

**Physical Organic Studies of Substituted Norbornyl Systems:
Aspects of Mechanisms and Chirality**

A thesis submitted in fulfilment of the requirements for the degree

of

DOCTOR OF PHILOSOPHY

IN CHEMISTRY

of

RHODES UNIVERSITY, SOUTH AFRICA

DEPARTMENT OF CHEMISTRY

Faculty of Science

by

ALICIA SINGH

January 2016



RHODES UNIVERSITY
Where leaders learn

To:

My dad who gave me my soft heart

&

My mom who gave me my strong backbone

Abstract

Fenchone and camphor are essential natural products that are available optically pure and contribute to the chiral pool in asymmetric synthesis. Further, they are both derivatives of norbornane, a structure that undergoes a remarkable diversity of rearrangements in acidic conditions. This work explores two aspects of the camphor/fenchone derived systems.

Firstly an attempt to clarify rearrangement mechanisms on a camphor system successfully *via* deuterium labelling and unsuccessfully *via* derivatization of fenchone (with rearrangement) to produce other ^{13}C -labelled camphor substitutions, has resulted in confirmation of a theoretically proposed, highly concerted Wagner-Meerwein, 6,2 - hydride shift, Wagner-Meerwein rearrangement in competition with an associated 2,3-methide shift. Kinetics and activation parameters for many steps have been resolved in this rearrangement of the deuterium labelled camphor-derived tosylate system to two pairs of isotopomers. Further, the kinetics and formation of an unexpected pair of dimers encountered during the scheme for ^{13}C labelling are investigated in detail. These dimers (forming during the initial stages of the synthetic scheme) are unusual in that they are not expected rotamers of each other, but diastereomers resulting from chirality of a sulfur atom in a sulfite moiety. A feasible mechanism of formation that matches the kinetics has been proposed in this unexpectedly complex system, and thermodynamic parameters have been determined.

The second aspect of substituted norbornyl systems pertains to their chirality, and the influence of this chirality on reaction mixtures, with an aim to identify novel chiral micellar catalysts for use in heterogeneous reaction mixtures. Headway has been made towards the synthesis of the appropriate surfactants to be used in the construction of these micelles, but extensive molecular dynamics simulations have illustrated the feasibility of forming the stable chiral micelles in a dual-solvent system, and detail precisely the influence of chirality on surrounding media.

These studies add important physical organic data as well as show the immense possibilities pertaining to substituted norbornane systems.

Contents

INTRODUCTION.....	1
1 Bicyclic monoterpenes containing the bicyclohept[2.2.1]ane skeleton.....	1
1.1 Reactivity of bicyclohept[2.2.1]yl derivatives	2
1.1.1 Free radical reactions / photochemical reactions	3
1.1.2 Carbocationic rearrangements of substituted bicyclohept[2.2.1]yl derivatives	5
1.1.2.1 Reactions involving loss of structural integrity	5
1.1.2.2 The Wagner-Meerwein rearrangement.....	6
1.1.2.3 Hydride and methide shifts.....	7
1.1.2.4 The camphene hydrochloride rearrangement.....	9
1.2 Non-classical carbocations – an historical perspective	10
1.2.1 The non-classical carbocation controversy.....	13
1.2.2 Evidence for the non-classical 2-norbornyl carbocation	14
1.3 Structure of bicyclohept[2.2.1]yl derivatives	16
1.3.1 Camphor and fenchol derivatives in asymmetric synthesis.....	16
1.3.1.1 Asymmetric synthesis	16
1.3.1.2 Camphor in asymmetric synthesis:	16
1.3.1.3 Fenchol/fenchone in asymmetric synthesis.....	17
1.3.2 Camphor and fenchone derivatives in surfactants	18
1.4 Surfactants and colloids	19
1.4.1 Formation of micelles	20
1.4.1.1 Interfaces and boundaries	20
1.4.1.2 Formation of micelles from surfactants.....	21
1.4.1.3 Thermodynamics of micellization	23
1.4.2 Krafft temperature:	24
1.5 Classification of micelles	25
1.5.1 Types of surfactants used in the generation of micelles	25
1.5.1.1 Amphiphilic block copolymers:	25
1.5.1.2 Anionic surfactants	27
1.5.1.3 Cationic surfactants:	28
1.5.1.4 Non-ionic surfactants:.....	29
1.5.1.5 Zwitterionic surfactants:	29
1.5.2 Shape and size	30
1.5.3 Packing factor	32

1.5.4	Use of micelles in catalysis.....	33
1.6	Forces driving development of micellar catalysts.....	33
1.6.1	Micro-emulsions and micellar catalysis.....	33
1.6.2	Physical uses of microemulsions.....	34
1.6.3	Microheterogeneous catalysis.....	35
1.7	Chiral micelles in organic synthesis.....	35
1.8	Solvent chirality.....	39
1.9	Characterization of micellar systems (chiral and achiral).....	41
1.9.1	Small angle scattering (SAS).....	41
1.9.2	Nuclear magnetic resonance (NMR).....	44
1.9.3	Molecular modelling.....	45
1.9.4	Molecular dynamics.....	45
1.10	Aims of the present study.....	48
DISCUSSION – REACTIVITY STUDIES		49
2	Rearrangement of a spirobornyl tosylate	49
2.1	Preparation of the spirobornyl tosylate 63	50
2.2	Kinetic analysis of the decomposition of the tosylate	50
2.2.1	Attempted preparation of a ¹³ C labelled analog of the scaffold 67	52
2.2.1.1	Synthesis of fenchene 71	53
2.2.1.2	Kinetics and the formation of isomers.....	58
2.2.1.3	The mechanism of formation of isomers.....	59
2.2.1.4	Variable temperature studies:.....	63
2.2.1.5	Computational study.....	65
2.2.2	Synthesis of fenchene:.....	69
2.2.3	Methylation of xylyl-substituted norcamphor:.....	71
2.3	Deuterium labelling for kinetic studies	74
2.3.1	Synthesis of 2D labelled exo-tosyl spirocamphor systems and subsequent kinetics of decomposition	75
2.3.2	Determination of rate law for the competing racemization in the rearrangement of a xylyl-substituted camphene	81
2.3.3	Kinetics analysis:.....	83
2.3.4	Theoretical studies:.....	86
2.4	Conclusion of the kinetic mechanistic studies.....	87
DISCUSSION – STRUCTURE STUDIES		89

3	Camphor and fenchone in the formation of chiral surfactants for the generation of chiral micelles. The chiral influence of the substituted norbornyl systems.	89
3.1	Synthesis of surfactants	89
3.2	Synthesis of fenchone-derived sulfonamides	91
3.2.1	Mass spectroscopic studies on the series of fenchone-derived sulfonamides	98
3.2.1.1	The mass spectrum of the picolylamine-derived sulfonamide 101a	98
3.2.1.2	The mass spectrum of the furfurylamine-derived sulfonamide 101b	102
3.2.1.3	Mass spectrum of the adamantylamine derived fenchone-sulfonamide 101d	104
3.2.1.4	Mass spectrum of aniline derived fenchone-sulfonamide 101c	105
3.2.1.5	Summary of features of mass spectrometry of 101a-d	107
3.3	Reductions of fenchone-sulfonamides	107
3.4	Synthesis of ethers 104 from the hydroxy sulfonamides 102	109
3.5	Preliminary micelle modelling and dynamics simulation studies:	117
3.5.1	Exploratory work	117
3.5.2	Systematic setup within the scope of CHARMM software	120
3.5.2.1	Construction of surfactants and assembly into a model of a micelle	120
3.5.2.2	Molecular dynamics simulations at 310 K for the constructed, solvated micelles	124
3.5.3	Packing factor of surfactants	130
3.5.4	Solvent chirality:	131
3.5.5	Final modelling:	135
3.5.6	Micelle conclusion	152
	CONCLUSIONS	153
	EXPERIMENTAL	155
4	Experimental details	155
4.1	Fenchone derivatives	155
4.1.1	10-Fenchonesulfonic acid 97	155
4.1.2	10-Fenchonesulfonyl chloride 100	156
4.1.3	2-Hydroxy-10-fenchonesulfonic acid 98	156
4.2	Series of fenchone-10-sulfonamides	157
4.2.1	N-(Picolyl)fenchone-10-sulfonamide 101a	157
4.2.2	N-(2-Furfuryl)fenchone-10-Sulfonamide 101b	158
4.2.3	N-(Aniline)fenchone-10-sulfonamide 101c	159
4.2.4	N-(Adamantyl)fenchone-10-Sulfonamide 101d	160
4.2.5	2-Hydroxy-N-(picolyl)fenchane-10-sulfonamide 102a	161
4.2.6	2-Hydroxy-N-(furfuryl)fenchane-10-sulfonamide 102b	161

4.2.7	2-Hydroxy-N-(aniline)fenchane-10-sulfonamide 102c	162
4.2.8	2-Hydroxy-N-(adamantly)fenchane-10-sulfonamide 102d	163
4.3	Synthesis of camphor-10-sulfonamides:.....	164
4.3.1	N-(Picolyl)camphor-10-sulfonamide 128a	164
4.3.2	N-(Furfuryl)camphor-10-sulfonamide 128b	165
4.3.3	N-(Aniline)camphor-10-sulfonamide 128c	165
4.3.4	N-(1-Adamantyl)camphor-10-sulfonamide 128d	166
4.4	Camphor-sulfonamide reductions:	167
4.4.1	2-Hydroxy-N-(picolyl)camphane-10-sulfonamide 129a	167
4.4.2	2-Hydroxy-N-(furfuryl)camphane-10-sulfonamide 129b	167
4.4.3	2-Hydroxy-N-(aniline)camphane-10-sulfonamide 129c	168
4.4.4	2-Hydroxy-N-(adamantly)camphane-10-sulfonamide 129d	169
4.5	Attempted ether and ester synthesis:	170
4.6	Fenchene synthesis:	173
4.6.1	3,3'-Di-o-xylynorcamphor 86	175
4.6.2	Attempted synthesis of 1-methyl-3,3'-di-o-xylynorcamphor 87	176
4.6.3	3,3'-Di-o-xylylcamphor 67	176
4.6.4	2-Hydroxy-3,3'-di-o-xylylcamphor 62	177
4.6.5	Deuterated 2-hydroxy-3,3'-di-o-xylylcamphor 62^D	177
4.6.6	Spiro[camphene-7,2'-indane] 64	178
4.6.7	Spiro[bornane-3,2'-indane]-2-tosylate 63	179
4.6.8	Racemic-spiro[camphene-6,2'indane] 65	179
4.7	Mechanistic study:	180
4.7.1	LAD rearrangement	180
4.7.1.1	General procedure:.....	180
4.8	Mechanistic study:	190
4.8.1	Dimer study:	190
4.8.1.1	General procedure:.....	190
BIBLIOGRAPHY		196

Acknowledgements

Firstly, I would like to thank my supervisor Dr. Kevin Lobb for his immense patience, advice, wisdom. Without the endless time, guidance and encouragement this PhD would not be possible. I cannot thank you enough for all the support you have given me over the years. My co-supervisor Prof Perry Kaye, thank you for your infinite guidance and motivation throughout my research.

My family who have constantly been my rock, parents and my grandparents who worked endlessly to provide for my education; the most valuable gift I will ever receive, words cannot express my gratitude. To my sister, Tiacia Singh, my forever best friend, for always putting things in perspective and always having my back, I thank you.

To my colleagues, friends and family, Clive, Vimla, Rosh and in the department to Dr. Klein for the constant encouragement and counsel and to Dr. Khanye, Dr. Mashazi, and Dr. Veale for constantly listening to my troubles and never failing to come up with some advice for me to try. To Aveshen, Christiana, Sumedh, Kavir, Bola, Rola, Chris, Oliver, Wesley, the 'tearoom crew' and all my lab mates without whom this journey would have not been as fun and entertaining, thank you endlessly. To Iviwe and Masego, I cannot thank you girls enough for the endless chats, laughs and inspirations brought into my life by two such beautiful souls.

I would like to thank the University of Stellenbosch for high resolution mass spectroscopy and the CHPC for generous allocation of computer resources.

Thank you to all the Rhodes University support and technical staff for constantly going above and beyond to ensure our comfort and success.

Thank you to NRF and the Henderson Foundation for funding.

Introduction

Studies on Reactivity and Structure of Substituted Norbornane as Presented in Fenchone and Camphor-Derived Systems

1 Bicyclic monoterpenes containing the bicyclohept[2.2.1]ane skeleton

The bicyclohept[2.2.1]ane (norbornane) **2** skeleton may be classified as a bicyclic monoterpene; some derivatives include camphane, bornane and fenchane. Camphor **1** and fenchone **3** are both naturally occurring organic molecules and due to similarities in structure, these molecules have very similar chemical and physical properties.¹ Camphor has a rich and extensive history stemming from the East where it was used by the Chinese as a circulatory stimulant from where it spread to Europe and was used as a fumigant during the plague in the 14th century.²

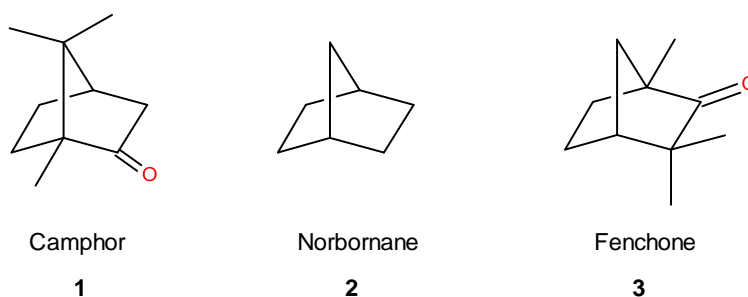
The natural source of camphor is the camphor tree, *Cinnamomum camphora* (Figure 1A)², which is indigenous to Japan, Taiwan and China. Optically active (1*R*)-(+)-camphor is distilled from the wood (Figure 1B).²



Figure 1. *Cinnamomum camphora*.²

Our interest, however, lies not in the medicinal properties, but the structural and chemical properties of these bicyclics. Some of the most fascinating features of these systems are its rigid structure and rare steric characteristics. The core bicyclic structure of interest, norbornane **2**, is a saturated hydrocarbon with a skeleton composed of a cyclohexane ring with a methylene group bridging across positions 1 and 4, forming the bicyclic system.³

Norbornane itself is achiral, and it is the substituents on the norbornane skeleton which are of interest as they define the reactivity and bring about chirality in the system.



1.1 Reactivity of bicyclohept[2.2.1]yl derivatives

Substituted norbornyl systems are known for their unexpected and surprising cationic rearrangements. In 1899⁴ Wagner realised that these rearrangements were similar to those observed during the dehydration of pinacolyl alcohol to tetramethylethylene, and in 1922 Meerwein⁵ suggested the involvement of the norbornyl cation during the rearrangement of natural terpenes, giving rise to the well known Wagner-Meerwein rearrangements.⁴ Disagreement regarding rearrangements of these systems have led to the controversies regarding the nature of the norbornyl-type carbocations themselves. There has also been confusion as to whether some of the observed experimental data reflected the presence of static penta-coordinate (non-classical) carbonium ion systems or rapidly equilibrating trivalent carbenium ions (Figure 2).⁴

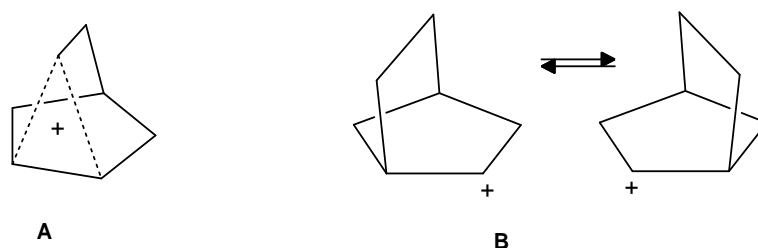
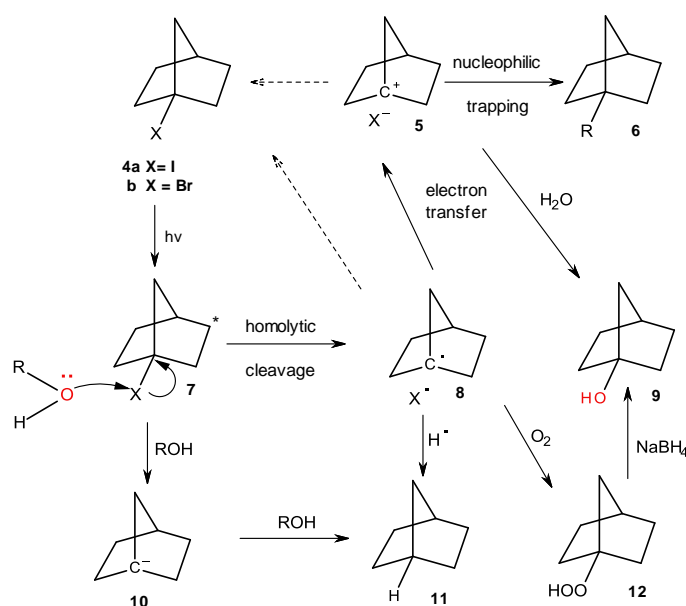


Figure 2. **A & B:** Symmetrical static non-classical 2-norbornyl carbocation (with bridging pentavalent carbonium species). Equilibrating trivalent carbenium carbocations.

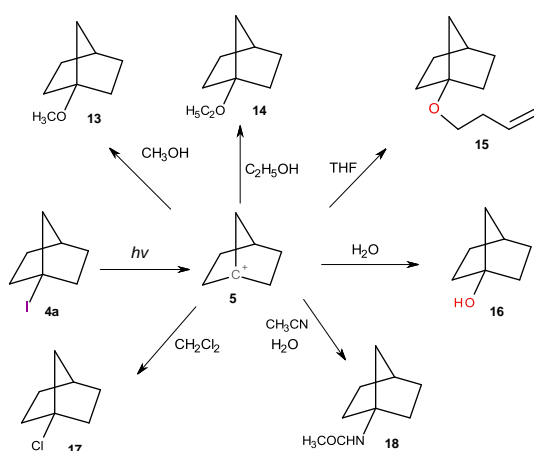
The interplay between structure and reactivity of the seemingly simple 2-norbornyl (bicyclo[2.2.1]heptyl) cation sparked a heated debate which is now known as the non-classical ion controversy.⁶ As will be discussed, these systems show diverse transformations.

1.1.1 Free radical reactions / photochemical reactions

It is worth starting the discussion with photo-excitation of norbornyl halides **4**, due to its simplicity of mechanism. A study conducted by Kropp *et al* involved the excitation of halonorbornanes to yield various substituted norbornanes such as 1-alkylnorbornanes **6**, 1-hydroperoxynorbornane **12**, and 1-hydroxynorbornane **9** (Schemes 1 and 2). Scheme 1 shows a proposed mechanism in which the stable bridgehead carbanion **10** and the bridgehead radical **8** may be an intermediate *en route* to the products. The bridgehead carbocation is highly unstable due to its inability to adopt a planar conformation, yet Scheme 2 illustrates how versatile this process is.



Scheme 1. Photochemical reactions of halonorbornanes.



Scheme 2. Possible products derived from norbornane cation.

Ultimately it is possible that irradiation at 254 nm of iodonorbornane **4a** produces the 1-norbornyl cation **5**, which upon reaction with various solvents gives access to an extensive range of useful final products such as the ethers 1-methoxynorbornane **13**, 1-ethoxynorbornane **14** and 1-(3-buten-1-yloxy)norbornane **15**, the alcohol **16** and the amide **18**. However, pertinent to this study is the discussion of the formation of carbocations, where rearrangement is also possible.

1.1.2 Carbocationic rearrangements of substituted bicyclohept[2.2.1]yl derivatives

The sheer complexity and diversity of skeletal rearrangements in norbornyl systems provides for a rich base in the historic literature and still captures the interest of chemists today. Substituted norbornyl systems have a tendency to undergo multistage transformation processes such as hydride and methide shifts, Wagner-Meerwein rearrangements and combinations of these such that even racemization is possible; these processes involve a variety of carbocation intermediates and products which may be classical or non-classical in nature.⁸

1.1.2.1 Reactions involving loss of structural integrity

The controversial nature of the 2-norbornyl cation lives on even after decades of debate and discussion, and one aspect is its reactivity and mechanisms leading to rearrangement. In the two-year span 2014 to 2015 a new study arose that was not immune to controversy regarding the rearrangement of the 2-norbornyl carbocation using mass spectrometry. During the study, an attempt to obtain an infrared spectrum of the 2-norbornyl cation in the gas phase by Mosley *et al*⁹ provided the unexpected observation that the 2-norbornyl carbocation rearranges to the 1,3-dimethylcyclopentenyl carbocation (Figure 3). This conclusion was reached by comparison of the experimental vibrational spectrum of the C-H fingerprint region to that generated computationally,¹⁰ and it was noted that the experimental data was not a match for the 2-norbornyl carbocation, but rather corresponded to the isomeric 1,3-dimethylcyclopentenyl cation. Further it was found that the 1,3-dimethylcyclopentenyl ion (Figure 3 B) was 19.0 kcal mol⁻¹ more stable than the 2-norbornyl cation (Figure 3 A).⁹ This has sparked further interest into what reaction pathways are available to the 2-norbornyl carbocation.

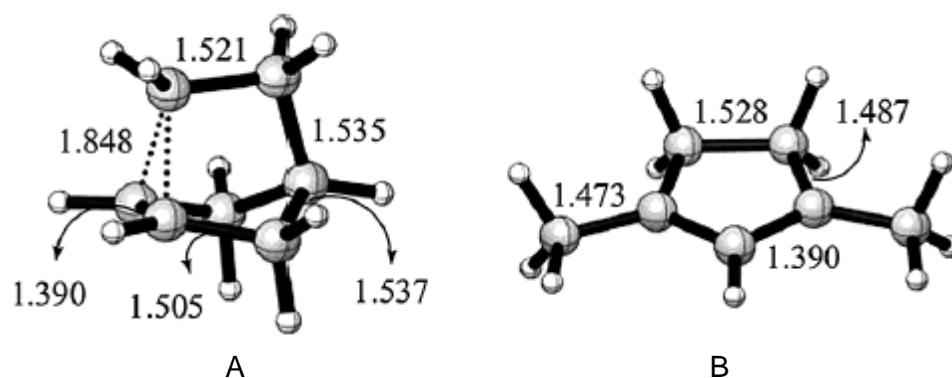
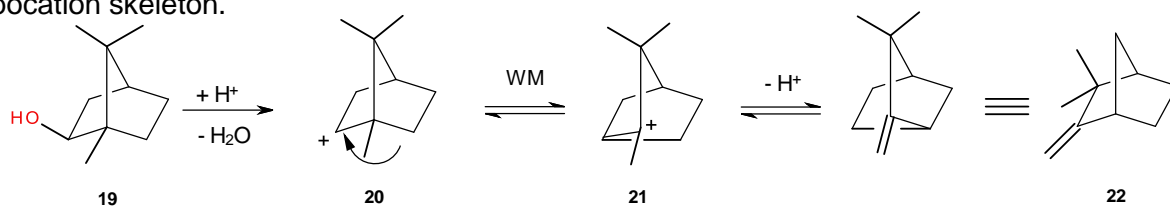


Figure 3. MP2/6-311G(2d,2p) optimized structures of the 2-norbornyl (A) and 1,3-dimethylcyclopentenyl (B) cations (*used with permission*).¹¹

The mechanism of isomerization from the 2-norbornyl cation to the 1,3-dimethylcyclopentenyl cation is difficult to identify. To address this question, Merino *et al.*¹¹ used Born-Oppenheimer molecular dynamics simulations to explore possible rearrangement pathways. The results of this study presented two possible complex pathways by which isomerization could occur, both involving ring opening by increasing the distance of the non-classical bridge. They also proposed that both rearrangement pathways are viable, given that the difference in activation energies of their first steps is only 1.0 kcal mol⁻¹. The study revealed the first possible pathway is longer and involves a series of ring openings resulting in acyclic allylic cations, while these intermediates are bypassed in a second, shorter route. Both pathways involve the formation of the methylcyclohexenyl cation, which undergoes a ring contraction and subsequent methyl and hydride shifts, resulting in the 1,3-dimethylcyclopentenyl cation. Lobb¹⁰ recently disputed these findings with a study showing that the isomerization route of the 2-norbornyl cation does not occur *via* ring opening of the non-classical cationic centre as reported by Merino, but rather through the cleavage of the C3-C4 bond occurring at 9.7 kcal mol⁻¹ lower than the previously stated level required for activation. He also illustrated that it was not possible to state or define a single isomerization mechanism from the 2-norbornyl to its isomer, but that the isomerization occurred *via* numerous (>10⁹) possible pathways.

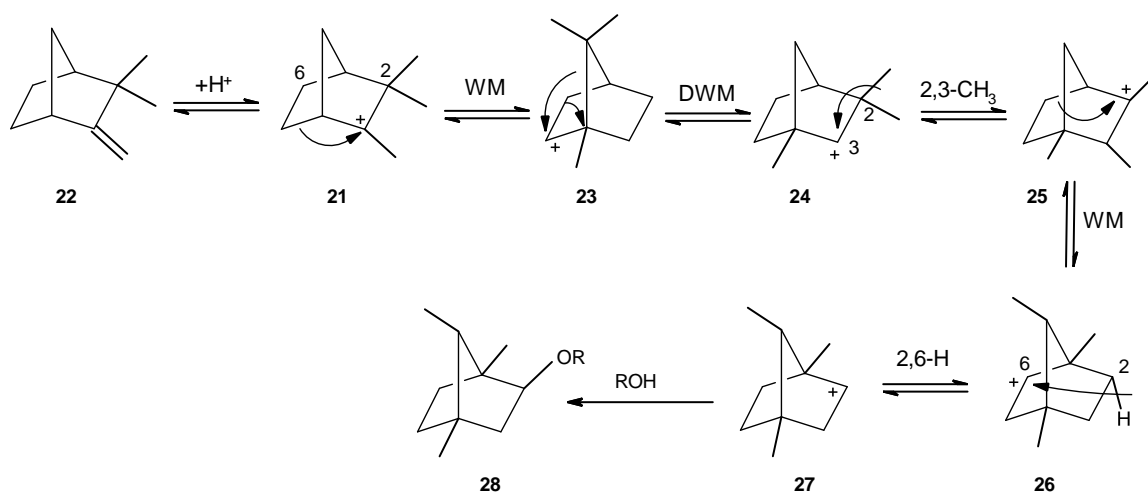
1.1.2.2 The Wagner-Meerwein rearrangement

As mentioned before, the extraordinary ability of carbocations to undergo numerous unusual rearrangements has caught the attention of many organic chemists. Between 1860-1925 the pinacol rearrangement and ring rearrangements of terpenes (such as, the dehydration of borneol and isoborneol to camphene) were identified.⁴ It was Wagner who put the pieces together and reported that these reactions proceed through carbocations.^{5,6} Meerwein described this discovery as 'Wagner's astonishing insight'.¹² The break-through made by Wagner was of the revolutionary idea that the acid-catalysed dehydration of borneol **19** into camphene **22** (Scheme 3) occurred *via* intra-molecular rearrangement.¹³ This mechanistic pathway is now what is referred to as the Wagner-Meerwein rearrangement (or Wagner-Meerwein shift). This rearrangement involves an intra-molecular 1,2-skeletal bond shift in the carbocation skeleton.



Scheme 3. Formation of camphene from isoborneol illustrating the Wagner-Meerwein shift.

Wagner-Meerwein shifts (and the double Wagner-Meerwein shift, which involves two bonds moving simultaneously) are crucial parts of many synthetically important reactions. Reactions, for instance involving (+)- α -fenchene and (-)-camphene with aliphatic-aromatic alcohols produce a product where the carbocation is trapped, subsequent to several carbocation intermediates.⁸ More than one of the steps involved is a Wagner-Meerwein transformation. It may be noted that many reactions proceed not through one single rearrangement step, but through many rearrangements, involving multiple distinct Wagner-Meerwein transformations. Scheme 4 shows the mechanism in the case where (-)-camphene **22** reacts with a primary alcohol to form the ethoxide **28** *via* a series of steps.

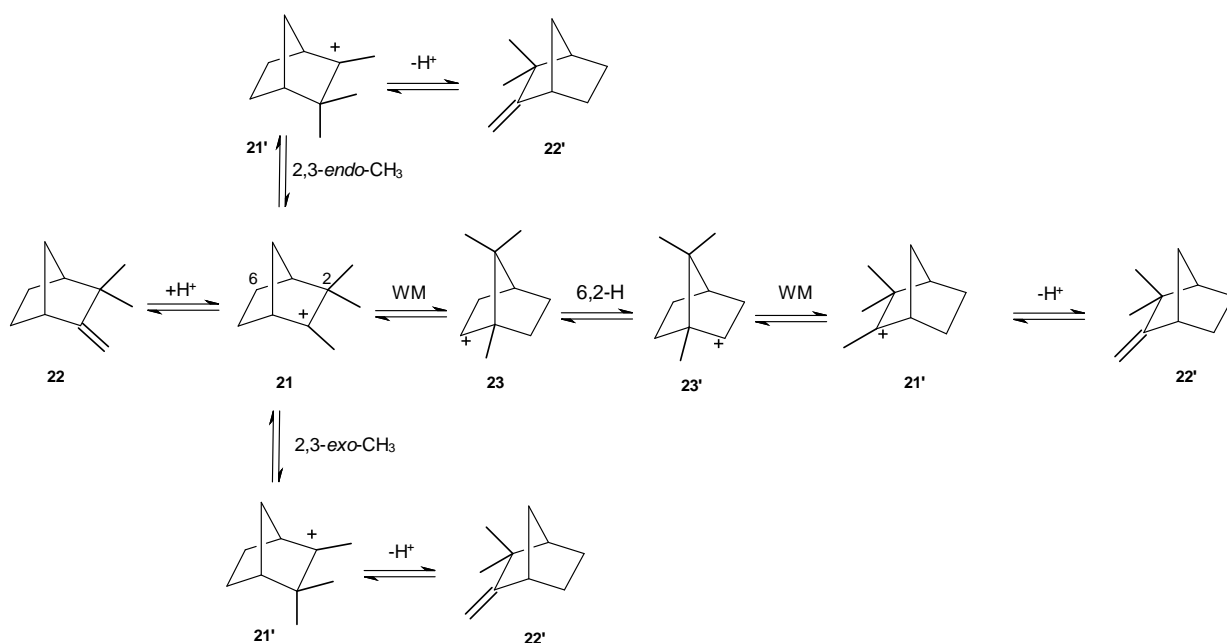


Scheme 4. Wagner-Meerwein (WM) transformations can be useful in synthetic pathways, particularly where the norbornyl skeleton is present.

1.1.2.3 Hydride and methide shifts

Prominent in rearrangement pathways, the substituted norbornyl skeleton is prone to the hydride and methide shifts (Scheme 6). According to NMR studies, it appears that the 3,2-hydride shift of the norbornyl cation generated in acidic media at low temperatures is much slower than the Wagner-Meerwein and 6,2-hydride shifts.^{14,15} Using ^{14}C labelled norbornyl systems, Roberts¹⁶ presented evidence that 6,2-hydride shifts also occur in non-classical ions (which will be discussed presently). Taking into account the ease of these shifts, in order to obtain NMR evidence of the static norbornyl or substituted norbornyl carbocations, low temperature NMR techniques have to be employed. NMR studies conducted at -70°C can freeze out the 3,2-hydride shift; however the 2-norbornyl cation must be cooled further to -159°C to freeze out 2,6-hydride shifts and Wagner-Meerwein rearrangements.¹⁷

These hydride and methide shifts also occur in Scheme 6; this interplay between the Wagner-Meerwein and the shifts illustrates the range and versatility, and influences which various rearrangements can have on a reaction mechanism. The rearranged camphene-derived cation **24**, which is formed through the isobornyl cation intermediate (Scheme 5) (**23**) via Wagner-Meerwein rearrangement, undergoes racemization. This racemization was initially attributed to a 3,2-methyl shift to form cation **21'** (referred to as the Nametkin rearrangement).¹⁸ It was concluded that this rearrangement involves no less than three competitive cationic racemization pathways¹⁸ (Scheme 5): (1) an *exo*-3,2-methyl shift to form **21'**, (2) a Wagner-Meerwein shift to form **23**, followed by a 6,2-hydride shift to form **23'** and eventually **21'** and (3) an *endo*-3,2-methyl shift in the protonated camphene cation to also form **21'**.

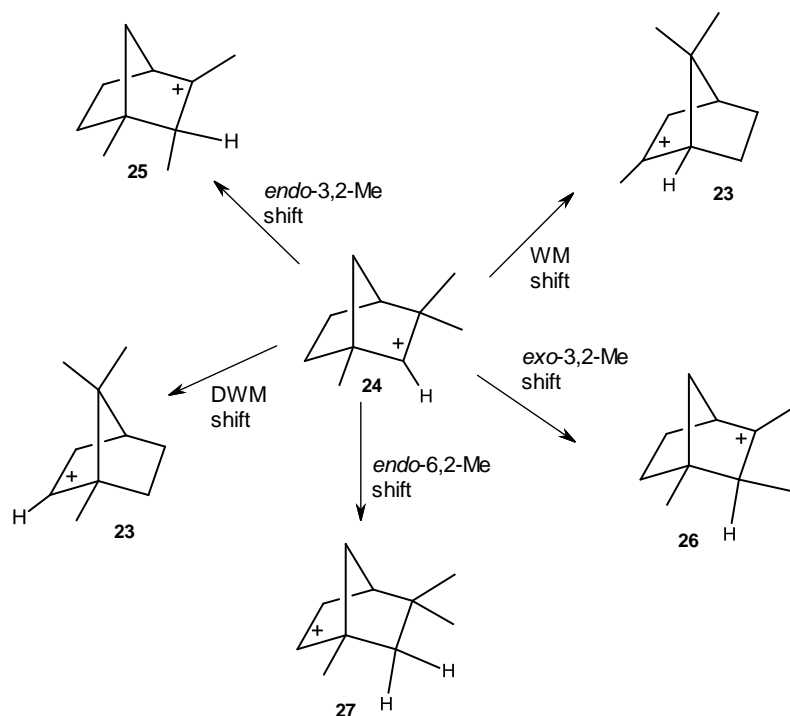


Scheme 5. Racemization pathways for camphene.

Rearrangement rates for the *exo* and *endo* processes can be quantitatively determined from NMR signal-broadening data.¹⁹ During acid catalysis, the difference in rates has been quantified as follows:

$$\frac{k(\text{camphene racemization via } \textit{exo} - \textit{methyl shift})}{k(\text{camphene racemization via } \textit{WM} - 6,2 - \textit{WM shift})} = \frac{2.8 \times 10^{-5} \text{ s}^{-1}}{2.2 \times 10^{-5} \text{ s}^{-1}} = 1.3$$

From the literature, it is evident that the *exo*-methyl shifts are faster than the competing *endo*-shifts.



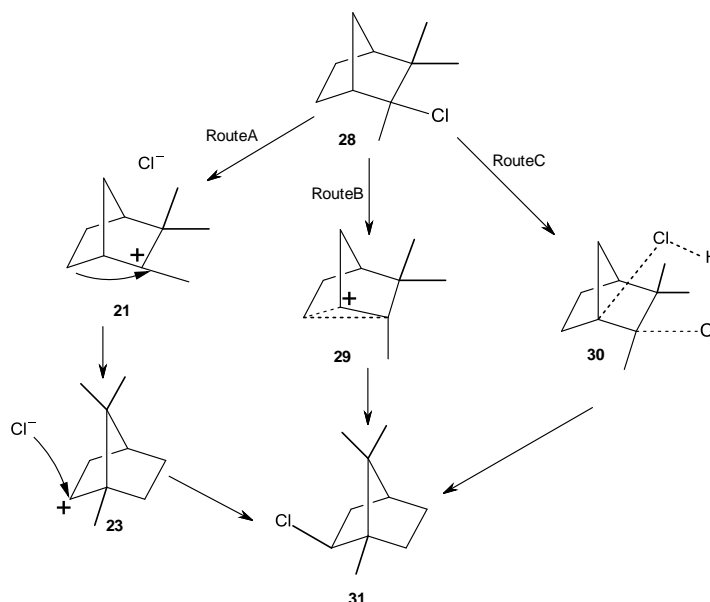
Scheme 6. Various possible rearrangements available to the 1,3,3-trimethylnorbornyl system.

1.1.2.4 The camphene hydrochloride rearrangement

Heavily dependent on the Wagner-Meerwein rearrangement is the mechanism of camphene hydrochloride rearrangement. The formation of isobornyl chloride by means of camphene hydrochloride rearrangement has been extensively studied and is fraught with controversy. Smith²⁰ conducted a thorough literature investigation into the camphene hydrochloride rearrangement and identified some flaws in two of the earliest postulated mechanisms. The two accepted routes (Scheme 7, routes A and B) did not address the rate enhancement (due to acid-catalysis), nor the rearrangement stereoselectivity (formation of only *exo*-product).²⁰ The two mechanisms (routes A and B) proceeded *via* two different pathways, route A involving a 'classical' carbocation **21** and route B containing the 'non-classical' ion **29**.

A kinetics study undertaken by Bartlett and Pöckel²¹ concluded that the hydrogen chloride catalysed rearrangement of camphene hydrochloride was primarily second order. Kinetic studies carried out in nitrobenzene solvent showed that the rearrangement involves one molecule of camphene hydrochloride and one molecule of hydrogen chloride.

Smith²⁰ took a theoretical route to explore and test new possible mechanistic pathways using density functional theory (DFT). The possibility of the process occurring *via* a cyclic transition state **30** was proposed in Scheme 7 route C, in which the role of the hydrogen chloride was not only for acid-catalysis, but also to influence the stereochemistry.



Scheme 7. Various routes exhibiting hydrogen chloride rearrangement.

This mechanism has been refuted by Sorensen *et al.*²² based on solvation energy calculation, reaffirming the case for carbocation intermediates and a Wagner-Meerwein shift, while Schleyer *et al.*²³ have identified a mechanism involving ion pairs, a compromise between routes A and B, and route C.

1.2 Non-Classical Carbocations – an historical perspective

As alluded to earlier, one of the most fundamental and original ideas in physical organic chemistry was the suggestion of the existence of carbocations. The concept of charged ions was initially posed within the realm of inorganic chemistry, but is now an essential tool in describing the mechanisms that occur in the transformations of organic compounds, and carbocations, especially derived from hydrocarbons, have been isolated and characterized. However, carbocations also exist as fleeting charged intermediates occurring during the course of reactions leading from non-ionic reactants to non-ionic products.¹⁷

From the late 1960s to the early 1980s carbocations became the focus of extensive experimental and theoretical studies regarding structure, stability and reactivity. Although this flurry of publications has slowed down, the effect has been to raise the status of carbocations to where they are regarded as arguably one of the most important intermediates in organic chemistry. So much so that in January 2001 a two-day symposium entitled “100 years on carbocations” was hosted by Professor George Olah.⁴

The earliest studies on carbocations were carried out in Britain (Ingold & Hughes) and Germany (Meerwein) in the 1920s and 1930s. These studies heralded detailed studies of organic chemical reactions and their mechanisms, hence shedding light on and sparking interest in the concept of positively charged hydrocarbons, to which was given the term carbocation.^{24,25} The term carbocation was not however, sufficient to describe a new type of positively charged carbon structure. The term ‘non-classical ion’ was originally proposed to explain experimental results of solvolysis from a particular standpoint. These non-classical carbocations exhibited the phenomenon of a carbon being bonded to five neighbouring atoms (a carbonium ion), of which some bonds were only partial, as opposed to the more conventional ‘classical’ carbocations (carbenium ions with three neighbouring atoms) with fully constructed bonds.²⁶ At the center of this discussion is the 2-norbornyl carbocation. The central issues surrounding the 2-norbornyl cation story have persisted: firstly, what is the structure of the cation under stable ion conditions in the absence of nucleophiles; and secondly, what are the structures of transition states resulting in the 2-norbornyl intermediates under solvolytic conditions?.²⁷

A 1949 communication by Winstein and Trifan²⁸ revealed an insightful clue into the structure of the 2-norbornyl carbocation. An investigation into the relative rates of acetolysis at 45°C of *p*-toluenesulfonates or *p*-bromobenzenesulfonates showed a remarkable difference. It was noted that the the *exo*-norbornyl **34** species loses its leaving group (to form a carbocation) at a rate 350 times greater than its *endo* counterpart **33** (*exo:endo* rates: 350:1) during this carbocation formation. During the same study it was also noted that the *endo*-norbornyl *p*-toluenesulfonate yields only the *exo*-norbornyl acetate **35** (although this *exo* product is racemic).

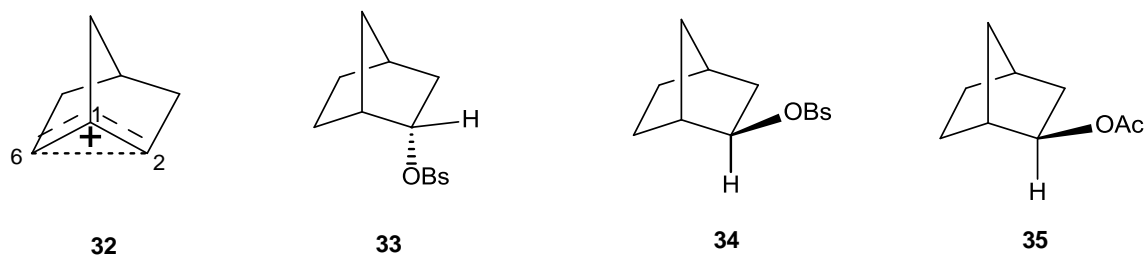


Figure 4. Solvolysis products of the norbornyl ion.

It was suggested the ionization of **34** proceeds through the non-classical cation **32**. The cation holds a plane of symmetry bisecting through the bond between carbon 1 and 2 and passing through carbon 6, hence the reaction with acetic acid is equally likely at both carbons 1 and 2, *via* the face of the structure opposite to the bridging carbon 6, resulting in the racemic *exo*-acetate **35**.^{27,28} This effect is further enhanced by the fact that the C1-C6 σ bond of the *exo*-brosylate **34** allows for neighbouring group assistance (anchimeric assistance) resulting in rate enhancement. In contrast the C1-C6 bond of the *endo*-species **33** is not suitably positioned to allow for anchimeric assistance that would aid solvolysis of the *endo*-brosylate.²⁹ When applying solvent more ionizing than acetic acid, the *exo* vs. *endo* trend is enhanced. The solvolysis rate constant ratios for *p*-toluenesulfonate analogues of *exo*-species **34** and *endo*-species **33** were found to be 281 for acetic acid, followed by 1122 in trifluoroacetic acid, and 1694 for formic acid.³⁰

Further evidence can be seen from kinetic studies on the acetolyses of *exo* and *endo*-2-norbornyl tosylates, where activation-free energies of $\Delta G^\ddagger = 27.1 \text{ kcal mol}^{-1}$ for the *endo* species and $22.6 \text{ kcal mol}^{-1}$ for the *exo*-isomer were measured, showing a ΔG^\ddagger of approximately 6 kcal mol^{-1} kinetics advantage for the *exo* over the *endo*-tosylate.³¹ Upon comparison with a 'classical' alkyl cation the 2-norbornyl cation is energetically similar in stability to a tertiary cation such as the *tert*-butyl cation and around $8\text{-}16 \text{ kcal mol}^{-1}$ more stable than secondary cations.³²

1.2.1 *The non-classical carbocation controversy*

In 1961, Herbert Brown contradicted current thinking when he presented a paper to the London Chemical Society. He addressed the issue of the non-classical carbonium ion intermediates concerning the solvolysis results: according to Brown, the results were not being produced with “the same care and same sound experimental basis as that which is customary in other areas of experimental organic chemistry”.⁴ What followed was decades of work attempting to gain evidence either proving or disproving the existence of the 2-norbornyl non-classical carbocation. The Brown-Winstein non-classical ion controversy came down to two opposing explanations of the same, non-disputed experimental data.

The origins of the non-classical carbocation may be found in 1939,³³ when Wilson put forward some progressive suggestions, but this did not gain general acceptance. Following Winstein, and by the 1960's the arguments pertaining to the existence of these systems had the full attention of prominent chemists of the likes of Herbert Brown (seen as the antagonist), versus Saul Winstein and George Olah, who supported the existence of the non-classical carbonium ion.

The previously discussed solvolysis studies of the *exo* and *endo* 2-norbornyl brosylates gave rise to the then proposed σ -delocalized, bridged norbornyl ion intermediate. Brown's interpretation was that steric effects could explain the solvolysis rates. Brown in turn proposed that solvolysis occurs *via* achimerically unassisted ionization and that the rate and the formation of only the *exo* isomer was a result of steric hindrance to ionization, particularly in the case of the *endo* isomer. Looking at the *exo/endo* solvolysis rates, according to Brown's explanation, the *exo* rate was not fast, but in fact, it was the *endo* rate that was slow.

Winstein's concept of the non-classical norbornyl cation inferred that the bridged ion is stabilized relative to a secondary ion by C-C σ bond delocalization. Brown put forward an argument stating that the available data were consistent with describing the intermediate as a rapidly equilibrating classical secondary ion.³¹ The observed Wagner-Meerwein shift resulting in the inter-conversion of the two ions was assumed to be rapid, relative to the capture of the nucleophile. The occurrence of such a rapid rearrangement would account for the isolation of a racemic product, and therefore Brown suggested that with such a migration, attack of the nucleophile from the *exo* direction would always be preferred.³⁴

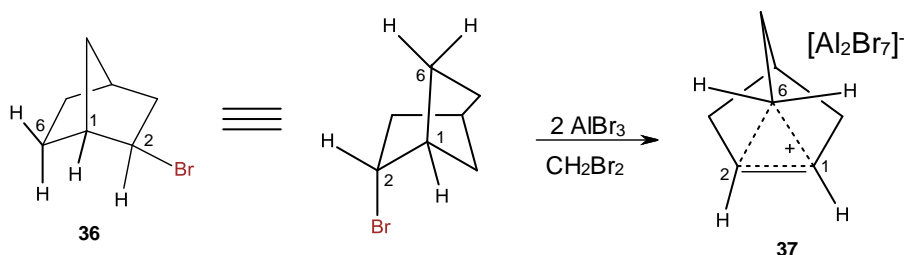
1.2.2 Evidence for the non-classical 2-norbornyl carbocation

At the 1962 Brookhaven Mechanism Conference, Olah presented findings on long-lived carbocations.⁴ According to his account he was spoken to privately by Winstein and Brown, who both expressed doubt on the validity of (the young) Olah's conclusions. However, accepting the possibility that Olah's findings were valid, each scientist asked Olah to apply his methods in the hope of obtaining further evidence to validate either the "non-classical" (Winstein) or "classical" (Brown) nature of the 2-norbornyl cation. The key to attaining stable, long-lived alkyl cations was the use of superacids, in particular protic superacids such as fluorosulfonic acid (FSO₃H), triflic acid (CF₃SO₃H) and magic acid (FSO₃H-SbF₅)⁴ and the technique used to view these carbocations was *via* NMR spectroscopy. ¹H and ¹³C spectroscopic studies in poorly nucleophilic solvents allowed for successful observation of the elusive norbornyl cation. A low temperature NMR experiment of the non-classical norbornyl cation was conducted in SO₂ClF and SO₂F₂ at -159°C; at this temperature all rearrangements (such as hydride shifts and Wagner-Meerwein) were dormant,³⁵ and the non-classical nature of the carbocation was evident.

In the middle of all of this flurry of studies on long-lived cations, it is worth remembering that in 1964 Schleyer reported the first direct observation of the ion as [SbF₆]⁻ salt.¹⁵ Further ¹³C spectroscopic studies of the cation showed upfield shifts being intrinsic rather than a rapid equilibration between isomers.³⁶ Although this NMR evidence was met with conviction by those supporting the classical ion theory, conclusions were rejected on the basis of the long NMR time scales.⁹ However, at -159°C, these arguments do not hold.

As further confirmation, core electron spectroscopy (ESCA) was conducted on the 2-norbornyl system, and this technique provided undisputable evidence as to the nature of the cation in question (the timescale is much shorter than that for NMR). Theoretical studies conducted by Allen and Goetz³⁷ entailing geometry-optimized *ab initio* calculations applying both STO-3G and 4-31G basis sets, reinforced what was determined from the ESCA spectrum results. These calculations have been done at even higher levels of theory more recently (such as MP2/6-311G(2d,2p))^{10,11} and the results are always consistent with a non-classical 2-norbornyl carbocation. There is a consistency between experimental and theoretical analyses, which all confirm that the 2-norbornyl carbocation is a single non-classical carbocation and not a pair of equilibrating classical ions.

Long after these conclusions were made the controversy of the norbornyl cation raged for almost two decades. As recently as 2013 Scholz *et al.*³⁸ presented a solution to this long-standing debate in the form of an x-ray crystal structure of the 2-norbornyl carbocation.



Scheme 8. Formation of the 2-norbornyl cation (**37**) in crystalline form for the purpose of x-ray diffraction.

The 2-norbornyl cation **37** was formed as a crystalline salt by reacting 2-exo-norbornyl bromide **36** in dibromomethane (CH_2Br_2) solution with aluminium tribromide (Scheme 8), and subjecting the crystals produced to x-ray diffraction, providing crystallographic proof of the bridged, non-classical cation. This may be viewed as a conclusion to the controversy, although there are many papers claiming to be such. Three 2-norbornyl moieties from the crystal structure are reproduced in Figure 4.

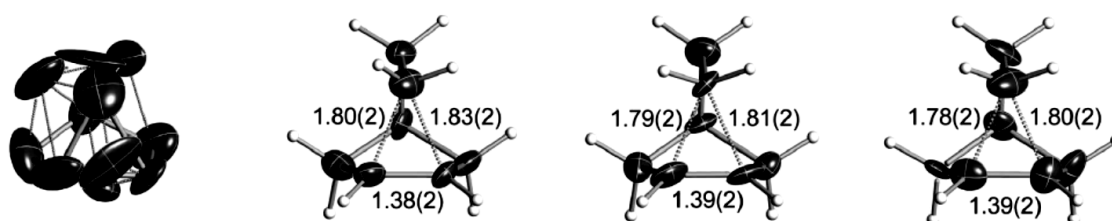


Figure 5. The crystal structure of the 2-norbornyl cation as $[\text{C}_7\text{H}_{11}]^+[\text{Al}_2\text{Br}_2]^- \cdot \text{CH}_2\text{Br}_2$. The figures from left to right represent the electron density maxima of the cation with the far left being the most disordered at 120 K, compared to those following which are three independent non-classical cation variations at 40 K (*used with permission*).³⁸

1.3 Structure of bicyclohept[2.2.1]yl derivatives

1.3.1 Camphor and fenchol derivatives in asymmetric synthesis

1.3.1.1 Asymmetric synthesis

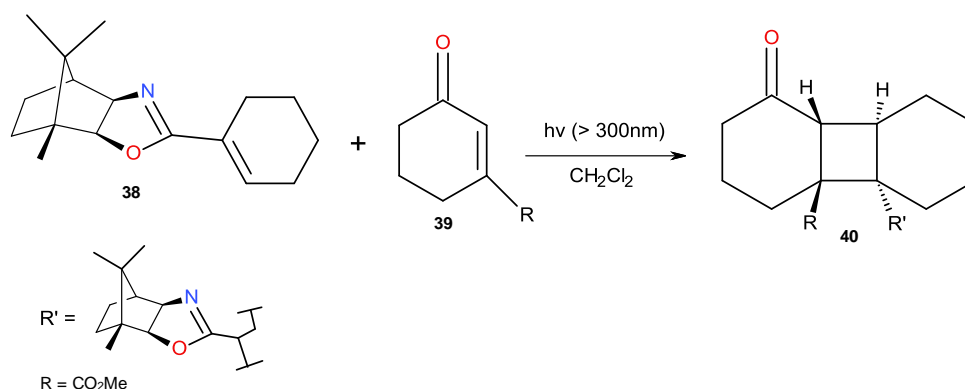
Asymmetric synthesis entails the creation of asymmetric centres with the aim of producing enantiomers or diastereomers in unequal proportions. This may be achieved by the creation of new asymmetric centres, either in achiral molecules through the use of chiral reagents or catalysts, or in molecules already possessing asymmetric centres, where further modification is influenced by the existing chirality, resulting in the formation of new diastereomers in unequal amounts.

Biological activity is often linked to the interactions of a particular stereoisomer with its respective biological receptor. This distinction between stereoisomers occurs due to the asymmetric nature of the environment around the receptors. Considering pharmaceuticals, many commercially available drugs contain at least one stereocentre, yet only one of its stereoisomers might exhibit the required beneficial properties whilst the other(s) could be ineffective and even hazardous. The infamous and tragic teratogenic effects of racemic thalidomide, which was marketed as a sedative hypnotic drug, were found to be due to one of the enantiomers while the other was effective in its intended purpose.³⁹

1.3.1.2 Camphor in asymmetric synthesis

Camphor has been used for hundreds of years as a rubefacient, mild analgesic, lip-balm, cold sore ointment, for the treatment of fibrosis and muscle stiffness. Of particular interest in natural camphor is its optical activity, and more importantly its optical purity.⁴⁰ Optical purity is an essential factor in asymmetric synthesis.

Camphor-derived chiral auxiliaries have often been used as chiral induction agents in asymmetric synthesis. Zhao *et al.*⁴¹ reported the asymmetric molecular [2+2] photoaddition reaction in the production of cyclobutanes (Scheme 9). Strained cyclobutanes have the ability to undergo transformations into other essential ring systems, allowing for the formation of complex carbon skeletons.⁴² Camphor was chosen to be the ideal candidate for this asymmetric induction reaction because of the steric hindrance owing to the methyl groups. Camphor served as a great source of an optically pure starting material for the formation of the chiral auxiliary attached compound **38**, resulting in an efficient method affording enantiomerically pure cyclobutanes **40** by reaction with the α,β -unsaturated cyclohexanone **39**.



Scheme 9. A camphor-derived chiral auxiliary in an asymmetric Diels-Alder cycloaddition.⁴¹

Recently, chiral *O,N,O*-tridentate phenol ligands **41** (Figure 5) constructed from a camphor backbone were found to be effective as chiral catalysts for the enantioselective addition of diethylzinc to aromatic aldehydes.⁴³ Optically pure secondary alcohols are important intermediates in the synthesis of various pharmaceuticals. One efficient method for the preparation of these alcohols involves the asymmetric addition of diethylzinc to aldehydes. Camphor was used in the development of new tridentate aminodiols ligands, which proved very successful, resulting in high enantioselectivities between 80-95%.⁴³

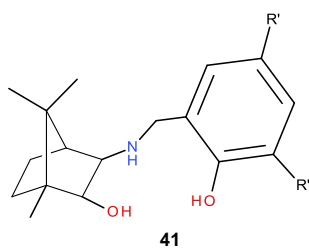


Figure 5. Structure of the *O,N,O*-tridentate ligand.

1.3.1.3 Fenchol/fenchone in asymmetric synthesis

Despite of the many structural and chemical similarities between the camphor **1** and fenchone **3** systems, camphor has been extensively employed in various asymmetric synthesis applications whereas fenchone is seldom used. There are, however, cases in which fenchone, like camphor, has been used to make chiral ligands. A particular example is where Blanco *et al.*,⁴⁴ explored various fenchol-based palladium-phosphorus halide catalysts in alkyl-aryl cross-coupling reactions. Two of the ligands, **42** and **43** are shown in Figure 6.

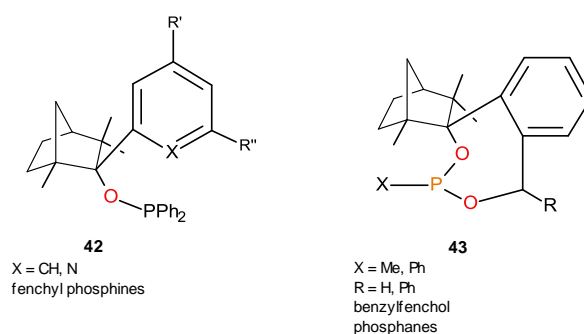


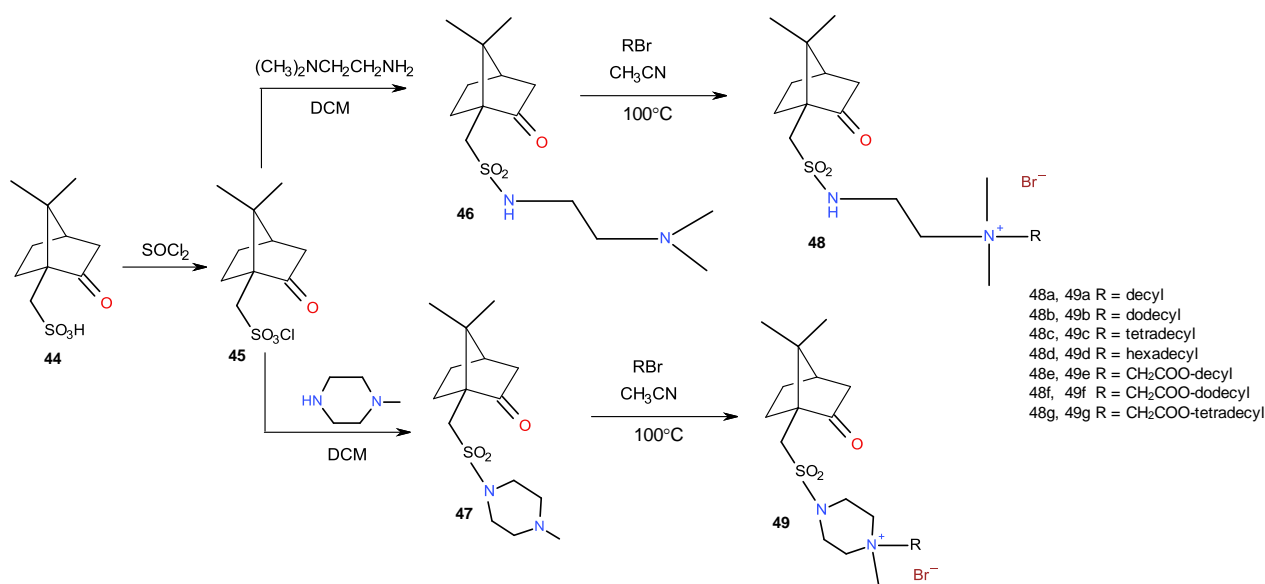
Figure 6. Fenchol-based phosphorus ligands.

These fenchol-based ligands were used to make chiral catalysts in chiral organolithium aggregates as well as in enantioselective organozinc catalysts.

1.3.2 Camphor and fenchone derivatives in surfactants

There are various methods to induce chirality into a system during synthesis; an asymmetric environment can be created by using an already chiral compound or chiral catalyst, or *via* a strategic symmetry-breaking object near a prochiral species.⁴⁵ Micelles can be viewed as microreactors that provide the advantages of conducting reactions in water by enhancing the solubility of nonpolar reagents and catalyst, but chiral micelles have the added benefits of aiding stereoselectivity by providing a chiral environment. By taking advantage of working at a molecular level through supramolecular chemistry one is able to gain control and govern both structural and dynamic properties of a system *via* non-covalent, intermolecular interactions.

Recently a series of homochiral quaternary ammonium sulfonamides containing the camphor moiety has been derived for testing against antimicrobial and antifungal agents (Scheme 10).⁴⁶ Surfactant type molecules synthesized with the attachment of *n*-alkyl chains between C4 to C18 proved to be most effective in antimicrobial activity. From the camphor-10-sulfonic acid **44** starting material various surfactants such as *N*-{2-(((1*S*,4*R*)-7,7-dimethyl-2-oxobicyclo[2.2.1]heptan-1-yl)methylsulfonamido)ethyl}-*N,N*-dimethyltetra-decan-1-aminium bromide **48c**⁴⁶ were prepared.



Scheme 10. Synthesis of quaternary ammonium salts derived from camphor-10-sulfonic acid.

What is interesting about this study is that the camphor skeleton was introduced not for its chirality, but for its antimicrobial properties. This, combined with the antimicrobial properties of the quaternary ammonium sulfonamide, was intended to increase the antimicrobial properties in the surfactant and the micelle generated. However, in the context of this study this illustrates the feasibility of constructing viable chiral surfactants to make micelles where chirality is evident.

1.4 Surfactants and Colloids

Very few areas within the field of chemistry have exhibited such rapid growth and evolution than the study of surface and colloid science, especially surface activity related to surface active materials,⁴⁷ these materials being commonly known interchangeably as surfactants or amphiphiles. The term amphiphile was defined by Paul Winsor more than 50 years ago, a combination of 2 Greek words: *amphi* meaning “double”, or “around” and *philos*, an expression of friendship or affinity.⁴⁸ Surfactants are molecules comprising two characteristic regions, namely a head and tail region, with one part having marked polar characteristics and the other apolar or *vice versa*. Surface science has generally been overlooked in the past however, considering emulsions, dispersions, foaming agents and wetting agents. The influence which

surface chemistry holds quickly becomes clear, and its relevance in one's day-to-day life. The importance of interface and phase chemistry extends from biological membrane formation and function in living cells, to dealing with problems of how liquids wet the walls of a rocket's fuel tank in a low gravity environment.⁴⁹ Considering the widespread applications of colloidal systems, including, but not limited to products of food technology, pharmaceutical and cosmetic preparation, paints, dyes, various processes involving mineral extraction, oil recovery and water treatment, chemists are pushed to understand and manipulate interfaces through the use of surface active agents.⁵⁰ Even through its long history, the study into these surfactant systems has only recently gathered interest. The earliest applications of colloidal systems were the use by alchemists for the production of colloid gold (an attempt to make the Elixir of Life) and Purple of Cassius used to make ruby glass.⁵⁰ Later (1856) the first systematic study of colloid gold was conducted by Michael Faraday, from which stemmed theories concerning the factors responsible for the formation and stabilization of such dispersions.⁵⁰ The lack of research and understanding in the field of colloid science compared to other fields of chemistry is largely attributable to the difficulty in preparing well-characterized colloidal materials with reproducible results. However more recent developments in preparation methods, coupled with the application of modern instrumentation such as high-resolution and scanning electron microscopy, laser light scattering experiments and nuclear magnetic resonance techniques have greatly aided our understanding of such colloidal systems and surfactant behaviour.⁵¹ These surfactants may also be used in the generation of micelles, which are themselves a colloidal system.

1.4.1 Formation of micelles

1.4.1.1 Interfaces and boundaries

An interface can be defined as a boundary between at least two immiscible phases.⁴⁹ In this area of chemistry the main concern with these multiphase systems is controlling and manipulating the phase boundary or the interfacial interactions. Molecules or materials exhibiting the ability to modify these interfacial interactions by means of greater adsorption at interfaces are collectively known as surface active agents or surfactants. Such surfactants cause solubilisation, a phenomenon whereby the solubility of solvophobic molecules is enhanced in a solvent medium.⁵² The aggregation of the amphiphiles results in the formation of microenvironments favourable to the solubilisation of these solvophobic molecules. Considering, on the one hand, that an aqueous environment containing aggregations of surfactants such as micelles, bilayers and vesicles may increase the solubility of poorly water-soluble hydrocarbons by many orders of magnitude, and on the other hand, in a similar way reverse micelles may promote the solubility of polar molecules such as water, amino acids

and proteins, in non-polar solvents.⁵² The molecules at the interface generally have properties different to that of their bulk material, and therefore have a definite free energy associated with each unit of the interfacial area.⁵³ Molecules at an interface usually have a higher potential energy than those within the bulk; this is due to the molecules at the interface experiencing a net force from neighbouring molecular interactions, which are significantly different to those from its own bulk.⁵³ When considering an interface, the central interfacial effects, which depend on the excess potential energy of surfaces, are capillarity and adsorption. Capillarity refers to any effect resulting from a tension at a liquid surface, and adsorption refers to adhesion of a solute by an interface. The process of adsorption results in the reduction of the surface free energy of the adsorbing surface and is a spontaneous process.⁵¹ Due to the amphiphilic nature of the surfactant molecules making up the micelle there is always an equilibration between the different forces of the solvent medium to find the most energetically favourable state. This need to find a state of maximum favourable interactions within the solvent environment results in surfactants spending most of their time at the interface between the two solvents.⁵⁴

1.4.1.2 Formation of micelles from surfactants

For the formation of normal micelles the amphiphiles are molecules made up of a hydrophilic head group and a hydrophobic tail region; due to this unique dual nature such molecules are able to interact with both polar and non-polar environments.⁵⁵ It is this amphiphilic character, coupled with the thermodynamic hydrophobic properties of the tails, that results in self-assembly of surfactants.⁵⁶ A reverse argument exists for where the head group is hydrophobic and the tail is hydrophilic. In this case, unfavourable interactions between tails and water can be minimized by aggregation of surfactants into micelles, resulting in the hydrophilic head surface region being exposed to water, and the hydrophobic tail region shielded at the core. In a process involving normal kinetic motion a surfactant molecule will make its way to the surface of the bulk solvent (e.g. water), thus the hydrophobic region of the amphiphile is no longer in contact with the water, and the energy disruption of the system is reduced (Figure 7). This phenomenon results in a congregation of surfactant molecules at the water surface. The length of the hydrophobic tail is also important. As the hydrophobic tail length increases the amphiphiles reduce the high surface tension of water;⁵⁵ this occurs because the longer the hydrophobic region of the molecule, the more energetically favourable it is to exclude the hydrocarbon portion from the bulk aqueous media. However, as the amphiphile concentration increases, and the interfaces become saturated, the system continues its efforts to minimise the free energy, and therefore, at a specific narrow concentration of amphiphile in solution, several amphiphiles will self-assemble into colloid-sized structures.⁵⁷ The formation of a

micelle from its respective surfactants is a stepwise process, which begins with a single surfactant monomer adding to the aggregation at a time.⁵³ Micelle aggregation can take various forms such as spherical and cylindrical micelles, bi-layer membranes, inverted hexagonal structures and inverted micelles; these formations are largely dependent on the hydrophilic region.⁵⁸ However, usually a micelle will have a nearly spherical shape, during the formation process the minimum free energy state within the system is reached.⁵⁵ As the amphiphile concentration increases, the free energy of the system rises due to the unfavourable interaction between the aqueous environment and the amphiphile hydrophobic region, in order to minimise the entropy of the system, these spherical micellar systems are formed.⁵⁷ These micelles then remain in the solvent system as thermodynamically stable, dispersed species with specific properties.

The lowest concentration at which spherical micelles form is termed the critical micelle concentration (CMC), and formation of micelles is characterized by a sharp discontinuity of bulk properties such as surface tension, conductivity, light scattering, self-diffusion and the molality of dissolved compounds.⁵⁵

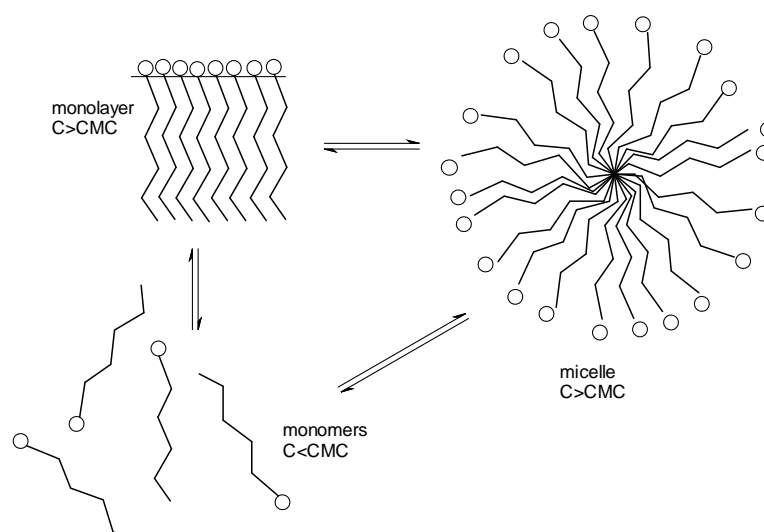
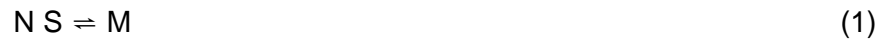


Figure 7: A surfactant can exist as different phases depending upon the concentration of the sample.

1.4.1.3 Thermodynamics of micellization

For simplicity, consider a case of a non-ionic surfactant, where⁵³ the association of N single molecules, S, forms a micelle M:



By the law of mass action we can write for the equilibrium constant K:

$$K = [M] / [S]^N \quad (2)$$

Representing the concentration of the monomer as C_s and that of the micelles as C_m but representing the concentration of surfactant in monomeric units:

$$K = C_m / C_s^N \quad (3)$$

where the total concentration of surfactant is given by $C = C_s + C_m$. The free energy of micellization is:

$$\begin{aligned} -\Delta G &= RT \ln K \\ &= RT \ln C_m - NRT \ln C_s \end{aligned} \quad (4)$$

or expressing the free energy as that required to insert one monomer unit into the micelle:

$$-\Delta G^\circ = -(\Delta G/N) = (RT/N) \ln C_m - RT \ln C_s \quad (5)$$

For many micellar units N will be to the order of 100, hence:

$$\Delta G^\circ \approx RT \ln C_s \quad (6)$$

Making the assumption that above CMC all additional surfactants added form new micelles, then the concentration of the monomeric material remains the same as the CMC value.

Therefore we have

$$C_s = [\text{CMC}] \quad (7)$$

and:

$$\Delta G^\circ = RT \ln[\text{CMC}] \quad (8)$$

Thus, if the critical micellar concentration, the CMC is known, the free energy of micellization is easily calculated.

1.4.2 Krafft temperature:

The Krafft temperature T_K is one of the physical properties of the micellar system that governs micelle formation. Even though most ionic surfactants have ample solubility in water, the extent of solubility is influenced by changes in the length of the hydrophobic tail, the nature of the head group, the valency of the counter ion and the bulk solution environment. At any temperature below T_K surfactant molecules will separate from the aqueous solvent. As surfactant concentration increases the monomer will crash out of solution rendering it ineffective for any intended purpose, while above T_K surfactants will be soluble regardless of concentration.⁵⁹ Generally, it is observed that the solubility of the surfactant material will undergo a sharp, distinct, discontinuous increase at a certain characteristic temperature, commonly referred to as the Krafft temperature, T_K .⁶⁰ The Krafft temperature is a narrow temperature range above which the solubility of a surfactant rises sharply; at this temperature the solubility of the surfactant becomes equal to the critical micelle concentration.⁶¹

$$T_K = k_c n - k_i \quad (9)$$

Equation 9 shows that T_K is related directly to the number of carbons in hydrocarbon chain (n), k_i is a constant depending on ionic head group and k_c is either 5.5 for both anionic and cationic surfactants with a single hydrocarbon chain and univalent counter-ion or 11 for divalent double chain surfactants.⁵⁹

1.5 Classification of micelles

1.5.1 Types of surfactants used in the generation of micelles

1.5.1.1 Amphiphilic block copolymers:

Amphiphilic block copolymers (Figure 8) have attracted much attention in recent decades, especially in the drug design and delivery field, in efforts to maximize and enhance therapeutic activity while minimizing negative side-effects.⁶² These self-assembled colloidal systems consist of copolymers that are formed by the polymerization of two monomers, one hydrophobic and one hydrophilic, commonly referred to as polymeric micelles.⁶³ Such systems typically are made up of biocompatible, biodegradable hydrophilic polymer blocks such as polyesters or poly(aminoacids) covalently bonded to a biocompatible hydrophilic polymer, a classic example being polyethylene glycol.^{57,62} The controlled architectures, narrow molecular weight distributions, and well-defined molecular weights are ideal for self-assembly into micelles. The polymeric micelles formed also have potential uses as nanoreactors, drug delivery devices and structure directive templates.⁶⁴

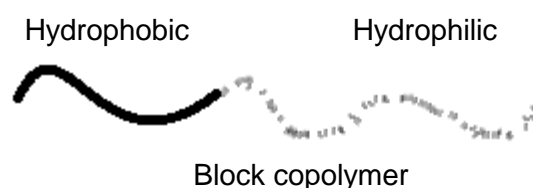


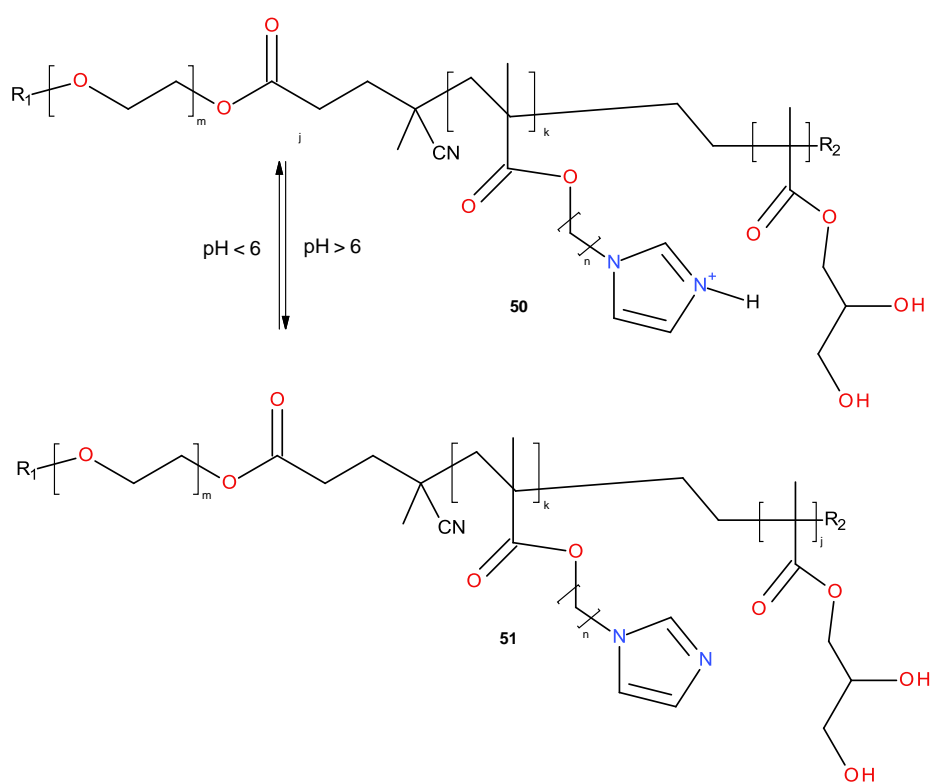
Figure 8: Block copolymer prior to self-assembly.

It is the combination of polymers that allows for such unique and useful properties. The hydrophobic core region assists in the solubilisation of hydrophobic drugs *via* non-covalent hydrogen bonding and hydrophobic interactions, while the hydrophilic surface is exposed to the external aqueous environment.⁶⁵ This design of drug encapsulation helps in protecting the bioactive agent against degradation and promotes prolonged systemic circulation.⁶³

One particular area in which polymeric micelles have proven to be invaluable is in the delivery of antibiotics. One particular study conducted by Radovic-Moreno *et al.*⁶⁶ concerned the development of antibacterial nanoparticles suitable for systemic administration, and the administration of drug-encapsulated, pH responsive, surface charge-switching poly(D,L-lactic-co-glycolic acid)-*b*-poly(L-histidine)-*b*-poly-(ethyleneglycol)(PLGA-PLH-PEG) nanoparticles as carriers for Vancomycin. This design allows the drug to remain unreactive at pH 7.4 and initiate drug release in an acidic environment characteristic of bacterial infections, and this is

accomplished by pH-sensitive nanoparticle surface charge switching where the imidazole groups of the PLH are protonated at low pH (Scheme 11)

Matini *et al.*⁶⁷ utilized a similar strategy in devising responsive materials to undergo conformational changes within a pH range. The purpose of the study was to devise a range of amphiphilic block co-polymers to form self-assembled systems to act as pH-responsive carriers for potential drug delivery applications. pH-sensitive polymers incorporating imidazole units were incorporated into the polymer backbone design to react between pH 5-8. The protonated **50** and unprotonated **51** forms are present at below and above pH 6 respectively. Association to form polymer nanoparticles happens with the uncharged **51**.



Scheme 11. Self-assembly of pH-responsive triblock co-polymers. Deprotonation of the central imidazole-containing blocks above a critical pH range causes self-association of hydrophobic components and formation of polymer nanoparticles.

1.5.1.2 Anionic surfactants

In anionic surfactants, the surface active portion of the surfactant holds a negative charge dissociation in water. These are ubiquitous within the field of micelle chemistry, with major subgroups within this class including alkali carboxylates, sulfates, sulfonates, and phosphates.⁶⁸

In recent years, emphasis has been on the production of anionic surfactants that are tuneable in some respect. For example, a surfactant derived from erucic acid **52** (Figure 9) has been shown to be highly responsive to changes in pH and temperature.⁶⁹ The erucic acid forms a hydrogel at low temperatures and high pH, and the combination of these two factors may be easily used to modify its macroscopic properties.

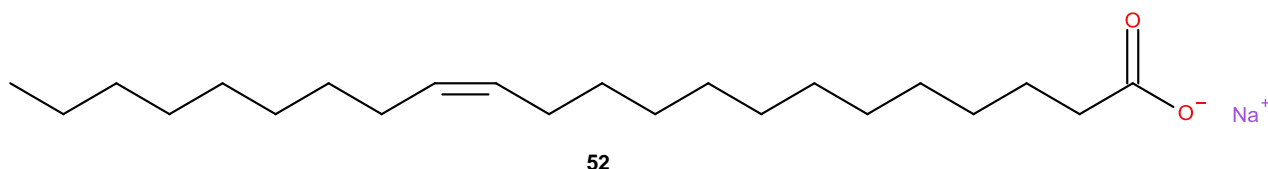


Figure 9. Erucic acid sodium salt, which acts as an anionic surfactant.

Anionic surfactants have gained interest also in the pharmaceutical field for the generation of drug delivery carriers. For example, an anionic surfactant based on 8-(dec-9-en-1-yloxy)octyl dihydrogen phosphate (PMES), **53** (Figure 10) was coupled with mesoporous silica nanoparticles (MSNs) forming a drug delivery carrier for resveratrol.⁷⁰

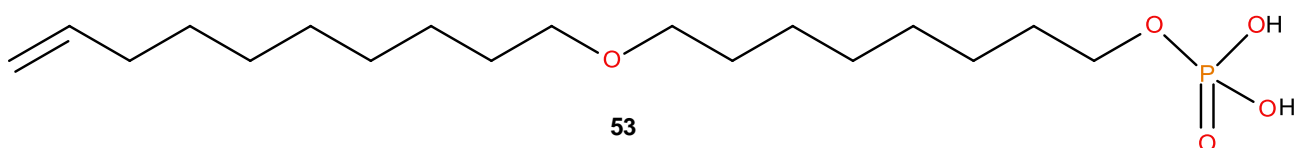


Figure 10. 8-(dec-9-en-1-yloxy)octyl dihydrogen phosphate (PMES) used in drug delivery.

This combination afforded effective and efficient intracellular release of resveratrol to the point where therapeutic efficiency in Chinese hamster ovary (CHO) cells was increased 13 times.⁷⁰

1.5.1.3 Cationic surfactants

In cationic surfactants, the surface active portion of the surfactant holds a positive charge when dissociated in water. These surfactants form micelles containing major subgroups of alkali carboxylates, sulfates, sulfonates, and phosphates. One such example is cetyltrimethylammonium bromide (CTAB) $C_{12}H_{25}N^+Me_3Br^-$, **54** (Figure 11) which has a plethora of uses. For example there is a recent study of the effect of the addition of CTAB on the morphology of thin films of semi-conductor zinc oxide.⁷¹

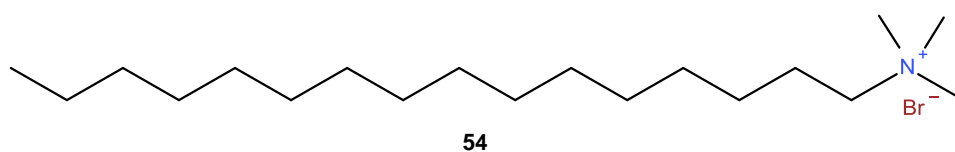


Figure 11. Cetyltrimethylammonium bromide.

It was noted that addition of the CTAB resulted in regular size and shape as well as uniform structure of crystallites on ZnO within the thin file, a significant property for the effectiveness of the film.

Furthermore, cationic surfactants have also proven their use in pharmaceuticals, forming part of drug delivery carriers. Cationic surfactants such as didodecyldimethylammonium bromide (DMAB), **55** (Figure 12) have been used along with poly(lactide-co-glycolide) (PLGA) in the formation of nanoparticles to deliver Paclitaxel.⁷²

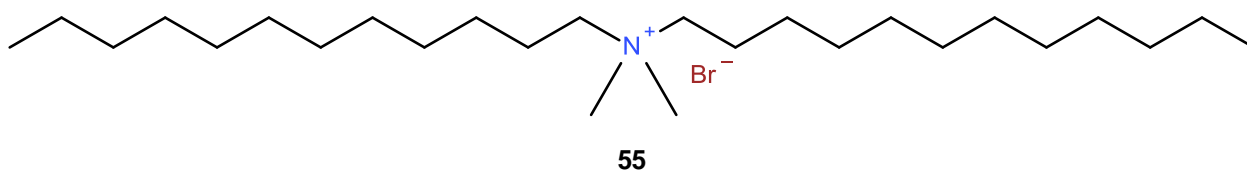


Figure 12. Didodecyldimethylammonium bromide used in drug delivery.

The choice of cationic or anionic surfactant in the generation of micelles for drug delivery will depend on several factors, including the nature of the drug being delivered and the biological environment at the target of the drug.⁷³

1.5.1.4 Non-ionic surfactants

Non-ionic surfactants typically are derivatives of ethylene oxide with a heteroatom, attached to an active hydrogen such as alkyl phenols, sugar esters, amine oxides and fatty amines.⁴⁹ Much attention in recent years has been focused on the use of non-ionic surfactants in oil recovery. A process of chemical flooding (using the non-ionic surfactant) is a technique most commonly used to enhance oil recovery. A microemulsion is able to mobilize the remaining oil by reducing the interfacial tension between the oil and water. Conventionally *n*-octane is used as the oil phase, while triglyceride microemulsions derived from pine oil are now increasingly used.⁷⁴

1.5.1.5 Zwitterionic surfactants

In this type of surfactant, the surface active portion of the surfactant contains both positive and negative charges. This gives differing properties to the aggregation compared with the other types of surfactants. Zwitterionic surfactants have a variety of uses, for example in biosensors. Peroxidases are vital heme enzymes that catalyse the oxidation of a number of electron donors using H₂O₂ as the electron acceptor. Surfactants such as 3-(1-tetradecyl-3-imidazolio)propanesulfonate (ImS3-14), **56** (Figure 13) may be used to disperse gold nanoparticles for the creation of a biocompatible environment for enzyme immobilization.⁷⁵

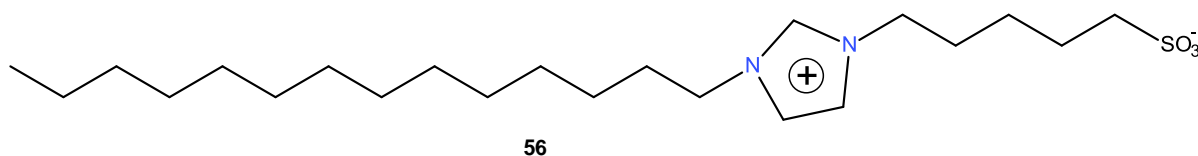
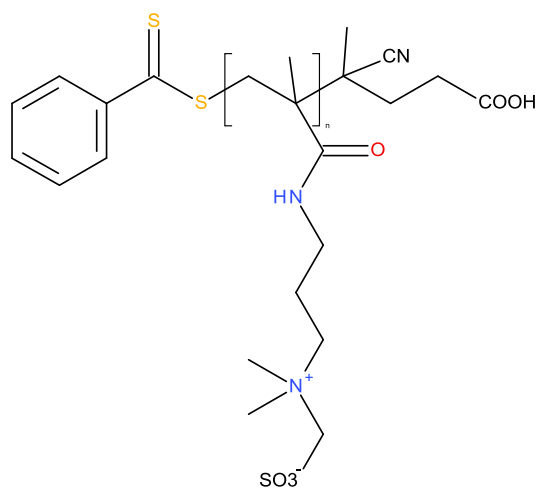


Figure 13. Zwitterionic surfactant used in drug delivery.

Recently, Geagea *et al.*⁷⁶ developed a new label for electrochemical biosensors involving the development of silver nanoparticles coated with a both zwitterionic and biotinylated zwitterionic polymers. The silver is prone to electrochemical oxidation, contributing to signal enhancement as the zwitterionic polymers grafted onto the silver surface provide stability. The presence of the carboxylic acid at the polymer terminal, **57** (Figure 14) allows for versatility and further biofunctionalization with a range of bioreceptors.



57

Figure 14. Zwitterionic polymer synthesized by reverse addition fragmentation chain transfer polymerization of *N,N*-dimethyl-(methacrylamido-propyl)ammonium propanesulfonate.

1.5.2 Shape and size

Considering the formation of micelles, if the only influencing factor was the aggregation of surfactant molecules, the micelle size would grow infinitely to form bilayer type structures. This does not happen as repulsive forces limit the micelle size and attractive forces supporting micelle growth. The electrostatic and steric interactions between the polar head groups give rise to these repulsive forces.⁵⁷ With ionic amphiphiles, the polar head of each surfactant molecule is charged, and it repels the neighbouring amphiphiles in a micelle resulting in the micelle head groups being pushed apart. This electrostatic repulsion results in a curved surface, causing a spherical shape, with the radius governed by the alkyl chain length as the head groups are further apart compared to the tail portion. However, if the neighbouring head group is pushed too far away, solvent molecules will enter the interior of the micelle increasing the free energy of the structure, which is known as the hydrophobic effect. A balance between the opposing forces within the structure then determines the optimum shape of the micelle. The size of the micelle is then a combination of the area occupied per alkyl chain and the total surface area, which is determined by the spacing of the head groups at the micelle surface.

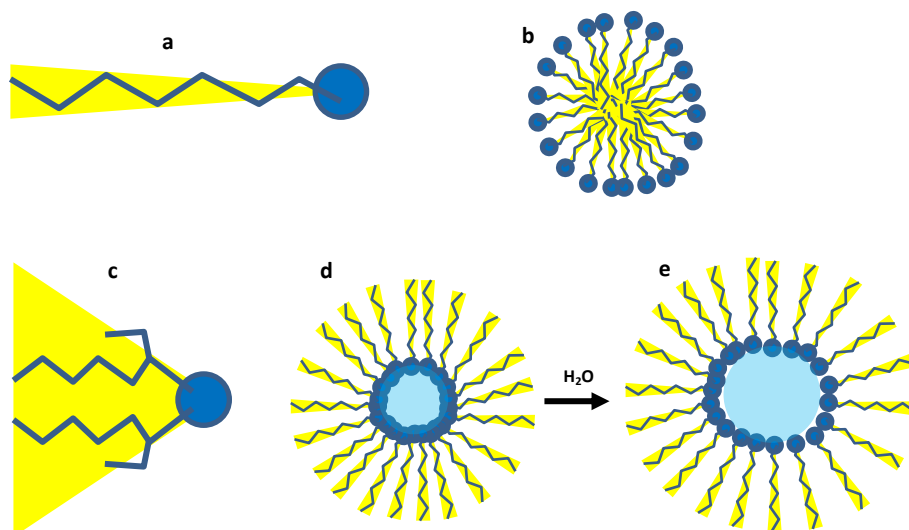


Figure 15. The various types and shapes of micelles able to form.⁷⁷

The size and shape of a micelle is largely dependent on both the constitution and the length of the surfactant molecule. If the amphiphile has a large polar head group and small hydrophobic chain (Figure 15 a), then the molecules will tend to aggregate into the structure of a normal micelle, where the chains form the inner micellar core and the polar head groups form the outer surface (Figure 15 b). The entire colloidal system is dynamic and the surfactant molecules involved in the formation of the original micelle are able to move freely and are thus continuously in exchange with other surfactant molecules in the aqueous bulk phase. The overall spherical micelle structure is maintained as it takes a timescale of microseconds for all of the surfactant molecules of the micelle to be replaced by others.⁷⁷ If the surfactant has a small polar head group and branched hydrocarbon chain (Figure 15 c), a spherical reverse micelle is possible (with appropriate solvent) where the head groups form the inner micelle core and the chains make up the outer surface (Figure 15 d). This type of micelle is more commonly referred to as a water-in-oil droplet⁵⁷ and water is free to diffuse into the core of this type of micelle (Figure 15 e). Considering normal micelles, the positioning of solutes is dependent on its hydrophobicity, concentration and nature of the surfactant. Counter-ion species oppositely charged to that of the headgroups of the micelle will bind tightly to such groups *via* coulombic attraction.⁷⁸ Non-polar species possessing delocalized electrons (e.g. aromatics) could also find their way to the polar head-groups rather than remaining within the micellar core.

1.5.3 Packing factor

The formation and self-assembly of amphiphilic systems is not only governed by thermodynamic considerations (as mentioned earlier in 1.4.2), but also by geometrical influences. The type of structure formed by aggregation of surfactants is largely determined by its packing factor, i.e. the ratio of the volume of the hydrophobic tail, v , to the length of this tail, l , multiplied by the effective surface area per head group, a .⁷⁹

The packing factor, equation 10:

$$p = \frac{v}{al} \quad (10)$$

The values that p holds is directly related to the shapes of the micelles formed (Table 1 and Figure 16).

Table 1. Packing factor parameters governing shape of aggregation.

Shape	Minimum value for p	Maximum value for p
Spherical	0.000	0.333
Globular	0.333	0.406
Worm-like	0.406	0.500
Vesicles	0.500	1.000

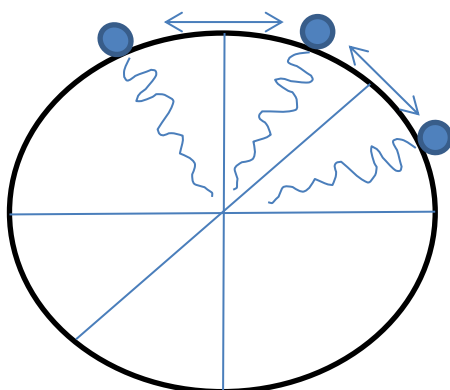


Figure 16. Schematic of head group forces governing micelle packing factor.

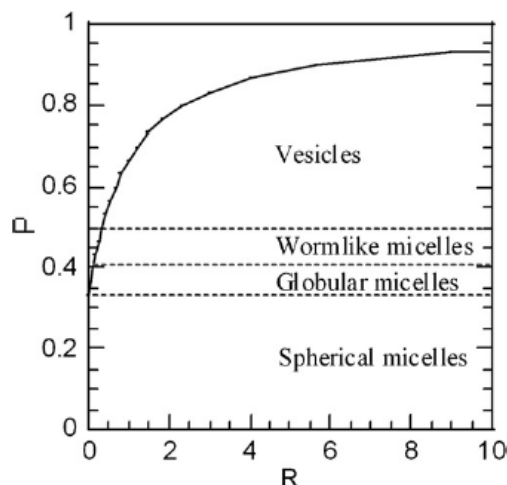


Figure 17. Graph showing average packing factor P plotted against R , lipid/detergent molar ratio.⁷⁹

The graph relating the lipid/detergent ratio to packing factor (Figure 17) indicates the flexibility available in pre-determining a proposed packing factor given various surfactants to aid in designing systems with specified requirements.⁷⁹

1.5.4 Use of micelles in catalysis

In describing the various surfactants, several uses of micelles were alluded to. In this section, we explore more generally the uses of and, later on, design modifications in the surfactants that may be introduced to improve physical and chemical properties of the micelles.

1.6 Forces driving development of micellar catalysts

Historically, synthetic reactions have been judged mainly by efficiency and stereoselectivity. However, as we move into the era of green chemistry other aspects such as safety and environmental sustainability are gaining importance when choosing reaction criteria. It is now essential to make sure reactions are optimized in terms of reagent usage, recycled catalysts and the use of eco-friendly reaction media. In this context, water seems the most advantageous, although water comes with various difficulties, particularly poor solubility of non-polar organic reagents. This problem may be overcome with micellar reaction environments along with their ability for micellar catalysis.⁸⁰

1.6.1 Micro-emulsions and micellar catalysis

Microheterogeneous micellar systems have great potential in terms of the non-conventional environments they present. Microemulsions are dispersions of two immiscible liquids made

with a surfactant. Essentially such systems are small-scale versions of macro-emulsions, with a droplet size approximately 100 Å, about 100 times smaller than a typical emulsion droplet size. The science that can occur within these solutions is not seen in homogeneous solutions and the majority of studies conducted on these micro emulsions employ water as the polar component with most experiments making use of a standard anionic surfactant Aerosol-OT (AOT) (sodium di-ethylhexylsulfosuccinate).⁸¹ However, researchers have studied waterless microemulsions where the aqueous water polar phase is replaced by polar solvents that possess relatively high dielectric constants; these non-aqueous microemulsions have attracted interest from a fundamental and a practical perspective, in the potential diversifying properties and uses of these systems.⁸¹

Catalysis will always play an essential role in overcoming the energy barrier of many reactions, and recently the catalytic properties of enzymes have proved particularly useful, due to the unique properties they exhibit as a result of their complex molecular structures.⁸² Enzymes have the ability to perform with high selectivity and under mild reaction conditions, hence various methods have been devised to enhance the kinetics of enzyme reactions.⁸³ One of these methods includes the use of micellar systems and microemulsions to improve catalytic reactions. Micellar conditions have been shown to increase the activity of some enzymes compared to reference buffered solutions.⁸⁴ In this case, reverse micelles are usually used due to their water core where biological molecules such as enzymes can be solubilized and protected, preserving the enzyme's activity.

1.6.2 Physical uses of microemulsions

Oil-in-water (o/w) and water-in-oil (w/o) microemulsions can be viewed by scientists as mobile, tailored-to-size microreactors where guest molecules can be introduced to perform reactions. Surfactants have proven their worth and practicality in a variety of fields, one of them being in the oil industry particularly in Enhanced Oil Recovery (EOR) processes. After primary and secondary production from a reservoir, up to 70% of the original oil remains on the reservoir rock.⁸⁵ Hence developing economically feasible methods of tertiary recovery has been a priority of petroleum engineers to increase overall oil recovery. With continually increasing oil prices research into EOR has gathered remarkable interest, particularly the exploration of surfactant processes.⁸⁶ A process known as surfactant flooding is employed where a slug of surfactant solution, made up as micro-emulsion, is injected into the reservoir from injection wells specifically spatially arranged. The residual oil is then swept towards production wells along with the slug by a further injection of water.⁸⁵

Apart from their use as microreactors, a field emerging from such systems of particular interest to chemists is that of microheterogeneous catalysis.

1.6.3 Microheterogeneous catalysis

Microheterogeneous catalysis may offer advantages when compared to other types of catalysis, its foremost feature being its versatility. For example, systems made up of surfactants exposed to an external stimulus (such as light, pH variation, etc.) may experience a major change in the nature of the catalytic effect, thus fatty acid soaps aggregate into micelles in a high pH buffer, while a decrease in the pH of the environment leads to micelles transforming into bilayer vesicles.⁸⁷

Normal and reverse micelles have attracted a lot of attention because a wide range of reactions such as oxidation, hydroformylation, carbonylation, dehalogenation, free radical polymerization, enzymatic reactions, ligand substitution reactions, electron transfer reactions, etc., can be studied within them.⁸⁷ Such systems are sometimes preferred as it provides the option of localization of reactants within these microenvironments, enabling catalysing and control of such reactions. Microemulsions may be used to induce regioselectivity for organic reactions, and some microheterogeneous systems may be able to mimic important characteristics of biological systems.⁸⁷

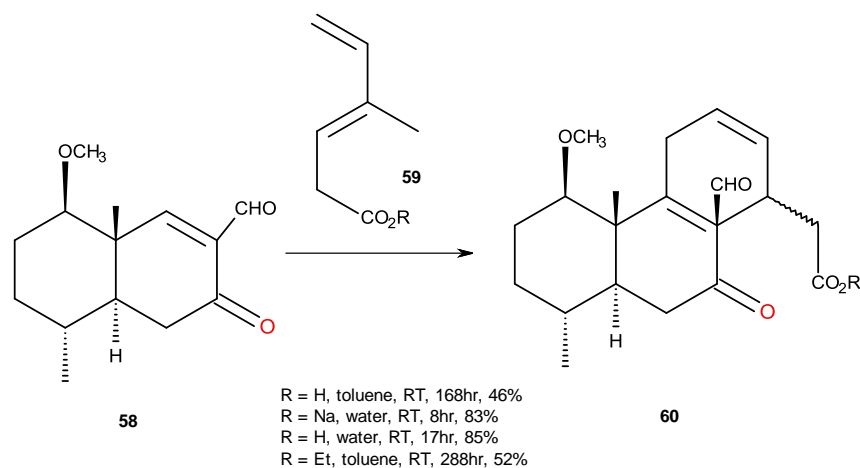
Systems with mimetic ability can divide into self-assembled systems (normal and reverse micelles, microemulsions, vesicles, and liquid crystals), supramolecular hosts (macrocyclic polyethers such as crown ethers, coronands, cryptands and podands, cyclodextrins) and amphiphilic polymers. These systems are broadly termed microheterogeneous systems, because of their colloidal dimensions despite large numbers of molecules per system.⁷⁸

1.7 Chiral micelles in organic synthesis

Chirality of supramolecular systems are of particular interest to chemists, not only due to their essential role in life and material sciences,⁶⁴ but also due to the identified potential of these systems in asymmetric synthesis. The chiral influence of the supramolecular structures, which is usually attained *via* non-covalent interactions, presents opportunities for various applications such as asymmetric catalysis and asymmetric auto-catalysis, nonlinear optics,⁶⁴ molecular recognition and self-assembly, and in molecular device design. Such systems may also be useful tools for the determination of the absolute configuration of chiral compounds.⁶⁴ Chiral micellar media offer a cleaner reaction medium than the traditional methods, and they

provide advantages such as solubilisation of reagents as well as concentration and pre-orientation of reactants.⁸⁸ The spark of interest around chirality stems predominantly (as mentioned earlier) from the fact that many drugs are only active as a certain enantiomer, and syntheses need to ensure the production of this correct enantiomer. As per the 1992 Federal Food and Drug Administration mandate, producers of pharmaceuticals evaluate the effects of individual enantiomers separately and verify the enantiomeric purity of chiral drugs.⁸⁹

For the purposes of asymmetric synthesis, a focus of this study is on the effects of chiral surfactants on regular organic reactions from a stereochemical viewpoint. This follows progress in the literature on the application of chiral surfactants for enantioselective synthesis. For example, Goldberg *et al.*⁹⁰ made use of chiral surfactants during the reduction of ketones to form chiral alcohols, with enantiomeric excess of less than 2%, followed by Zhang *et al.*⁹¹ using a surfactant based on menthylamine in organic reductions, resulting in enantioselectivities up to 17%. Hailes *et al.*,⁹² have also managed to synthesize chiral quaternary ammonium chloride surfactants based on (*S*)-leucinol, and the produced micellar structures have shown to significantly influence the outcome of Diels-Alder cycloadditions.⁹³ The Diels-Alder reaction is one of great importance in organic synthesis as it is a key step in many reactions, yielding compounds of six-membered rings, and this has been the focus of several studies involving micelles. In 1983 Grieco *et al.*,⁹⁴ conducted preliminary investigations of Diels-Alder reactions of the vinyl ketone, **58** with the diene, **59** producing the adduct **60**, carried out in aqueous media that was determined to be micellar (Scheme 12).⁸⁸



Scheme 12. Micelle mediated Diels-Alder processes.

This study of the intermolecular Diels-Alder reaction showed moderate yields when carried out in toluene, yet a definite improvement in yields for water as a solvent. The sodium salt of the diene was used and it was deduced that this contributed to the further acceleration of the reaction. Grieco determined that this acceleration was caused by the aggregation of the diene molecule in a micellar manner solubilising the dienophile.⁸⁸

As the Diels-Alder reaction is a [4+2] cycloaddition where a diene and a dienophile react to produce a six-membered ring,⁹⁵ the cycloaddition allows for the formation of four new stereocentres in a single reaction step. During the reaction, the approach of the double bonds is crucial for successful movement of electron pairs between molecular orbitals, hence the reaction is stereospecific and therefore the absolute configuration of the newly formed asymmetric centres can be controlled (Figure 18).

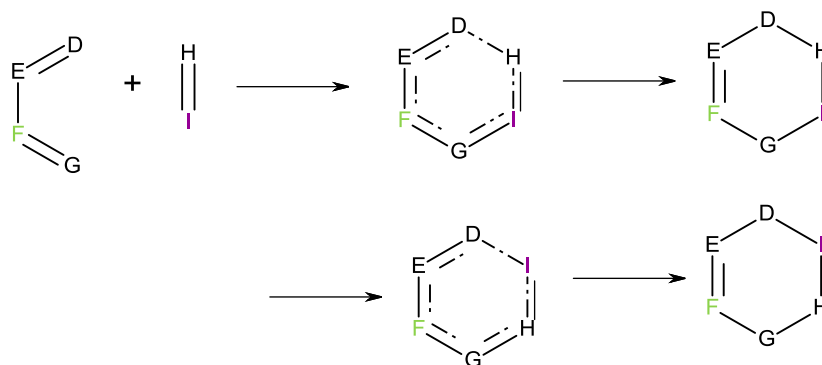


Figure 18. A schematic representation of a Diels-Alder reaction, showing the adaptability of the reaction shown by the fact that heteroatoms are allowed in any positions of a-f. Products (a) and (b) are two regioisomeric products.⁹⁵

The Diels-Alder reaction is a textbook example of a reaction in which the outcome is indifferent towards choice of solvent and solvent effects. During investigations to increase rate and stereoselectivity of Diels-Alder reactions it was determined that the most effective changes were observed upon introduction of a Lewis acid.⁹⁵

Diels-Alder reactions are great candidates for a two-solvent micellar system, as these ring forming reactions can be effectively conducted in an aqueous reaction medium where rates of reaction are significantly higher compared to those performed in organic solvents.⁹⁴ Various methods to enhance reaction rates have been employed, such as ionic liquids used as solvent instead of water, and thus far the most effective is the addition of Lewis acids, acting as catalysts into the aqueous media.⁹⁶ Diego-Castro and Hailes⁹⁷ undertook a study to investigate the performance of Diels-Alder reactions using chiral micellar media. A (*S*)-leucine-derived surfactant, **61** (Figure 19) was the chiral source used to catalyse a reaction between cyclopentadiene and nonyl acrylate. In the presence of the chiral surfactant, chiral induction was only observed in the *endo*-species and was minimal in the *exo*-form.

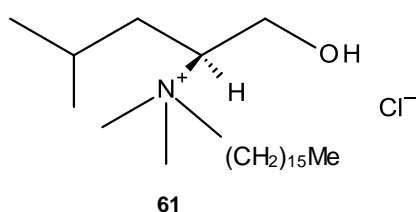


Figure 19. (*S*)-Leucine-derived surfactant.

Considering the effect of the addition of cyclopentadiene to nonyl acrylate in water containing the surfactant, good yields were observed, while enantioselectivities were poor. These observations mirror those seen during the micellar catalysis attempts of Rispen and Engberts,⁹⁴ where a rationalization of these results draws attention to the importance of the ideal positioning of the reaction reagents relative to the surfactant catalytic centre.

1.8 Solvent chirality

Supramolecular chirality is a phenomenon which arises from the non-symmetrical spatial arrangement of a system's components where assemblies are due to noncovalent interactions,⁹¹ and this chirality is dependent on both the chirality of the molecular constituents and the manner of their assembly. Therefore, through non-covalent bonds either chiral or achiral molecules can be assembled into chiral microstructures. An important point to consider when dealing with large assembly systems is how the chirality at the supramolecular level relates to the chirality at a molecular level. Once such chiral microenvironments are formed, they may behave differently to the individual chiral component molecules. In some cases, it is possible to regulate and control these environments *via* external conditions such as pH, temperature and solvents.⁹¹ Functions that individual chiral molecules could not previously perform may be possible under the varied conditions.⁹¹

In the case of dual-solvent micellar systems, the polar and non-polar solvents are usually water and an organic solvent; this organic solvent is generally an achiral, long chain hydrocarbon. As a focus within this research is the generation of chiral reaction environments within these supramolecular systems, this study will address how placing a chiral molecule (surfactant) amidst the environment of an achiral solvent (hexane) will induce chirality, and in turn cause solvent chirality resulting in an asymmetric reaction environment. Transfer of chirality will occur within a certain proximity to the chiral molecule, which may be referred to as the 'chiral zone'.³⁹

Consider two optically inactive but chirally-metastable molecules and possible solvents, gauche *n*-butane and cyclohexane.⁹⁸ These molecules may be considered to be achiral molecules, for example, *n*-butane has three rotational isomers, a pair of gauche enantiomers and one *trans* form. Likewise, cyclohexane has two conformational achiral enantiomers and an enantiomeric pair of twist boat conformations.⁹⁸ However, , no detectable optical activity can be observed in either due to their dynamic behaviour, small population and ultra-short lifetime in the thermally excited states.⁹⁸

Chiral molecules or species that can be detected chiroptically may be classified into two parts depending on how chirality is induced, whether due to intra- or inter-molecular processes. The intra-molecular route is attributed to stereogenic centres within the species itself.⁹⁸ This can be considered to be a direct chiral induction bias. However, inter-molecular chirality arises from external influences acting upon the molecule. These influences are considered to be indirect, and much weaker chiral induction biases.⁹⁸ When looking at these inter-molecular influences, one must look at the system in terms of how a target chiral molecule interacts in a liquid state.⁹⁸ Separately, four distinct solvent-molecule influences must be considered:

- A chiral molecule is surrounded by solvent molecules
- An achiral molecule is surrounded by chiral solvent molecules
- A chiral molecule is surrounded by chiral solvent molecules
- An achiral molecule is surrounded by achiral solvent molecules

Such indirect influences are generally very small in magnitude, but the extent of these biases may be amplified by solvent quality. Chiroptical properties in the ground state and photoexcited states of optically inactive molecules, supramolecular structures and polymers are affected greatly by the surrounding molecules through non-covalent interactions between chiral and solvent molecules⁹⁸.

When considering a system such as a solvent where all molecules are the same yet there is an induced chirality, there is a need internally to rank the molecules by degree (amount) of chirality as illustrated in Figure 20.⁹⁹

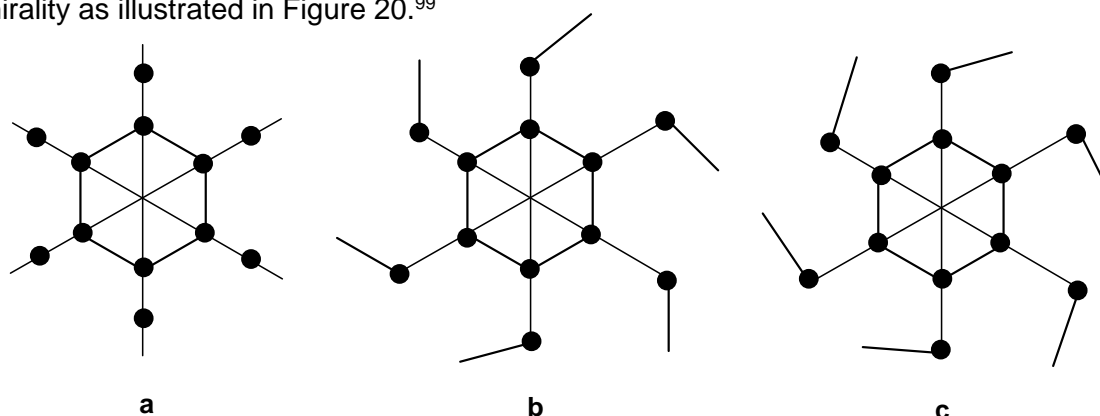


Figure 20. Three geometries of the same molecules to be ranked in terms of degree of chirality (a) achiral, (b) chiral and (c) 'more' chiral.

Due to the fact that there can be various versions of a chiral structure there is a need to define two means to measure chirality.⁹⁹ If we informally and arbitrarily assign the terms right-handed (R) and left-handed (L) to systems with opposite chirality, then:

- A degree of chirality: is a scalar function Ψ that disappears if a system is achiral and has equal value for the system and its mirror image: $\Psi(R) = \Psi(L)$.
- A chirality index: is a pseudo-scalar function X that disappears if a system is achiral and has equal and opposite values of the system and its mirror image: $X(R) = -X(L)$.

Considering a simple illustration Figure 21,⁹⁹ any system in continuous motion will interconvert between the (R) and (L) configurations and by that must pass through an achiral configuration, at which point a switch in sign of the chirality index occurs, passing through zero.

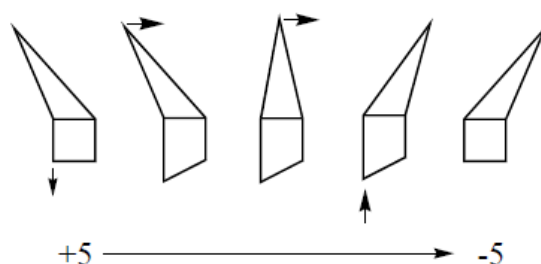


Figure 21. The dependence of chiral index upon structure.

1.9 Characterization of micellar systems (chiral and achiral)

1.9.1 Small angle scattering (SAS)

Small angle scattering is based on the scattering of radiation (x-rays, neutrons, light) from such particles.¹⁰⁰ Colloidal particles are too small to be seen under microscopic conditions, however, when a beam of light is passed through a system containing certain molecules larger than the surrounding bulk molecules, then the light is scattered. SAS can be used to study systems with a structural length scale ranging between 10-1000 Å.¹⁰¹ The technique is particularly used in the analysis of shapes and sizes of particles dispersed in a homogeneous medium, with particular interest in macromolecules such as biological molecules, polymers and micelles in a solvent.¹⁰¹ Different length scales of molecules can be investigated, depending on the wavelength of radiation used. Synchrotron and neutron sources coupled with sensitive detectors and CCD cameras have made this technique one of the best in the analysis of dispersed systems in solution.¹⁰⁰

SAS encompasses two complementary techniques, Small Angle X-ray Scattering (SAXS), and Small Angle Neutron Scattering (SANS). For example, we look at SANS (Figure 22). SANS is a diffraction experiment where a monochromatic beam of neutrons is directed at a sample, and in turn the neutrons are scattered by nuclear interactions within the sample.

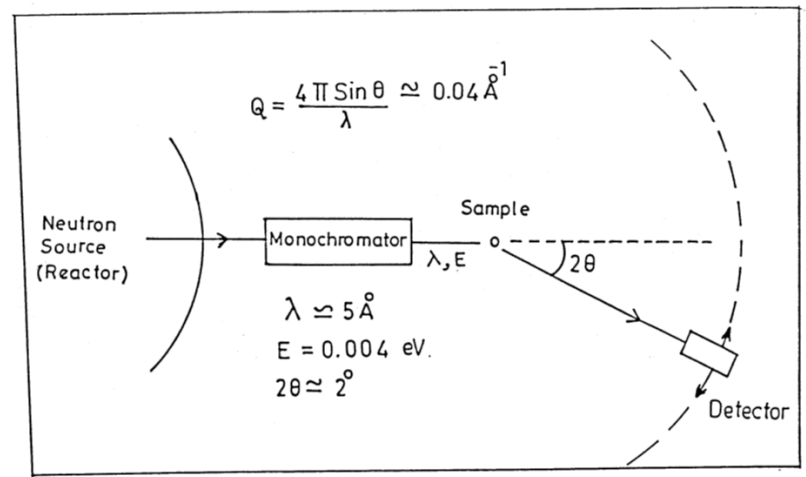


Figure 22. Schematic details of SANS experiment.¹⁰¹

The wave vector transfer Q is calculated according to Equation 11:

$$Q = 4\pi \sin \theta / \lambda \quad (11)$$

Where λ is the incident neutron wavelength and 2θ is the scattering angle. In these experiments, Q is usually small, ranging from 0.001 to 1.0 \AA^{-1} and the wavelength of neutrons is typically 4 to 10 \AA . The smallest Q values occur at small scattering angles ($\sim 1^\circ$), which is why the technique is called small angle neutron scattering.¹⁰⁰

During a SANS experiment, the coherent differential scattering cross section ($d\Sigma/d\Omega$) is measured as a function of wave vector transfer Q . For a system of mono-dispersed particles, equation 12 holds:

$$(d\Sigma/d\Omega) (Q) = n (\rho_p - \rho_s)^2 V^2 P(Q) S(Q) \quad (12)$$

where:

- n is the number density of particles, ρ_p and ρ_s , are respectively, the scattering length densities of the particle and the solvent.
- V is the volume of the particle.
- $P(Q)$ is the intraparticle structure factor, dependent upon the shape and size of the particle.
- $S(Q)$ is the interparticle structure factor, dependent upon the spatial arrangement of particles and is therefore sensitive to the interparticle interactions.

Scattered neutron intensity in the SANS experiment depends on $(\rho_p - \rho_s)^2$, the square of the difference between the average scattering length density of the particle and the average scattering length density of the solvent.¹⁰⁰

Recent kinetic studies by Jensen *et al.*,¹⁰² on the well-known sodium dodecyl sulfate (SDS) surfactant in aqueous sodium chloride (NaCl) were conducted using SAXS. Even though SDS techniques have been extensively studied and used in structure determination. The study of SDS behaviour under various conditions as well as computer simulation studies have been conducted.¹⁰³⁻¹⁰⁵ Due to the fast-moving nature of surfactants, time-resolved SAS and SAXS were employed to look closely into the evolution of surfactants within orders of milliseconds. This particular study utilized the SAXS technique to follow the transition of surfactant molecules from individual globular micelles to worm-like elongated micelles. SDS is an anionic surfactant and has a negative head group charge causing electrostatic repulsion between neighbouring charged head groups resulting in a larger outer radius, and therefore larger micelles. During the course of the study, the ionic strength of the solvent was increased by the addition of NaCl, causing the effective head-group area to decrease and the surfactants to then rearrange into a worm-like cylindrical aggregation as seen in Figure 23.¹⁰²

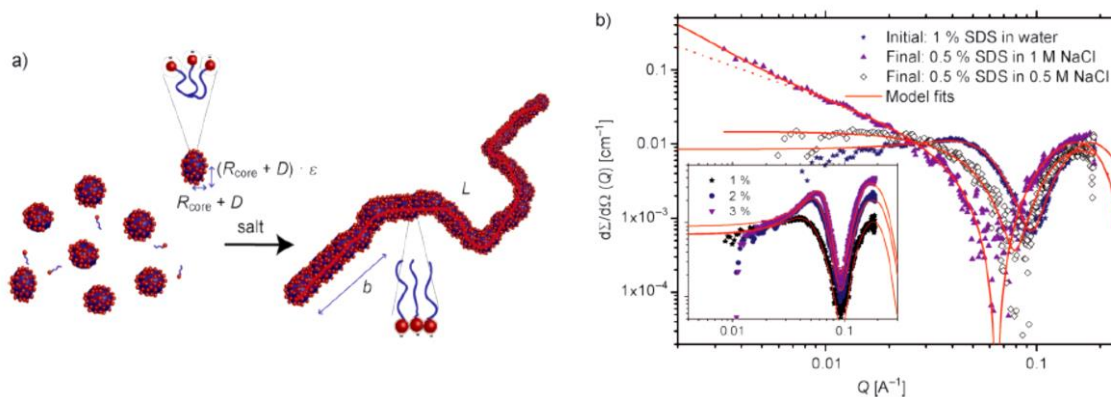


Figure 23. a) Systematic representation of the transformation of surfactants from spherical geometry to cylindrical micelles. b) SAXS data representing the absolute scattering intensity vs. the modulus of the scattering momentum (Q) starting from the original SDS in water solution through to the increasing ionic strength (*used with permission*).¹⁰²

1.9.2 Nuclear magnetic resonance (NMR)

Nuclear magnetic resonance (NMR) spectroscopy is a common technique in organic chemistry used to acquire information about molecular dynamics and structure through weak interactions of nuclear spins within the molecular environment.¹⁰⁶ NMR spectroscopy is frequently used to characterize surface and colloidal systems. A structure formed through aggregation is often much larger than its constituent molecules and therefore moves at a much slower rate. Regular organic molecules travel with speeds of approximately 10^{-12} s and may be characterized from chemical shift and spin-spin coupling, compared to aggregated systems which move on average between 10^{-9} – 10^{-10} s where different spin interactions such as dipole-dipole, quadrupole coupling and chemical anisotropy must be considered.¹⁰⁶ Apart from structural studies, NMR spectroscopy can be particularly useful due to the unique nature of amphiphiles, as it is important to study the molecular motion related to the aggregated system from a kinetics and thermodynamic perspective on a microscopic scale. One area of particular interest pertains to the rearrangement of colloidal systems in response to a change in chemical environment. ^1H NMR techniques allow one to directly follow the shape transformations which these aggregates undergo with, for example ^1H NMR and NMR self-diffusion experiments respond to alterations in the chemical environments of surfactants, providing information on micelle shape changes.¹⁰⁷

Lu *et al.*¹⁰⁸ conducted an NMR study investigating the effect of increasing ionic strength of three types of well-known surfactants; TX-100 (non-ionic surfactant), sodium dodecyl benzene sulfonate (SDBS, anionic surfactant) and tetradecyl trimethyl ammonium bromide (TTAB,

cationic surfactant), as well as the influence of room temperature and pressure. The experiments were conducted under aqueous conditions in D₂O with a small pulse angle of 30° instead of the conventional 90° sequence to ensure complete recovery of longitudinal magnetization. NMR techniques were successfully used to investigate micelle transformation of the three surfactants. Notably, chemical shifts of protons near the head group changed faster compared to protons further down the long hydrophobic chains, indicating that spherical micelles are likely to undergo a shape change from spherical to ellipsoidal or rod-like. The technique gave consistent results over the three types of surfactants with all suggesting a multi-step complicated transformation processes.

1.9.3 Molecular modelling

There has undoubtedly been a steady, rapid increase in the computing power available to computational chemists. Therefore, increasingly complex molecular systems may be simulated for longer periods. Hence, in recent decades computational chemistry has become a field of growing popularity and interest amongst theoretical and experimental chemists. Within this field, chemists now have the ability to resolve experimental problems *via* computational means. Scientist may construct and compute a real world model of both measurable and immeasurable properties and compare these results with those obtained experimentally.

1.9.4 Molecular dynamics

The tool of molecular dynamics (MD) solves Newton's equations of motion for a given molecular system, and provides trajectories for atoms present within the system boundaries; from these trajectories, multiple properties may be calculated.¹⁰⁹ The intention of such computer simulations is to compute macroscopic behaviour from microscopic interactions. The primary considerations of microscopic aspects are:¹¹⁰

- The understanding and interpretation of experimental results.
- Semi-quantitative estimates of experimental results.
- The capability to interpolate or extrapolate experimental data into regions that are difficult to access within a laboratory.

The study of chemistry entails the investigation of atomistic properties of molecular systems, and therein lies the basic challenge in the concept of computational chemistry. To describe or predict:¹¹⁰

- The structure and stability of a molecular system.
- The free energy of different states of a molecular system.
- Reaction processes within molecular systems in terms of interactions at an atomic level.

Considering these challenges, the first addresses the topic of which state of a system has the lowest energy. Taken further one begins to deal with the prediction of the relative free energy of different states, and lastly the prediction of the dynamic process involving the change of states.

Computational chemistry has been an asset applied to the study of the structure and thermodynamics of micelles. Simulations may be divided into two categories; in the first micelles of a certain size and shape are assumed to exist and the simulations investigate their structure and short time dynamics. The second method studies the process of spontaneous micelle formation.

The experimental work conducted on micelle systems investigates of aggregate shape and its fluctuations, chain conformations, penetration of water into the core, extent of counter ion coupling with respective headgroups, and behaviour of solutes.¹⁰⁹ Even with the growing interest in computational chemistry, simulations and dynamics studies of micelles have not progressed very far. One of the proposed reasons for this lack of progress is that it may not be possible to simulate the actual self-assembly of micelles in realistic models; therefore before a simulation can be set up, one must first specify the size of the proposed micelle for study.¹⁰⁹ Under experimental conditions aggregates have a wide range of sizes and may have varying shapes that could influence individual micelle properties.

With the current accessible means to experimentally and theoretically analyse and examine micellar systems and surfactants including NMR, EPR, light scattering, small angle neutron scattering, Monte Carlo simulations and molecular dynamics (MD) simulations,¹¹¹ coupling of both experimental and computation techniques provides insight into properties such as hydrogen bonding, diffusion, re-orientation with response to stimuli, shape and size changes.¹¹¹ With progress and greater computing power, increasingly complex systems such as large micellar systems can now be examined. In general, two approaches are employed when modelling micelle systems: full micelles where surfactants, counter ions and solvent molecules are simulated, and constrained micelles in which the system components are not specified, but rather an external spherical potential is implied.

Molecular dynamics simulations have been successfully used to resolve and examine the structure of spherical micelles and their interactions with solvent.¹¹² These simulations generally involved 10-20 surfactants with up to 1000 water molecules, run for a few hundred picoseconds.¹¹² However under these time conditions, dynamic properties of micelles become difficult and almost impossible to study as residence times of individual surfactants in the micelle is usually $10^{-5} - 10^{-6}$ s, whereas micelle lifetimes last between $10^{-3} - 10^{-1}$ s.⁹⁵

Realistic model simulation is limited to a few nanoseconds, whereas the crucial aspects of micellar solutions such as surfactant exchange, micellar formation and break-up can occur on a millisecond timescale.¹⁰⁹ Examples of earlier studies include those performed using sodium octanoate whose surfactants contains 10 heavy atoms and micelles, made up of approximately 15 monomers. The numbers of atoms making up this system was more manageable computationally.¹¹¹

Molecular modelling and simulation studies tend to encounter similar problems (Table 2), that is, how to efficiently scan a vast space to determine all possible molecular conformations, to depict the system itself at a global energy minimum in thermal equilibrium, as well as the basic problem of obtaining a sufficiently accurate energy function of the force field for all molecules involved in making up the system of interest.

Table 2. Various classifications of molecular systems; the shaded area is amenable to computer simulation application.

	Crystalline Solid State	Liquid State Macromolecules	Gas Phase
Quantum Mechanics	Possible	Impossible	Possible
Classical Statistical Mechanics	Easy	Computer simulation	Trivial

The computational work required to effectively handle long-range electrostatic forces of larger ionic surfactants has been the main reason for the lack of advancement of larger and longer simulation and molecular dynamics studies. When considering micellar solutions, conditions have to be set up such that there are no interactions between the periodic images; this requirement thus results in very large systems.¹¹¹

In the current study the various assumptions, approximations and limitations will be addressed when constructing the molecular system. The prominent limitations encountered were classical mechanics of point masses, system size, time scale of involved processes, and accuracy of force fields.¹¹⁰

1.10 Aims of the present study

This thesis looks at two aspects of the camphor/fenchone system with different focuses.

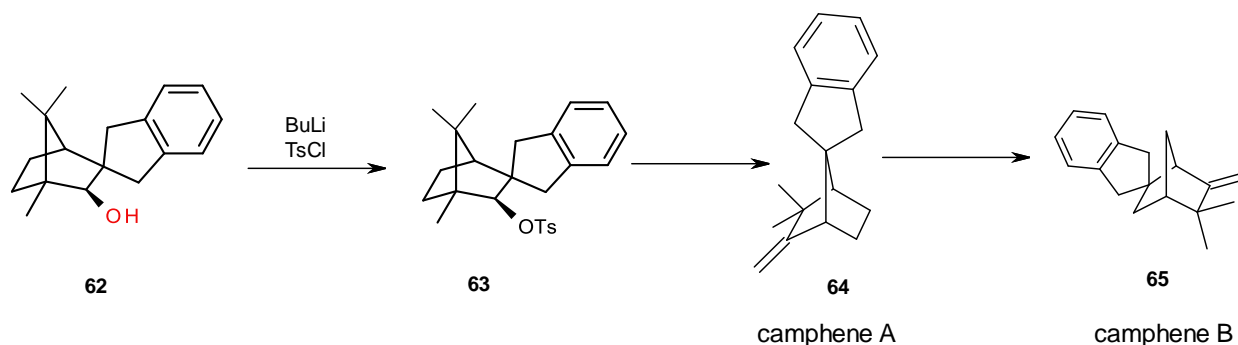
1. Reactivity of substituted norbornyl systems.
 - a. Attempt to synthesize a ¹³C-labelled spirobornyl tosylate and the investigation of its reactivity and mechanism of transformation, and
 - b. Failing which using its ²H-labelled isotopologue to the same purpose,
 - c. Investigation of the kinetics and reactivity of unexpected transformations along the way.
2. The chirality of substituted norbornyl systems
 - a. Design and synthesis of camphor and fenchone-derived chiral surfactants.
 - b. Evaluation of their feasibility and stability of the derived micelles *in silico*,
 - c. *In silico* investigation of the chiral influence of the micelles on the micro-environment.

Discussion – Reactivity Studies

2 Rearrangement of a spirobornyl tosylate

A transformation reported in the literature involved an NMR ^1H kinetic study¹¹³ which followed the decomposition of a tosylate **63** to the camphene products **64** and **65** (Scheme 13). In this study activation energies were determined for the successive transformations – the first being from the tosylate **63** to camphene **64** with an associated $\Delta G^\ddagger = 24.2 \text{ kcal mol}^{-1}$, followed by the conversion from camphene **64** to camphene **65** with its respective free energy of activation of $\Delta G^\ddagger (298\text{K}) = 22 \text{ kcal mol}^{-1}$. Other parameters, such as the entropies of activation were $14 \text{ cal mol}^{-1} \text{ K}^{-1}$ for **63** to **64** and approximately $-25 \text{ cal mol}^{-1} \text{ K}^{-1}$ for **64** to **65**, consistent with the dissociation in the first step and rearrangement in the second. However, an earlier study identified both enantiomers of the camphene **65** within a crystal structure,¹¹³ indicating that racemization occurred under the reaction conditions. However, the rate of racemization could not be determined, as enantiomers are indistinguishable under normal NMR spectroscopic conditions.

Since optically pure materials (such as the camphenes produced) could be of value in asymmetric synthesis, it would be useful to avoid racemization. Therefore, of interest in this study was a means for characterizing the racemization process.



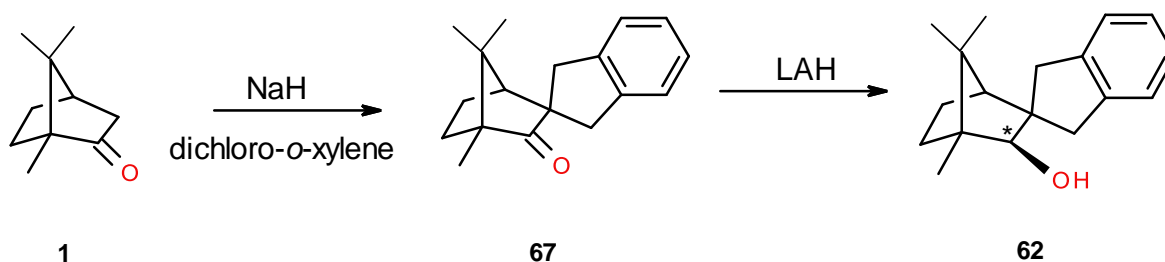
Scheme 13. Formation and decomposition of a spirobornyl tosylate.

Therefore, two of the subsidiary aims of this study were to:

- (a) Determine whether racemization occurred in the initial formation of camphene **64**
- (b) If not, whether the transformation from camphene **64** to camphene **65** occurred faster than the racemization process, enabling optically pure camphene **65** to be isolatable.

2.1 Preparation of the spirobornyl tosylate **63**

Preparation of the tosylate followed the literature¹¹³ where optically pure camphor was reacted with α,α' -dichloro-*o*-xylene in the presence of a base sodium hydride. The excess sodium hydride provided for sequential removal of both hydrogens α to the ketone and insertion of the xylyl group on the terpenoid skeleton. Following chromatographic purification, the adduct **67** was reduced in dry THF with lithium aluminium hydride (Scheme 14) to form the *exo*-alcohol adduct **62**. Removal of the hydroxyl hydrogen using butyl lithium and introduction of tosyl chloride, produced the tosylate **63**, which, after workup was recrystallized at 0°C (Scheme 13).



Scheme 14. Synthesis of the spirobornyl scaffold.

2.2 Kinetic analysis of the decomposition of tosylate **63**

Decomposition of the tosylate **63** was followed using ¹H NMR spectroscopy at a fixed temperature, according to the literature methods.¹¹³ Figure 24 shows a stacked ¹H NMR plot of the decomposition of the tosylate **63** and the subsequent formation of both camphene products.

Shown in Figure 24 is the decay of the tosylate **63** (green arrow), formation of the first product camphene A **64**, followed by its transformation (red arrows) into camphene B **65** (black arrow), producing the racemic mixture. The product was not isolated, nor was its optical activity measured, but racemization was confirmed in later experiments.

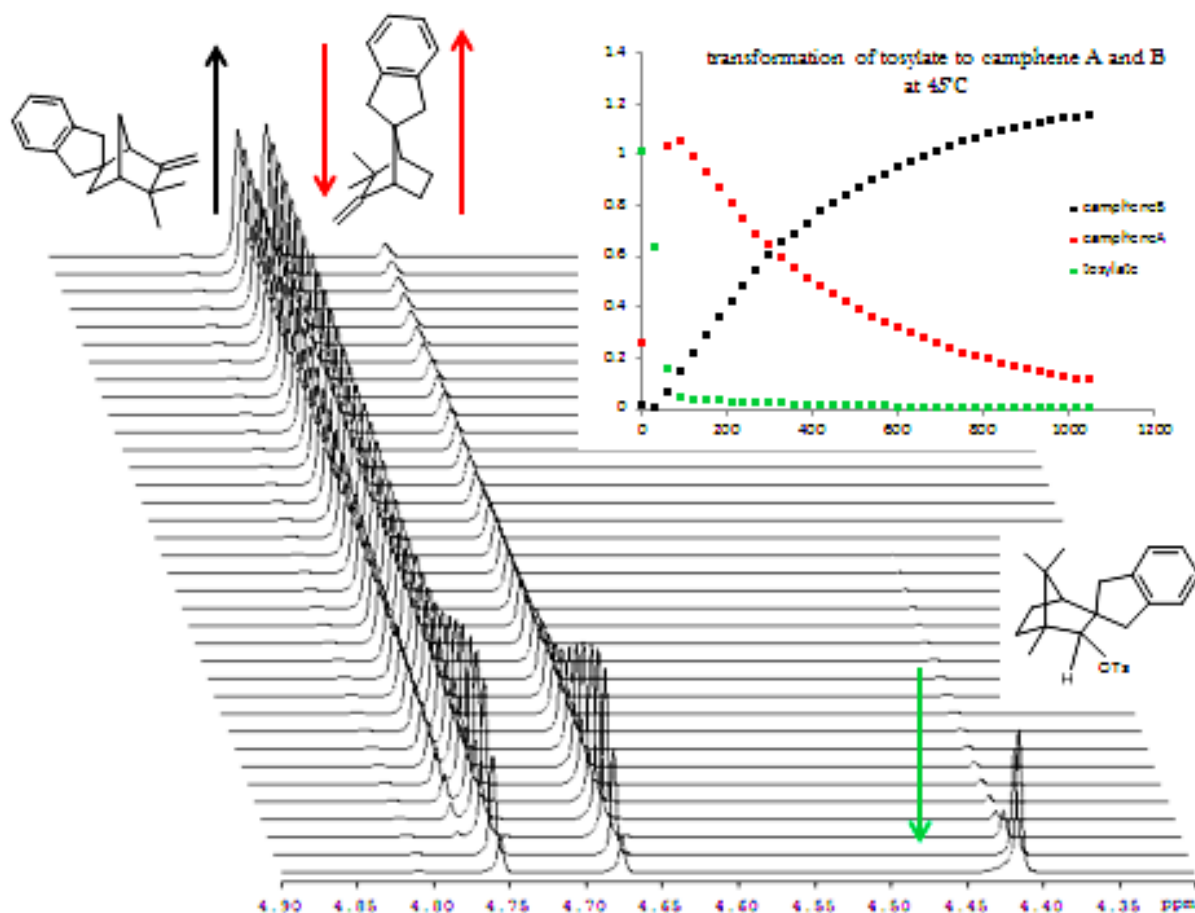


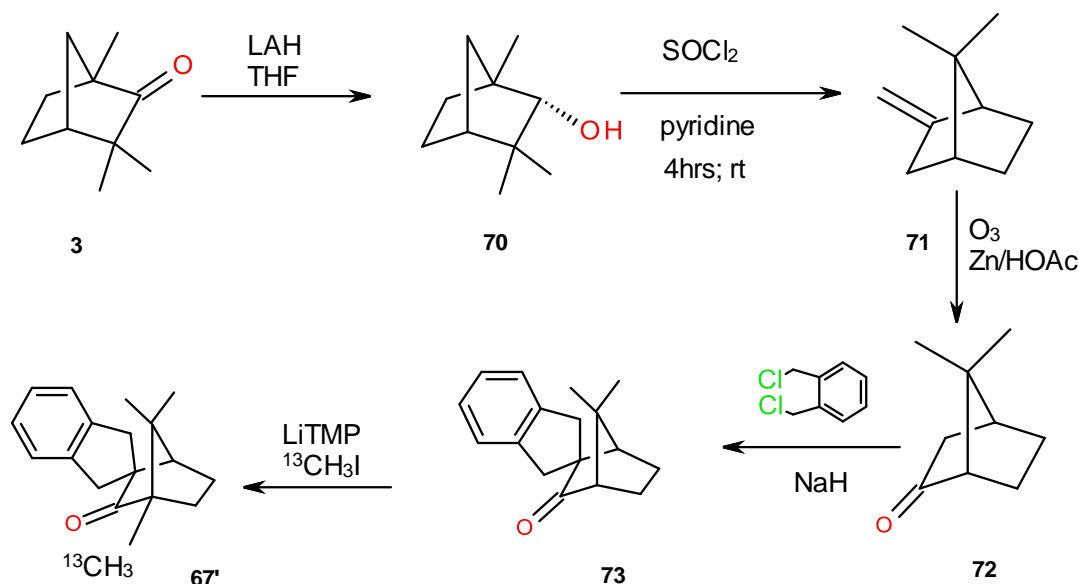
Figure 24. Raw ^1H NMR data and a plot of the integral values vs. time as a repeat of the reported kinetic transformation in literature.¹¹³

Of course, it was not possible to detect any racemization at this point. In order to uncover the complexity and variety of rearrangement routes seen in these substituted norbornyl systems this study was focussed on following such rearrangements through NMR spectroscopy using isotopically labelled analogues (isotopologues) of **63** in an attempt to confirm mechanisms, and identify the processes and the rates of racemization. The two bicyclic moieties used as starting points to synthesize these isotopologues were camphor (**1**) and fenchone (**3**), both naturally occurring molecules readily available in high optical purity.

Our investigation into the rearrangements of isotopologues was initially based on that shown in Scheme 15, involving five synthetic steps giving a ^{13}C labelled spirobornyl tosylate derivative (**67'**).

2.2.1 Attempted preparation of a ^{13}C labelled analogue of the scaffold 67

Racemization of the tosylate involves several consecutive transformations that interchange the methyl groups. Thus, the first strategy proposed for following the racemization step involved the following synthetic scheme to ensure that at least one of the methyl groups in the precursor to the tosylate was ^{13}C labelled (Scheme 15).



Scheme 15. Proposed scheme for the production of the ^{13}C -labelled precursors.

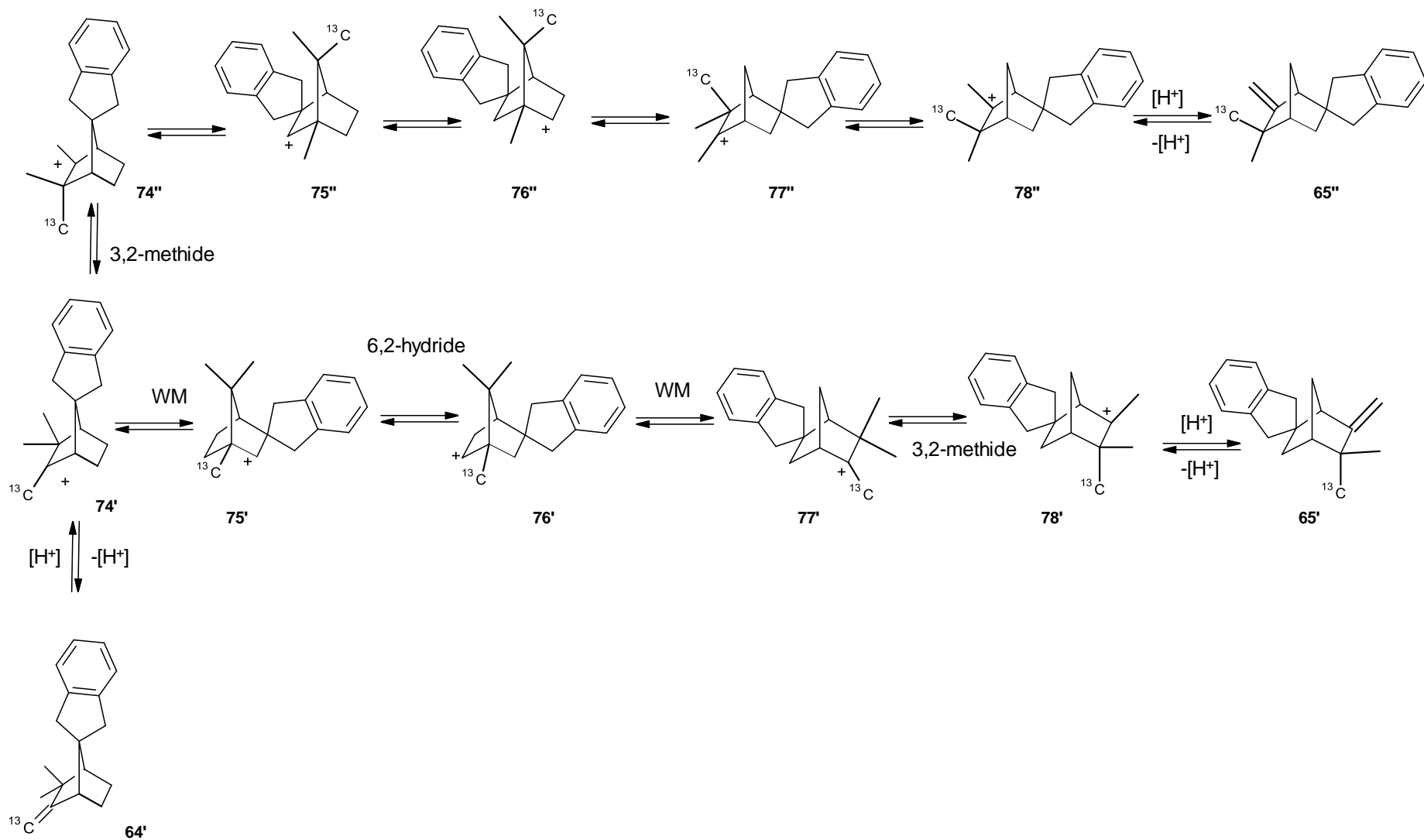
This scheme involves reaction between fenchol **70** and thionyl chloride in pyridine to give fenchene **71**, an oxidative cleavage of the double bond (with many options available, the first attempt was to use ozone as the oxidizing agent) to introduce the carbonyl group, forming apocamphor **72**, followed by introduction of the xylyl group forming **73**, and a final stage alkylation with ^{13}C -labelled methyl iodide to form **67'**, the ^{13}C -labelled enantiomer of **67**. For this there are two notable aspects; firstly, the synthetic scheme provides the commercially unavailable fenchene **71** and secondly, it provides the ^{13}C labelling of its derivative *via* a difficult methylation at a bridgehead carbon. The enolization of this bridgehead carbon at position 1 is difficult (requiring an extremely powerful base)^{114,115} due to the strained geometry at the bridgehead position and inability of this configuration to adopt a planar enolate anion. Part of the rationale behind this step was that in particular, optimization of the substitution at the bridgehead position would in itself lead the way for other studies to explore unusual substitutions on the norbornyl skeleton.¹¹⁶

The ^{13}C labelling strategy had as its basis a proposed mechanism for the rearrangement of the labelled carbocation **74'** (Scheme 16) that would produce a range of isotopomers. It was presumed that if racemization occurred during the transformation of camphene A **64** to camphene B **65** we could predict the exact isotopomers formed. Following protonation of labelled camphene A **64'** to produce the cation **74'**, the racemization process was proposed to involve a methide shift which would produce a pair of enantiomers of isotopomers **74'** and **74''**. Each of these isotopomers would undergo a series of Wagner-Meerwin, 6,2-hydride, Wagner-Meerwein, and 3,2-methide shifts, producing enantiomers of the isotopomers of camphene B **65'** and **65''**. The ^{13}C labelling would clearly define the racemization and would be fully distinguishable in a ^{13}C NMR spectrum.

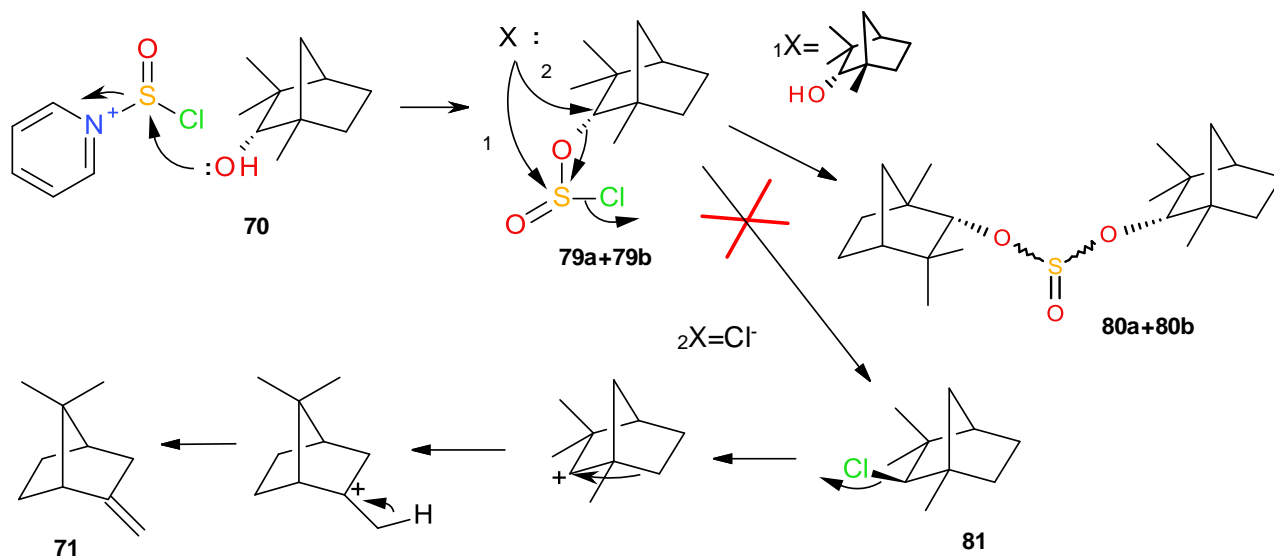
This synthetic scheme has serendipitously resulted in interesting and unexpected results leading to extensive, in-depth physical-organic studies regarding kinetics and mechanisms of other transformations. Ultimately (see later on in the study), this scheme was abandoned in favour of a much simpler approach.

2.2.1.1 Synthesis of fenchene **71**

Fenchene **71** (Scheme 17), was synthesized following literature procedures.^{117,118} Thus, fenchol **70** was reacted with thionyl chloride in pyridine in expectation of forming fenchyl chloride **81**, with inversion of configuration *via* an $\text{S}_{\text{N}}2$ mechanism (rather than retention of configuration *via* the intimate ion pair ($\text{S}_{\text{N}}\text{i}$) mechanism which is favoured in the absence of pyridine.) Fenchyl chloride **81** was then expected to undergo dehalogenation, a Wagner-Meerwein rearrangement and, finally, deprotonation to produce the desired fenchene **71**. Work-up afforded a white crystalline product, ^1H NMR analysis of which revealed the absence of the expected vinylic proton signals at *ca.* 4.7 ppm, indicating that fenchene **71** was not present in the product mixture. However, there was evidence of the formation of two closely related products. A pair of doublets characterized the predominant product at 3.94 and 4.10 ppm with a small coupling constant of 2 Hz. The minor product, on the other hand, exhibited a pair of overlapping doublets at 4.02 ppm (initially considered a triplet). These products have been identified as the difenchyl sulfites **80a** and **80b**, which are formed by the sequential reaction of two molecules of fenchol **70** with thionyl chloride.



Scheme 16. Mechanism for rearrangement of ^{13}C -labelled camphene A **64'** to ^{13}C -labelled camphene B **65'** and **65''**.



Scheme 17: Proposed synthesis of fenchene **71**.

The products (**80a/80b**) were then purified by recrystallization from hexane for further characterization. The ^1H NMR spectrum of the major product indicated the presence of six methyl singlets, compared to the three methyl groups present in the fenchol (**70**) starting material. Fenchene **71** contains only two methyl groups and hence this product was unambiguously ruled out. Multiplicity-edited HSQC (Figure 25) confirmed the multiplicity of all the carbon atoms present. As will be discussed to later, inter conversion between the major and minor products was observed and therefore it was not possible to obtain either in pure form. Considering the NMR spectra evidence up to this point, we initially assigned the diterpene ether structures to the two products.

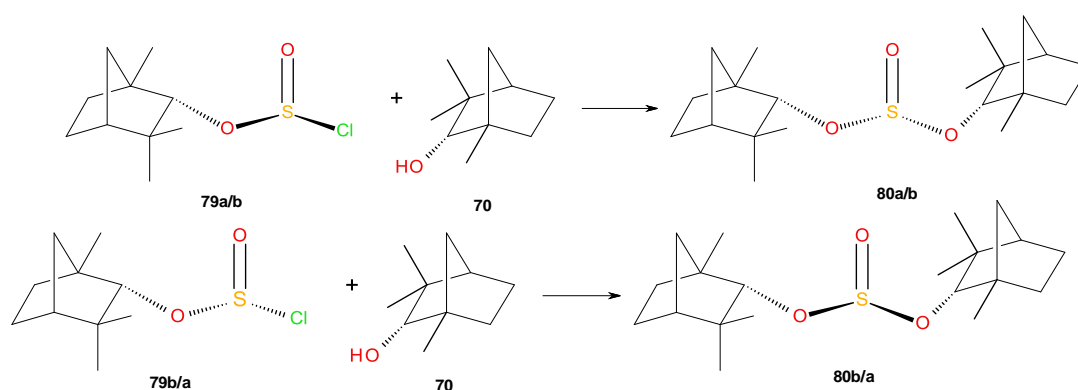
Analogous ethers, such as a diisobornyl ether are produced in oxidative processes used to convert the exocyclic alkene camphene to the alcohol isoborneol.¹¹⁹ Dimers involving a fenchane skeleton are also known where the linkage is an alkene.¹²⁰ In this research group, similar dimers have been encountered involving a camphor skeleton, also with an ether linkage.¹²¹

Elemental analysis however, showed the presence of sulfur that could not be confirmed with available NMR techniques. The structures were then reassigned as sulfite esters (**80a** and **80b**) which have the molecular formula $\text{C}_{20}\text{H}_{34}\text{SO}_3$ and are consistent with the full set of NMR and the elemental analysis data (Table 3). The origin of the major and minor products (Scheme 18: **80a** and **80b**) could be attributed to the stereochemical differences of the sulfur

atom linking both fenchol units forming the dimer. Synthesis of the dimer was repeated with yields reaching 72%. Changing the order of addition of reactants did not affect this outcome (Table 4).

Table 3: Elemental data for products **80a** and **80b**.

Element	C	H	N	S
%	67.8	9.5	0.0	8.3
Expected: diterpene ether	82.7	11.7	-	-
Expected: sulfite ester	67.8	9.6	-	9.0



Scheme 18. The formation of and the stereochemistry at the sulfur centre of **80a** and **80b**.

Table 4. Effect of varying the reaction conditions for formation of the dimer.

Reaction	Time (h)	Temperature	Moles SOCl ₂	Result	%yield (dimer)
A	2	Room Temperature	1	Dimer	72
B	2	50 °C	1	Dimer	65
C	18	Room Temperature	1	Dimer	71
D	2	Room Temperature	4	Dimer/fenchene	32
E ^a	2	Room Temperature	1	Dimer	72

^a Fenchol added in small amounts to stirred pyridine and SOCl₂

Table 4 shows some of the results of the attempted fenchene syntheses under various reaction conditions, highlighting formation of the dimer as major product. Fenchene itself was generally not observed at all. In each attempt, only one variable was altered at a time

compared to the original reaction conditions. The best yields were obtained at room temperature.

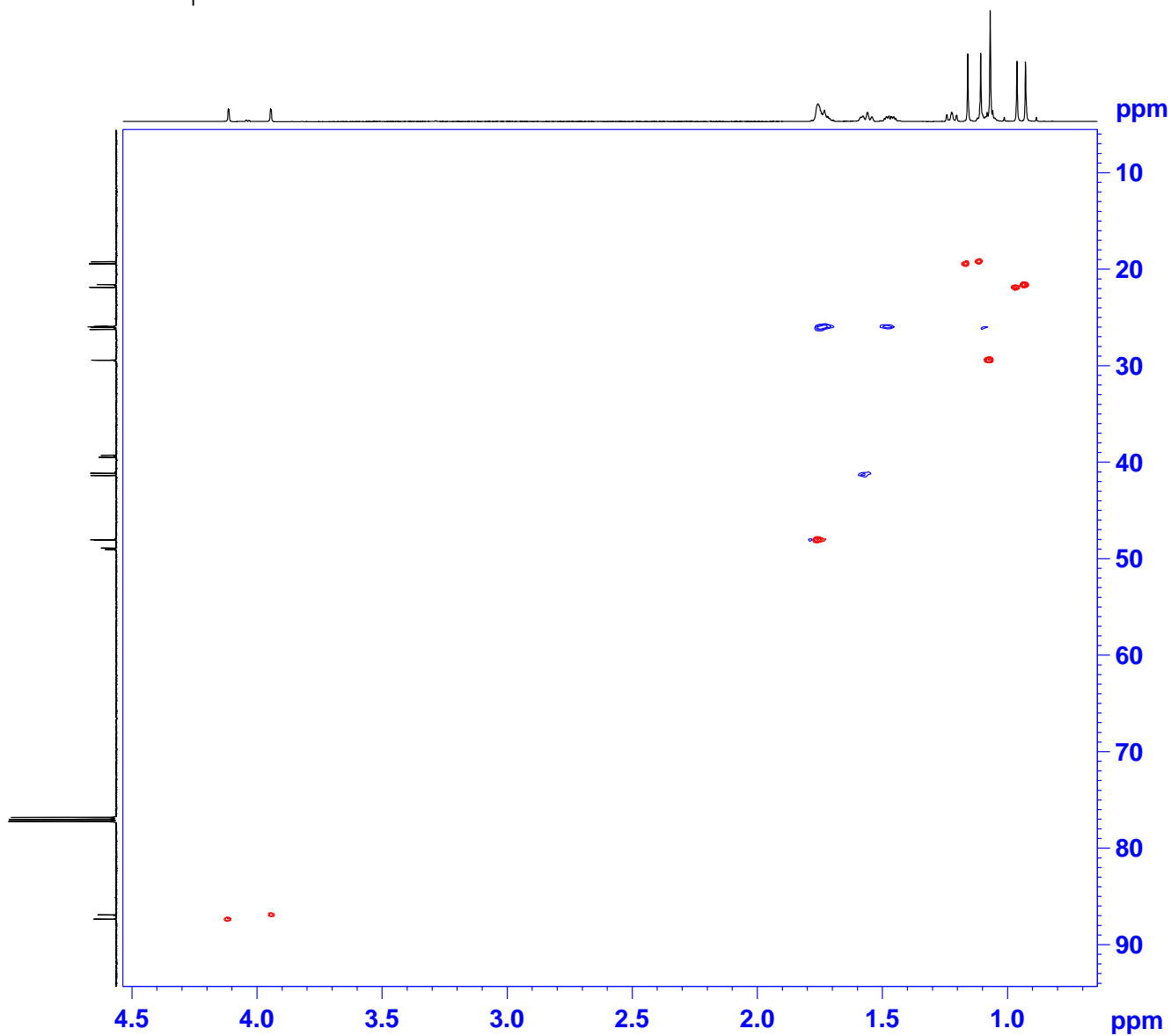
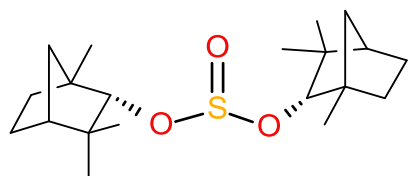


Figure 25. 600 MHz multiplicity-edited HSQC spectra of the major diastereomer of **80a** and **80b** in CDCl₃.

Where the possibility of carbocation formation exists on substituted norbornyl systems, it is not inconceivable that rearrangement may take place simultaneously. The rearrangement of camphene hydrochloride (which is close in structure to the fenchyl chloride that was expected as an intermediate) has been studied extensively and is known to readily rearrange to isobornyl chloride (see the preceding discussion in Section 1.1.2.4, Scheme 7).²³ The similarity was taken into account in this study. However, the multiplicity of the carbon atoms and the mechanism of formation of the sulfite together provide strong evidence against rearrangement processes taking place in this reaction. This study is unusual in this respect for a substituted norbornyl system under these conditions.

2.2.1.2 Kinetics of formation of isomers **80a** and **80b**

To gain a further understanding into the formation of the dimer (and to perhaps limit its formation and favour the fenchene product) a ¹H NMR kinetics study was initiated, with the reaction followed over a range of temperatures. The fenchol, thionyl chloride, pyridine and 1,3,5-trimethoxybenzene (TMB, used as an internal standard) were combined at 0°C and a stock solution was made up to 5 mL in CDCl₃. The reaction mixture was equally distributed in NMR tubes and kept in dry ice to retard any reaction from occurring prior to the kinetics run. After acquisition of spectra over time intervals, the regions specific to the study were integrated on one of the spectra and an in-house auxiliary program kl_kinint (within Bruker Topspin 2.1) was used to collate the values of integrals in these regions throughout the course of the experiment.¹²²

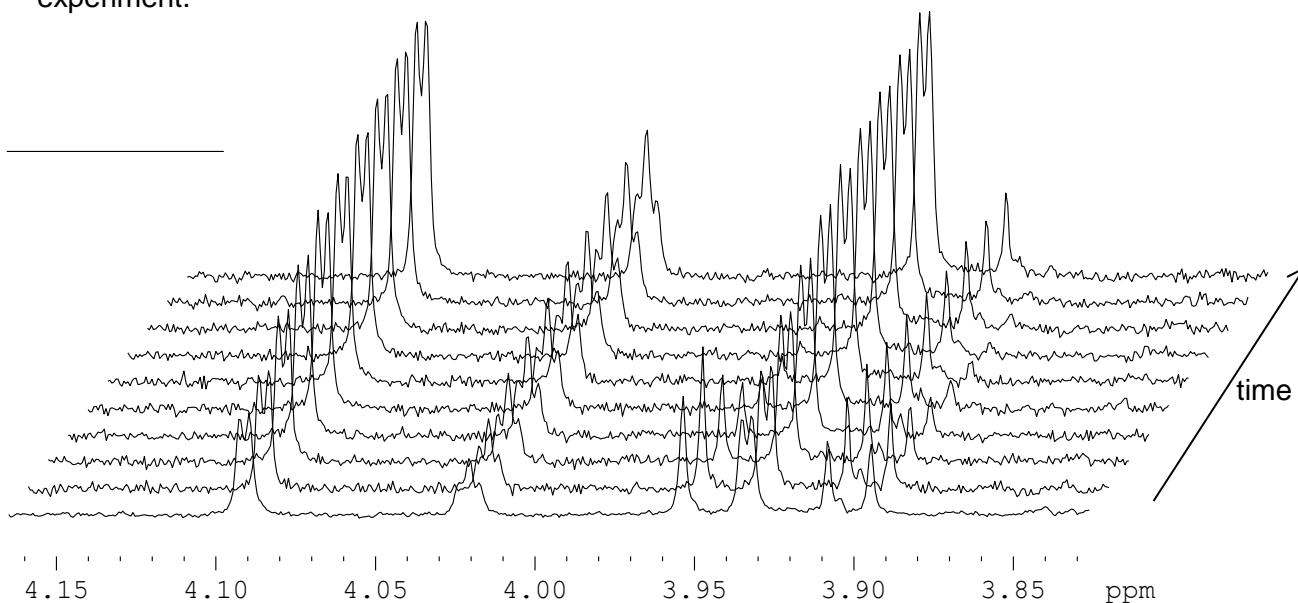


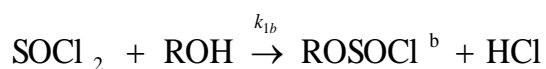
Figure 26. Formation of **80a** & **80b** signals during the course of a single NMR study.

A complication was the slow decomposition of the TMB standard, hence the TMB data was not used over the long-term analysis, rather the TMB standard allowed initial concentrations to be determined, and a mass balance was used to ensure that the integration was reliable during the course of the experiment. The reason for the decomposition of the TMB standard was evident retrospectively. Thionyl chloride had been used to prepare diaryl sulfoxides, for example,¹²³ and although the TMB may have been too hindered to form a dimer, it is possible that chlorosulfination may have occur at an aromatic position on the trimethoxybenzene standard.

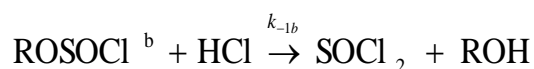
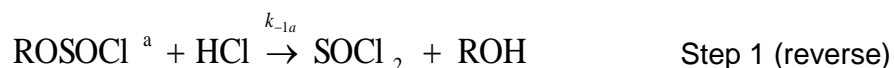
Figure 26 shows the formation of the pair of doublets at 3.94 ppm and 4.09 ppm (corresponding to the 2-*exo* and 2'-*exo* ¹H signals from **80a**), the overlapping pair of doublets at 4.02 ppm (corresponding to **80b**) during a typical kinetics run at 298 K with NMR spectra recorded at 5 min intervals. This trend was consistent over all range of temperatures between 20-45°C. It was noted, however, that the initial step, involving formation of the thionyl chloride - fenchol conjugate, could be considered to be instantaneous, as indicated by the presence of the 2-*endo*-H signal of the fenchol-thionyl chloride adduct **79a/b** at 3.29 ppm from the very first spectrum in the series, while no fenchol 2-*exo*-H signal was evident. The kinetics therefore follows the transformation that occurs because of a second fenchol (**3**) moiety attacking the thionyl chloride - fenchol adduct with the resultant formation of the dimer product. Even though the rate of formation of the minor product was considerably slower, both isomers formed simultaneously. The pair of doublets for the minor product, however, was not resolved at all of the temperatures in CDCl₃. Of course, while it is not possible to resolve the two diastereomers of the initial adduct, both must be present for the formation of the two diastereomeric products. Further, consideration of the interconversion between possible diastereomers was included in the kinetic model.

2.2.1.3 The mechanism of formation of isomers

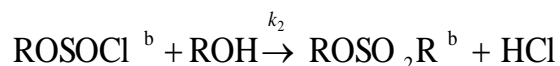
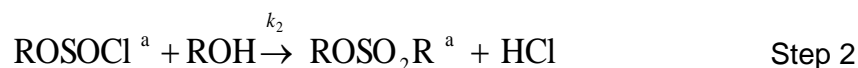
The mechanism of dimer formation must be overall second order with respect the fenchol and first order with respect to the thionyl chloride. The full mechanistic scheme (with all possibilities considered) follows. As there are diastereomers, two pathways, a and b, must be followed for each step. Therefore, the initial reaction of thionyl chloride with fenchol produces two products.



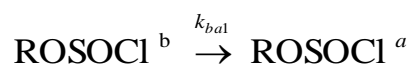
To allow for the reversibility of this step in the kinetic model the following two steps are included.



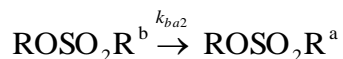
The final formation of the two diastereomeric dimers is by reaction of the intermediates with a second molecule of fenchol.



Other processes which are possible are inter-conversion between stereoisomers due to inversion at the sulfur center

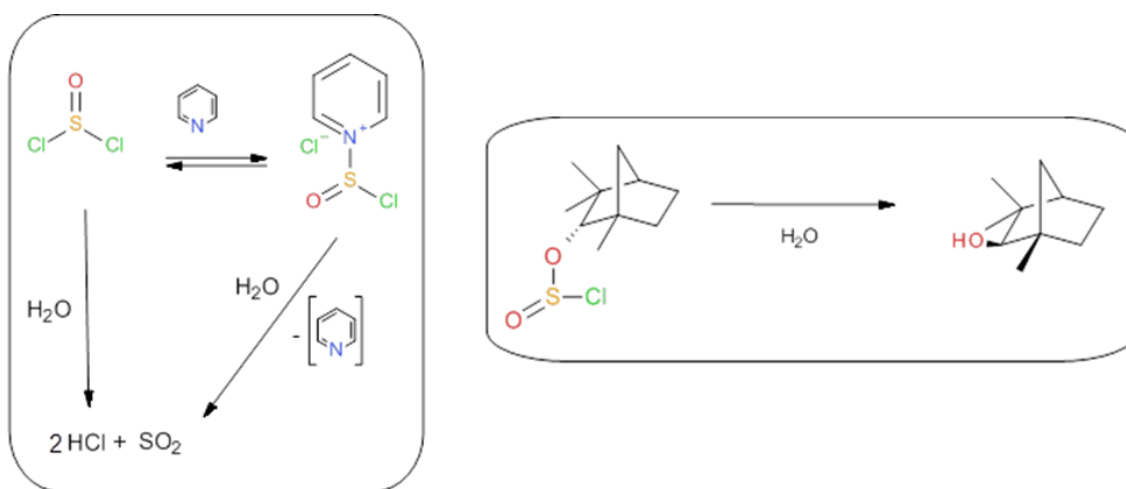


The second inter-conversion is possible with the final product



The fact that thionyl chloride is present and involved in the reaction is problematic since it is not detected in the ^1H NMR spectrum. One way to estimate its amount is by its initial amount in the reaction mixture, less the quantity of fenchol-thionyl chloride adducts. However, the

precision of this calculation can be affected by the presence of water in the reaction mixture, since thionyl chloride reacts readily with water. The water might be present in small quantity because of condensation during the transfer of cold reagents to the NMR tubes. However, it may be that the effect of water is overestimated in this case. That the dimer products are formed at all suggests that nucleophilic attack on the thionyl chloride-pyridium complex by the fenchol has a much higher rate compared to the attack on the complex by water, possibly because the concentration of water present was considerably less than the concentration of the fenchol. Scheme 19 summarizes the possible water involvement.



Scheme 19. Summary of competing processes that could occur in the presence of water.

In a similar vein, one could also consider the formation of pyridinium complexes and hydrolyses thereof in the overall description of the kinetics, but ultimately none of these was found to have a detectable influence on the rate laws for formation of the dimer under the conditions used.

To summarize, the rate constants considered are shown in Table 5, together with the informal designators used when assigning a theoretical fit to the experimental data.

Table 5. All rate constants used for theoretical fit. ROH is fenchol, and a and b denote diastereomers of the respective adducts **79** and **80**.

$\text{ROSOCI}^{\text{a}} (\mathbf{79a}) + \text{ROH} \rightarrow \text{ROSOOR}^{\text{a}} (\mathbf{80a}) + \text{HCl}$	k_1
$\text{ROSOCI}^{\text{b}} (\mathbf{79b}) + \text{ROH} \rightarrow \text{ROSOOR}^{\text{b}} (\mathbf{80b}) + \text{HCl}$	k_2
$\mathbf{80a} + \text{HCl} \rightarrow \text{ROSOCI}^{\text{a}} + \text{fenchol}$	k_3
$\mathbf{80b} + \text{HCl} \rightarrow \text{ROSOCI}^{\text{b}} + \text{fenchol}$	k_4
$\text{ROSOCI}^{\text{a}} \rightarrow \text{ROSOCI}^{\text{b}}$	k_5
$\text{ROSOCI}^{\text{b}} \rightarrow \text{ROSOCI}^{\text{a}}$	k_6
$\mathbf{80a} \rightarrow \mathbf{80b}$	k_7
$\mathbf{80b} \rightarrow \mathbf{80a}$	k_8
$\text{SOCl}_2 + \text{fenchol} \rightarrow \text{ROSOCI}^{\text{a}} + \text{HCl}$	k_9
$\text{SOCl}_2 + \text{fenchol} \rightarrow \text{ROSOCI}^{\text{b}} + \text{HCl}$	k_{10}
$\text{ROSOCI}^{\text{a}} + \text{HCl} \rightarrow \text{SOCl}_2 + \text{fenchol}$	k_{11}
$\text{ROSOCI}^{\text{b}} + \text{HCl} \rightarrow \text{SOCl}_2 + \text{fenchol}$	k_{12}

Rate constants k_1 and k_2 , along with k_9 and k_{10} , were assumed to predominate in governing the overall formation of each of the dimer products. In order to get an accurate theoretical to experimental fit, the more minor contributing reverse rates as well as inter conversions were taken into account, but only after the best fit with these predominating rate constants was determined.

Figure 27 shows a typical theoretical fit to the experimental data. For the theoretical fit, numerical application of Euler's method for integrating the series of ordinary differential equations was performed over 1 s time intervals within the Excel program. Use of the solver functionality refined the rate constants to a higher level of accuracy.

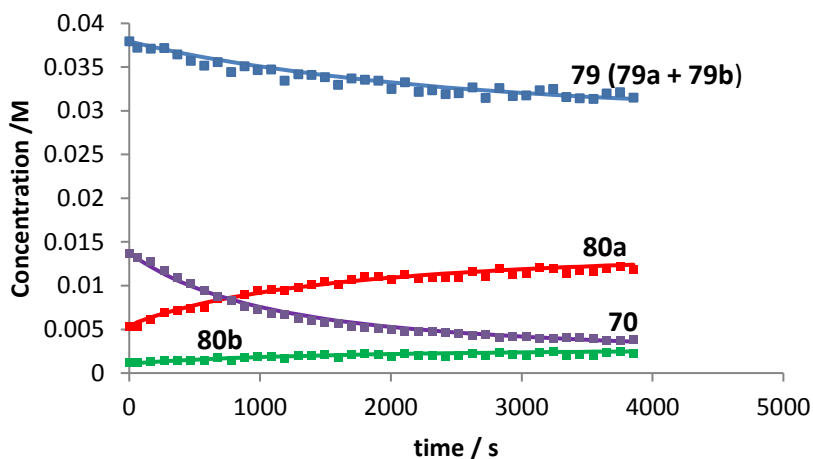


Figure 27. Experimental concentrations (dots) and theoretical fit (solid lines) for species during the kinetics run at 298 K.

For this fit, the initial ratio of the two fenchol-thionyl chloride adduct diastereomers **79a** and **79b** was also estimated from the initial experimental data, to provide the best overall match to the experimental data.

These data suggest good agreement between the experimental data and the proposed mechanistic steps. These data were reproduced at several temperatures, but activation data could not be determined. Inter-conversion processes (that may make the solution to the rate constants non-unique), account for this. Thus although there is a plausible rate law, determining the unique values of the rate constants was not possible.

2.2.1.4 Variable temperature studies:

In order to fully de-convolute the relationship between the minor and major product diastereomers a variable temperature study (^1H NMR VT- study) was conducted in $\text{DMSO-}d_6$. Variable temperature analysis typically is used to observe and characterize equilibria. In this particular case coalescence between the two species was not observed, as temperatures were changed (the apparent coalescence in the minor diastereomer is from the non-equivalent 2-H protons in a single diastereomer), and so all that was examined was the relative proportions of each diastereomer at each temperature. Figure 28 shows the variation in signal at various temperatures. Line shapes were not studied in detail due to differences in shimming caused by changes in temperature.

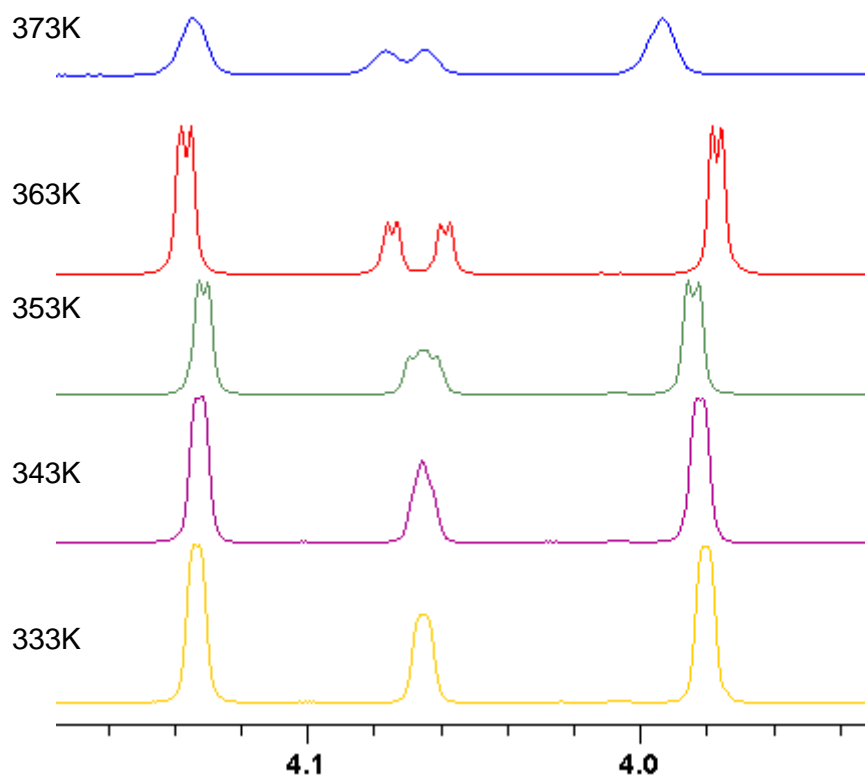


Figure 28. The effect of temperature on the 2-exo and 2'-exo ^1H signals.

By exploring the relative proportions of each stereoisomer at each temperature, K_{eq} was determined and the Van't Hoff plot of $\ln(K_{\text{eq}})$ vs $1/T$ was plotted (Figure 29). From this plot it was determined that the more stable diastereomer was $\Delta G = 2.25 \pm 0.38 \text{ kcal mol}^{-1}$ lower in energy than its counterpart but had greater entropy by $\Delta S = -4.0 \pm 1.0 \text{ J K}^{-1}$.

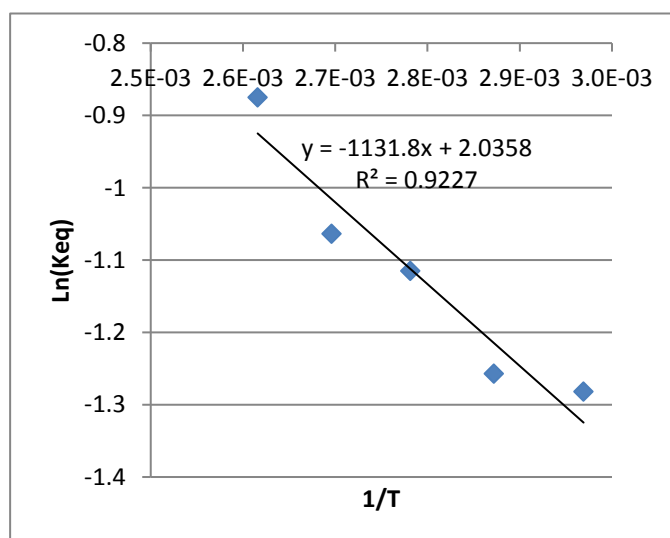


Figure 29. Van't Hoff plot for the exchange of the dimers at variable temperature.

2.2.1.5 Computational study

Initially it was not clear whether the species involved were rotamers of each other or actual diastereomers (sulfur diastereomers are unusual). As such, the initial modelling work was done to explore the conformational space of a single diastereomeric system. There are four relevant torsions and the exploration of this is not easy in terms of a four-dimensional potential energy surface.

Rotation about the two C-O bonds (at the AM1 level, Figure 30) in Gaussian 03 for a single diastereomer of **79** provided a 2-dimensional potential energy surface as illustrated in Figure 31. This figure suggests that there is a single conformation in the lowest energy “well” but the detail (6 positions per rotation) does not give the detail of very small local minima “wells”. At any temperature, these local minima will not attract a sizable population of rotamer. The inference is that this particular diastereomer must have a single predominant rotamer, and that the presence of rotamers may not be a suitable explanation for the observation of two separate species.

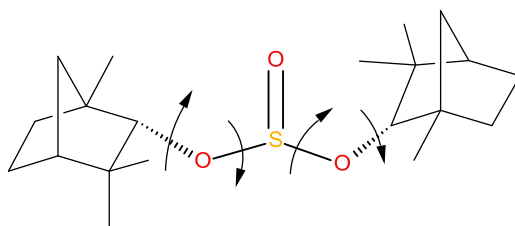


Figure 30. Torsion angles used in geometric analysis.

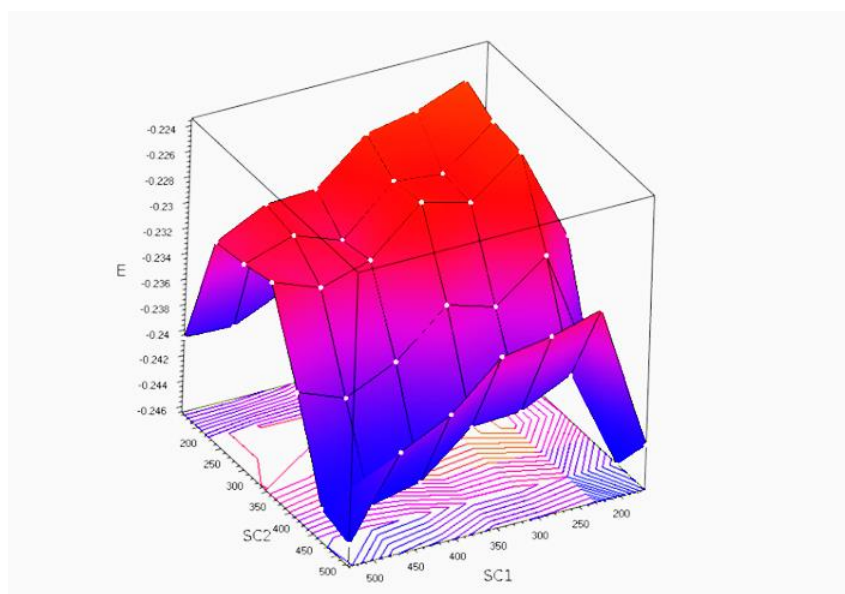


Figure 31. Change in energy of various conformations of the dimer throughout an energy scan with two torsions taken into account.

A criticism of the above analysis is that the rotation about the S-O bond is not taken into account. The possibility of rotation about the S-O bond affecting the outcome of this conformational search was therefore explored. A total of 6x6x6x6 conformers (shown in Figure 30) were generated using VEGA ZZ in a systematic way. Each of these conformers was optimized at the AM1 level in Gaussian 03. In some cases, the conformation produced by VEGA ZZ included atoms that were nearly overlapping, and thus the results from the AM1 work included bond breakage (as the strain was unrealistically high in some conformers). To analyze these results, another way of visualizing the modeling results was explored, since the outcome is essentially a 4-dimensional potential energy surface, requiring five dimensions if energy is included. A way to visualize this complex set of data is using parallel axes. Figure 32 shows the results of this situation. There are five parallel vertical axes which relate the energy (first vertical axis) to the torsion angles present in a particular conformation (remaining 4 vertical axes for the CCOS, COSO, OSOC and SOCC torsion angles), by a line connecting the 5 points. These lines (one for each conformer) are colored by energy value. The lowest two energy values are from rearrangement to low energy structures, with differing bonding patterns due to attempted AM1 optimization of a very high-energy conformation from the VEGA ZZ conformational search. As such, they are treated as artifacts.

The third-lowest energy value is of interest (red). Many conformations have this value for energy (marked red on the parallel axis graph). Many of them have a different set of torsion angles, and thus would have different ¹H NMR spectra. The evidence is such that, since we see a relatively simple spectrum, these rotamers must be interconverting on a time scale much shorter than the NMR timescale.

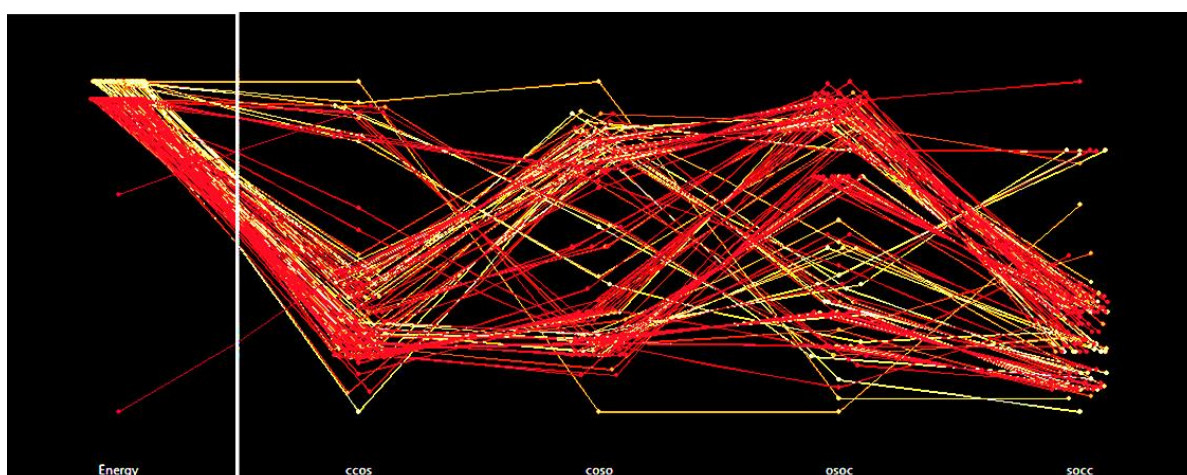


Figure 32. Parallel axis representation relating the energies of conformations to the torsion angles present in the conformation.

This detail highlights the evidence that the presence of rotamers cannot support the experimental data, and the most likely choice, given the possibility of stereoisomerism of the sulphur, is that of diastereomers.

Sulfur has a lone pair in the sulfite moiety, and as such will exhibit diastereomers with differing NMR spectra (if NMR active nuclei are observed). Thus, this was chosen as the most plausible explanation for the presence of two species that can interchange under the conditions described.

Another piece of evidence regarding the formation of the dimer is the generation of a successful transition state (at the B3LYP/6-31G(d) level). This transition state has only one imaginary frequency, and, following displacement about this frequency in one direction (followed by optimization) leads to one of the diastereomers (*in lieu* of an IRC calculation).

NMR calculations (GIAO at the same level of theory) indicate that both the 2'-*exo*-H and the 2-*exo*-H are distinct in the NMR spectrum (Figure 35).

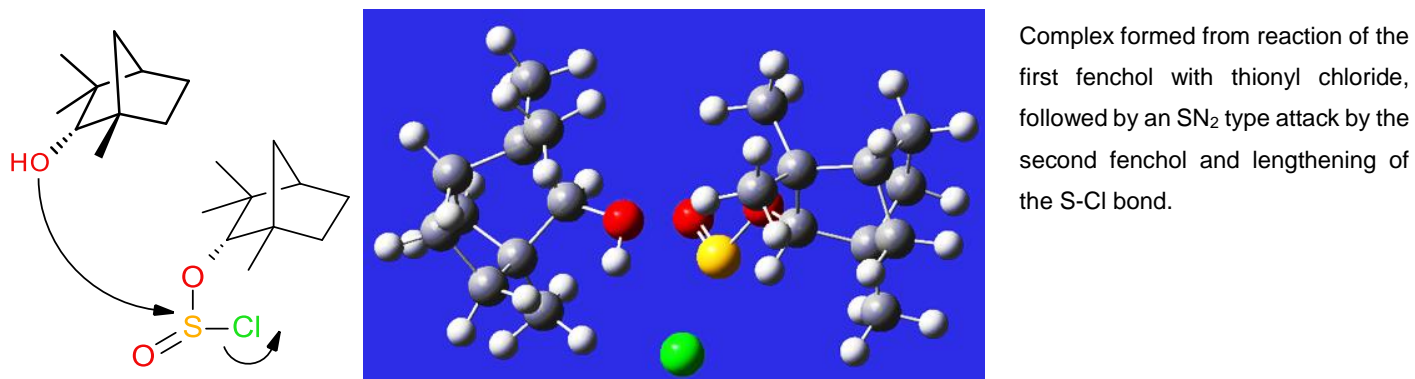
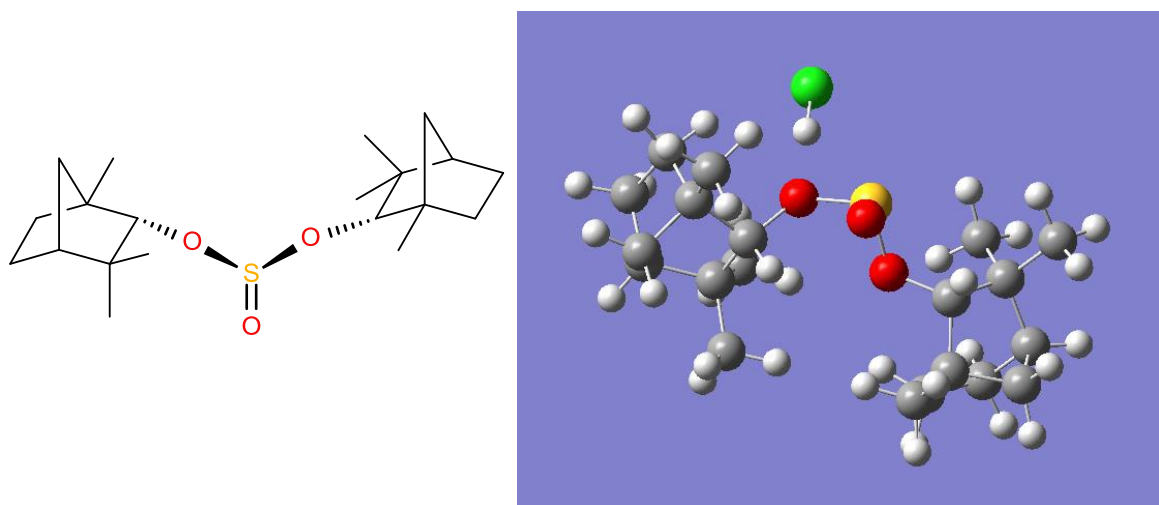


Figure 33. Transition state for the formation of a difenchyl sulfite (**80a/b**) diastereomer, by interaction of a single fenchol molecule (**3**) with the fenchol-thionyl chloride adduct (**79a/b**).

The evidence from the NMR spectra, elemental analysis, variable temperature work, and computational modelling are all in support of the assignment of these as the difenchyl sulfite esters.



The dimer is formed (optimising the transition state after displacement in one direction about the imaginary frequency. The HCl leaving group is hydrogen bonded to an oxygen.

Figure 34. The final product as a result of optimizing in one direction of the imaginary frequency (one diastereomer).

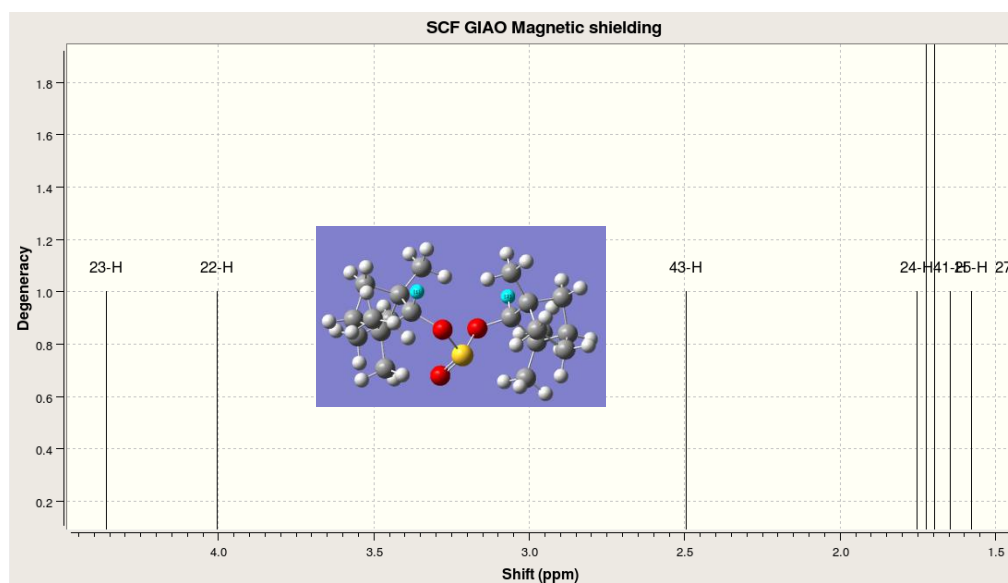
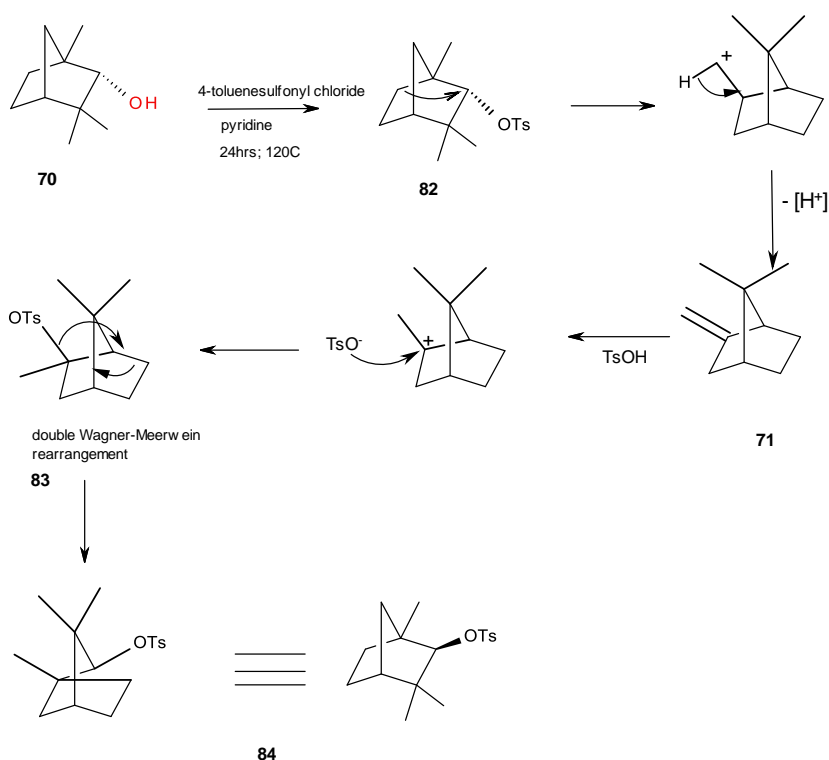


Figure 35. GIAO NMR calculation at B3LYP/6-31G(d) level of one adduct showing the distinct signals for 2-H on each fenchol skeleton. The cyan hydrogen atoms are hydrogens marked as 22 and 23 in the theoretical ^1H NMR spectrum.

2.2.2 Synthesis of fenchene:

After various failed attempts to synthesize fenchene from pyridine and thionyl chloride, another method from the literature was employed, by refluxing the fenchol with 4-toluenesulfonyl chloride in pyridine for 24 h.¹²⁴ The reaction mixture was first quenched with NaOH, and on the second attempt with NaHCO₃. Both times the crude product after work-up was a brown oil, where NMR spectrum showed that fenchene had been successfully synthesized, indicated by the presence of alkene hydrogens. However, when left standing the oil formed white crystals. NMR analysis of the crystals showed that the fenchene had disappeared, producing the suspected fenchyl-tosylate adduct **84** (Scheme 20), perhaps due to incomplete removal of tosic acid by these bases.

With the NaHCO₃ work-up, the hexane layer was passed through a plug of silica with the aim of removing any tosic acid, but this was unsuccessful and the fenchene reverted to the tosylate **84**.



Scheme 20. A possible explanation for the disappearance of fenchene.

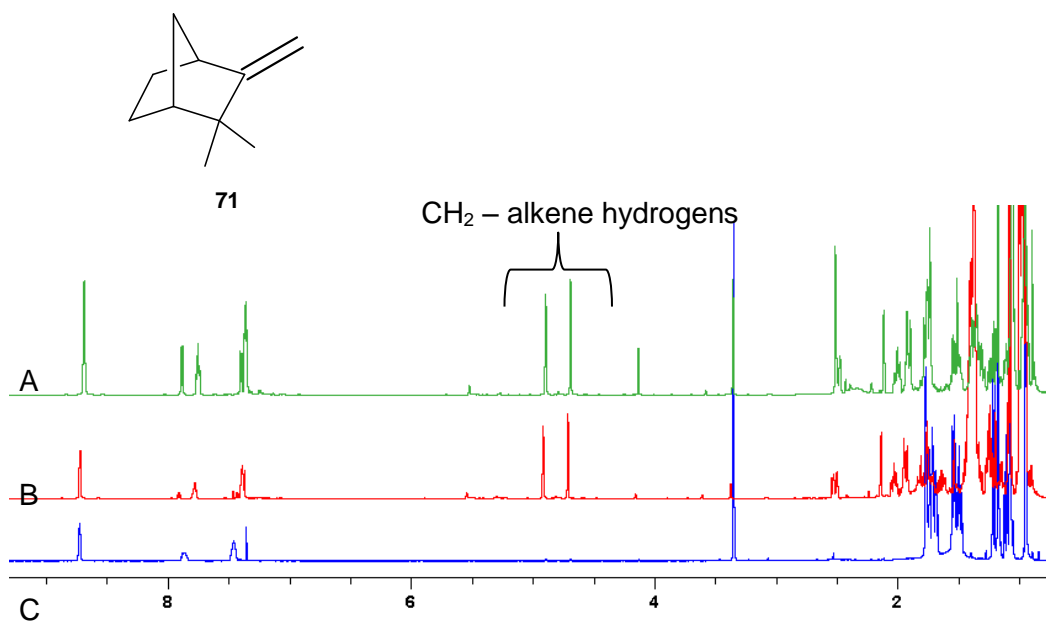


Figure 36. 600 MHz ^1H NMR spectra: A: Fenchene post workup with NaOH; B: Fenchene post workup with NaHCO_3 and silica plug; C: Showing disappearance of fenchene overnight.

The isolation and purification of fenchene proved frustrating. However, in a repeat experiment (Figure 36), use of NaHSO_3 during workup led to formation of a precipitate. The precipitate was filtered off and the solution extracted with hexane. TLC showed only a single spot. ^1H NMR spectra of the product showed pure fenchene (Figure 37). We tentatively attribute the success of this technique to (a) the formation of other oxidation states of the toxic acid sulfur, rendering the toxic acid unable to react in the undesired manner, or (b) the creation of a highly reductive environment preventing any oxidative changes in the fenchene product.

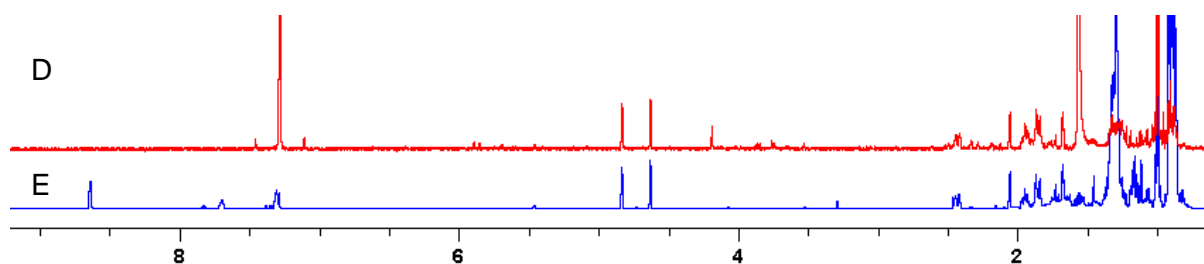
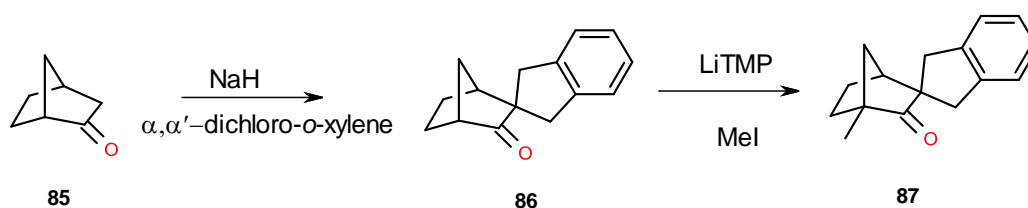


Figure 37. 600 MHz ^1H spectra: D: NaHSO_3 workup showing presence of fenchene only, E: NaHCO_3 where toxic acid is still present.

The fenchene was not taken forward according to Scheme 15; simultaneously with this study, a trial methylation reaction was attempted on a xylyl-substituted norcamphor derivative, in preparation for the final stages of the proposed synthetic scheme (Scheme 15).

2.2.3 Methylation of xylyl-substituted norcamphor:

In preparation for ^{13}C labelling of the xylyl-substituted apocamphor system in the ^{13}C labelling scheme (**73** to **67'**) an attempted methylation of a bridgehead carbon on apocamphor using methyl iodide (MeI) was performed. For this work a xylyl substituted norcamphor derivative **86** was synthesized (Scheme 21) from norcamphor **85**.



Scheme 21. Methyl addition to a bridgehead position.

The reaction required that the lithium 2,2,6,6-tetramethylpiperidide (LiTMP) base first be synthesized by reacting 2,2,6,6-tetramethylpiperidide (TMP) with butyllithium (BuLi) at -78°C in THF, to which the substituted norcamphor **86** was added, followed by the methyl iodide. Upon workup and analysis, it was concluded that the intended methylated product had not formed. However, analysis of the ^1H NMR spectrum revealed an interesting feature. Although pure LiTMP and 3,3-di-*o*-xylynorcamphor **86** were used, inspection of the spectrum (Figure 38) revealed numerous signals between 2.0-3.5 ppm that shed some interesting insights into the reactivity of this xylyl-norcamphor system.

Assessing the substituted norcamphor moiety in terms of available reaction sites (Table 6), it is clear that numerous products are possible. In terms of reactivity we had predicted that the bridgehead α -hydrogen labelled **a** would be reactive and was the intended methylation point. There was also the possibility that the benzylic protons labelled **b** and **c** would compete as reaction sites due to electron delocalization (pK_a of a ketone α -H is typically approximately 20 compared to that of benzylic hydrogens which are around 40). However, given the expected acidity order for the identified protons (**a** > **b,c** > **d**), it was anticipated that reaction at the bridgehead α -H (**a**) would still be favoured. In norbornyl systems, the β -H's at position 6 (**d**) are reactive under basic conditions.¹²⁵ Nevertheless, assuming that methylation could take place at any point **a-d** (and assuming that in the presence of LiTMP all of these protons are

accessible) multiple substitutions could occur and up to 100 possible products are possible. Although the reagents MeI and LiTMP were not used in excess, making significant multiple substitutions unlikely, this method was discarded and a simpler, more efficient procedure of deuterium labelling was employed.

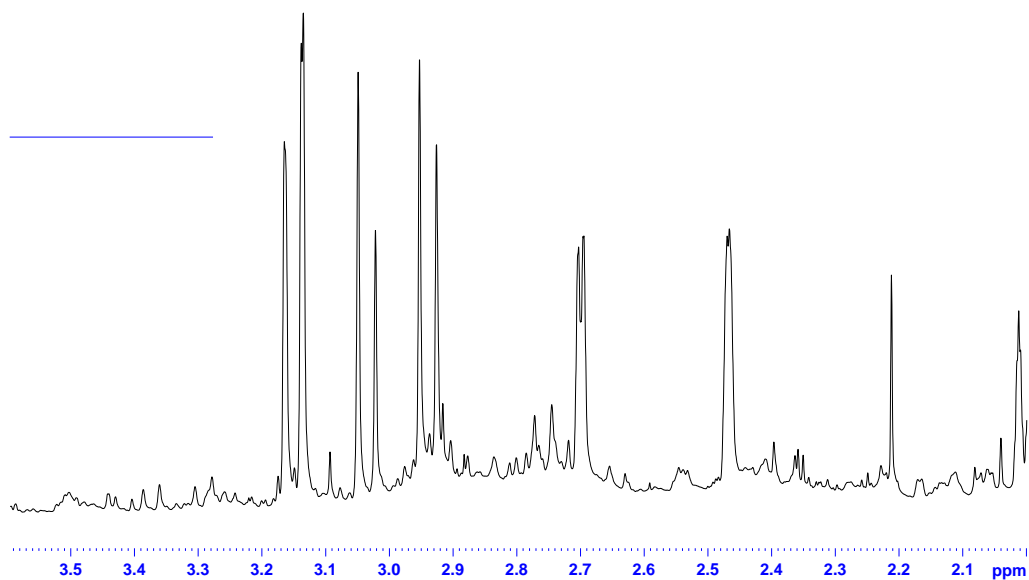



























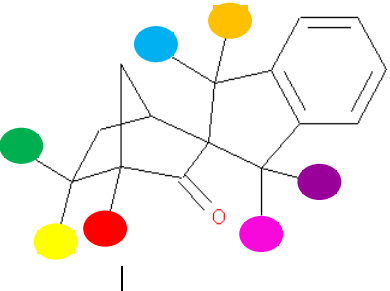


Figure 38. Multiple methylations are evident in the LiTMP mediated methylation of norcamphor.

Table 6. Some possible substitution patterns in the methylation of the xylylnorcamphor **86**.

Mono-substituted	Di-substituted	Tri-substituted	Tetra-substituted	Penta-substituted	Hexa-substituted
					
					
					
					
					
					
					



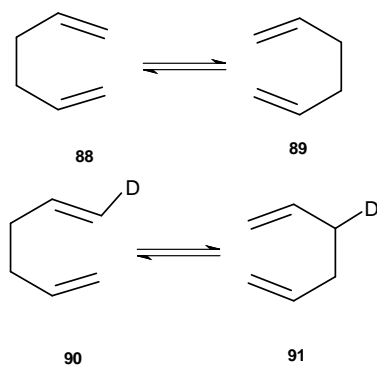
Although fenchene **71** was successfully synthesized, the anticipated complexities prompted us to abandon the approach outlined in Scheme 15 and the use of ^{13}C -labeled camphor. A new strategy involving deuterium labelling proved successful in achieving the original objective of following the reaction route, using a labelled isotopologue of the camphor derivative **67** to distinguish racemization pathways leading to the two enantiomers of camphene A **64** and camphene B **65**.

2.3 Deuterium labelling for kinetic studies

Typically, the primary concerns in chemical reactions are the isolation and identification of products. However, a more fundamental challenge involves elucidation of the reaction mechanism and the identification of reaction intermediates. NMR spectroscopy is commonly used in kinetic studies where isotope labelling aids in deciphering reaction pathways.

Deuterium labelling has been applied to norbornyl systems. For example, in a study conducted by Werstiuk *et al.*,¹²⁵ high-field ^2H NMR spectroscopy was used to investigate geminal deuterium isotope effects in 1,3,3-trimethylbicyclo[2.2.1]heptane-2-ones (fenchones). The study revealed that it is possible to use high-field ^2H NMR spectroscopy to directly obtain information on the degree of deuterium substitution and to identify chemically non-equivalent deuterons.

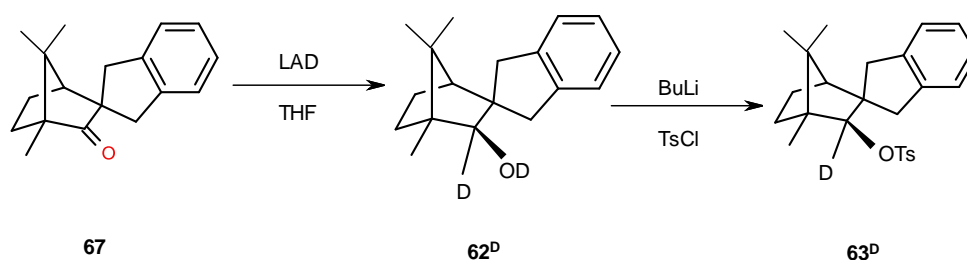
In the simple reported rearrangement¹²⁶ detailed in Scheme 22, both the reactant and the products **88** and **89** are the same. Deuterium labelling makes it possible to determine whether a reaction is taking place, and to distinguish between the two isotopomers in the NMR spectrum that would otherwise be chemically equivalent (since the deuterated analogues **90** and **91** are clearly different). Although the possibility of kinetic isotope effects was anticipated, these effects were later ruled out by computational methods.



Scheme 22. Deuterium labelling aids in degenerate rearrangement investigation.

2.3.1 Synthesis of 2D labelled *exo*-tosyl spirocamphor systems and subsequent kinetics of decomposition

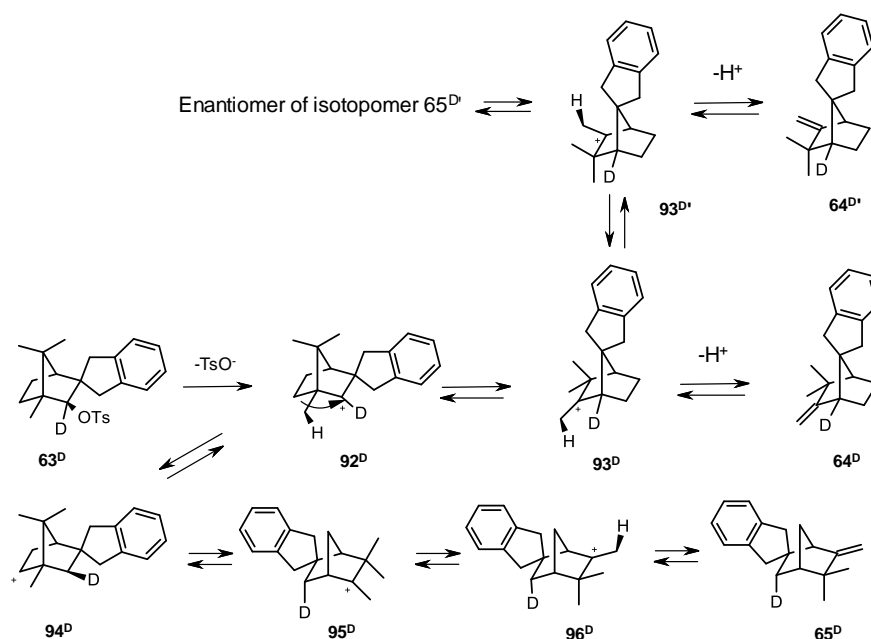
The strategy employed involved deuterium labelling at position 2 on the xylyl-substituted camphor skeleton **67** (Scheme 23). The deuterium at this position is not available for anticipated transformations and is not involved in any rate-determining step, however, its proximity to the reaction centre guided the investigation of possible kinetic isotope effects.



Scheme 23. Process of deuterium labelling.

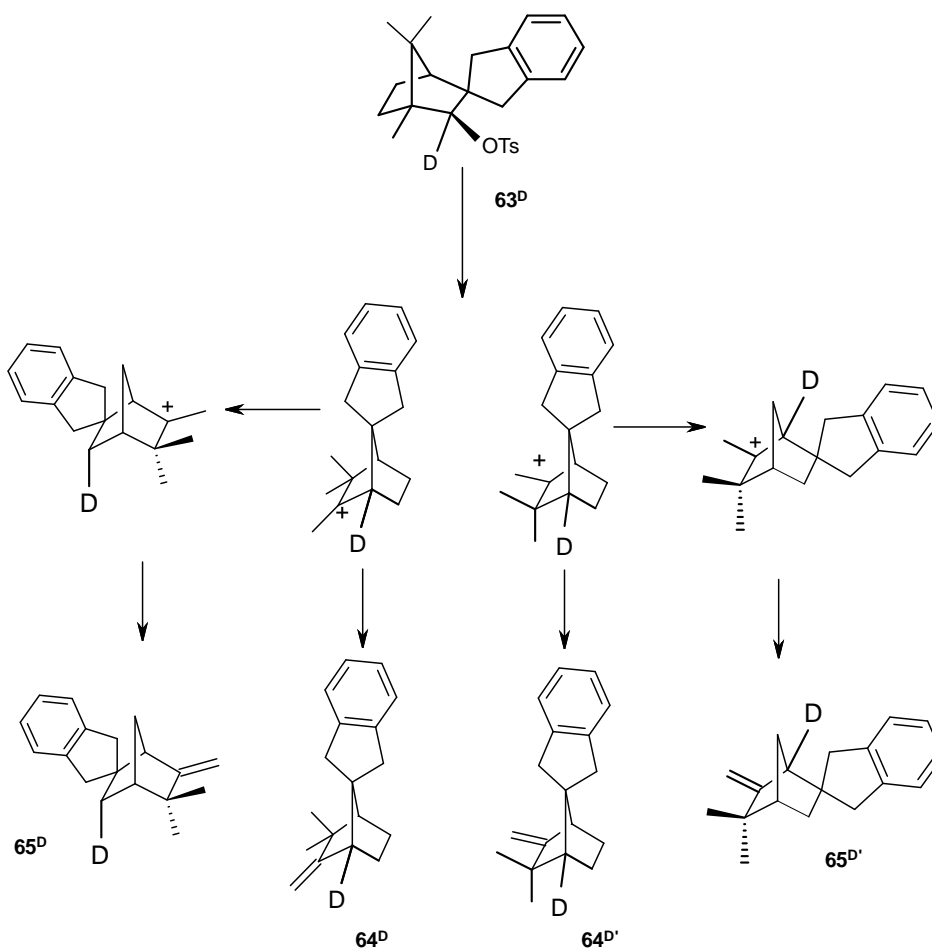
The xylyl-substituted camphor **67** was reduced with lithium aluminium deuteride (LAD) in dry THF to afford the deuterium labelled scaffold **62^D**. The alcohol was reacted with butyllithium and tosyl chloride to produce white needle-like crystals of **63^D** which served as the precursor for the kinetics study. This unstable product was stored at 0°C in minimal volume of ethyl acetate to minimise degradation. A standard was not used in this study, as the tosylate decomposition and subsequent rearrangements do not produce side products and the mass balance was maintained, confirming the stability of the product during the course of the kinetic study.

Scheme 24 traces the path of the deuterium label through the transformation (excluding the racemization) while Scheme 25 summarizes all deuterium labelled species that will be formed from transformations of the starting ²H labelled tosylate **63^D**. These schemes provide the rationale to distinguish and resolve camphene A (**64**) and its enantiomer, now represented by the isotopomers **64^D** and **64^{D'}**, similarly with camphene B (**65**) and its enantiomer as represented by the isotopomers **65^D** and **65^{D'}**.



Scheme 24. Mechanism rationalizing the expected position of deuterium in camphene products 64^D , $64^{D'}$ and 65^D .

The mechanism proposed involves loss of tosic acid and rearrangement to produce the carbocation 92^D , a methide shift to account for formation of the enantiomers (93^D and $93^{D'}$) at a rate slow enough for the mixture to retain optical activity, and a series of rearrangements allowing for the transformation of carbocation 92^D into intermediate 96^D . Carbocations 92^D and 94^D do not correspond to minima on the potential energy surface; the rearrangement from 93^D to 95^D ($93^D - 95^D$ or $93^{D'} - 95^{D'}$) is a highly concerted process involving a concerted Wagner-Meerwein, 6,2-hydride shift, Wagner-Meerwein process and the transformation from 95^D to 96^D ($95^D - 96^D$ or $95^{D'} - 96^{D'}$) is simply a methide shift. Loss of a proton from 93^D and 96^D accounts for the observation of the product camphenes 64^D and 65^D respectively. Dissociation of the tosylate (93^D) to form carbocation 92^D (Scheme 24) results in the production of tosic acid. It was previously determined¹¹³ that in $CDCl_3$ autocatalysis occurs as the dissociation is in fact catalysed by the tosic acid.



Scheme 25. Summary of deuterated products expected from transformations of the ²D labelled substrate.

This is a very straightforward system to work with, in that the decomposition of tosylate and the corresponding transformation and racemization processes can be observed *via* both ¹H and ²H NMR spectroscopy, and it occurs within a convenient timescale between 25°C and 55°C. Ultimately, the ²H NMR spectroscopy was used in a qualitative manner and not to calculate the concentrations of any species. Hence, default NMR parameters were used to acquire the ²H spectra, the T1 relaxation time for the deuterium was not measured, and the delays (in particular d1) were not optimized.

The labelled tosylate **63^D** was dissolved in bulk 5 mL CDCl₃, evenly distributed into NMR tubes and stored in dry ice to minimise degradation. Each sample could then be warmed to room temperature, placed into the NMR spectrometer at the required temperature and data collection could begin with a very short delay. It was noted that degradation to form products did occur faster at the higher temperatures, as expected. Therefore, ¹H and ²H NMR spectra

had to be acquired in shorter time intervals compared to the lower temperatures. The ^2H NMR spectra acquired at time intervals (Figure 39) clearly show the decomposition of the initial tosylate **63^D**, as observed by disappearance of the 2-*endo*-D signal at approximately 4.4 ppm, the formation of camphene A **64^D** (as seen by the deuterium at position 1 on the bornyl skeleton at 2.3 ppm), its racemization to **64^{D'}** (which moves the deuterium to position 4 and is seen at 1.5 ppm), and the subsequent formation of the major final product camphene B **65^D** (1.7 ppm) and the minor enantiomer of the isotopomer of camphene B **65^{D'}** (2.4 ppm) as a function of time.

Only ^1H data was used for further analysis and to obtain concentrations of all species involved (tosylate **63^D**, camphene A **64^D**, camphene A' **64^{D'}**, camphene B **65^D** and camphene B' **65^{D'}**). The ^1H spectrum was integrated according to regions illustrated in Figure 41. From these integrations, it was possible to calculate all individual concentrations at each time point during the kinetic runs. In some cases, it is possible to calculate concentrations of a single species or group of species from different integral information, and this was used to confirm the quality of the experimental data. Analysis of the kinetics data (Figure 40) shows the autocatalytic decay (or combination of first/second/third order decay) is observed together with the formation of all camphene species. Note that the leaving group, the TsOH, saturates at 0.21 M concentration at 318K and saturates at different concentrations for each temperature.

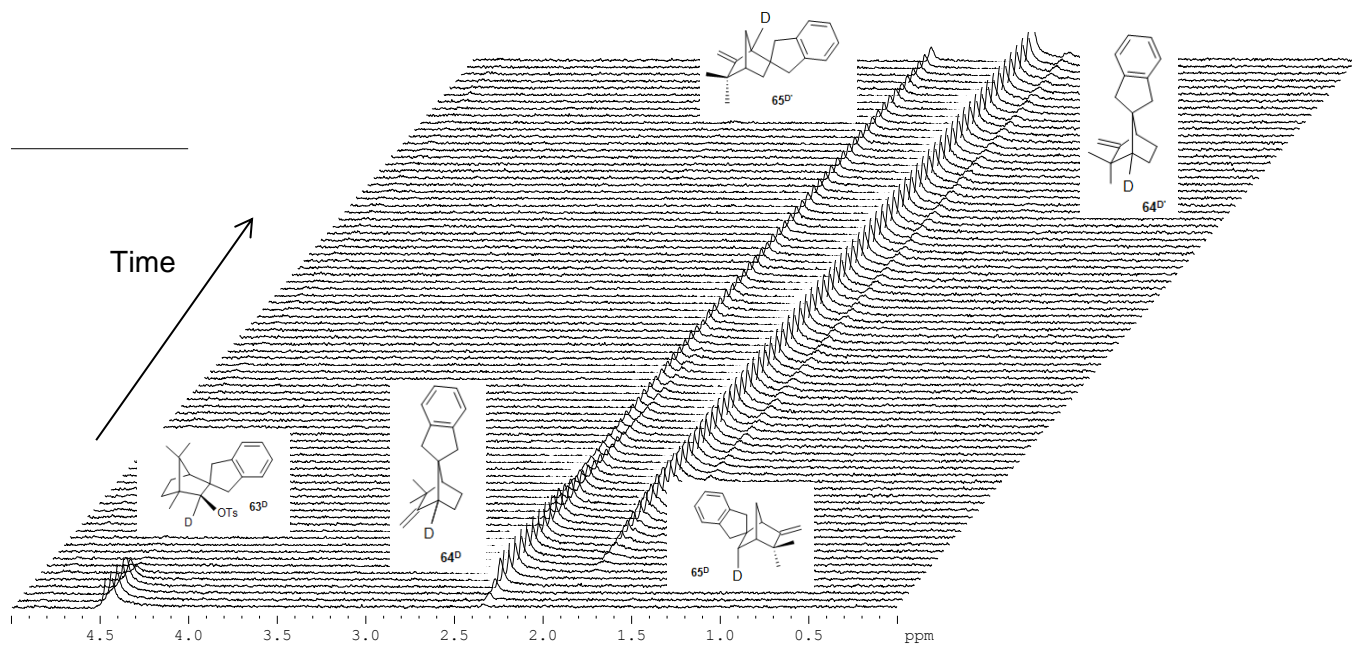


Figure 39. Stacked plot of 92 MHz ^2H NMR spectra showing the decomposition of tosylate and rearrangement products at 313 K in CDCl_3 . The disappearance of the 2-*endo*-D signal from the tosylate **63^D** corresponds to the appearance of the deuterium at position 4 on **64^D**. Signals from **64^{D'}**, **65^D** and **65^{D'}** are apparent in these spectra.

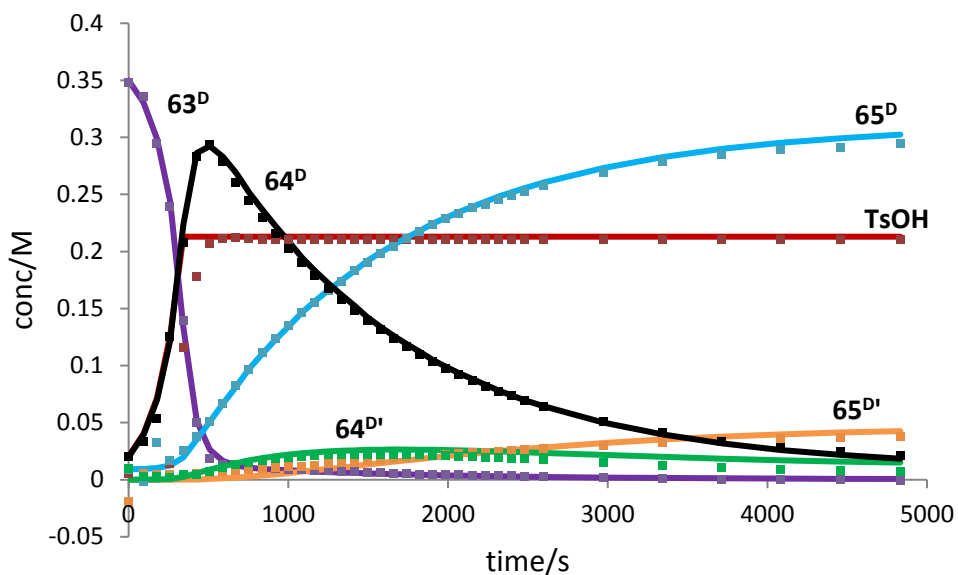


Figure 40. Molar concentration of all species in the decomposition of 63^D at 318 K derived from 1H data. The experimental data (points) are overlaid with the theoretical fit (lines).

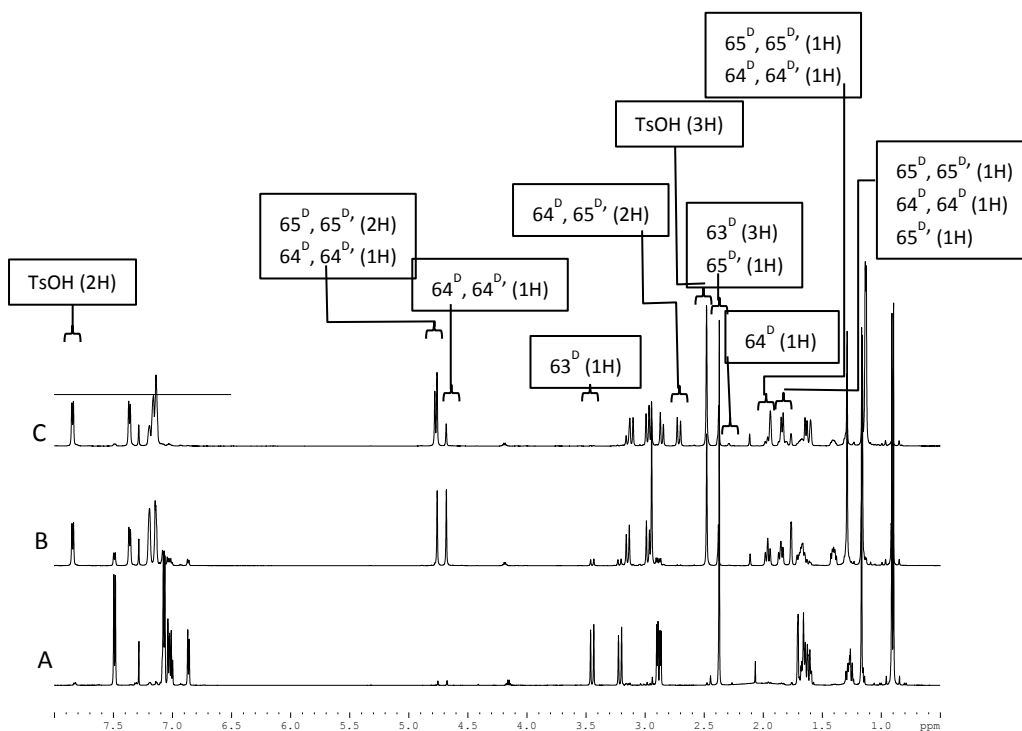
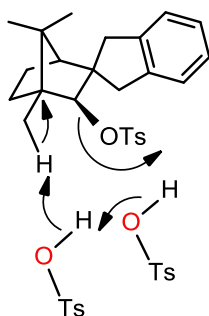


Figure 41. Integral regions used to calculate the concentrations of all species during the kinetics runs.

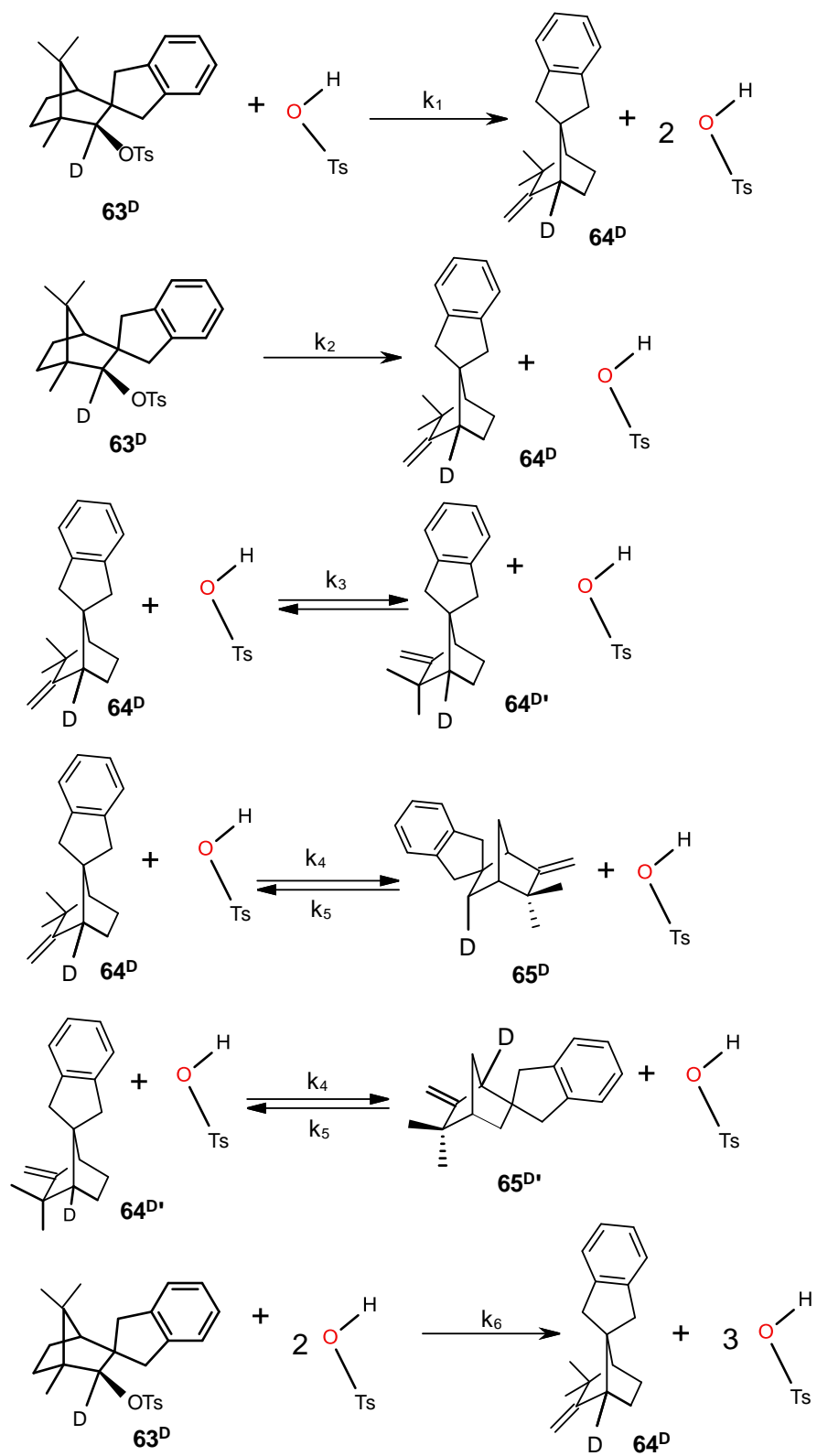
In Figure 41 three spectra from different time points during the 318 K kinetic run are shown. (A) is at the beginning of the kinetics run and consists predominantly of the tosylate **63^D** as seen by the presence of a proton at 3.5 ppm and signals in the aromatic region. (B) represents a spectrum further on into the kinetics run, consisting mainly of **64^D**, indicated by peaks between 4.7-4.8 ppm, before significant transformation to **65** and racemization. The appearance of the signal at 7.8 ppm is important to note, showing the formation for the tosic acid and (C) at the end of the run, where most of **64^D** has transformed into the second camphene product with alkene hydrogens around 4.8-4.9 ppm. The intensity of peak used to monitor the tosic acid had remained constant between B and C, signifying the saturation of the acid.

2.3.2 Determination of the rate law for the competing racemization in the rearrangement of a xylyl-substituted camphene

Considering the kinetic data retrieved according to the integration regions in Figure 41, and algebraic manipulation to offer the exact concentrations of the six species, we decided to investigate rate laws for all possible transformations, including relevant reversible transformations. From the rate expressions derived for the transformations summarised in Scheme 27, theoretical concentrations can be obtained using the initial concentrations of all species and numerical (Euler) integration of the series of differential equations for the proposed mechanistic steps. By varying the values of individual rate constants k_1 - k_6 , a theoretical concentration vs. time graph for the predicted model was obtained, in which the theoretical fits (Figure 40-solid lines) achieved for all species follow the experimental data (Figure 40-dots) closely. One important factor to note is the governing role played by the tosic acid (TsOH) during the rearrangement process. The presence of the tosic acid was a complicating factor in the kinetic analysis due to its relative insolubility in CDCl_3 , but it is required for autocatalysis to occur and therefore had to be accounted for in the theoretical fit. A third-order decomposition was also included according to the mechanism in Scheme 26.



Scheme 26. Formation of camphene **64** directly from **63** via a third order process.



Scheme 27. All possible processes involved in rate determination following decomposition of tosylate.

2.3.3 Kinetics analysis

The transformation was followed using ^1H and ^2H NMR spectra, although only the ^1H data was used for further analysis. All kinetic runs were conducted in CDCl_3 . The spectra were acquired on a 600 MHz Bruker Avance III spectrometer with a constant delay between the acquisitions of the individual 1-D spectra. For detection a broadband inverse detect probe was used for which temperature calibration data was available. The observations were repeated at different temperatures. The integration regions identified in Figure 41 were seen as crucial in collecting as much data on the transformations as possible. During analysis more than one integral region could be used to confirm the concentration of a particular species. One factor taken into account upon integration of selected regions is that the integration region itself should be wide enough to accommodate signal drift (resulting from temperature fluctuations as well as a change in the reaction medium) as the reaction proceeds (the system becomes very acidic during the course of the reaction as tosic acid is produced, and the tosic acid OH has a chemical shift that becomes successively deshielded as this acidity increases), yet simultaneously be narrow enough that accuracy is not lost. Concentration trends at all temperatures were similar to that observed at 318 K in Figure 40; the deuterated tosylate at an initial concentration 0.35 M decomposes until 0 M, and this decay is almost mirrored in the formation of the tosic acid until saturation is reached at 0.21 M. The tosic acid is involved in several second-order processes, resulting in the formation of major camphene products (**64^D** and **65^D**). We observed camphene **64^D** to increase quite rapidly until approximately 500 s whereupon **64^D** then rearranges and decreases, gradually resulting in the steady formation of camphene **65^D**. For a good theoretical to experiment fit, the reversibility between camphene products **64** and **65** had to be taken into account. It was also noted that racemization occurring upon camphene **64^D** formation. Minor racemization products followed a similar trend to the major products as **64^D** reached a maximum concentration of 0.022 M.

Table 7. Determined rate constants for the processes in Scheme 25.

T(K)	k_1^a	k_2	k_3	k_4	k_5^b	k_6	k_7
314.04	2.52E-06	1.35E-04	0.000341	0.002498	0.000108	0.110611	0.000392
319.81	ND	4.42E-04	0.000736	0.00318	ND	0.239201	0.001934
325.28	ND	7.46E-04	0.000717	0.003885	0.000162	0.547727	0.00457
331.17	ND	2.50E-03	0.001432	0.005731	0.000346	0.600528	0.004641
Process	63 +TsOH → 64 +2TsOH	63 → 64 +TsOH	64^D +TsOH → 64^D +TsOH	64 +TsOH → 65 +TsOH	65 +TsOH → 64 +TsOH	63 +2TsOH → 64 +3TsOH	64 +TsOH → 63
Units	$\text{M}^{-1}\text{s}^{-1}$	s^{-1}	$\text{M}^{-1}\text{s}^{-1}$	$\text{M}^{-1}\text{s}^{-1}$	$\text{M}^{-1}\text{s}^{-1}$	$\text{M}^{-2}\text{s}^{-1}$	$\text{M}^{-1}\text{s}^{-1}$

^a Since the decomposition of **63** is fast at high temperatures, it is not possible to reliably determine k_1 in these cases due to fewer data points. ^b k_5 is a small contributor in the process from **64** to **65** (involving k_3 , k_4 and k_5) and also is not determined reliably.

During the theoretical fit, the concentration of TsOH was allowed to reach the maximum level observed experimentally for each temperature. It was noticed that the autocatalytic decay did not perfectly match first or second order decomposition, nor was it a combination of the two. However, the addition of a supplementary third order component for the decomposition of the tosylate resulted in better matching of the theoretical to the experimental data. This finding may be attributed to a Grottuss-type mechanism (Scheme 26) for the transfer of a methyl proton to the oxygen of the leaving group, mediated by two TsOH molecules. Therefore, since the tosic acid played such a determining role in the overall decomposition, the third order (k_6) and first order (k_2) rates were allowed to govern the kinetic model for the tosylate decay. The reverse first order (k_7) was used as a means to prolong the presence of the tosylate even long after autocatalysis was complete. During the determination of the second order decomposition (k_1), the major problem encountered was that the required data could only be collected during the lower temperature kinetics runs, decomposition preceded too fast at the higher temperatures and too few data points were collected for a reliable determination of k_1 . At the later stages of the process, we see that the tosic acid is still very much involved in the rearrangement from camphene **64^D** to **65^D** (k_4) as well as in the formation of the minor racemization products **64^D** to **64^{D'}** (or **64^{D'}** to **64^D**). The reverse reaction rate (k_5) did improve the overall fit in some cases, but was not a significant overall contributor. Scheme 27 provides details of all steps used for theoretical data fits; most reaction rates are second order, highlighting the importance of the tosic acid in effecting the transformation. Once all fits were complete, Eyring plots (equation 13) were constructed to determine activation parameters ΔS^\ddagger and ΔH^\ddagger from the temperature dependence of the rate constants (Table 7 and 8).

$$\ln \left(\frac{k}{t} \right) = \frac{-\Delta H^\ddagger}{RT} + \ln \left(\frac{k'}{h} \right) + \frac{\Delta S^\ddagger}{R} \quad (13)$$

where k is the rate constant, T is temperature, ΔH^\ddagger is the enthalpy of activation, ΔS^\ddagger is the entropy of activation, R is molar gas constant, k' is Boltzmann constants and h is Plank's constant.

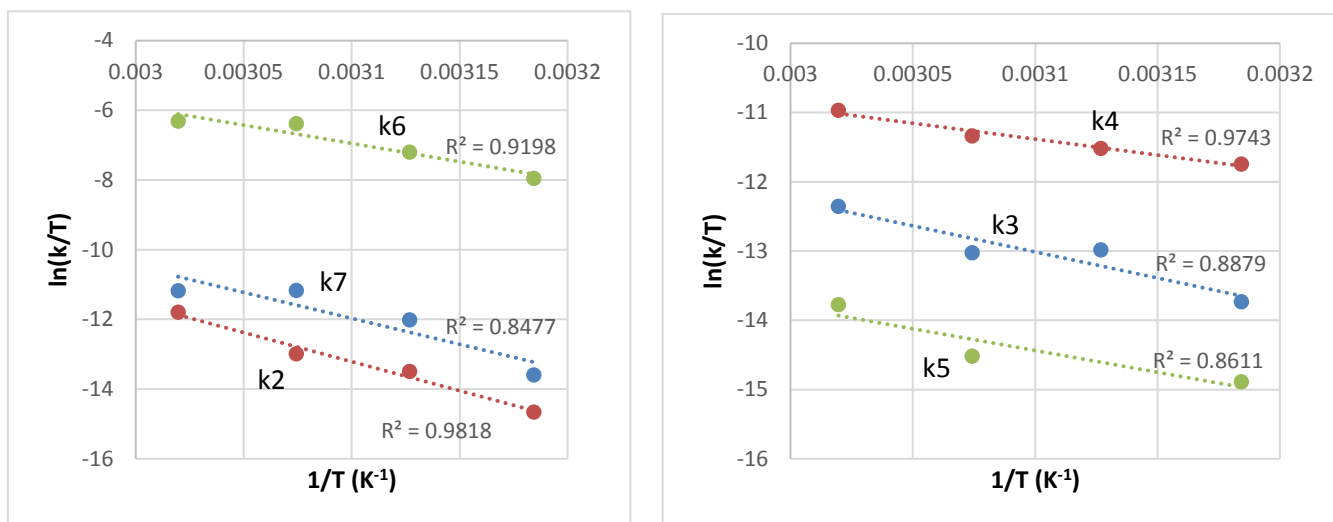


Figure 42. Eyring plots for six determined rate constants.

Table 8. Activation parameters (in kcal mol⁻¹) from the Eyring plots.

	ΔH^\ddagger (kal/mol)	Error (ΔH^\ddagger)	ΔS^\ddagger (cal/K/mol)	Error (ΔS^\ddagger)	ΔG^\ddagger (kcal/mol)	Error (ΔG^\ddagger)	E_a (kcal/mol)	Error (E_a)
k_2	33.2	7.0	29.3	21.4	24.4	13.3	33.8	7.0
k_3	15.0	3.8	-26.7	11.7	22.9	7.2	15.6	3.8
k_4	9.1	1.9	-41.5	5.8	21.5	3.6	9.7	1.9
k_5	12.5	5.0	-37.2	15.5	23.6	9.6	13.1	5.0
k_6	20.8	4.4	3.6	13.5	19.8	8.4	21.4	4.4
k_7	29.6	8.9	20.6	27.5	23.4	17.0	30.2	8.9

Overall, the experimentally determined value for ΔG^\ddagger for all processes was in the range 9-33 kcal mol⁻¹. ΔG^\ddagger for k_2 and k_7 were both in agreement with a previous study¹¹³ of ca. 24 kcal mol⁻¹, as was the transformation of **64**^D-**65**^D from ΔG^\ddagger for k_4 was determined to be 21.5, compared to previous results of 21.7 and 22.6 kcal mol⁻¹.

As the deuterium labelled system matches the experimental results of the previous study conducted with an unlabelled system, it is safe to say that no kinetic isotope effects were observed, and that the deuterium was not involved in the known transformations. Deuterium labelling at C-2 was successful and did not interfere with the rate of the decomposition and rearrangement processes.

2.3.4 Theoretical studies:

Based on the proposed mechanism (Scheme 24) and proceeding transformations, models of all likely camphene products were constructed, and as these transformations tend to involve carbocation intermediates, our models included possible intermediates (taking into both conformations of the xylyl-five membered ring). The theoretical study undertaken entailed geometry optimization, together with frequency analysis of all products and intermediates, done at the B3LYP/6-31+G(d,p) level of theory. As the study involved deuterium labelling, isotopes for each species had to be taken into account to prove or disprove a measurable kinetic isotope effect, and to be able to compare results to the previous study where racemization was unaccounted. The electronic energies for the pairs of isotopomers were expected to be equal, such that for each of **64^D** and **64^{D'}** there are two conformations and like conformations of **64^D** and **64^{D'}** are compared. Slight differences however were observed in the sum of electronic and thermal energies at 298 K (Table 9). The transition states for each of the unimolecular rearrangements proposed by the mechanism were also calculated at the same level of theory (Table 10). The largest difference in transition state is that for the highly-concerted rearrangement in which the 0.1 kcal mol⁻¹ difference may be attributed to the proximity of the heavier deuterium to the 2-C atom that is highly involved in the transition state. This results in an increase in free energy of activation for the transformation **93^D** to **95^D** of 0.1 kcal mol⁻¹, relative to the corresponding transformation of **93^{D'}** to **95^{D'}**. Given the errors in determination of activation parameters this kinetic isotope effect is negligible. Comparing the experimental and theoretical values it may be seen that ΔG^\ddagger (at 298 K) for k_3 (racemization of both conformers of **93^D** – **93^{D'}**) match within experimental error. (22.9 ± 7.2 kcal mol⁻¹ experimental vs. 19.75 kcal mol⁻¹ theoretical). Similarly, the ΔG^\ddagger (at 298 K) for k_4 (**64-65**) of 21.5 ± 3.6 kcal mol⁻¹ matches the highest energy barrier for the two-step transformation **93^D**-**95^D**-**96^D** (22.33 and 17.74 kcal mol⁻¹) or **93^{D'}**-**95^{D'}**-**96^{D'}** (22.23 and 13.73 kcal mol⁻¹). This suggests that the required protonation of the camphenes must involve a negligible energy barrier.

Table 9. B3LYP/6-31+G(d,p) level ΔG for intermediates and products (kcal mol⁻¹).

Structure	Conformer A (isotopomer a)	Conformer A (isotopomer b)	Conformer B (isotopomer a)	Conformer B (isotopomer b)
64 ^a	4.05	4.06	7.10	7.11
65 ^a	0.01	0.00	0.22	0.23
93 ^b	4.09	4.09	8.16	8.15
95 ^b	4.26	4.24	7.34	7.32
96 ^b	0.00	0.00	0.48	0.48

^a ΔG relative to lowest energy conformation/isotopomer of **65**^b ΔG relative to lowest energy conformation/isotopomer of **96**Table 10. B3LYP/6-31+G(d,p) level transition states energy ΔG relative to **93**^D (kcal mol⁻¹)

Transition States	ΔG
93 ^D - 93 ^{D'} <i>exo</i> -methide shift (A)	19.75
93 ^{D'} - 93 ^D <i>exo</i> -methide shift (B)	19.75
93 ^{D'} - 95 ^{D'} WM-6,2-hydride-WM	22.23
93 ^D - 95 ^D WM-6,2-hydride-WM	22.33
95 ^{D'} - 96 ^{D'} <i>exo</i> -methide shift	13.73
95 ^D - 96 ^D <i>exo</i> -methide shift	13.74

2.4 Conclusion of the Kinetic Mechanistic Studies

The attempted synthesis of a ¹³C labelled spirobornyl tosylate has in onestep produced a novel difenchyl sulfite. This sulfite presents as diastereomers, and inversion of the sulfur centre has been observed. Modelling, various NMR techniques and elemental analyses all support the assignment of this product as a sulfite rather than a dimeric ether. The kinetics of formation of this sulfite are in agreement with a proposed rate law. Activation parameters for this formation have not been determined but the difference in free energy between the diastereomers has been determined *via* variable temperature NMR studies. Flaws in the proposed ¹³C labelling synthetic scheme have been revealed, including the remarkable reactivity of the spirobornyl system in strongly basic media. A change in scheme to ²D labelling has allowed for the study of the rearrangement mechanism for the decomposition of **63**^D and the activation parameters for all steps are now known, including that for the racemization. The modelling data are in good agreement with the experimental data.

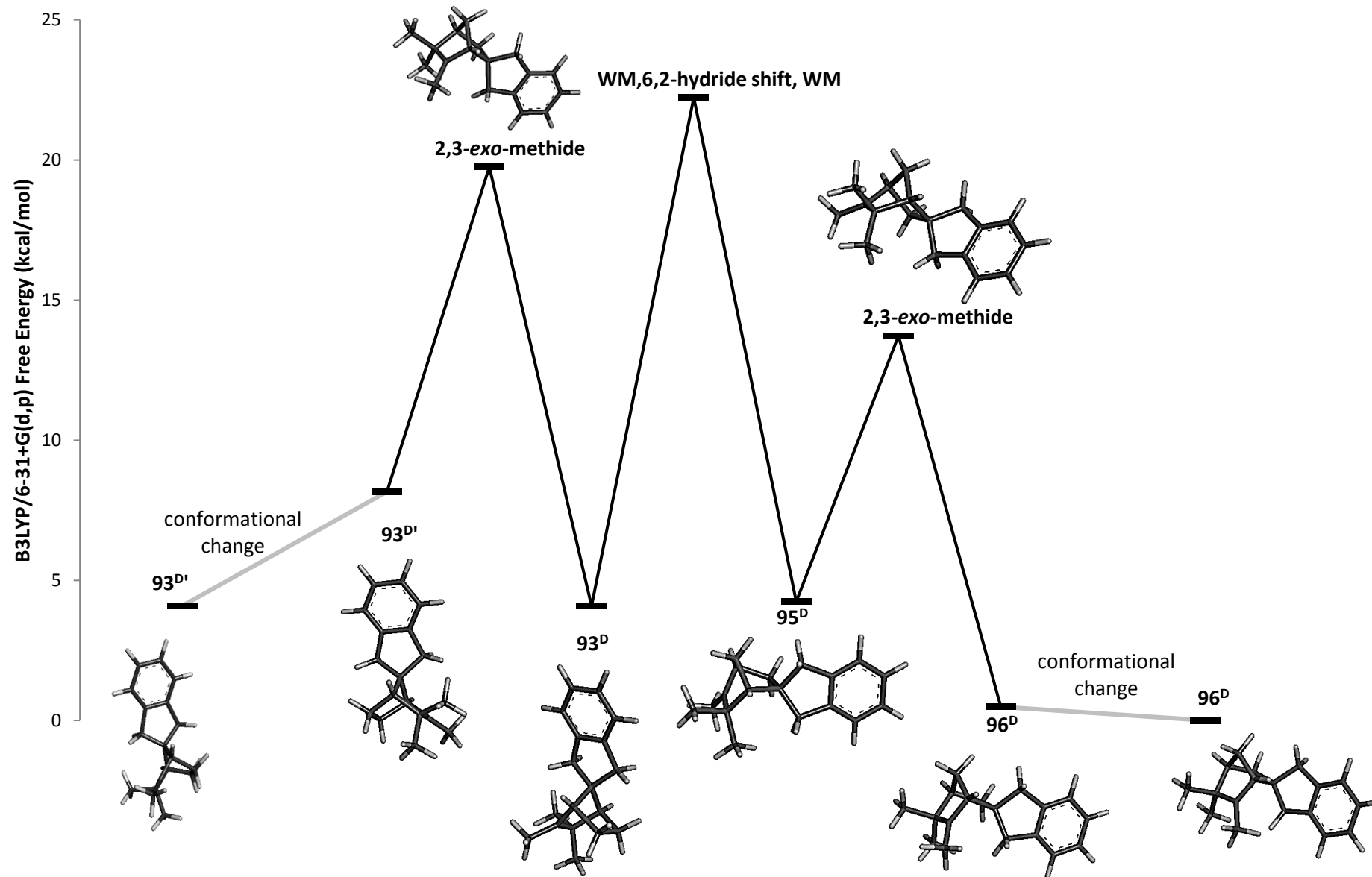


Figure 43. B3LYP/6-31+G(d,p) potential energy surface for the transformation from 64^D to 65^D including racemization.

Discussion - Structure

3 Camphor and fenchone in the formation of chiral surfactants for the generation of chiral micelles. The chiral influence of the substituted norbornyl systems

3.1 Synthesis of surfactants

As discussed in the introduction, bicyclohept[2.2.1]yl derivatives, namely camphor **1** and fenchone **3**, have been used in research as chiral auxiliaries in asymmetric synthesis. The current part of this study focuses on fenchone/fenchol-derived surfactants for the formulation of chiral micelles.

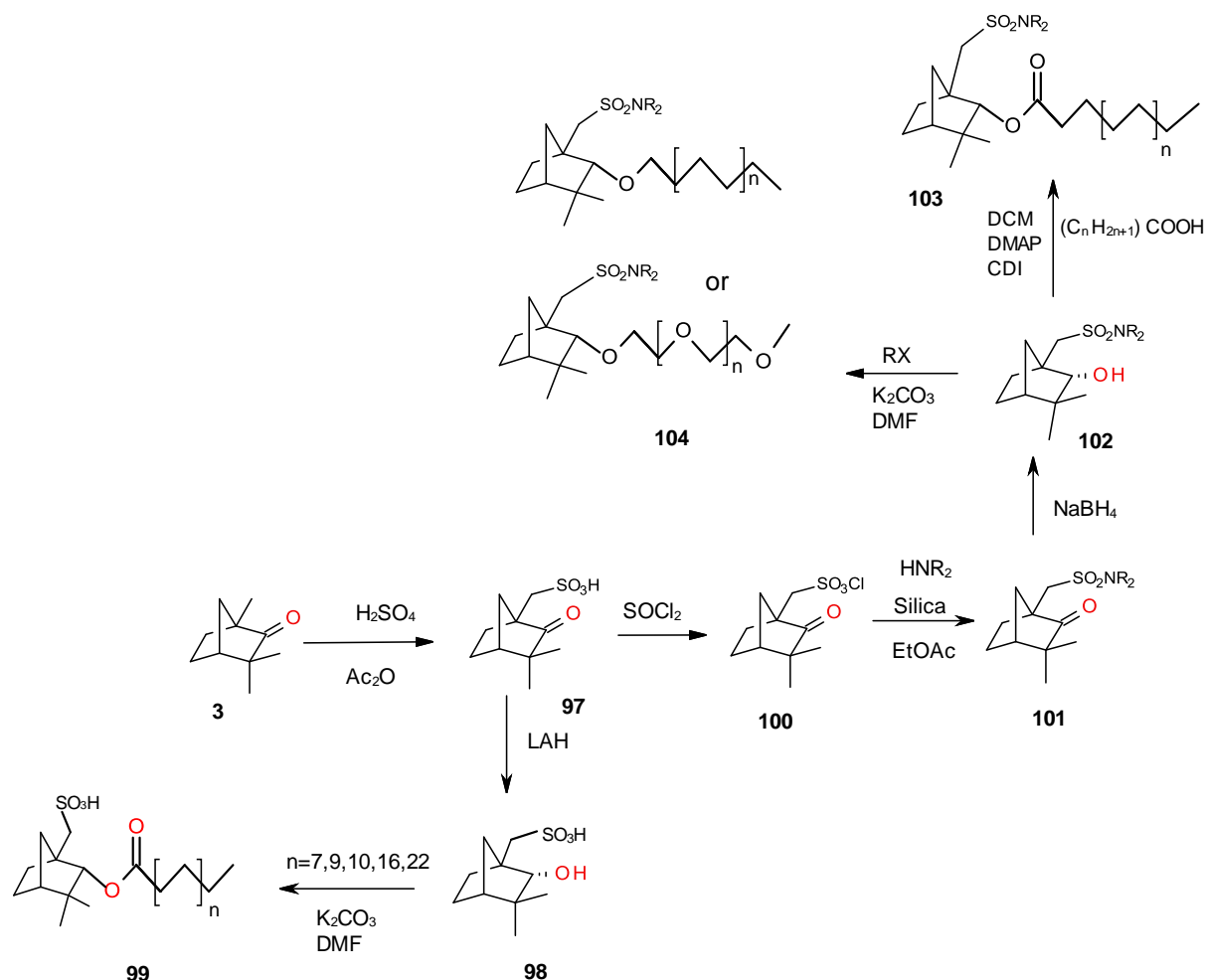
It was hypothesized that the incorporation of fenchone (or a derivative of fenchone) would allow for the introduction of chirality to the environment in proximity to the micelle.

Micelles may provide an environment where reaction acceleration is observed due to increased concentration and availability of substrate at the chiral interface. Part of the effect may be due to a “pseudophase” of the micelle that allows for solubilization and concentration of the more hydrophobic reactants.¹⁵⁶ When the micelle also catalyzes the reaction these systems may be very successful. A good example of this is the 106-fold increase in reaction rate observed by Otto *et.al.*¹⁵⁸ in which micelles composed of the anionic surfactant copper didodecyl sulfate catalyzed a Diels-Alder process between cyclopentadiene and a series of substituted vinylic ketones - the phenyl-1-(2-pyridyl)-2-propen-1-ones. In this particular case the availability of the copper center at the surface of the micelle meant extremely efficient catalysis of the reaction by the micelle. The Diels-Alder reaction between cyclopentadiene and *N*-ethylmaleimide has also been successfully mediated by reverse micelles in a water in oil environment.¹⁵⁸

Chiral surfactants forming chiral micelles have been successfully used in chiral resolution,¹⁵⁹ or as a form of a chiral shift reagent in NMR.¹⁶⁰ There has been some progress in the use of these as a chiral environment and for catalysis in asymmetric synthesis. Examples include the synthesis of oxiranes using chiral micelles composed of *N*-hexadecyl-*N,N*-dimethyl ephedrine bromide,¹⁶¹ in which a 57% diastereomeric excess was reported. the asymmetric reduction of ketones using chiral sulfonamide-derived surfactant systems with a 95% enantiomeric excess,¹⁶² and the Diels-Alder reaction of cyclopentadiene and nonyl acrylate using a (*L*)-leucine-derived surfactant, yielding up to 15% enantiomeric excess.⁹⁷

Part of the envisaged synthetic scheme was to have access to two different types of surfactants for the creation of both normal and reverse micelles, within the context of a two-solvent system. As part of on-going research within our group, Morita-Baylis-Hillman reactions play a large role, which are well known for long reaction times and relatively low yields, with products that are racemic mixtures.⁴⁰ Therefore an anticipated application was that the micelle could be used for catalytic purposes concerning the Morita-Baylis-Hillman reaction, as a substitute for the employment of the common nitrogen-based catalyst DABCO. This would serve two purposes – the micelle would provide both the catalysis and the chiral environment for asymmetric catalysis of the Morita-Baylis-Hillman reaction. Hence, the choice of substituent on the bicyclic system was a series of amides. Scheme 28 gives direct access to six different classes of chiral surfactants for the use in the generation of normal and reverse chiral micelles.

In Scheme 28 fenchone **3** undergoes sulfonation to fenchonesulfonic acid **97**. This may be reduced to the fenchol derivative **98** and then used to produce the series of esters **99**. Alternatively, the sulfonyl chloride **100** may be used to synthesize the series of amides **101**, which are then to be reduced to the fenchol derivative **102**, followed by formation of a series of esters with nonpolar tails **103** or ethers with polyethylene glycol tails, **104**.

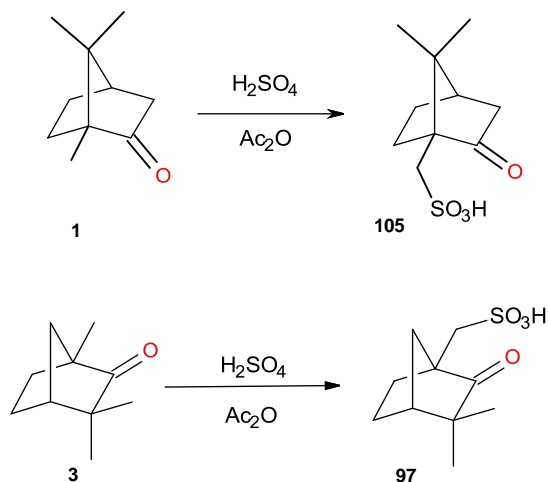


Scheme 28. Proposed reaction scheme for synthesis of normal and reverse surfactants.

3.2 Synthesis of fenchone derived sulfonamides

The initial step in the synthesis of both normal and reverse surfactants was to prepare commercially unavailable 10-fenchesulfonic acid **97** from fenchone **3**. Sulfonation of the bridgehead methyl group of fenchone was achieved using the Reychlers acid method¹²⁷ which is commonly used for the synthesis of 10-camphorsulfonic acid **105** from camphor **1** (Scheme 29). The fenchone was sulfonated with concentrated sulfuric acid (H_2SO_4) in acetic anhydride at room temperature for 72 h. However, yields did not exceed 42%. Attempts to optimize this reaction included, 1) after addition of sulfuric acid the reaction mixture was heated, 2) the original reaction method was used, and left to stir for a week at room temperature, however in neither case was any improvement in the yield obtained. The product, although insoluble in many organic solvents, was soluble in $\text{DMSO}-d_6$ and could be characterized by NMR spectroscopy. The ^1H NMR spectra of the sulfonated fenchone (Figure 44) shows the presence of only two unresolved methyl groups, as a singlet at 1.05 ppm, as opposed to the three methyl groups visible in the spectra of the fenchone **3** starting material. The presence of

two pairs of doublets corresponding to the nascent diastereotopic protons appear at 2.76 and 2.92 ppm. The product was of high purity and thus no further purification steps were taken.



Scheme 29. Synthesis of Reychlers acid **105** and of 10-fenphone sulfonic acid **97**.

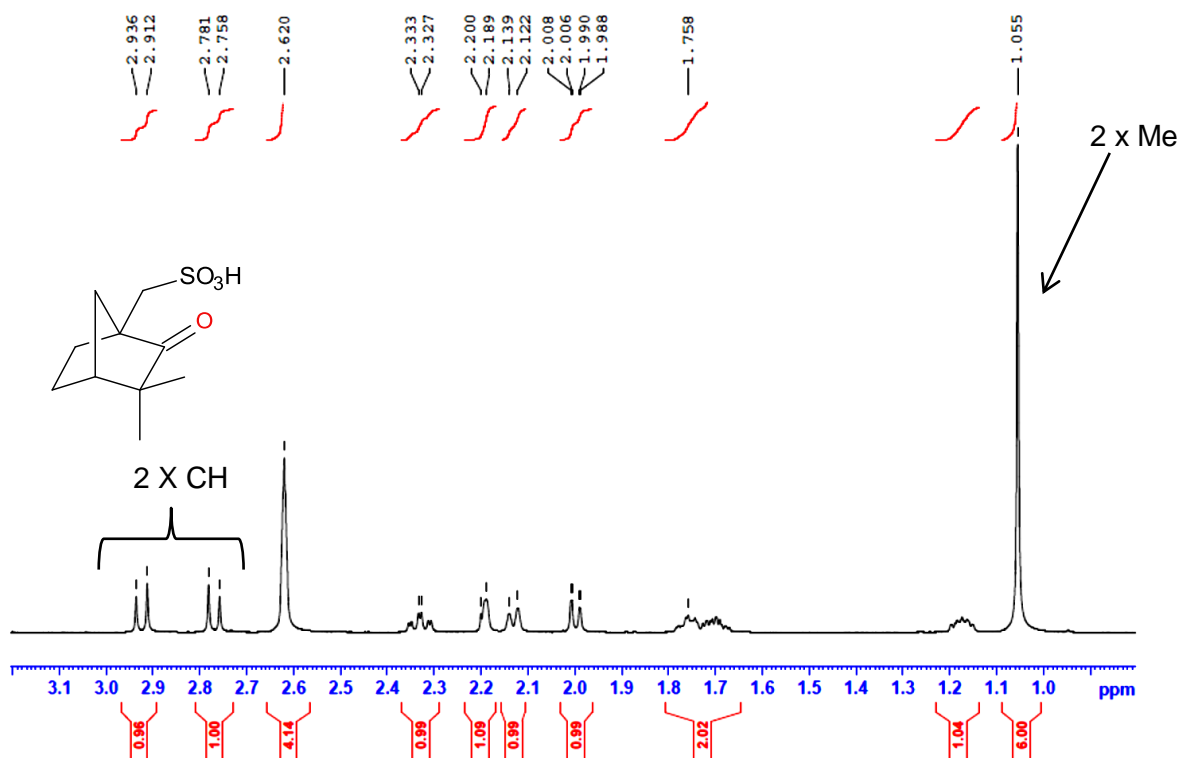
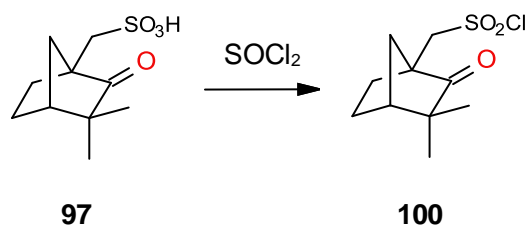


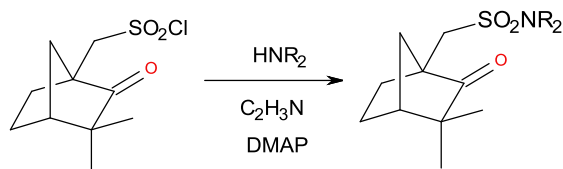
Figure 44. ^1H NMR spectrum of 10-fenphonesulfonic acid **97** (600 MHz, $\text{DMSO}-d_6$).

This sulfonic acid **97** was used directly in the second stage of the scheme to form the 10-fenchonesulfonyl chloride **100**, also a commercially unavailable precursor (Scheme 30).

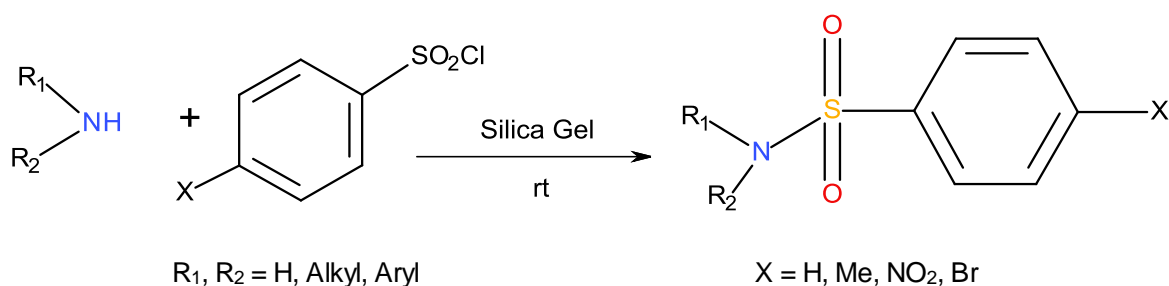


Scheme 30. Synthesis of commercially unavailable 10-fenchonesulfonyl chloride.

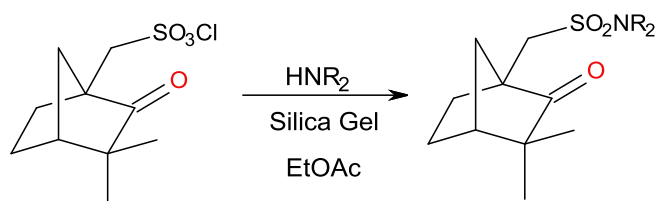
It was intended that the “head” region of surfactants for reverse micelles be constructed as fenchol-derived sulfonamides. Thus, a series of secondary amines were used to modify the head region for the surfactants. The first procedure (Scheme 31) followed was similar to that previously used by a member of the research group to convert 10-camphorsulfonyl chloride into camphor sulfonamide derivatives.¹²⁸



Scheme 31. First method for synthesizing sulfonamides.¹²⁸



Scheme 32. Method for synthesis of sulfonamides reported by Jafarpour *et al.*¹²⁹



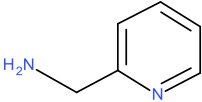
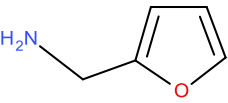
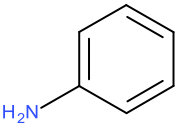
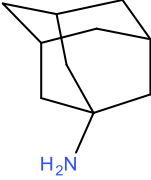
Scheme 33. Modified method for the synthesis of sulfonamides.

Procedure 1 (Scheme 31) entailed a reaction between the fenchonesulfonyl chloride (limiting reagent) and a series of amines (Table 11), in two equivalent excess in acetonitrile with DMAP at 0°C, under nitrogen for one hour. The procedure was tested on a reaction between the fenchonesulfonyl chloride and aniline (sterically and chemically considered the least complicated amine out of the chosen series), the reaction was followed using thin layer chromatography (TLC), and product formation was only observed after the reaction was left to stir overnight at room temperature, with a yield of 62%. A silica column was used for purification and the final yield of the isolated aniline derivative was 43%. A similar result was obtained for the other amines, but those with more sterically hindered moieties, such as 1-adamantylamine, had longer reaction times and lower yields.

In an attempt to find more efficient reaction conditions, a study by Jafarpour *et al.*¹²⁹ was considered (Scheme 32) where sulfonamides had been synthesised under mild and solvent-free conditions with silica gel offering catalytic assistance. The solvent free reaction method was followed as reported, but no reaction occurred, with the ¹H NMR spectrum showing the presence of only starting materials. Considering the steric bulk of both the fenchonesulfonyl chloride scaffold and the secondary amine, a second modified method was attempted, where ethyl acetate (EtOAc) was added in with the reaction mixture (Scheme 33). EtOAc was used as a solvent to ensure all materials were sufficiently dissolved. Considering these two factors, it was hoped that rates of reactions would increase, as well as product yields. Silica gel proved to be effective for catalytic purposes, owing to its uniform, large surface area (5-800 m² g⁻¹) and high porosity.¹³⁰ Silica-catalysed reactions are advantageous owing to its mild reaction conditions and high regioselectivity. The silica catalysed method was used for all sulfonamide syntheses, with advantages related to availability, inexpensiveness, and easy workup.¹³¹ It is interesting to note that Procedure 1 was conducted under dry conditions and was less

successful than the second, which used hygroscopic silica gel under atmospheric conditions. The reaction of the fenchonesulfonyl chloride with aniline was monitored with TLC and reached completion within approximately 45 min. Work-up entailed filtering off the silica gel and removal of the ethyl acetate. In this figure the diastereotopic signals from the product produced in both methods are evident. However, the diastereotopic signals from the sulfonyl chloride are not present in the crude mixture from the silica-mediated process. No further purification was required and the aniline substituted fenchone gave the product in 93% yield. Similar results were observed with other amines, with maximum reaction times being 2 h with excellent yields (Table 11).

Table 11. Amines used in the synthesis of the fenchone-derived sulfonamides **101**, and yields using methods 1 and 2.

Compound	Amine	Structure	Yield Method 1 (%)	Yield Method 2 (%)
101a	Picolylamine		45	97
101b	Furfurylamine		51	93
101c	Aniline		61	93
101d	Adamantylamine		51	72

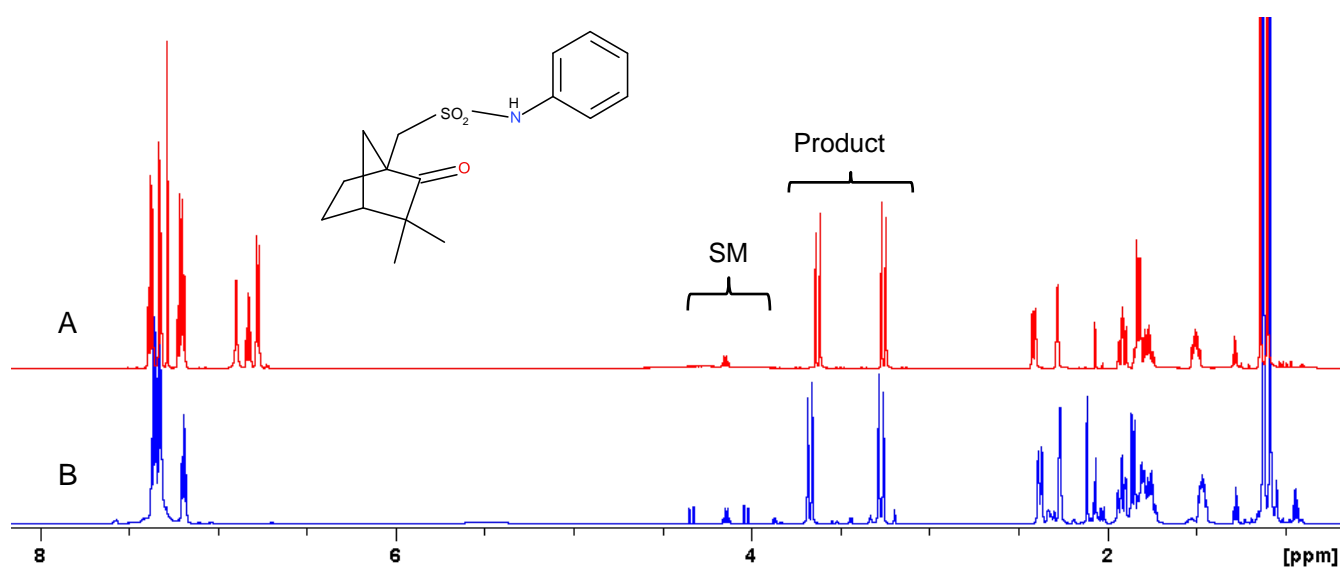


Figure 45. Showing ^1H spectra of crude products from both methods for sulfonamide synthesis. The aniline derived fenchone sulfonamide **101c**, from Method 1 (B) and Method 2 (A), (600 MHz, CDCl_3).

NMR 1-D and 2-D analysis of the furfurylamine-derived sulfonamide **101b** allowed for its unambiguous characterization. All the remaining products (**101a-101d**) of the series were characterized in a similar manner.

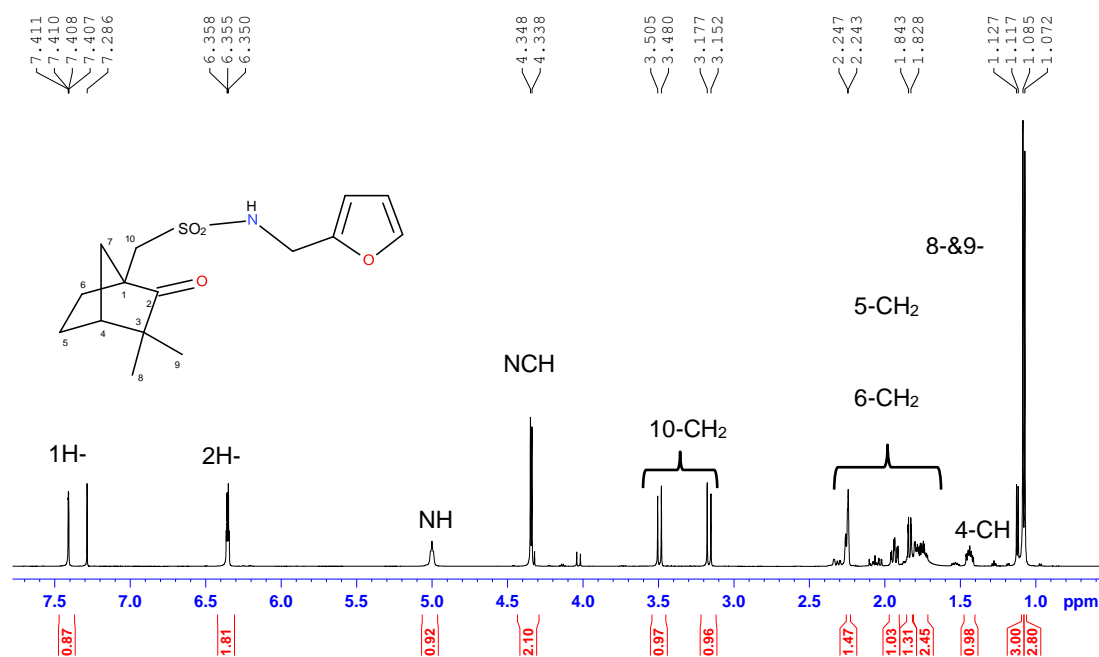


Figure 46. ^1H NMR spectrum of compound **101b** (600 MHz, CDCl_3).

In the ^1H spectrum (Figure 46) of **101b**, the diastereotopic protons are evident at 3.16 and 3.49 ppm, while the sulfonamide proton appears at 5.01 ppm. The three aromatic protons associated with the furfuryl moiety are resolved at 600 MHz as a double doublet at 7.41 ppm ($J_1 = 1.8$ Hz, $J_2 = 0.6$ Hz) and two overlapping signals at 6.26 ppm.

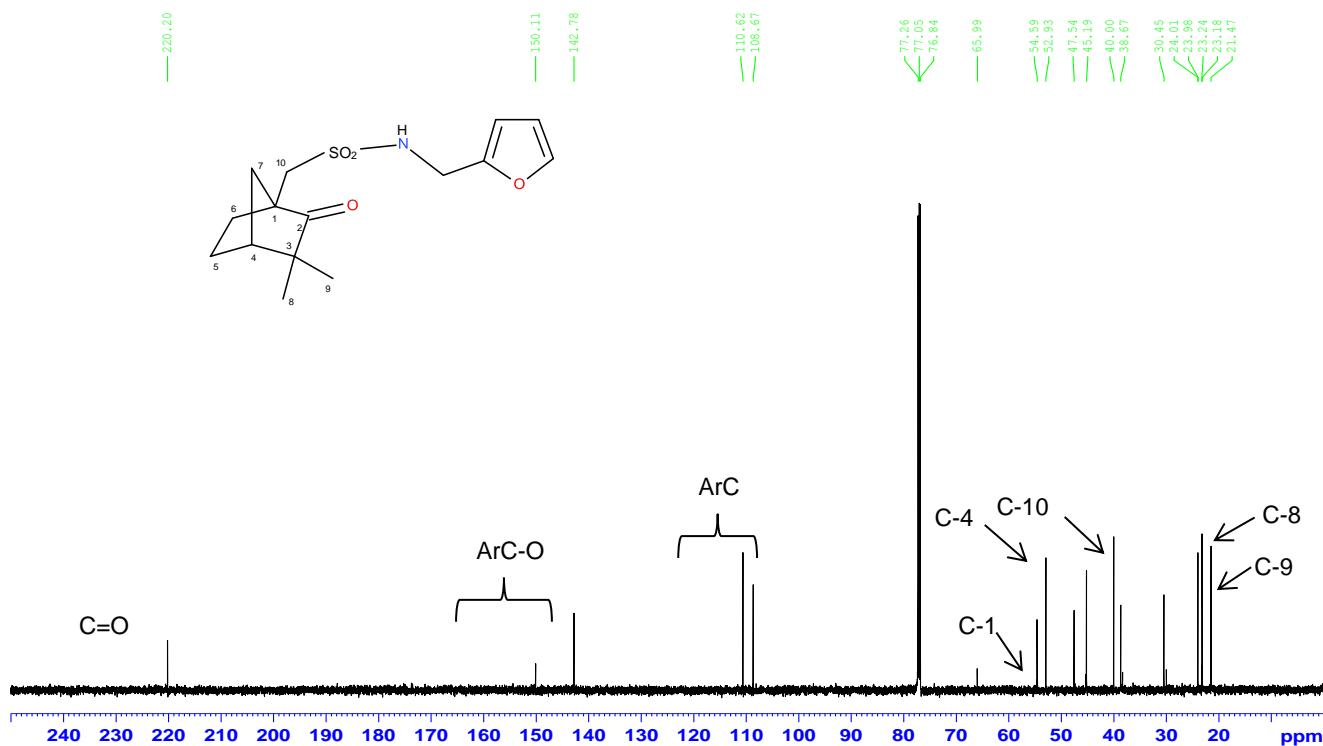


Figure 47. ^{13}C NMR spectrum of compound **101b**, (150 MHz, CDCl_3).

In the ^{13}C NMR spectrum (Figure 47), the carbons adjacent to the oxygen on the furfuryl moiety appear at 150.1 ppm (weak quaternary) and 142.7 ppm (more intense primary carbon). The carbonyl signal from the fenchone is evident at 220.2 ppm.

Although these compounds were destined for use in the generation of surfactants, the fenchone-derived sulfonamides were analogues of camphor-derived sulfonamides produced previously within the research group and for which mass spectrometry data was available. The decomposition and rearrangement possibilities of cations formed during mass spectrometry serve as a point of common interest between carbocation work and work concentrating on chirality in this section of the thesis.

3.2.1 Mass Spectroscopic Studies on the series of fenchone-derived sulfonamides

3.2.1.1 The mass spectrum of the sulfonamide **101a**

Mass spectrometry was performed on the array of fenchonesulfonamides. The positive electrospray ionization mass spectrum of the picolylamine-derived fenchonesulfonamide **101a** is presented in Figure 48. This spectrum, showing only the molecular ion M^+ , confirms the exact mass of the sulfonamide and also the isotopic mass distribution anticipated from this compound (affected by $^{32}\text{S}:^{33}\text{S}:^{34}\text{S}$, $^{12}\text{C}:^{13}\text{C}$, $^1\text{H}:^2\text{H}$ and $^{14}\text{N}:^{15}\text{N}$ and $^{16}\text{O}:^{17}\text{O}:^{18}\text{O}$ relative abundances). Table 12 shows the relative abundances of the molecular ion expected from the isotopic distribution close in mass to the most abundant peak, as expected for the $M+H$ ion $\text{C}_{16}\text{H}_{23}\text{O}_3\text{N}_2\text{S}$.

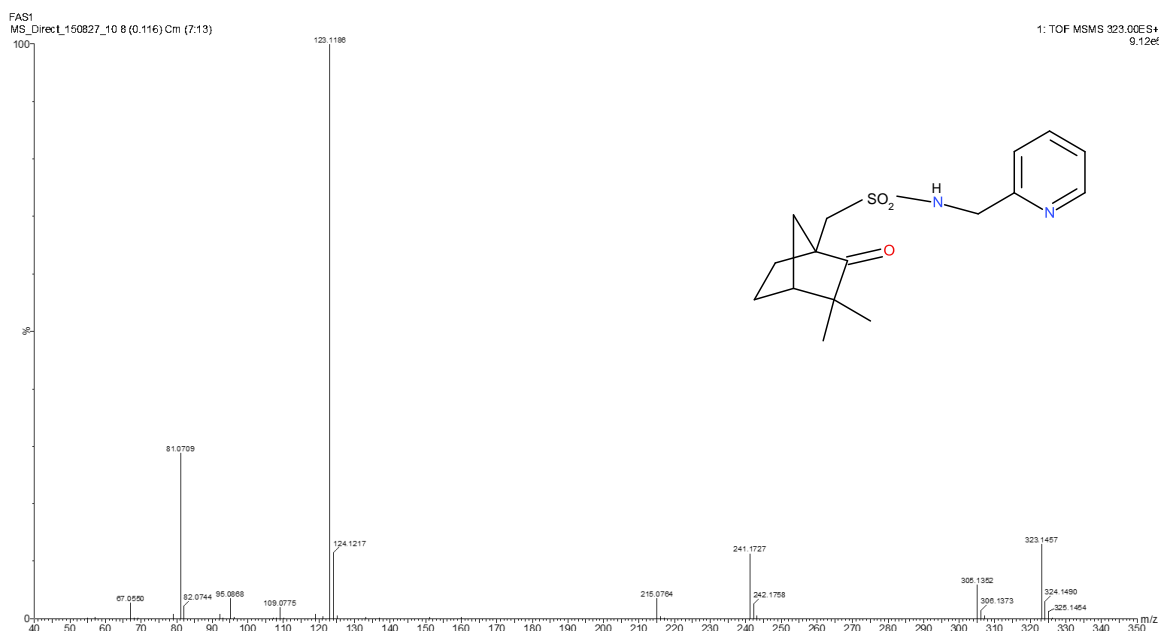
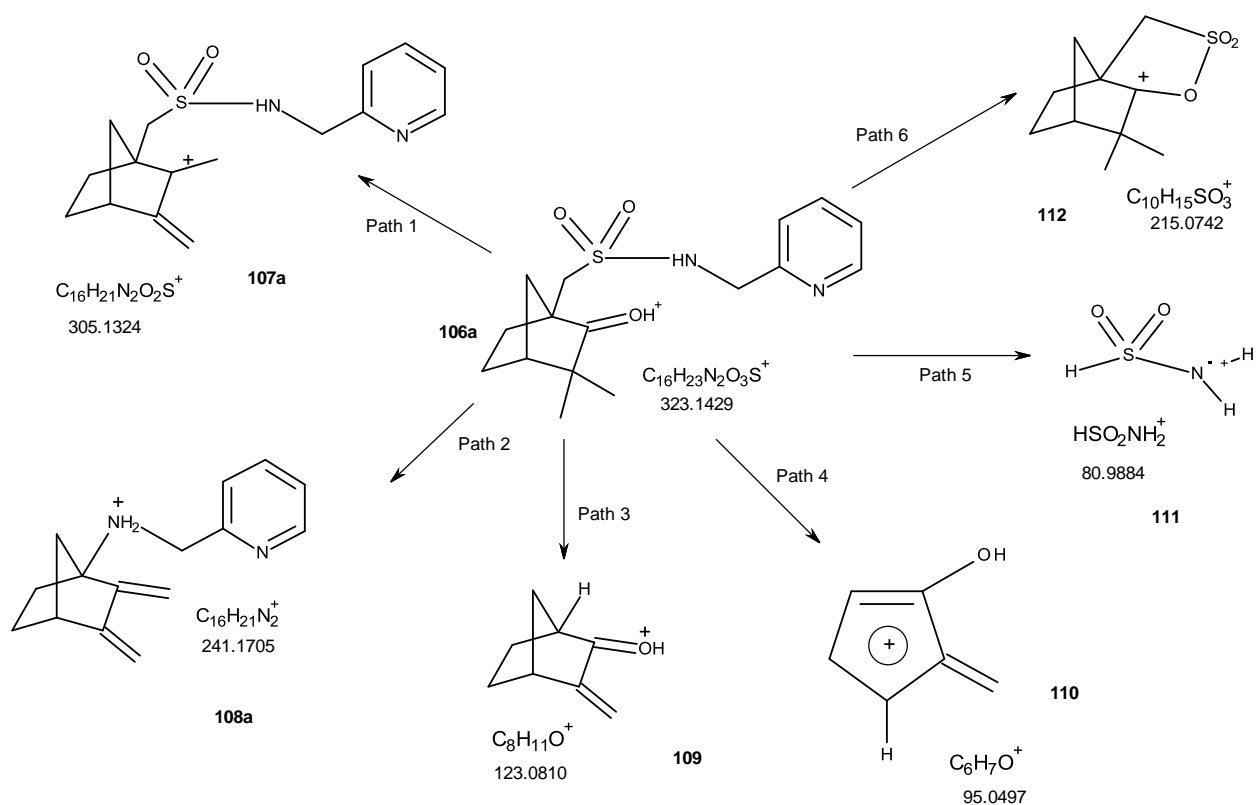


Figure 48. The EI mass spectrum of the protonated molecular ion of the picolylamine-derived sulfonamide **101a**.

Table 12. Relative abundance of isotopologues of $\text{C}_{16}\text{H}_{23}\text{O}_3\text{N}_2\text{S}$.

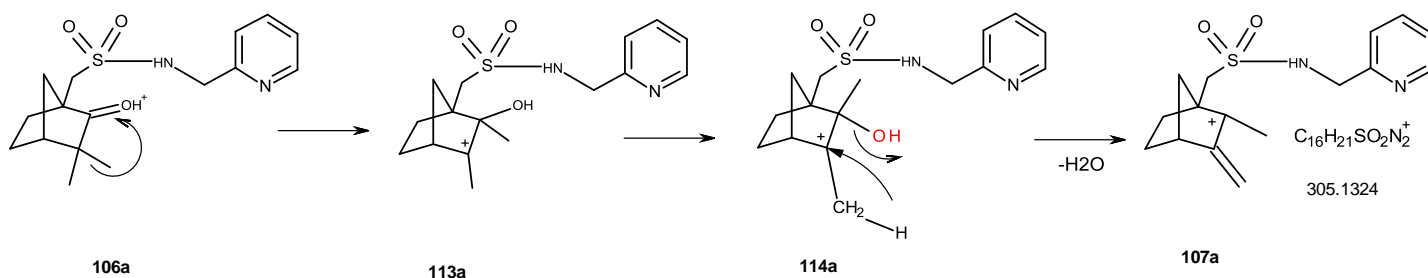
Mass	Relative Abundance
323.1429	100.00
324.1461	18.00
325.1393	5.00
326.1423	1.00



Scheme 34. Electrospray MS fragmentation pathways of the molecular ion **106a**.

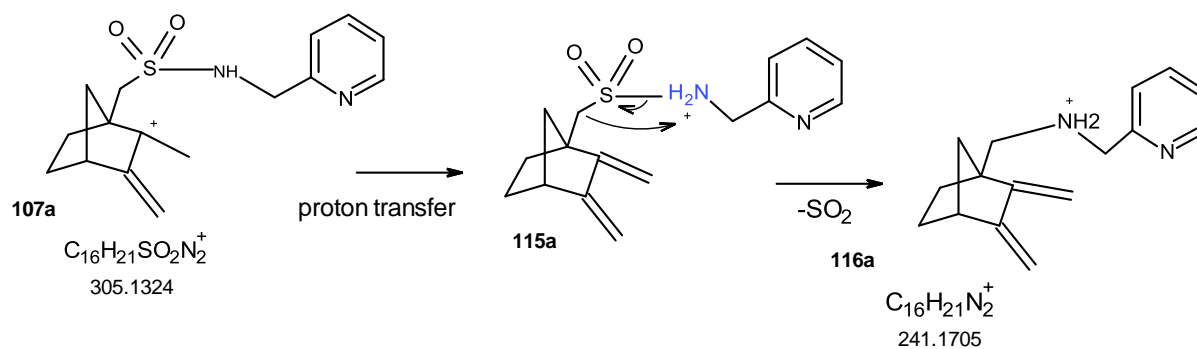
From all six pathways, paths 1, 3, 5 and 6 can be attributed from the initial protonation affording MH^+ **106a** (Scheme 34). Pathways 2 and 4 arise from sequential fragmentations.

Pathway 1 involves a migration of a methyl group, resulting in a tertiary alcohol and a stable tertiary carbocation intermediate, followed by the formation of a double bond from the loss of water, as the OH^- and H-CH_2 yield a tertiary carbocation **107a** ($m/z = 305.1324$) as illustrated in Scheme 35.



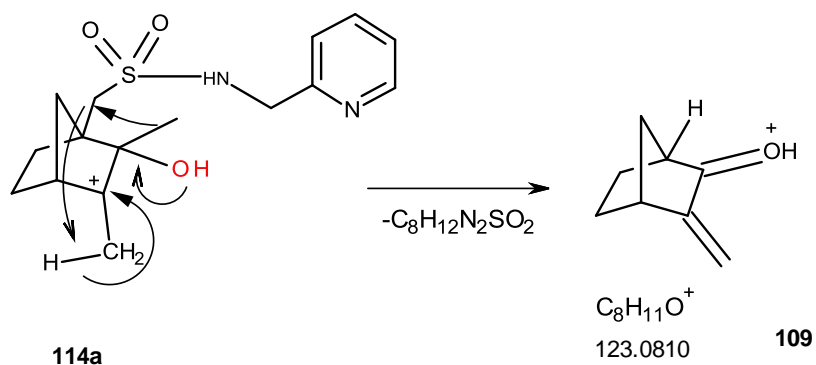
Scheme 35. Pathway 1 showing formation of carbocation **107a**.

Carbocation **107a** is further fragmented *via* the loss of sulfur dioxide to afford carbocation **116a** ($m/z = 241.1705$) in pathway 2 (Scheme 36).



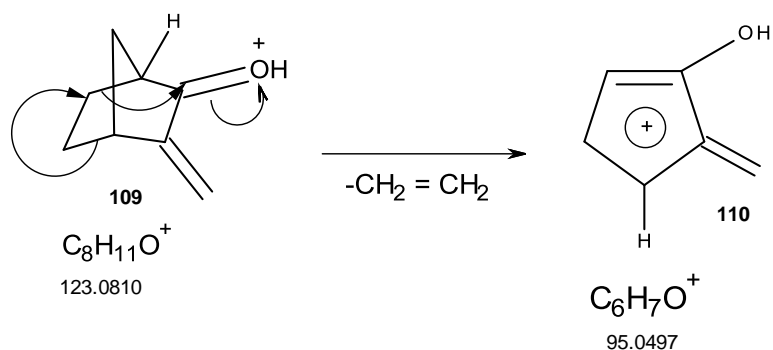
Scheme 36. Pathway 2 showing generation of fragment **116a**.

Rearrangement of **114a** results in loss of the sulfonamide group leading to carbocation **109** ($m/z = 123.0810$) (Scheme 37).



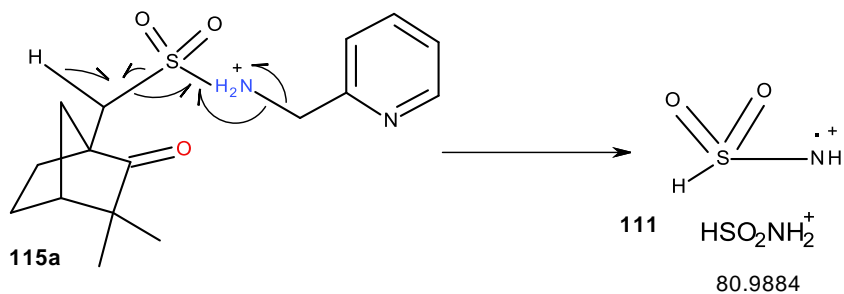
Scheme 37. Pathway 3 showing generation of fragment **109**.

A retro Diels-Alder type mechanism on carbocation **109** results in the loss of an alkene, producing a resonance stabilized carbocation **110** ($m/z = 95.0497$) (Scheme 38).



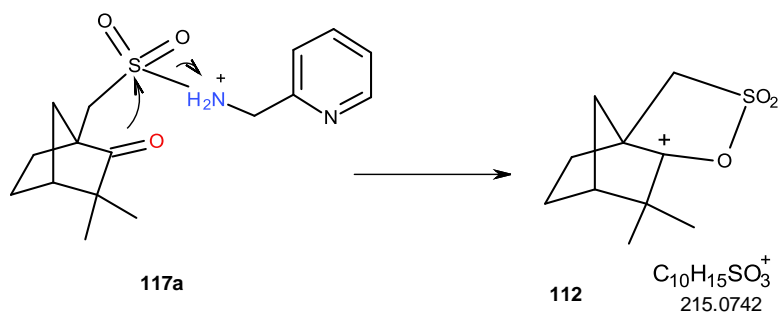
Scheme 38. Pathway 4 showing generation of fragment **110**.

Pathway 5 involves a homolytic type fission of the protonated molecular ion, producing a radical cation **111** ($m/z = 80.9884$) with the loss of both the aromatic and fenchone rings (Scheme 39).



Scheme 39. Pathway 5 showing generation of fragment **111**.

A prominent fragment identified originates from the initial protonated molecular ion, producing a resonance stabilized sultone **112** ($m/z = 215.0742$) (Scheme 40).



Scheme 40. Pathway 6 showing generation of fragment **112**.

3.2.1.2 The mass spectrum of the fufurylamine-derived sulfonamide **101b**

The electrospray ionization mass spectrum for **101b** is illustrated in Figure 49.

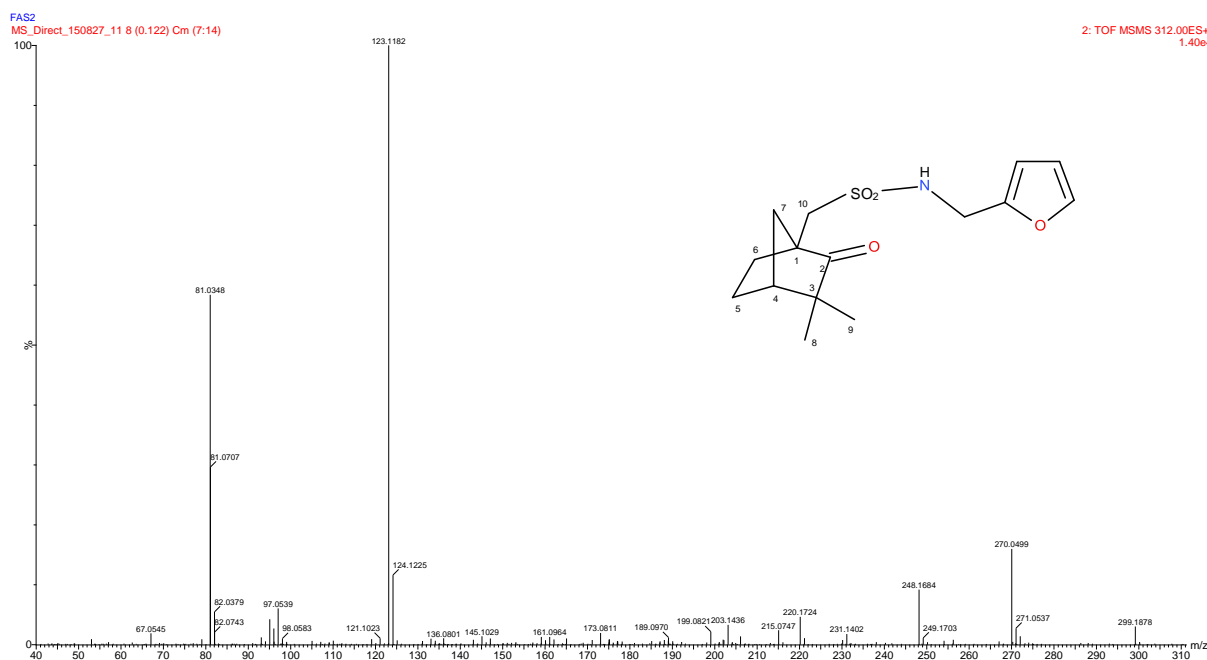
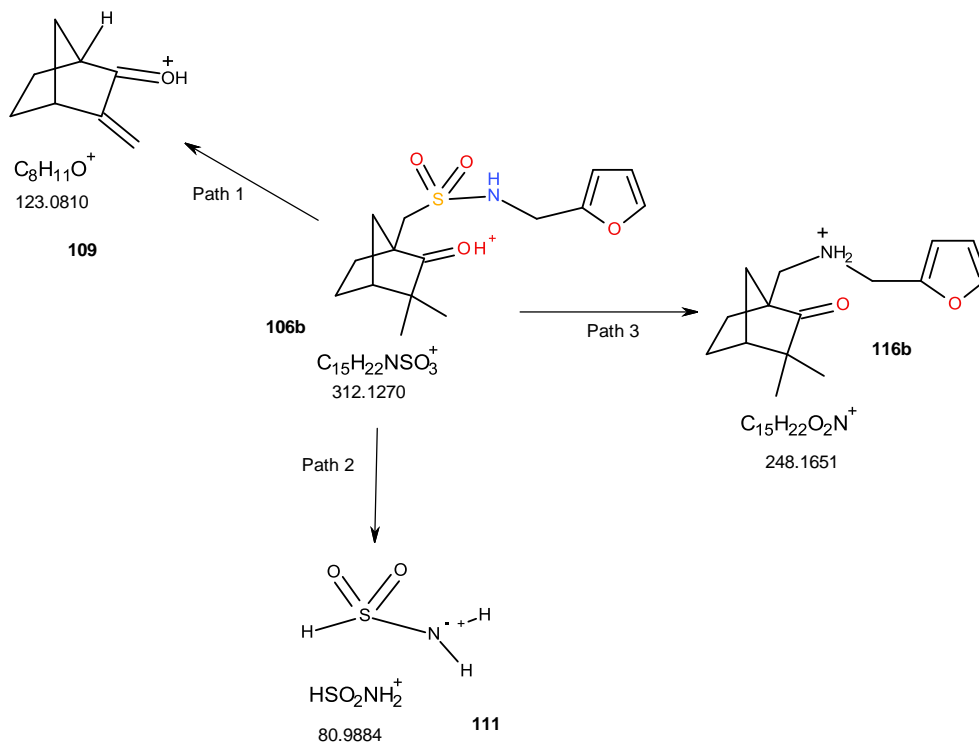


Figure 49. The EI mass spectrum of the protonated molecular ion of the fufurylamine-derived sulfonamide **101b**.

The predicted mass and molecular formula for compound **101b** was $311.15 \text{ g mol}^{-1}$ and $\text{C}_{15}\text{H}_{21}\text{O}_4\text{NS}$ respectively, which is in accordance with the mass spectrum of molecular ion mass of $312.12 \text{ g mol}^{-1}$. For this spectrum there is more fragmentation observed. Table 13 illustrates the expected pattern for the molecular ion.

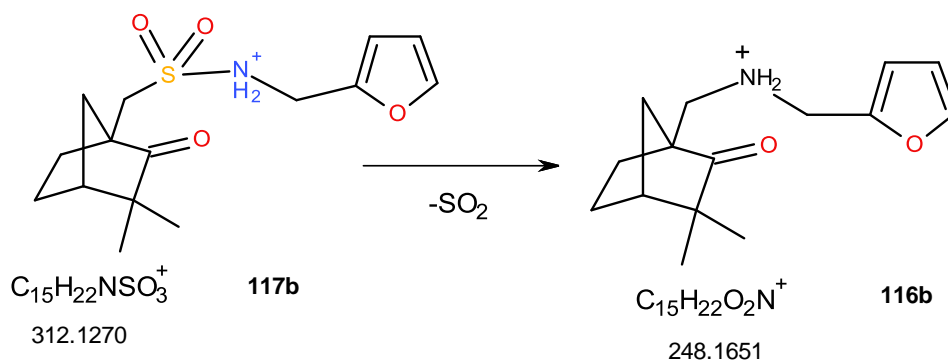
Table 13. Relative abundance of isotopologues of $\text{C}_{15}\text{H}_{22}\text{O}_4\text{NS}$.

Mass	Relative Abundance
312.1270	100.00
313.1302	18.00
314.1262	7.00
315.1278	1.00



Scheme 41. Electrospray MS fragmentation pathways of the protonated molecular ion **106b** of compound **101b**.

Fragmentation patterns of the protonation of the furfurylamine-derived sulfonamide molecular ion **106b** appear to be very similar to that for **106a**. Pathways 1 and 2 can be seen interpreted in Scheme 41. Pathway 3 yields a carbocation *via* the loss of sulfur dioxide from the molecular ion (Scheme 42).



Scheme 42. Pathway 3 showing generation of fragment **116b**.

3.2.1.3 Mass spectrum of the adamantylamine derived fenchone-sulfonamide **101d**

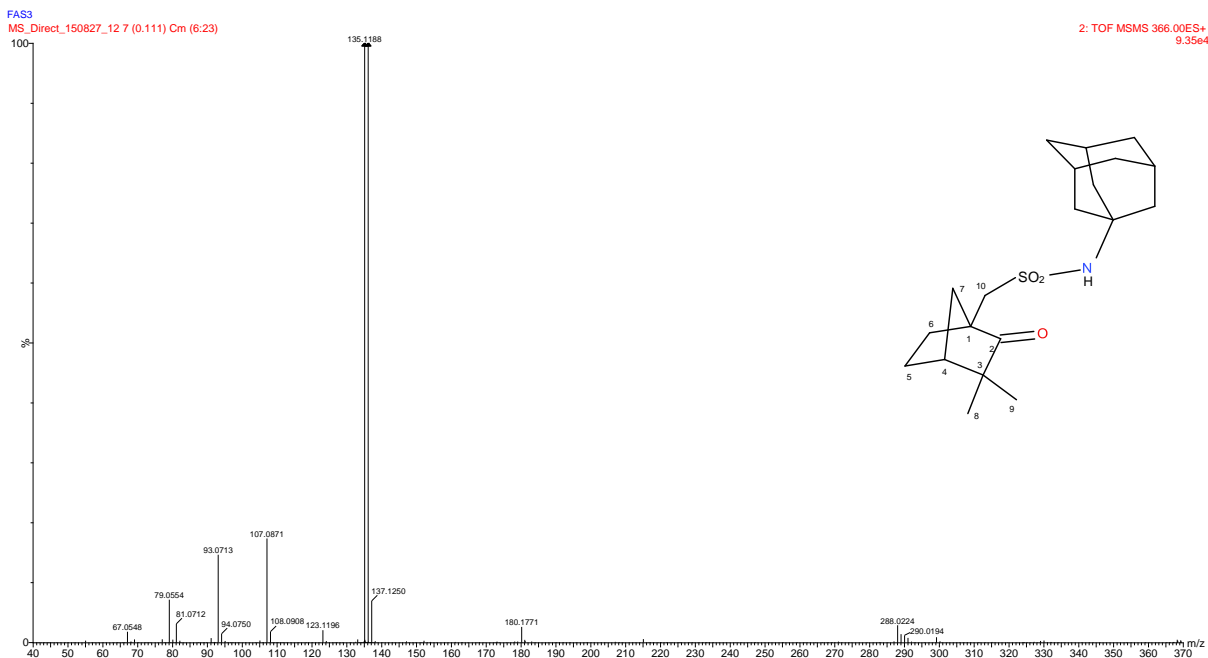


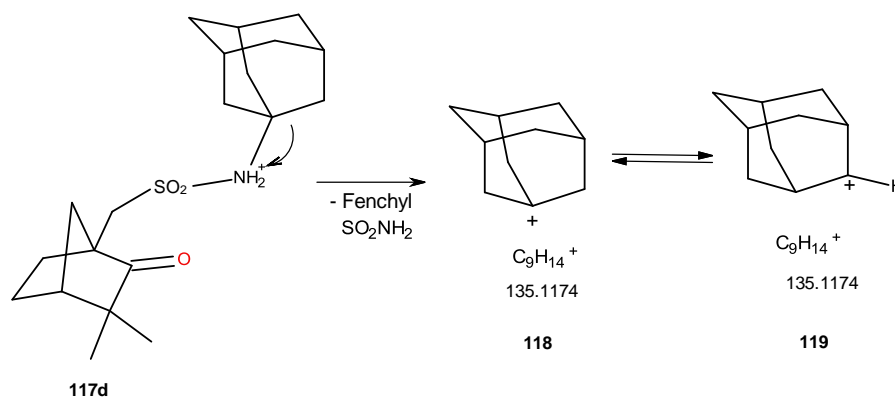
Figure 50. The EI mass spectrum of the protonated molecular ion of the adamantylamine-derived sulfonamide **101d**.

The predicted mass and molecular formula for compound **101d** was 365.20 g mol⁻¹ and C₂₀H₃₁O₃NS respectively, which is in accordance with the mass spectrum of molecular ion mass of 366.20 g mol⁻¹.

Table 14. Relative abundance of isotopologues of C₂₀H₃₂O₃NS **101d**.

Mass	Relative Abundance
366.2103	100.00
367.2136	23.00
368.2103	8.00
269.2115	1.00

The most prominent fragment identified after the fragmentation of the molecular ion A is the adamantyl cation, with the loss of the fenchyl-sulfonyl and amine moieties leading to a tertiary carbocation forming at the bridgehead position **118**, which then rearranged to the more stable secondary cation **119** ($m/z = 135.1174$).



Scheme 43. Fragmentation of **117d** to form the adamantyl cation **119**.

3.2.1.4 Mass spectrum of aniline derived fenchone-sulfonamide **101c**

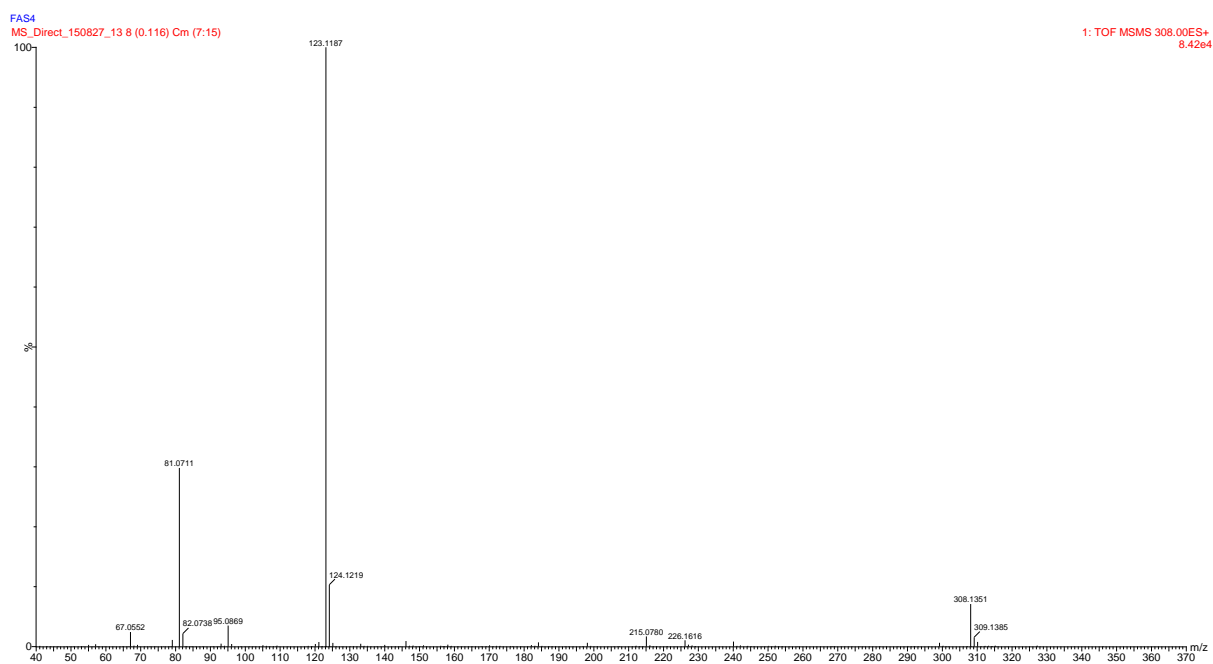


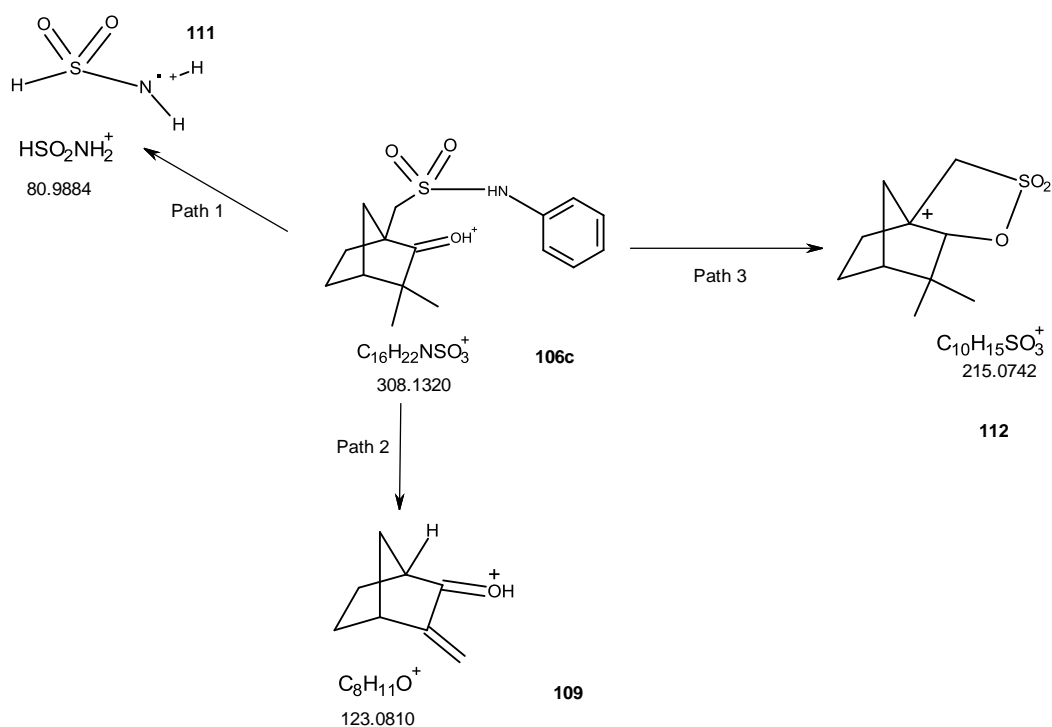
Figure 51. The EI mass spectrum of the protonated molecular ion of the aniline-derived sulfonamide **101d**.

The predicted mass and molecular formula for compound **101c** was 307.1242 g mol⁻¹ and C₁₆H₂₁O₃NS respectively which is in accordance with the mass spectrum of molecular ion mass of 308.1320 g mol⁻¹. For this spectrum there is more fragmentation observed.

Table 15. Relative abundance of isotopologues of C₁₆H₂₂O₃NS **106c**.

Mass	Relative Abundance
308.1320	100.00
309.1353	19.00
310.1314	7.00
311.1328	1.00

With regard to the MS/MS no new fragments were observed, and therefore pathways 1-3 are very similar to those predicted to occur for **101b** (Scheme 44).

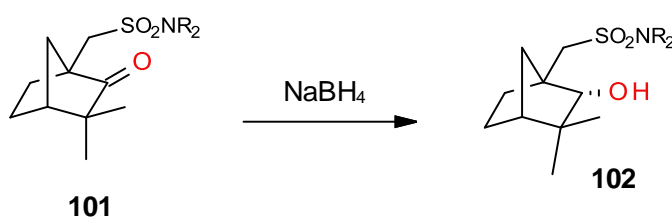


Scheme 44. Electrospray MS fragmentation pathways of the protonated molecular ion **106c** of compound **101c**.

3.2.1.5 Summary of features of mass spectrometry of 101a-d

The fragmentation of these systems shows features peculiar to the various moieties within the structures of **101a-d**. Common to all is the loss of SO₂ from the sulfonamide group, a peculiarity of the fenchone, that allows for loss of an oxygen from the fenchone group *via* rearrangements and the retro Diels-Alder process. Other aspects are peculiar to a particular species, such as the adamantyl derivative **101d**, where the adamantyl carbocation is evident in the spectrum. In short, not only has the synthesis of these sulfonamides been optimized to excellent yields, but these sulfonamides have been fully characterized using NMR, and also by their mass-fragmentation pathways.

3.3 Reductions of fenchonesulfonamides



Scheme 45. Reduction of fenchone-derived sulfonamides **101a-d**

Following the formation and characterization of the sulfonamides, reduction of the carbonyl group on the fenchone-derived sulfonamides skeleton (**101a-101d**) was to be carried out using mild reaction conditions, to ensure that reduction occurred only at the ketone moiety and avoid modification of the vulnerable sulfonamide bond. Double reduction of aromatic sulfonamides can occur, involving cleavage of both bonds of sulfur to carbon and nitrogen.¹³² Metal hydrides are commonly used for reductions; the choice lay between lithium aluminium hydride (LiAlH₄) and sodium borohydride (NaBH₄). LiAlH₄ is the more powerful of the two reducing agents, however, it is unselective and poses a threat to the sulfonamide moiety. Primary sulfonamides are resilient to reduction with LiAlH₄ but under the stringent anhydrous and more vigorous reaction conditions, secondary sulfonamides are susceptible to reduction.¹³³ In comparison, NaBH₄ is less reactive, therefore safeguarding the sulfonamide from hydrogenation, and reactions may be carried out at room temperature in protic solvents.^{134,135} Reactions (Scheme 45) were carried out in methanol with excess sodium borohydride, reducing agent was used because NaBH₄ reacts rapidly with methanol and metal borides further accelerate this breakdown, therefore a 2-fold excess was used to ensure consumption of all starting materials. Reactions were quenched with cold water and hydrochloric acid. Sulfonamides were extracted and isolated under acidic conditions successfully with yields ranging from 62-73% for all amine

derivatives except picolylamine. A ^1H NMR spectrum in CDCl_3 of the initial picolylamine sulfonamide extraction with ethyl acetate showed no product present. A ^1H water suppression NMR spectrum was used on the aqueous layer in a 10% D_2O :90% H_2O mix. The water signal was presaturated with a pulse train at 4.73 ppm and it was confirmed that the fenchone-picolylamine derived sulfonamide **102a** had remained in the water layer. Neutralization was used therefore in the work-up, to release the sulfonamide into the organic layer.

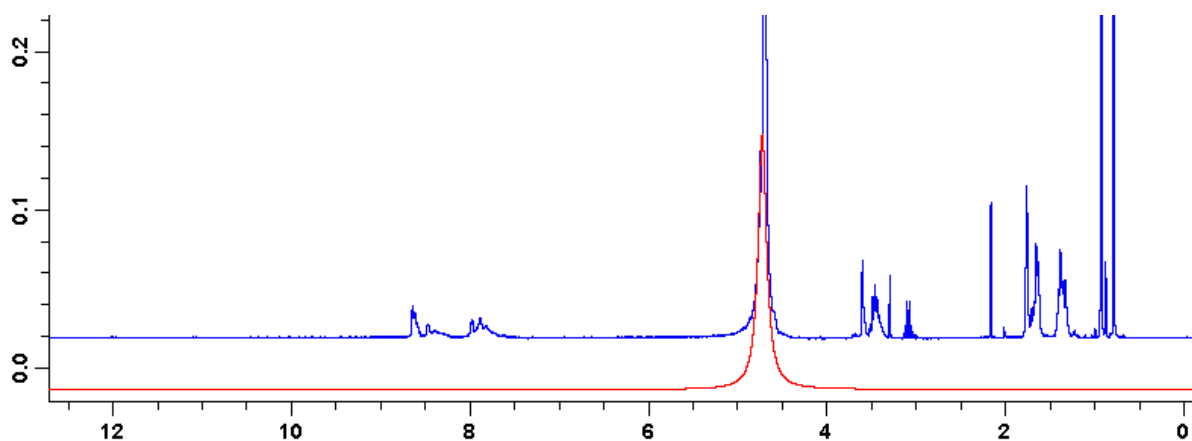


Figure 52. ^1H NMR spectrum with pre-saturation on the water signal (600MHz, 10% D_2O :90% H_2O), overlaid with proton spectrum of **102a**.

This highlighted for our study the acidity of the labile proton directly attached to the nitrogen of the sulfonamide group, and its role in solubility when conditions are not acidic enough to maintain the protonation. Serendipitously this observation aided the design and the hypothesis that picolylamine-derived surfactants could allow for the tuning of the ionic head-region of the surfactant. In a basic solution the surfactant will be anionic, while under acidic conditions a cationic system will be possible. This design may potentially be extended for conditions where the head-region is neutral, in which a hydrophilic polyethylene glycol tail can be used to create a surfactant suitable for the creation of reverse micelles (Figure 53).

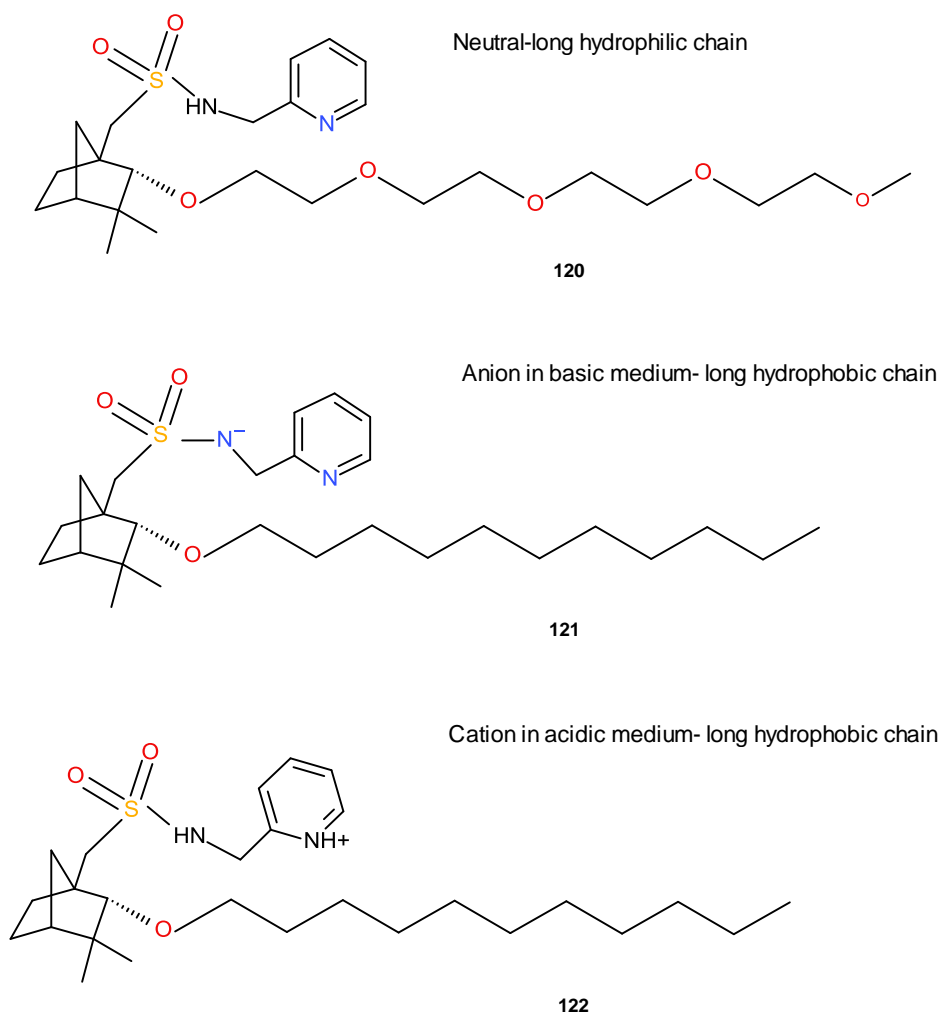


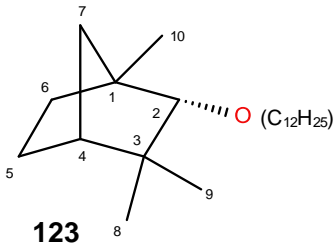
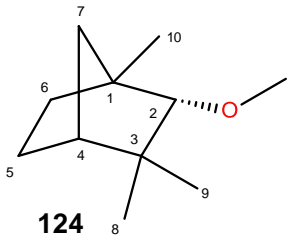
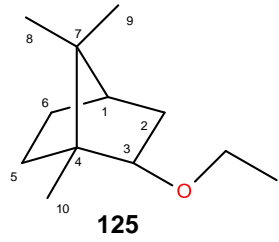
Figure 53. Generation of tunable chiral micelles from the picolylamine derived sulfonamide **102a**.

3.4 Synthesis of ethers **104** from the hydroxyl sulfonamides **102**.

The final step of the synthesis was to link the head and tail regions *via* an ether bond. An ether bond was chosen due to its relative chemical stability. Ethers generally are not reactive in the presence of dilute acids or bases and mild oxidizing and reducing agents, hence the risk of the surfactant itself undergoing cleavage, or reactions could be minimal and therefore the integrity of the micelle moiety would be preserved during applications. A reaction between the reduced aniline-derived system and bromohexane in ethanol with sodium hydroxide, stirred at room temperature for 15 h,¹³⁶ was the first attempted surfactant synthesis; unfortunately the success of the reaction was difficult to determine from the ¹H NMR spectrum, as it was too complex to assign any of the signals conclusively. The crude mixture was neutralized and preliminary purification was attempted by passing the mixture through a plug of silica gel to remove unreacted starting materials. ¹H NMR analysis showed no starting material present and at the same time no decipherable information on the ether product either. It seemed that

the starting materials had remained on the silica plug however, in the process, the surfactant may also have remained in the silica, or hydrolysis of the sulfonamide or some other process removed all trace of the desired product. Given the steric demands of this system, the ether synthesis was attempted on a variety of model systems (Table 16). Under these conditions, the complications due to the reactivity of the sulfonamide were removed. Varying the bicyclic structure, solvent, base, temperature and time of numerous reaction conditions¹³⁷⁻¹⁴⁰ all proved unsuccessful.

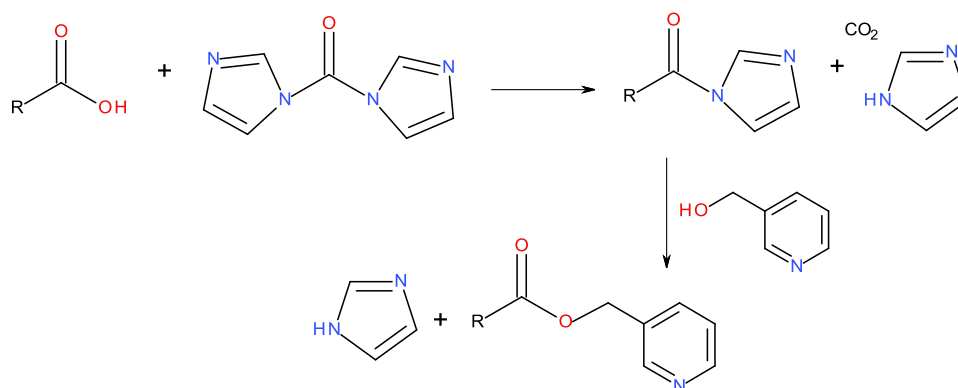
Table 16. Attempted synthesis of fenchol and borneol ethers as per Scheme 28.

 <p>123</p>	<p>1: fenchol, bromododecane, triethylamine, DMAP in THF under N₂, 80°C, 15h 2: fenchol, bromododecane, NaOH, ethanol, 25°C, 15h 3: fenchol, bromododecane, NaH, toluene, reflux, 18h 4: fenchol (dry), bromododecane, NaH, toluene, reflux, 18h 5: fenchol (dry), bromododecane, BuLi, THF, rt, 18h</p>
 <p>124</p>	<p>6: fenchol (dry), methyl iodide, NaH, toluene, reflux, 18h</p>
 <p>125</p>	<p>7: borneol (dry), ethylbromide, NaH, DMF, 25°C, 48h 8: borneol (dry), ethylbromide, silver tetrafluoroborate, acetone, reflux, 18h</p>

There were many suspected reasons as to why ether bond formation was not successful. The possible influence of the bulky methyl groups would be compounded by the presence of a sulfonamide group in proximity to the alcohol oxygen, which could prevent access of the base

to this hydroxyl proton, or, if the proton was abstracted, it could be that the long hydrocarbon chain could not move into the proximity of the alkoxide for bond formation to occur. Alternatively, if all of these steps are plausible, it may be that the transition state involving this bulky nucleophile in reaction with the alkyl halide in an S_N2 type arrangement is too high energetically to be feasible. As may be seen from the table, various solvents were tried and bases of varying strengths ranging from sodium hydroxide to butyllithium did not yield positive results.

An alternative plan was initiated with the view that the transition state in the Williamson ether synthesis was plausibly the most likely cause of problems. In order to overcome the problem of steric hindrance, the original idea of connecting head and tail regions was changed from the use of an ether bond to that of an ester. The intention was to use a coupling agent, namely 1,1'-carbonyldiimidazole (CDI) (Staab's reagent) (Scheme 46). CDI is commonly used as a coupling reagent, as a condensation or dehydration reagent in preparations of amides, esters, carbamates and so on.^{141,142}



Scheme 46. Reaction mechanisms for the formation of picolinyl ester derivatives with CDI.¹⁴³

The most sterically hindered step in this case is likely to involve attack of the bulky alcohol on the carbonyl carbon of the imidazolide, leading to a tetrahedral intermediate. This is expected to be less sterically demanding than S_N2 displacement of halide in an alkyl halide by the bulky alcohol, as the pentavalent transition state would have five groups around the reaction centre, including the bulky alcohol and a large halide.

The first attempt at this ester synthesis was also conducted on a model bicyclic system, borneol. Octanoic acid was stirred with dry DMF and CDI for 30 min, allowing for the evolution

of carbon dioxide and the complete formation of the imidazolid. The alcohol was then added and the reaction left to stir at room temperature overnight. NMR analysis of the crude mixture showed that the reaction had failed. The ^1H NMR spectrum showed the presence of all starting materials including the CDI, which led us to believe that the CDI had failed to form the carboxylic acid-CDI complex, resulting in no reaction occurring. It was suspected the CDI may have been only sparingly soluble in the DMF solvent.

A concurrent attempt at synthesizing the ester was with the fencholsulfonic acid (which directly produces a surfactant that may be used for the creation of a normal chiral micelle). This reaction involved reacting octanoic acid, with CDI in dry THF (Figure 54). The fencholsulfonic acid was added after 30 min and left to stir overnight. It was anticipated that reaction of the CDI with the sulfonic acid would not compete with the reaction with the alcohol due to congestion around the sulfur centre. However, from ^1H NMR analysis of the crude reaction mixture, there were signs that the reaction had proceeded, but the spectra showed numerous signals, with a best yield at 3% of the product. Further work-up and purification was not attempted on the sample.

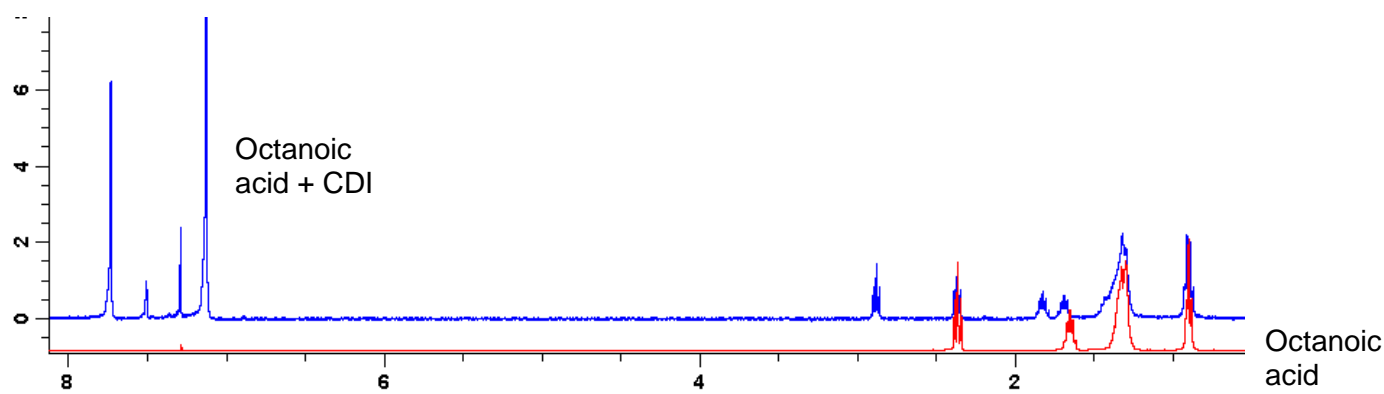


Figure 54. ^1H NMR spectrum of the product of the reaction between octanoic acid and CDI.

After these results and other failed attempts with various reaction conditions, other methods for producing esters were explored. Reaction between the fencholsulfonic acid and acetyl chloride in pyridine was investigated. The acetyl chloride does not have a long side chain and has a simple ^1H NMR spectrum, and was used in the hope of rationalizing why these reactions were not successful. ^1H NMR analysis of the crude reaction mixture again showed only the presence of starting materials.

To explore the issue of increased activation due to steric hindrance around the reactive centres, another method of ester synthesis was attempted on fenchol as a test system as a proof of concept. Octanoic acid and CDI were stirred together in acetonitrile and heated at 40°C for 30 min while the fenchol was stirred in a separate vessel with K₂CO₃ in the same solvent. After 30 min the alcohol and base mixture were added to the octanoic acid and CDI and stirred at 60°C for 4 h. The acetonitrile was removed and a ¹H NMR spectrum of the crude reaction mixture was run (Figure 55). Again, while starting materials were still present, there was evidence of a possible product. The potassium carbonate was reacted with the alcohol with the aim of generating highly reactive alkoxide. (While potassium carbonate is a relatively weak base, the possibility of forming a too small concentration of the alkoxide cannot be excluded.) A singlet at 4.38 ppm shows a definite change in the fenchol structure, which could be attributed to the HCOR proton. The NMR integrals indicate an approximate 30% conversion to the ether **126**.

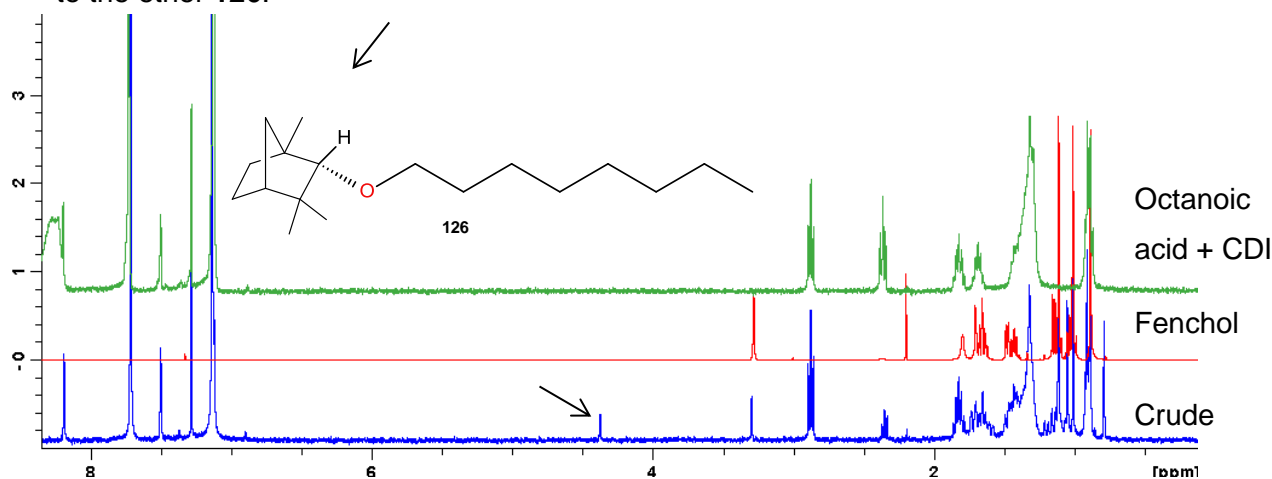
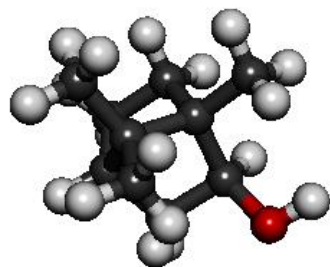
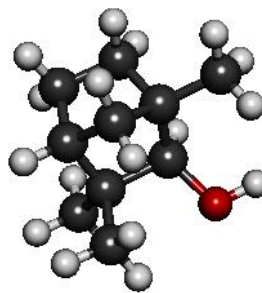


Figure 55. Synthesis of a fenchol-derived ether **126**.

The two methyl groups at position 3 on the fenchol skeleton are in close proximity to the alcohol group. As this was deemed a major point of interference, this would sufficiently explain why the ester formation would be difficult and hence the ether synthesis even more so. Considering that each reaction was tried countless times with varying parameters such as temperatures, solvents, reagents, and reaction times, we considered this route to have been fully explored, and discarded the fenchone scaffold and initiated work on camphor derivatives instead, in the hope that the region around the synthesized alcohol would be less hindered, thus allowing synthesis of the ether.



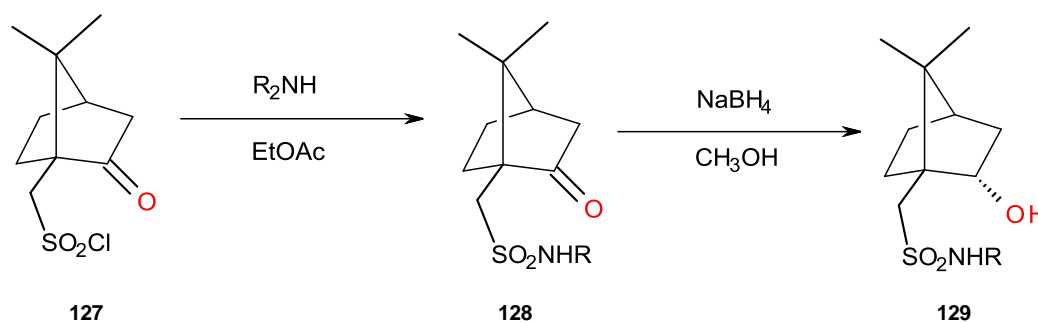
Camphor



Fenchol

Figure 56. Camphor **1** and fenchol **70**.

The same methodologies used for fenchone were applied to the synthesis of a family of camphor-derived sulfonamides. The starting material 10-camphorsulfonyl chloride **127** is commercially available and did not need to be synthesized. Camphor sulfonamides **128** were made following method 2 and yields were almost comparable as those obtained from the fenchol system (Table 17). The camphor sulfonamides were reduced with excess sodium borohydride in methanol.¹²⁸



Scheme 47. Camphor derived sulfonamides **128** and reduced sulfonamides **129**.

Table 17. Camphor-based sulfonamides **128** and reduced **129**.

R	128 yield (%)	129 yield (%)
Picolylamine a	97	49
Furfurylamine b	93	69
Aniline c	93	57
Adamantylamine d	72	33

Several attempts were made on both the ether and ester synthesis on the camphor system. The method giving the best ether yields entailed stirring reduced aniline-camphor sulfonamide with K_2CO_3 in DMF for 1 h, followed by the addition of bromododecane in minimal DMF dropwise and refluxing the reaction mixture for 18 h. The reaction time coupled with the high boiling point of solvent of over $150^\circ C$ provides insight into the high activation parameters required to overcome the steric hindrance inherent in the system. Solvent was removed and 1H NMR analysis of the crude mixture revealed the presence of starting materials and also possible product (Figure 57).

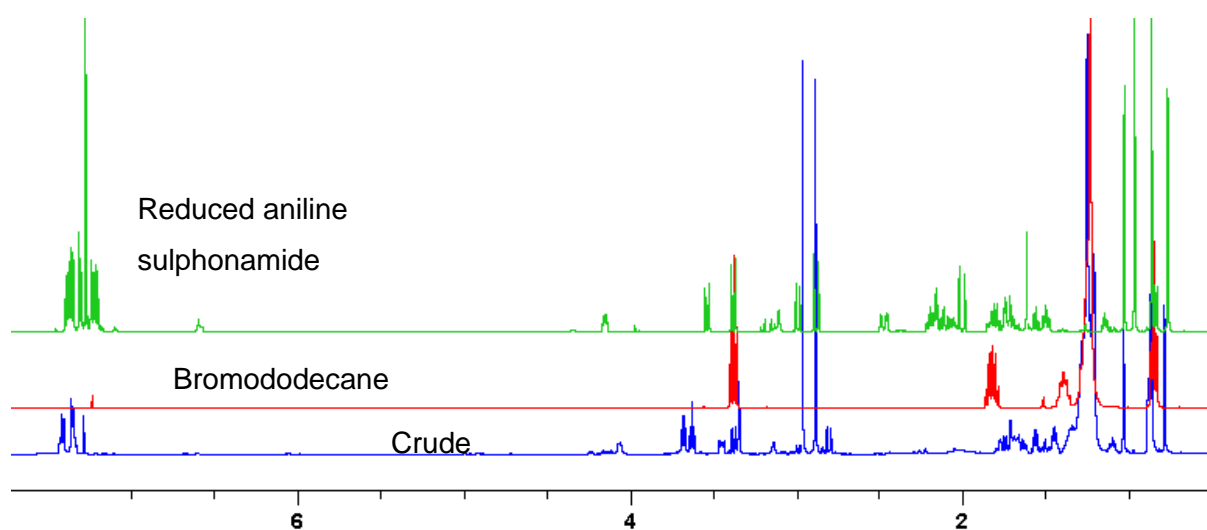


Figure 57. Comparison of 1H NMR signals of **129c**, bromododecane, and crude ether product **130c**.

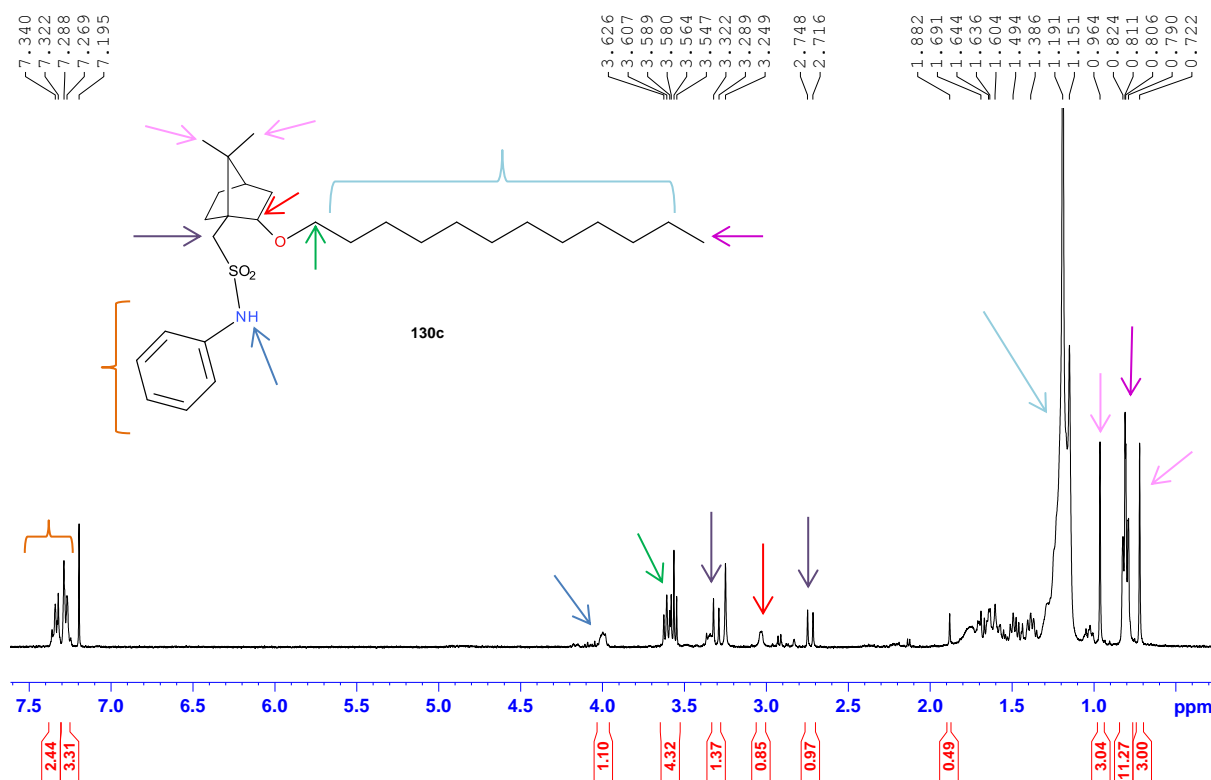


Figure 58. Assignment of signals in the ^1H NMR spectrum for product **130c**.

Considering the ^1H NMR spectrum (Figure 58), the main indicator in determining the success of this reaction would be the presence of a triplet in the region between 3.5-4.5 ppm integrating to two protons, indicated by the green arrow (Figure 58). There are multiple signals observed around 3.6 ppm which are consistent with $\text{CH}_2\text{-O}$ from the product close to the $\text{CH}_2\text{-Br}$ from the bromododecane starting material. The most prominent peak is that at 1.15 ppm from the bromododecane chain. Again there could be overlap of protons from product and starting materials. The head region of the surfactant is intact with both methyl groups from the camphor skeleton (pink arrows), the diastereotopic protons (black arrows), and aromatic protons from the aniline moiety (orange) all present. Workup of this product proved difficult due to its low mobility on silica. For use of this method in the production of surfactants the purification process will require optimization with respect to mobile and stationary phases within the chromatographic process.

A further attempt on the synthesis of the ethers was not pursued even though it is a feasible line of investigation in future. Surfactant synthesis was considered a proof of concept. The primary focus of the micelle study lay in the design of surfactant, molecular modelling and molecular dynamics of the micelle in the dual-solvent micellar system. Both the fenchol and camphor (reduced to isborneol) systems were considered during the construction of

surfactants for micelles, as the opposing *exo* vs. *endo* hydroxyl positions of the skeletons are assumed to have significant structural impact on the micelle systems formed.

3.5 Preliminary micelle modelling and dynamics simulation studies:

Key objectives of this study were, to design and predict the behaviour of chiral surfactants with respect to their aggregation in the desired binary solvent system, to predict the stability of these chiral micelles, and to understand the chiral influence these micelles would have on the solvent. The core of this study was therefore modelling which would provide the appropriate structural insight into the prediction of the behaviour of surfactants in solution as well as investigate the micelle itself in terms of molecular geometry and system energies.

Molecular dynamic studies were initiated to explore questions such as the extent to which water penetrates the micellar core (in the normal micellar systems), the nature of the hydrocarbon/water interface, and the extent of the sphere of influence of the chiral portion of the micelle on the nearby achiral hexane solvent.

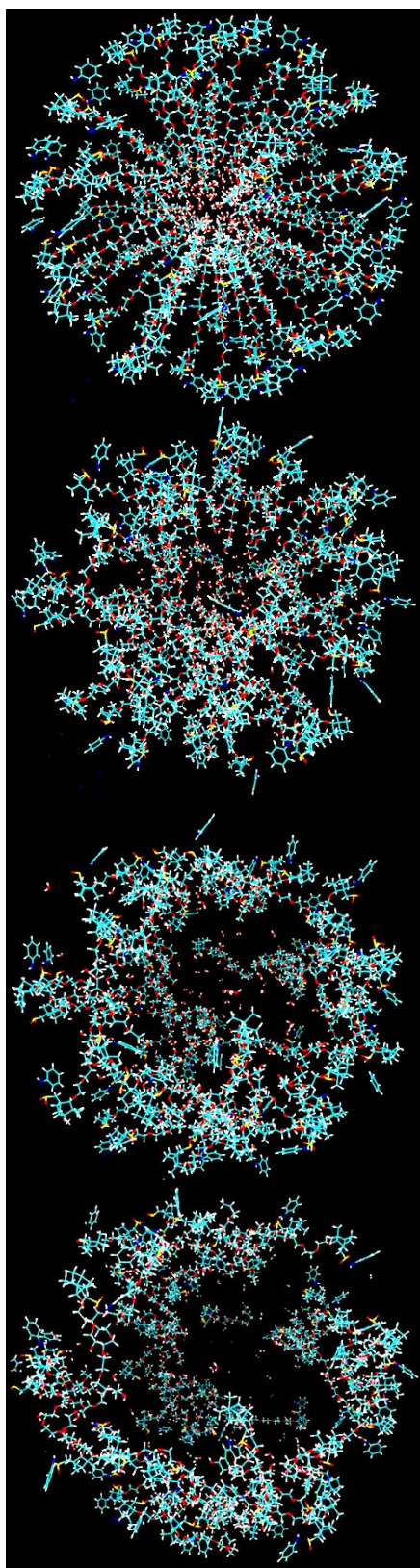
In the absence of data regarding the optimum size of the micelle in a two phase solvent system, several micelle sizes were constructed; each construction was dependant on the structure of the surfactant, the number of surfactants per micelle, as well as the inner core radius.

3.5.1 Exploratory Work

The initial foray into the dynamics of these systems used packmol¹⁴⁴ to aid in the packing of the various components prior to molecular dynamics. For ease VMD (Visual Molecular Dynamics)¹⁴⁵ was used together with NAMD (Nanoscale Molecular Dynamics)¹⁴⁶ to perform the dynamics.

Prior to work with CHARMM (Chemistry at HARvard Macromolecular Mechanics) the system had been set up in an automated way within the context of VMD with respect to force fields and a preliminary dynamics run had been performed using NAMD. Figure 58 illustrates the result of this unsuccessful simulation. It would appear that the pressure internal to the micelle was catastrophically greater than the surrounding pressure due to hexane solvent, and allowed for the explosion of the micellar system. There are several factors that may have contributed to this, including close contact within the core of the micelle, incorrect boundary conditions (such as for an isolated system), a low density of hexane, and/or too rapid heating

of the system. The force fields used for the micelle might also have been at fault. It was felt that the level of detail required for simulation within CHARMM would aid the understanding of these particular systems and provide more detail within the simulation, with an aim of constructing micelles that were stable within the simulation period using, validated force fields.



0 ps

Figure 56 shows a two-solvent phase micellar system, with the outer hexane molecules hidden. At time $t=0$ ps the surfactants have all tails pointed inwards forming a sphere with water molecules only filling the inner diameter of the micelle. This particular micelle was constructed from an aniline-derived sulfonamide with 100 surfactant molecules and an internal diameter of 4\AA .

As the simulation proceeds, the micelle immediately begins to break up. The spherical shape is no longer maintained. It appears that there may have been too many water molecules in the confined space of the internal core and the outward forces have been too strong causing the micelle to break apart.

The surfactant molecules drift further apart in and amongst the hexane molecules, with large gaps for the water molecules to leak out.

At the end of the simulation, the micelle was completely broken up, with the surfactant molecules too far apart to reassemble. The water, hexane and surfactant molecules have no apparent order of assembly.

This simulation was unsuccessful as the micelle was unable to withstand the simulation.



4 ps

Figure 59. Results of preliminary (1st trial) molecular dynamics simulation.

3.5.2 Systematic setup within the scope of CHARMM software

3.5.2.1 Construction of surfactants and assembly into a model of a micelle

The first step in the simulation of chiral micelles was the construction of the individual surfactants (Figure 60 and 61). Discovery Studio 3.5 Client was used to draw these 3D structures, which were optimized in terms of conformation *via* the conformational search facility AMMP) within the VEGAZZ suite of software.^{147,148} Figure 60 shows the construction of an aniline-fenchol-derived surfactant with a neutral head region and hydrophilic tail region.

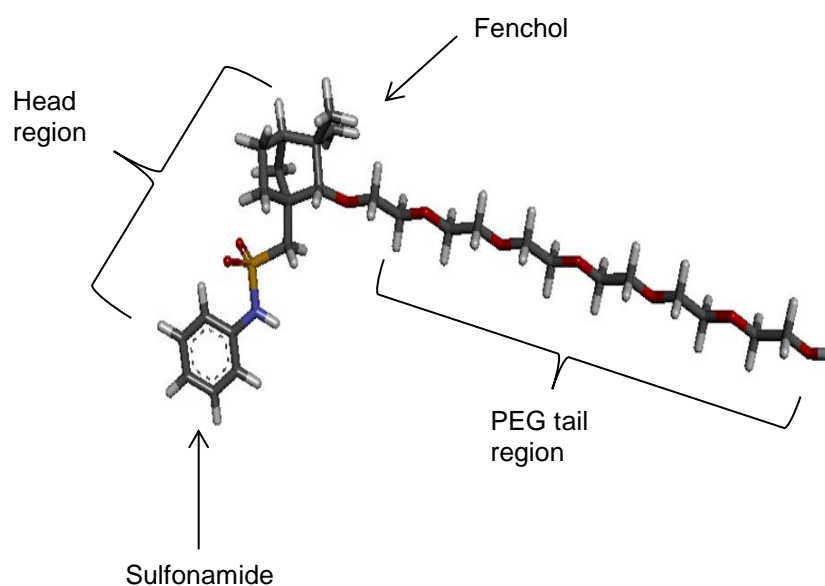


Figure 60. An example of an aniline-derived 3D surfactant molecule.

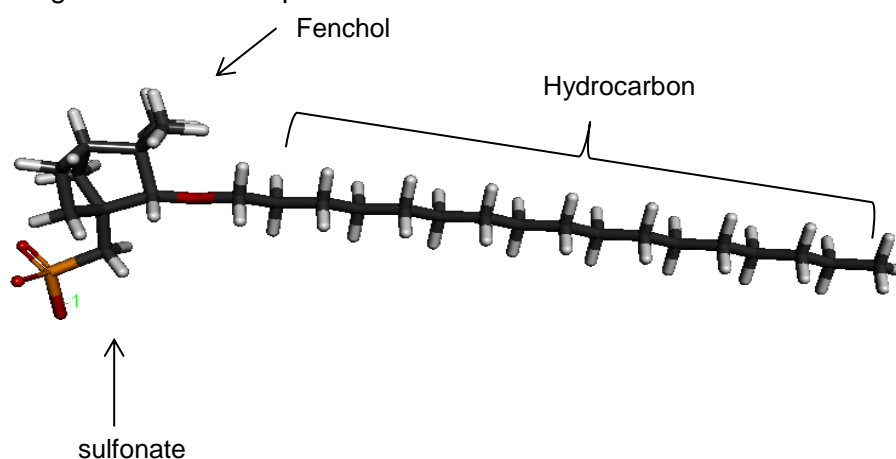


Figure 61. Normal surfactant with negatively charged sulfonate head region.

A full set of fenchol-derived surfactant and micelle systems was constructed; for the reverse micelle a series of sulfonamide-derived surfactants containing the ether linkage was formed

from picolylamine, furfurylamine, aniline and adamantylamine was constructed and the sulfonic acid-derived surfactant was used as a representative for the normal micelle. Each micelle was varied by surfactant with the number of surfactants ranging from 20-50 molecules per hemisphere (for a total of 40-100 surfactants per spherical micelle) and an internal diameter between 4-7 Å. The entire micellar system consisted of hexane, water and surfactant molecules within the dimensions of a 100 x 100 x 100 Å cube. In order to cope with movement of solvent at the edges of the simulation cell, periodic boundary conditions were used for the simulation. Thus solvent leaving the simulation on one face reappears on the opposite face for a simulation of this symmetry (Figure 62).

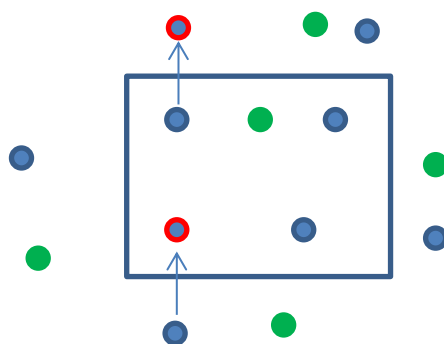


Figure 62. Showing concept of period conditions.

Surfactant force fields were generated using the CGenFF (CHARMM General Force Field),^{149,150} and the simulations were conducted using the software CHARMM which is a program well-suited for molecular dynamics of large systems such as bio-macromolecules, using molecular mechanics and even QM/MM techniques. The CHARMM program provides , an all-atom force field that works well with a wide range of molecular simulations, from the more basic simulations which are being minimization of structures and production runs of molecular dynamics trajectories to complex abilities such as correlation analysis.^{151,152} In 2009 CGenFF, a general force field was introduced, covering a wide range of organic groups present in biological and drug-like molecules, including a variety of heterocyclic scaffolds. This has typically been used in exploring receptor drug interactions. Respective surfactant force fields were generated and extracted through the CGenFF program using the CHARMM 36 force field.

Each surfactant was then assembled into a micelle in the pdb format using an in-house script.¹⁵³ This script solves the problem of equally spacing the required number of surfactants

over the surface of a sphere. An elegant way to solve this problem uses insight from the arrangement of seeds within a sunflower.¹⁵⁴ This phyllotaxic arrangement has been described by botanists and even has been used to arrange mirrors on satellites for orbiting the earth. The basis of the script is that the surfactants spiral outwards from the centre at a fixed angle $\gamma = 2\pi \left(1 - \frac{1}{\phi}\right)$ where ϕ is the golden ratio 1.618. The surfactants are arranged to point towards the centre of the sphere, based on the centre of mass of the surfactant and the greatest extent of the tail. A CHARMM input script is created together with the appropriate set of coordinates (.crd) for all of the surfactants within the micelle. The CHARMM script takes in these coordinates, together with the CGenFF force field parameters and solvents pentane (hexane was used later in this work) and water and creates a protein structure file (PSF) for the micelle containing all of the required topology of the micellar system, along with the coordinates (.crd) file for the full system. The PSF contains lists of every bond, bond angle, torsion angle and improper torsion angle as well as information required to generate hydrogen bonds and non-bonded interactions. This information is essential for the calculation of the energy of the system.

Figure 63 shows a 3D representation of a fully constructed micelle system. With the pentane molecules hidden it can be observed that the water molecules (green) fill the core of the micelle, including the inner radius as well as along the long chains. It is this interaction between the water and the chains that should result in the micelle retaining its shape. Hiding the water molecules, one can clearly see the arrangement of the surfactants into a spherical shape with the tails all pointing inwards and the head region at the interface between the water and hexane.

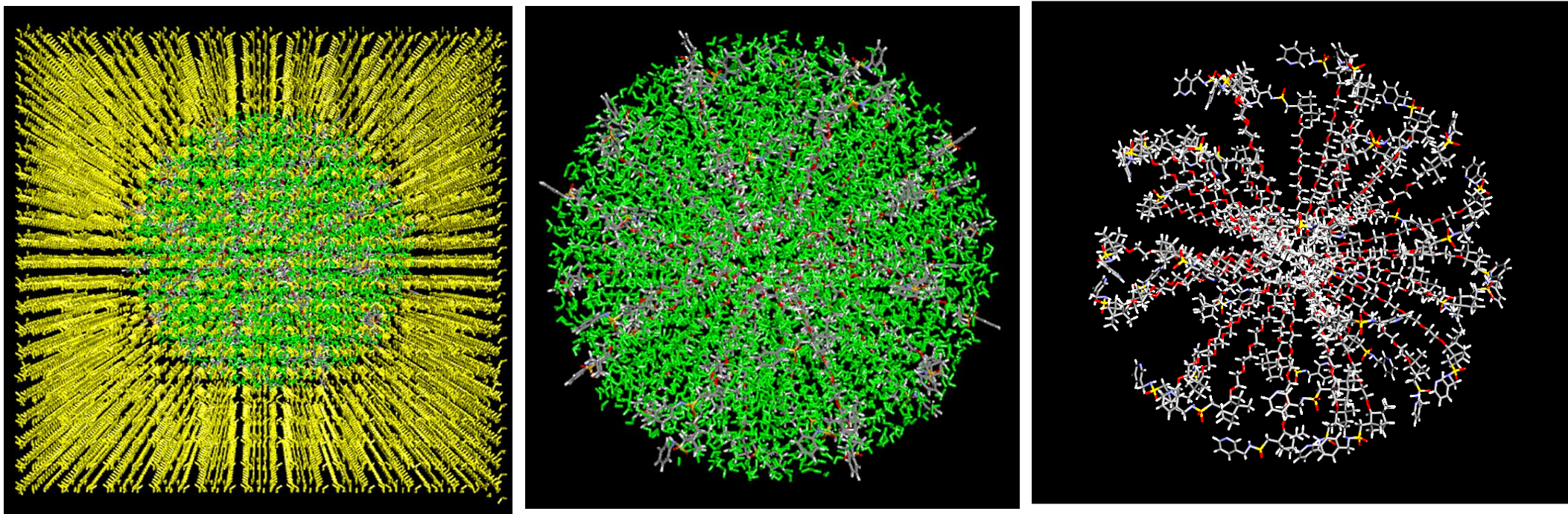


Figure 63. Constructed micelle with water (green) filling the core of the micelle, and surrounded with pentane (yellow).

3.5.2.2 Molecular dynamics simulations at 310 K for the constructed solvated micelles

After construction, three steps were required to proceed with the dynamics simulation (Figure 64) and these are detailed in the following paragraphs.

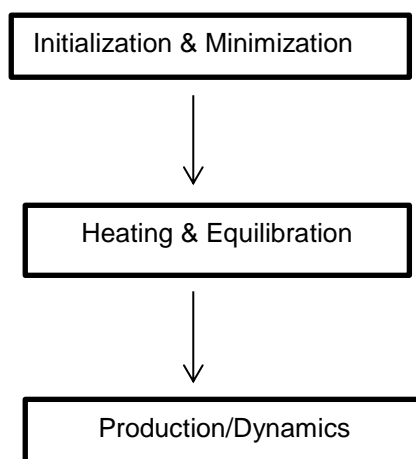


Figure 64: General overview of steps required for set-up of dynamics simulation

3.5.2.2.1 Initialization and Minimization

Prior to the molecular dynamics simulation, an energy minimization was conducted on the system. This minimization was carried out for the primary purpose of removal of any strong van der Waal's interactions that may lead to structural distortions, resulting in an unstable simulation. At this point, the system consisted of a 100 Å box with of surfactants (pre-constructed micelles), water and pentane molecules arranged in the appropriate regions of space with the appropriate density. The systems were minimized for 200 steps using a steepest descent algorithm, and then *via* Newton-Raphson for a further 100 steps.

3.5.2.2.2 Heating

During this stage, initial velocities at a low temperature are assigned to each atom of the system and Newton's equations of motion are combined to propagate the system in time. It is at a low temperature and initial velocities where the simulation begins. Periodically, new velocities are assigned at a slightly higher temperature as the simulation continues. This process of heating is repeated until the desired temperature is reached. This system was slowly heated from a temperature of 110 K to 310 K over 100000 steps (with 1 fs time step). The leap-frog verlet integrator was used.

3.5.2.2.3 Equilibration

The simulation of the system continued at 310 K for 200000 steps for a total duration of 200 ps simulation. During this time several properties are monitored, particularly the structure, pressure, temperature changes and energies. The purpose of this equilibration phase is to run the simulation until these properties become stable with respect to time. During equilibration, the system is allowed to reach equilibrium where there are fewer large movements due to stresses in the way the model has been constructed. Also, molecules have time to become more disordered and realistic to experimental conditions.

3.5.2.2.4 Production

The final step was to run the simulation under the same conditions as equilibration. Rotation and translation were cancelled every 10 steps. In the production phase 350000 steps of dynamics was performed corresponding to a total of 3.5 ps simulation. It is during the production phase that thermodynamics parameters are calculated and structural features are monitored.

During the production dynamics, some specific choices are as follows. Constant pressure/temperature based dynamics (using a Hoover thermostat at 310 K) was used together with the EWald summation method in the form of Particle-Mesh-EWald (PME) which was employed to aid with long-range non-bonded interactions (appropriate to working with PBC). PME only works correctly for systems with a zero total charge. The particle-mesh provides a defining grid to limit long-range interactions in all dimensions. For the purpose of this project the fast Fourier transform (FFT) was used “fftx48, ffty48, fftz48” to consider charges 48 points in each dimension. A cut-off radius at 16 Å, “cutnb16” was used to increase efficiency in the generation of the non-bonded pair list. To avoid computing bonded interactions between chemically bonded species (atoms 1-2, 1-3 and in some cases 1-4), these pairs were excluded from non-bonded energy calculations.

It is also worth noting at this point that the pentane (yellow, Figure 63) was very ordered prior to equilibration. Simulations run with pentane at such a low level of entropy resulted in a collapse of the box (the micelle ended up being surrounded by pentane, and there was no traversal of pentane through the boundaries); the ordering caused large gaps within the cube which could not withstand the duration of the simulation, resulting in collapse during minimization and initial heating. For the final simulations a box of hexane at higher density (which had also gone through a heating process) was constructed and used.

Aside from the pentane density, the CHARMM-based molecular dynamics simulation proceeded successfully; the simulation of the micelle was consistent with the aim that the water molecules would not push the surfactant molecules, breaking up the system. The water was equally distributed in the diameter as well as along the surfactant chains, and the intermolecular forces held the system together well under the temperature of simulation. The model was modified, and various micellar systems were constructed with the purpose of finding an optimum condition for micelle setup that would have greatest stability during the entire dynamics simulation.

The main aims of the research were to construct chiral micelles to be used both in asymmetric synthesis as well as for catalytic purposes. Therefore, each unit cell could be considered to be a micro-asymmetric reaction environment. The surface assembled from the fenchol-sulfonamide head region of the micelle forms the interface area in which reactions are to take place. It is important therefore for this interface region to remain stable and intact during the simulation period. The balance and constancy of the hydrophobic-hydrophilic interactions are essential in construction of a stable micro-micellar system, which can then be translated into macromolecular reaction conditions.

Considering as an extreme the results from the preliminary dynamics simulation in the previous sections, the micellar interface was not maintained and the micelle could not act as a contained reaction environment. Similarly, excessive mobility of the surfactant with little opportunity for the chiral head to remain at the interface was deemed to be an undesirable trait for a surfactant.

In order to more accurately determine the exact construction of a micelle to maintain stability during the entire dynamics run, a systematic investigation during the simulations was conducted by changing numbers of surfactants per micelle as well as internal diameters to find optimum conditions. The size of the internal diameter is of particular importance as it inherently governs the number of water molecules that the micelle can hold. Figure 65 shows the dimensions of the micelle measured in order to make judgement, while Figure 66 shows graphs which indicate the periodic change in dimensions along the x, y and z axis of the aniline-derived micelle with time. This was used as a guide as to which configuration of micelle would be most ideal. It is important to remember that this simulation is on a very small timescale; over longer time-scales, diffusion of surfactants in and out of the micelle would be expected. In Figure 66 the graphs 20.7 and 50.4 (corresponding to a micelle with $20 \times 2 = 40$ surfactants and internal diameter of 7 \AA , and a micelle with $50 \times 2 = 100$ surfactants with

internal diameter of 4 Å) show the most fluctuation; the micelle constructed from a total of 40 surfactants and internal diameter of 7 Å was the least stable. In this case the number of surfactants was too few, and the micelle too sparse, for an internal diameter of 7 Å, hence there were not enough surfactants to contain the number of water molecules filling the core, causing the micelle to expand too much along each axis. For the case of the micelle with 100 surfactants and an internal diameter of 4 Å fluctuation; was present this case may be explained as with an internal diameter of 4 Å there was not enough room for 100 surfactant tails closer to the core, resulting in strong repulsive forces which caused the micelle to oscillate to such a large extent. At this point it was confirmed that both the number of surfactants per micelle and internal diameter ratio had to be chosen suitably for a micelle in simulation. For the other two cases in Figure 66 (20.4 and 50.7), these constructions endured the duration of the simulations run successfully. We see that in these cases the micelle was stable over all three dimensions during the simulation and these influenced the choice of setup to take forward to the final simulations. Of these two choices, the micelle containing 100 surfactants had a higher density of chiral “heads” at the surface of the micelle. Thus from these preliminary observations, the decision was made to use micelles containing 100 surfactants with an internal diameter of 7 Å for the final simulations.

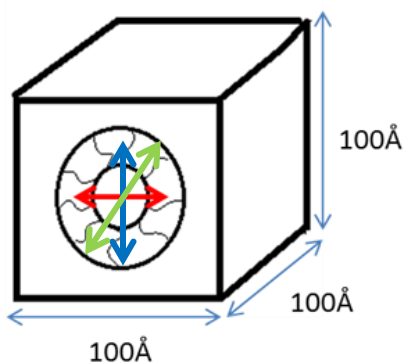


Figure 65. Representation of the simulation cell, and the dimensions of the micelle that were monitored.

Figure 67 shows a successful molecular dynamics simulation of an aniline-derived micelle system which lasted the entire 4 ps duration. At time $t = 0$ ps the hydrophobic head groups of the surfactants formed the outer surface of the micelle exposed to the hexane while the hydrophilic PEG chains formed the micelle core. Surfactants appeared to be homogeneously dispersed along the micelle with all tails pointing inwards. As production proceeded, we found a good balance between the attractive and repulsive forces, maintaining the spherical shape

of the micelle throughout with a good periodic motion during the course of the simulation, as predicted from graph 50.7 of Figure 66. At the end of the simulation it was found that all the water molecules were still contained within the micelle core. However, an interesting and unexpected phenomenon was observed; there was a great change in the displacement of the surfactant tails. The long chains appeared to have moved from a position perpendicular to the surface of the micelle to a more horizontal position, closer to the surface of the micelle.

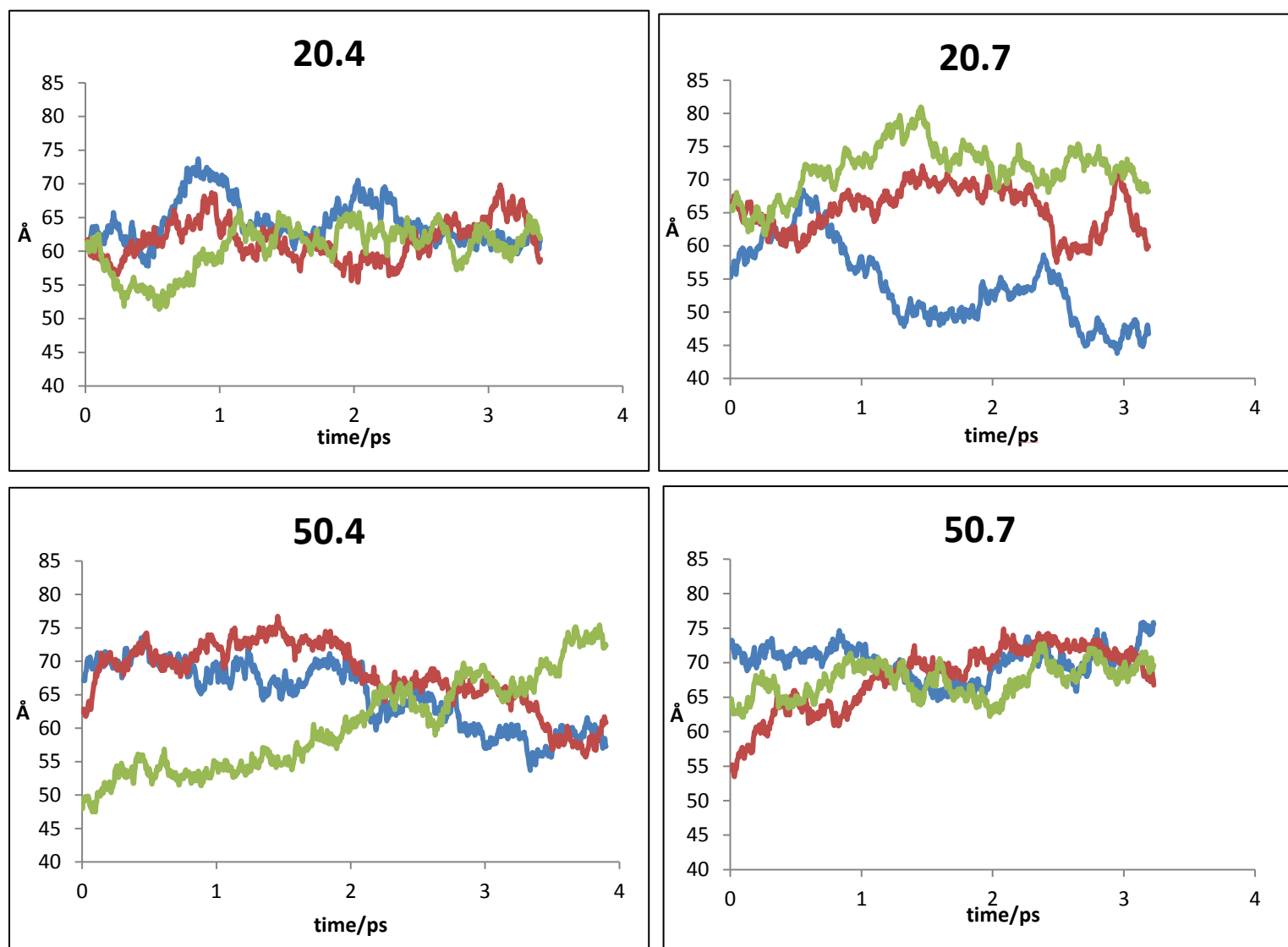


Figure 66. Progression of the dimensions of the micelle in three axes for four of the aniline-fenchol based micelles. The notation 20.4 indicates 20 surfactants per hemisphere (40 surfactants total) surrounding a hollow of radius 4 Å. All inner space is filled with water, and outer space is filled with pentane.

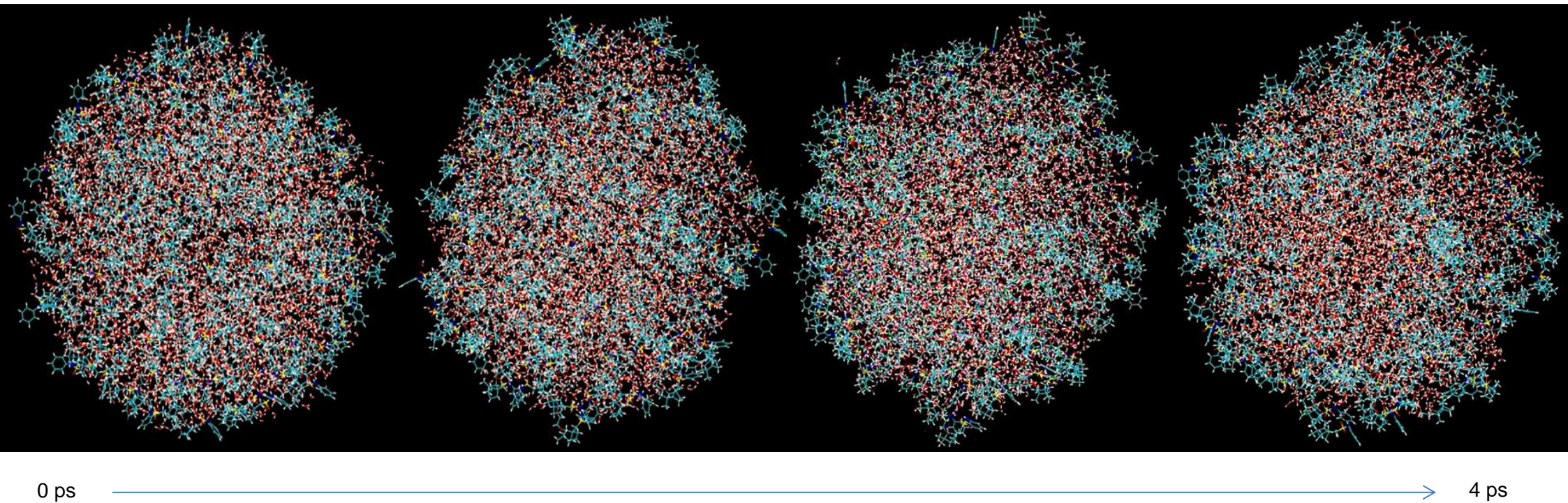


Figure 67. Evolution of the micelle under 4 ps of dynamics. The surfactants together with the inner phase of water are shown. The pentane remains hidden.

The surfactants during simulation ended up non-linear with many “kinks” along the long chains. The water molecules interacted along the length of the chains, yet throughout the production there was no breaking up of the micelle or leakage of water into the hexane. This bending of the surfactant chains about the ether bond may influence the properties of the micelle as the tails sit near the surface and the water molecules occupy a cohesive block within the core. A cause for the bending of the tail is possibly an entropic advantage. Another reason for this observation may suggest favourable water-water interactions, exceeding that of the water-polyethylene glycol, resulting in a thermodynamic force driving the polyethylene glycol from the centre to the surface of the micelle. Considering the vast changes of the positions of the surfactant tails, the sulfonamide head regions remain on the surface at the interface between the hexane and water solvents.

3.5.3 Packing Factor of Surfactants

As a further confirmation of the expected shape of the micelle upon assembly, the packing factors for each of the sulfonamide-derived surfactants were calculated. The formation and self-assembly of amphiphilic systems is governed by thermodynamic and geometrical influences. The type of structure formed by aggregation of surfactants is largely determined by its packing factor, P ; that is the ratio of the volume of the hydrophobic tail, v , to the length of this tail, l , multiplied by the effective surface area per head group, a . The value of P thus dictates the shape of the aggregate, in our particular case for spherical micelles, $0 < P \leq 0.3$. Looking at the cone shape (Figure 68) of an individual surfactant, on average the calculated packing factor for the surfactants was approximately 0.3 (Table 18) indicating experimentally that each surfactant would self-assemble into spherical micelles. It can also be inferred that in this study the size and shape of the sulfonamide head group in terms of steric bulk had no great bearing on aggregation or the general shape of the micelle.

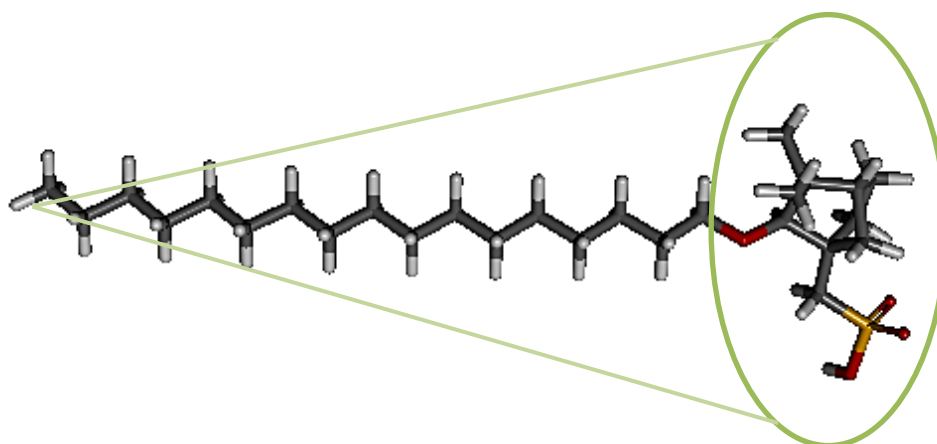


Figure 68. Extents of surfactant used to calculate the packing factor.

Table 18. The packing factors for a variety of surfactants.

Compound	Sulfonamide:	Packing Factor ($\text{\AA}^3 \text{\AA}^{-1} \text{\AA}^{-2}$)
S1	Aniline	0.286
S2	Benzylamine	0.297
S3	Furfurylamine	0.291
S4	Picolylamine	0.304

3.5.4 Solvent chirality:

Given that the micellar system was constructed from chiral surfactants in a two-solvent system made of water and pentane, the possibility of chirality transfer was investigated. In a set-up where an achiral solvent is placed in close proximity to a chiral molecule, the environment becomes chiral and may be regarded as asymmetric. This concept was further investigated with molecular modelling; as the surface of the micelle is chiral it was anticipated that the pentane molecules in such close proximity would experience instantaneous induced chirality, resulting in a resultant chiral zone being present as a possible reaction environment.

As there has been interest in this induced chirality, there has been development in the literature of methods of quantifying the degree of chirality, commonly referred to as indices of chirality. Buda *et al.*¹⁵⁵ have defined the measure of chirality within two categories; the first is those indices which measure the extent to which the chiral molecule in question differs from its achiral reference object, and the second is a measurement of the extent to which two enantiomers differ from each other. The dynamics trajectories provided an ideal source of information for this type of study as the only chiral input was the bicyclic fenchol system, yet the measurement could be made on the pentane to determine the chiral influence. Therefore, there was a means in this study to quantify chirality.

Quantification requirements used to set up the parameters for calculations were that at a molecular level, non-zero pentane molecules were chiral.

This should not change upon rotation and translation but should switch signs upon reflection, providing a pseudo scalar measure.

The term gyration tensor, G_0 , was used to describe the pseudo scalar behaviour or the instantaneous chirality of the achiral solvent molecules.

$$G_0 = \frac{1}{3} TrG$$

$$= \frac{1}{3} \sum \rho(\mathbf{r}_1)\rho(\mathbf{r}_2)\rho(\mathbf{r}_3)\rho(\mathbf{r}_4) \cdot \frac{[(\mathbf{r}_{12} \times \mathbf{r}_{34}) \cdot \mathbf{r}_{14}](r_{12} \cdot r_{23})(r_{23} \cdot r_{34})}{(r_{12} r_{23} r_{34})^n r_{14}^m} \quad (14)$$

Where the mass of the atom was used for $\rho(r)$, the r_{ij} are the vectors defined by atom i and atom j , a value of 2 was used for n and a value of 1 for m . The term was summed for all quadruples of atoms within the molecule of interest. With Equation 14, one is able to interpret chirality of the micelle model. G_0 maybe be defined as the isotropic chirality index and this quantity allows for the allocation of a non-zero numerical assignment for chiral molecules, as well as the change of chirality upon translation.

Equation 14 was applied initially to the achiral solvent resulting in Figure 69, where shades of red and blue were used to indicate degrees of chirality.

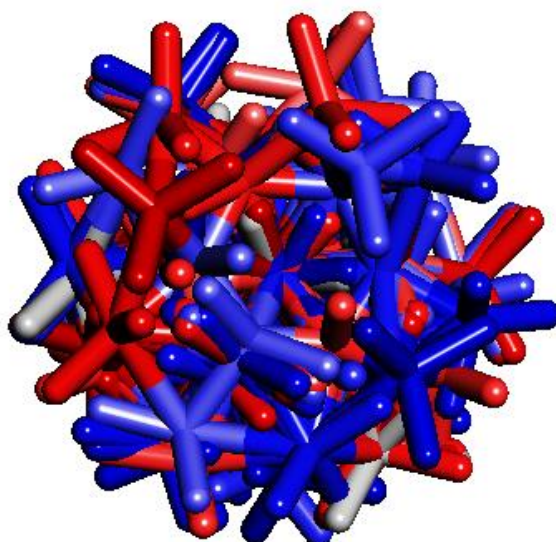


Figure 69. A conformational search for pentane has provided many conformers shown superimposed. The colour shows degree of induced chirality for pentane, where red infers positive chirality, blue infers negative chirality (in relation to Equation 14) and colour intensity indicates the degree of chirality.

Equation 14 was then applied to a fully constructed micelle system (to only the pentane molecules present), and showed promising preliminary results as seen in Figure 70.

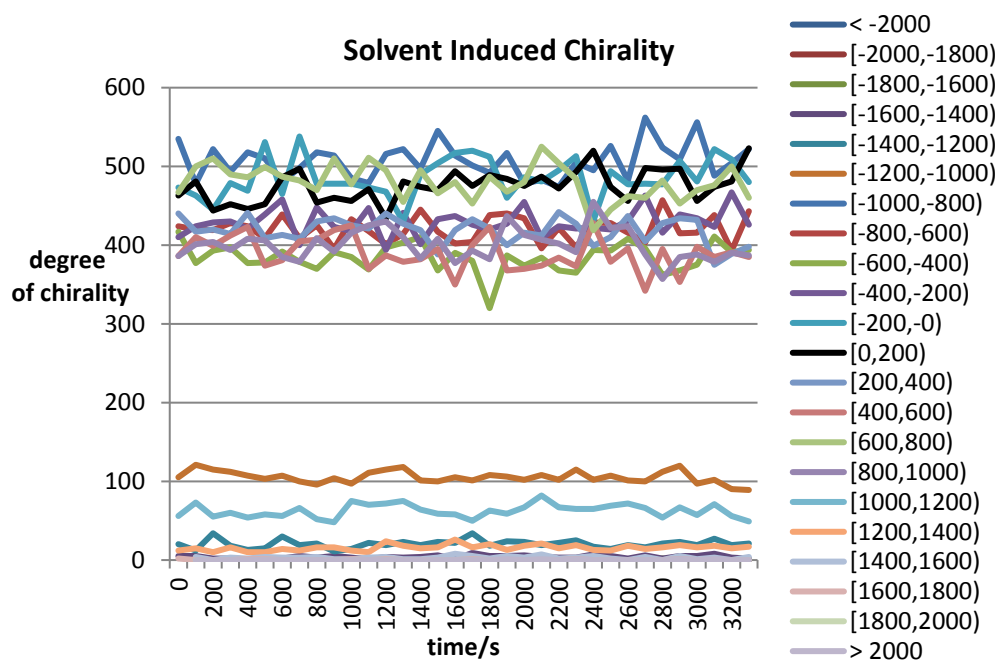


Figure 70. Numbers of pentane molecules with a specific range of chirality during simulation.

Figure 70 is difficult to interpret. It appears that there are large numbers of pentane molecules with a small degree of chirality, and much fewer with extreme indices of chirality. It is difficult to determine, for instance, even though there are more molecules in the band (-1200, -1000) than in the band (1000,1200), whether one chirality or another predominates during the simulation.

Observing the chirality directly in the simulation is more subjective. The chirality visualized in Figure 71 shows a single point during the dynamics; it would appear that there are more blue pentane structures than red ones, particularly when observing the surface of the micelle.

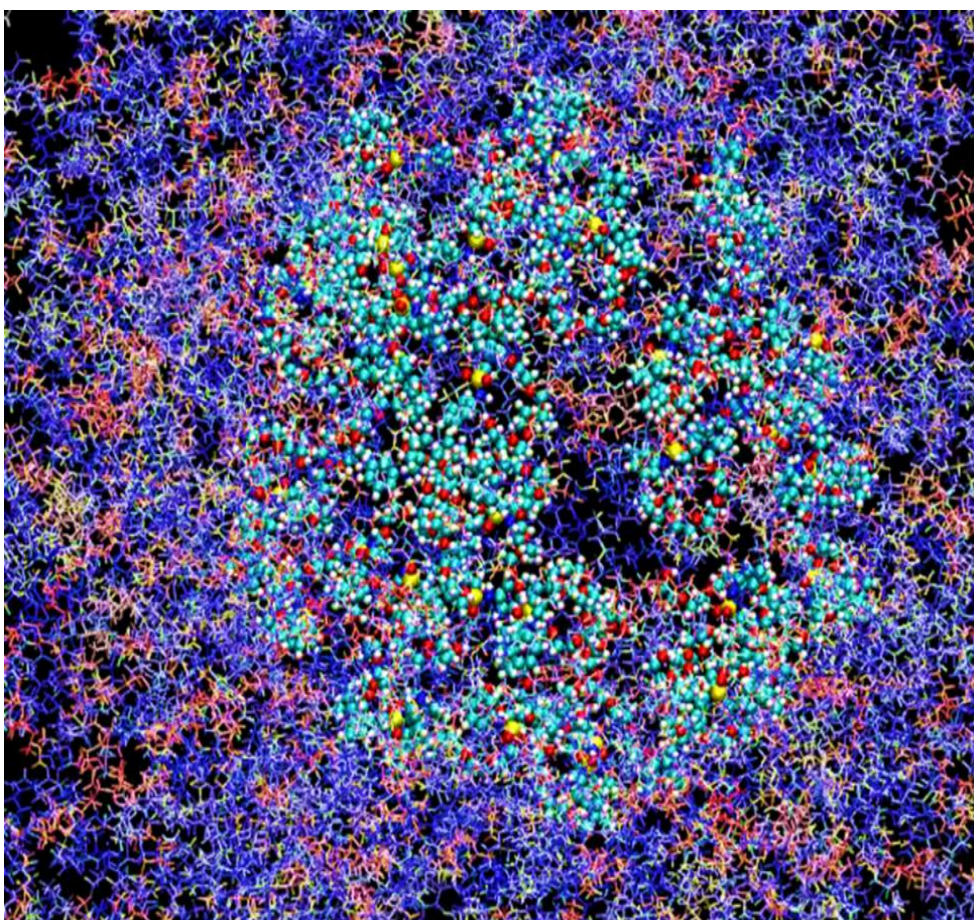


Figure 71. Chirality (blue and red) of solvent pentane at a point during the dynamics simulation.

3.5.5 Final modelling:

Given the difficulties with interpreting the chirality data, and with the use of un-equilibrated pentane, modifications were made for the final molecular dynamics runs. Firstly, hexane was used (with a wider scope for chirality than pentane) and a conformational search in VEGAZZ provided conformations of hexane. The ratios of the populations of conformers (using the Boltzmann ratio at 310 K) were determined, and Packmol was used to combine this ratio of conformations into a 110 Å cube at the appropriate density for hexane. This was then equilibrated within CHARMM prior to the simulations.

Secondly, care was taken with respect to the design of the surfactant. For the final molecular modelling simulations, attention was paid to the picolylamine-derived surfactants for the creation of the micellar systems. This choice was due to the pH responsive nature of the picolylamine moiety that makes the system not only chiral but also tuneable. Under acidic conditions the picolylamine aromatic nitrogen may be protonated, while under very basic conditions the sulfonamide is deprotonated. Neutral conditions also exist. Zwitterions are unlikely given the pK_a and pK_b of these groups. Other neutral sulfonamide-derived surfactants were also constructed and simulated. The synthesis of surfactants during the previous section of the study guided the design here, and the modelling results we hope will prove valuable in feeding back into future synthesis of surfactants, bearing in mind the desired characteristics of the final micelles. Surfactants were constructed *in silico* with both fenchol and camphor systems and as suggested from the preliminary results, the molecular dynamics simulation was to be performed on a 100 surfactant micelle with a 7 Å internal diameter filled and surrounded by both water and hexane solvent molecules for each micelle of interest.

In addition to the fenchol/fenchone derived systems, a series of camphor-based systems was also constructed. The reasoning behind this was that as the “tail” connects to the “head” *endo* to the norbornyl structure in the fenchone-derived systems, and this arrangement is *exo* in the camphor based systems, the head will be oriented differently at the interface for these two different systems, and the influence of chirality may well be different. The camphor-based surfactants are shown in Figures 72, 73 and 74.

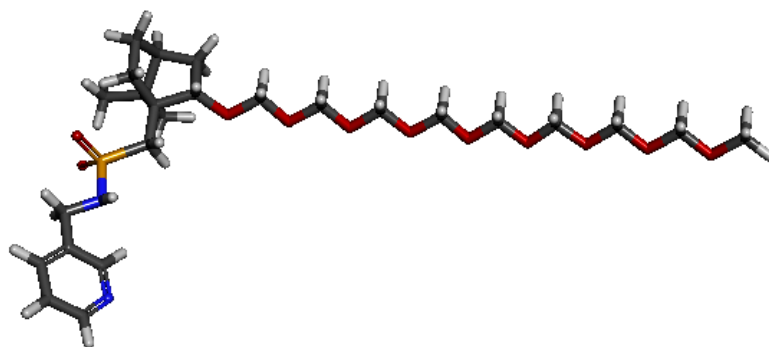


Figure 72. A neutral camphor sulfonamide/picolylamine/polyethylene glycol-derived surfactant.

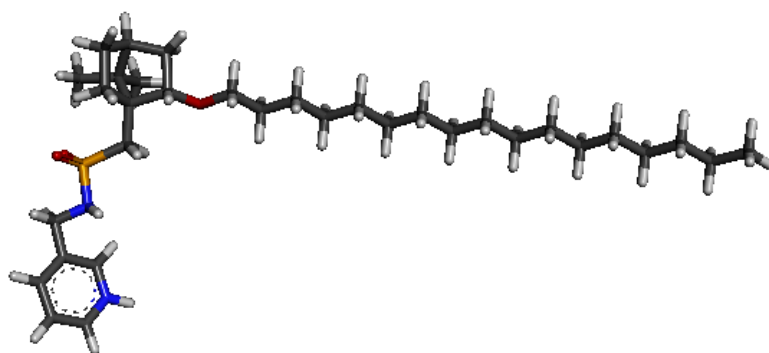


Figure 73. A cationic camphor sulfonamide/picolylamine derived surfactant.

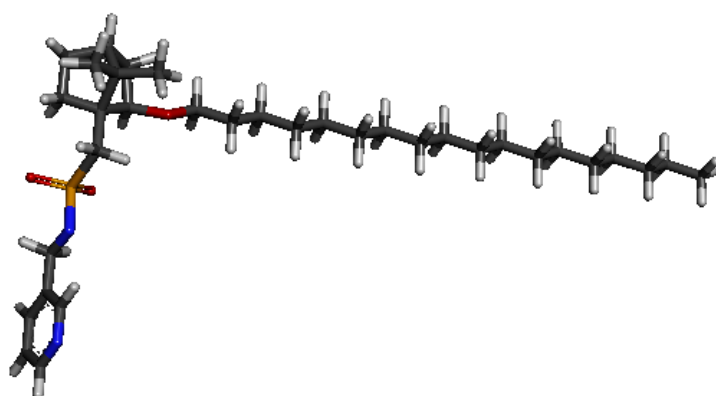


Figure 74. An anionic camphor sulfonamide/picolylamine derived surfactant.

The construction of the micelles required force fields for the surfactants which were obtained from the CGenFF server. For the anions, force field parameters were added for bonding to a nitrogen anion in the negatively charged sulfonamide moiety, a particular bonding case not

supported by CGenFF. After the micelle was generated, these force fields were used within the CHARMM program for the simulation.

Table 19 shows all sulfonamide surfactants constructed into micelles for final modelling in water/hexane, with the key used in the later discussion.

Table19. The key components of the derived sulfonamides used as surfactants in the micelle simulations

Key	Head	Amine	Alkyl	Charge
FANE	Fenchone	Aniline	Hexaethyleneglycol	Neutral
FBNE	Fenchone	Benzylamine	Hexaethyleneglycol	Neutral
FINE	Fenchone	Imidazole	Hexaethyleneglycol	Neutral
FPIP	Fenchone	Piperidine	Hexaethyleneglycol	Neutral
FFNE	Fenchone	Fufurylamine	Hexaethyleneglycol	Neutral
FPNE	Fenchone	Picolylamine	Hexaethyleneglycol	Neutral
CPNE	Camphor	Picolylamine	Hexaethyleneglycol	Neutral
FPBUA	Fenchone	Picolylamine	<i>n</i> -Octadecoxy	10 Anion/90 Neutral
CPBUA	Camphor	Picolylamine	<i>n</i> -Octadecoxy	10 Anion/90 Neutral
FPBUC	Fenchone	Picolylamine	<i>n</i> -Octadecoxy	10 Cation/90 Neutral
CPBUC	Camphor	Picolylamine	<i>n</i> -Octadecoxy	10 Cation/90 Neutral

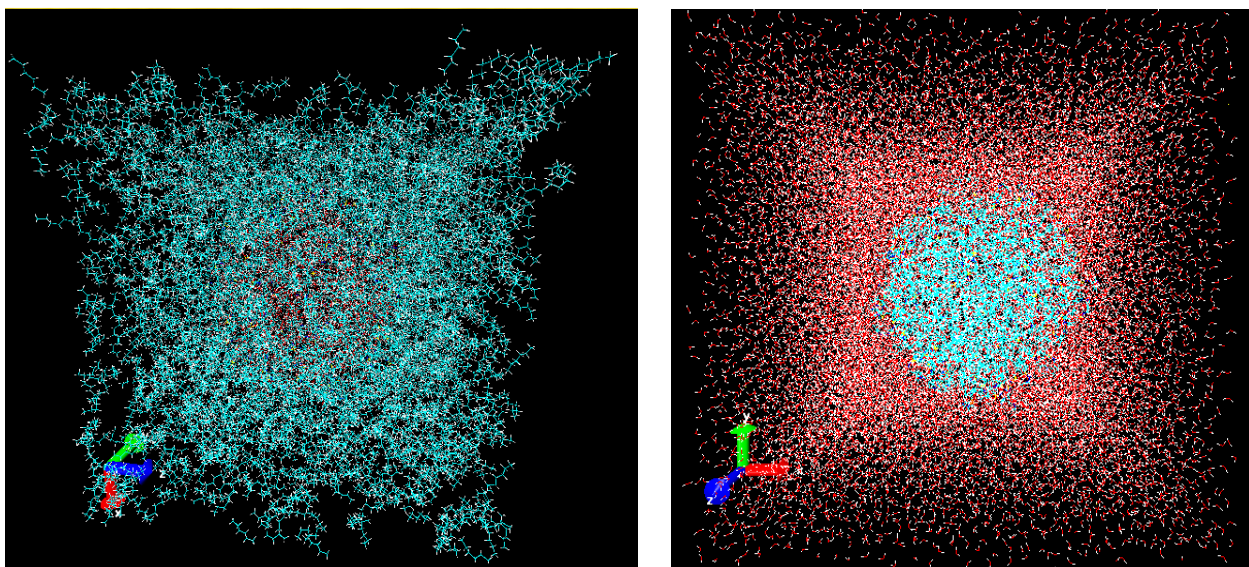
Prior to dynamics the micelle was constructed as detailed in the previous section and solvated as follows – for the neutral surfactants the inner region of the micelle (populated by the polyethylene glycol tails) was solvated with water, while the outer region was solvated with hexane. For the charged systems the reverse was true, where the inner region was solvated with hexane. When considering solvation of the micellar system, our main concern was not the behaviour of the bulk hexane and water molecules, but rather how the micelles interact with the solvent as well as amongst the surfactant molecules themselves. For these simulations, as before, the shape of the unit cell chosen was a 100 x 100 x 100 Å cube with periodic boundary conditions.

Given the tune-ability of the picolylamine-derived surfactants, these may be protonated or deprotonated given a change in pH environment. The cationic and anionic micelles have an overall charge and require neutralization from negative and anionic counter ions respectively,

prior to minimization. For a more accurate representation during dynamics simulations, an excess concentration of counter ions of 0.15 M of KCl or NaCl was added to the system. On addition of ions, random solvent molecules were replaced. It was noticed, however, that the unit cell for the charged micelles was not able to withstand the simulation and expanded enormously during the beginning stages. However, given that the charged micelles contained 100 surfactants, a charge of positive or negative 100 resulted in a repulsion too great for the micelle to endure during simulation.

The strategy was then to modify the charged micelles to the situation where 90% of the surfactants were unionized, leaving for only 10% cations or anions with the aim of reducing the impact of repulsive charges. This modification proved successful as the micelles maintained stability during the simulation. This was a reasonable assumption to make, as, if the aqueous phase is one pH unit away from the pK_a or pK_b in the direction that favours ionization, then 10% of the surfactant molecules will be ionized.

Figure 75 shows examples of the “water in oil” and “oil in water” micelles respectively. Given the size of the hexane molecules, the bounds of the periodic boundary conditions appear more ragged with hexane as the outer solvent.



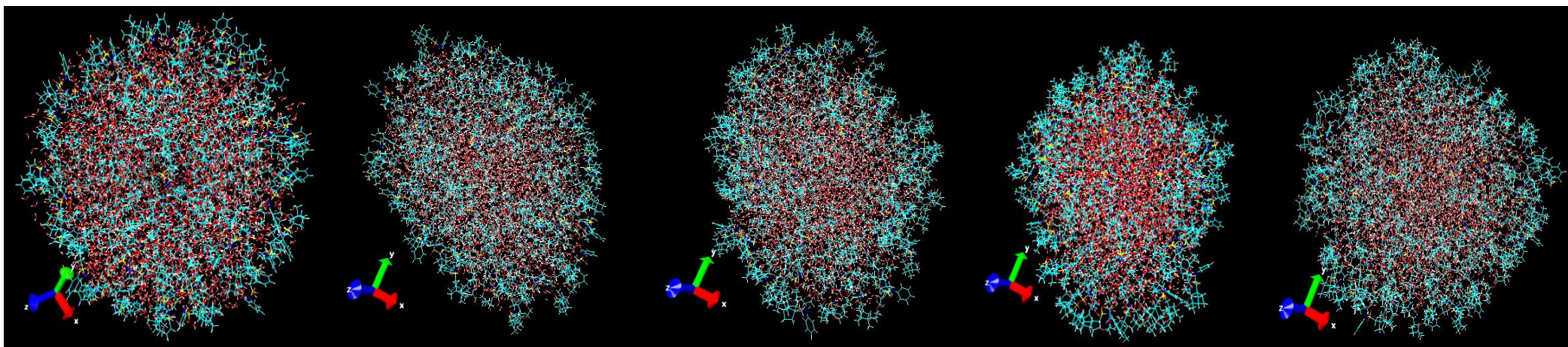
A

B

Figure 75: A. micellar system with hexane (blue) as the bulk solvent surrounding the micelle and aqueous core. B: charged micellar system with water as the bulk solvent (red and white) surrounding the micelle and hexane core.

Both systems, (Figure 75 A and B) are shown at the end of the simulation after approximately 600 ps. It can be seen that the unit cell wall maintains its shape and the micelle itself is able to withstand the entire simulation without breaking apart. In all cases, the core solvent remained confined among the surfactant polar and non-polar tails.

FANE



CPBUA

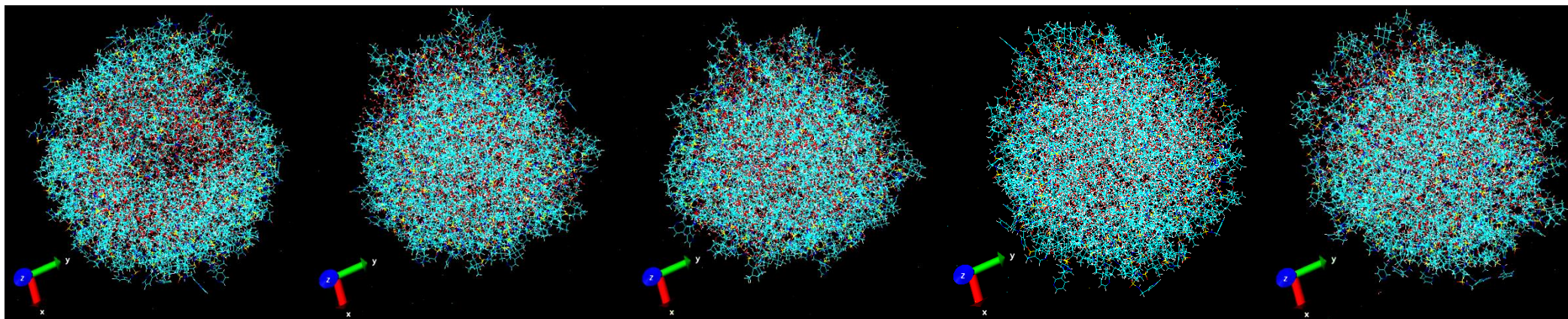


Figure 76. Evolution of the uncharged micelle FANE (top) with the hexane molecules hidden, and the charged micelle CPBUA (bottom) with water molecules hidden, during the 600 ps of dynamics.

For ease of computation, the equilibration and production dynamics were combined into a single simulation, where the start of the dynamics indicates the equilibration period, and the latter stages the longer-term behaviour of the system. The total simulation time of 600 ps was long enough for observation of these behaviours.

Figure 76 shows snapshots of the simulation of the micelle with time. It can be seen that the micelle has an overall spherical shape at the beginning of the simulation (at frame = 0 ps). As expected for the micelle consisting of neutral surfactants, the surface is comprised of hydrophobic groups surrounded by the bulk solvent, hexane, while the water is distributed amongst the polyethylene glycol chains at the micelle core. At the start of the simulation the aniline sulfonamide head groups at the surface are fairly homogenous, and with time there is a noticeable change in shape. Although the structure remains globular-like, it does take on a more ellipsoidal shape. Considering the average variations of the radii along each x, y and z axis, the largest extent reached is approximately 70 Å. The equilibration shape of the micelle is therefore ellipsoidal exhibiting overall good flexibility and retention of core water molecules.

Considering the kinetic and potential energy graphs (Figures 77, 78 and 79, **KE** and **PE**), overall the trends are very similar; for the neutral micelles with the bulk solvent being water there is a noticeable drop in energy at the beginning which is attributed to the equilibration of the entire system. After approximately 200 ps the potential energy of the system is stabilized and remains constant until the end of the simulation, implying an overall balance between repulsive and attractive forces of the micellar system. A few anomalies are to be noted: FPIP, FPNE and CPNE do begin to undergo equilibration as seen in the drop in energy, but there is a substantial downward drift past 200 ps with no distinct equilibration end point and no apparent stabilization. Kinetics graphs **KE** in Figures 77, 78 and 79 show the same overall trend, with no distinct variances, indicating a constant temperature throughout simulations of all micellar systems both neutral and ionic.

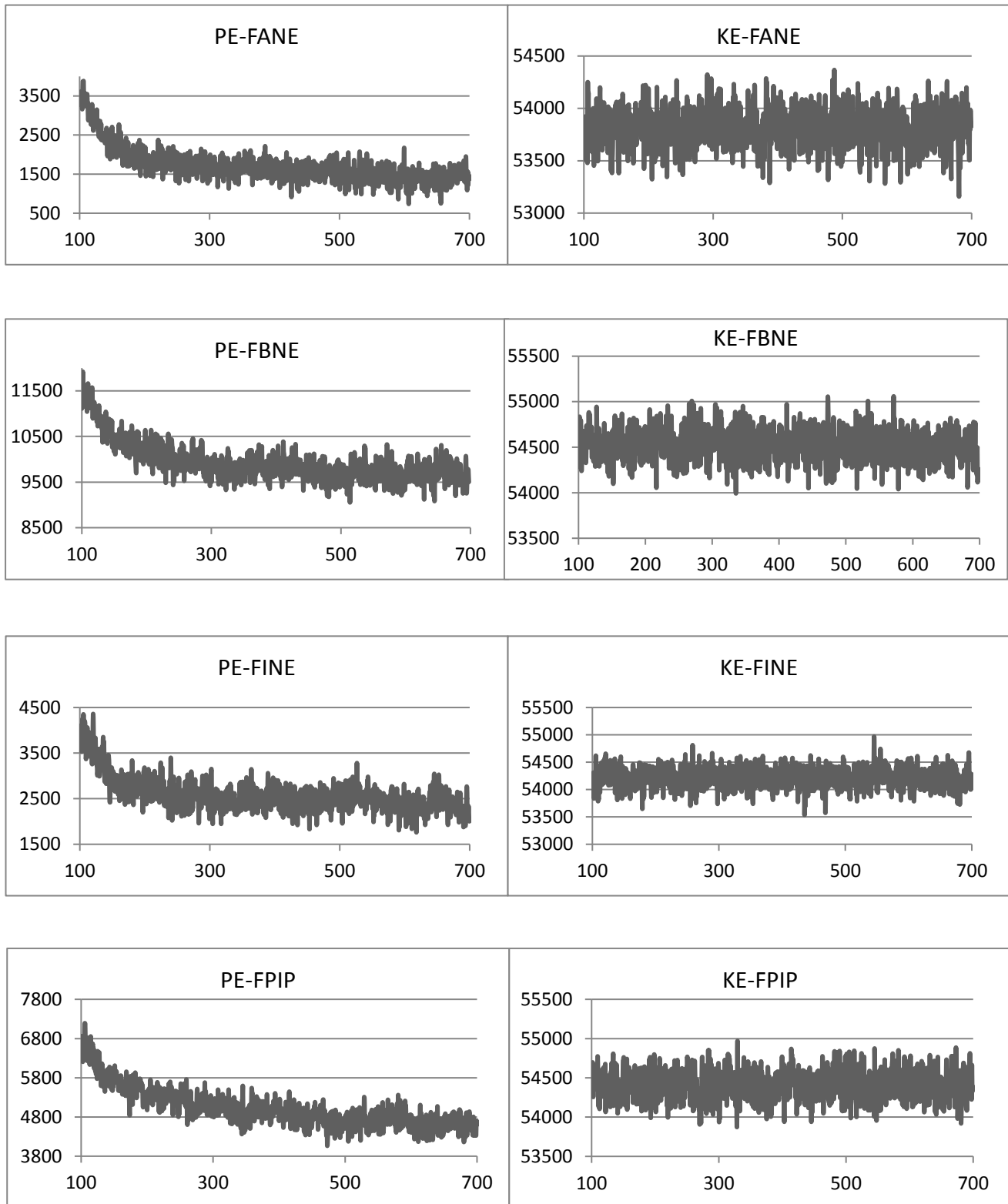


Figure 77. Kinetic and potential energy during course of 600 ps of dynamics. The horizontal axis starts at the end of the heating cycle of 100 ps.

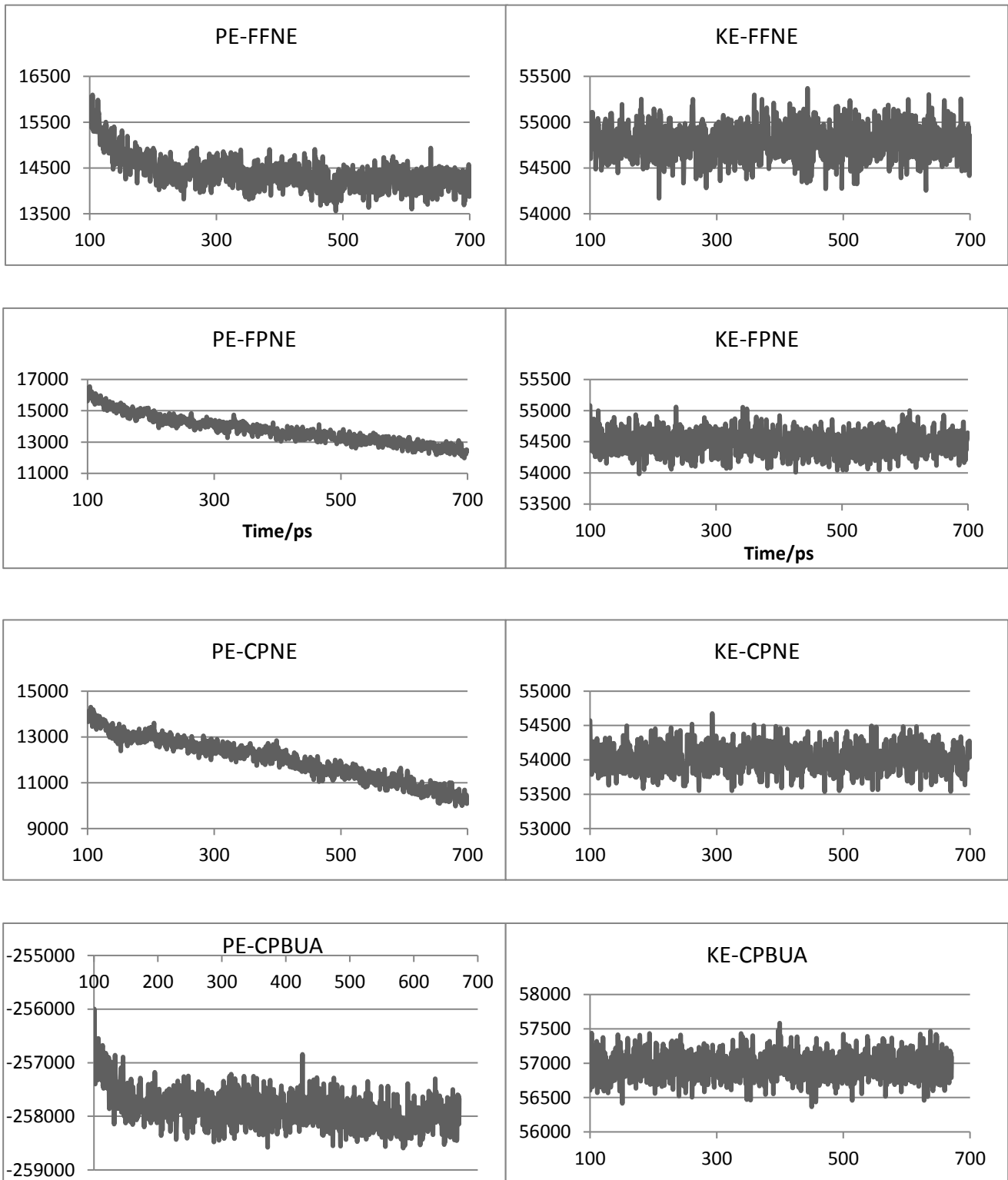


Figure 78. Kinetic and potential energy during course of 600 ps of dynamics. The horizontal axis starts at the end of the heating cycle of 100 ps.

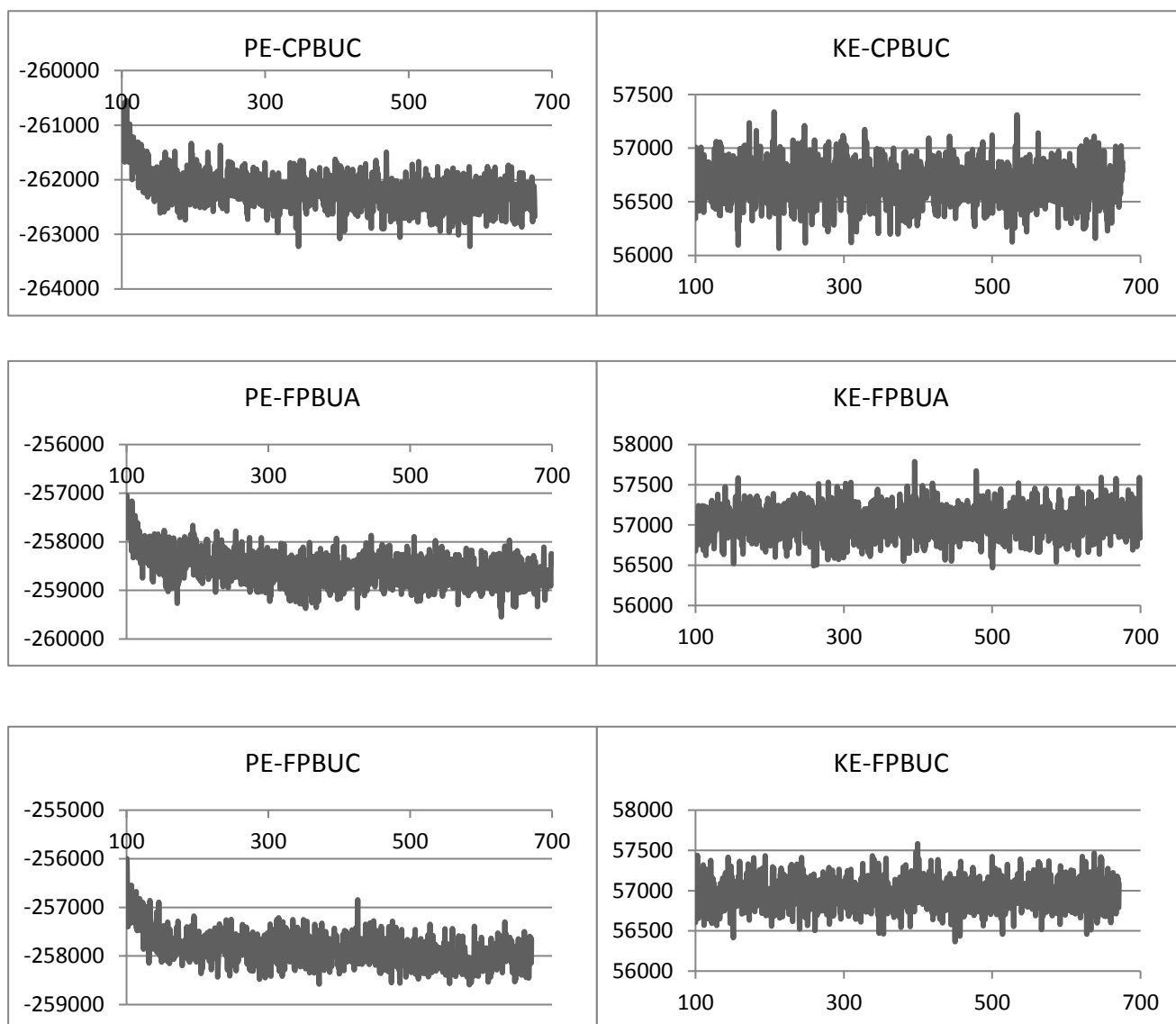


Figure 79. Kinetic and potential energy during course of 600 ps of dynamics. The horizontal axis starts at the end of the heating cycle of 100 ps.

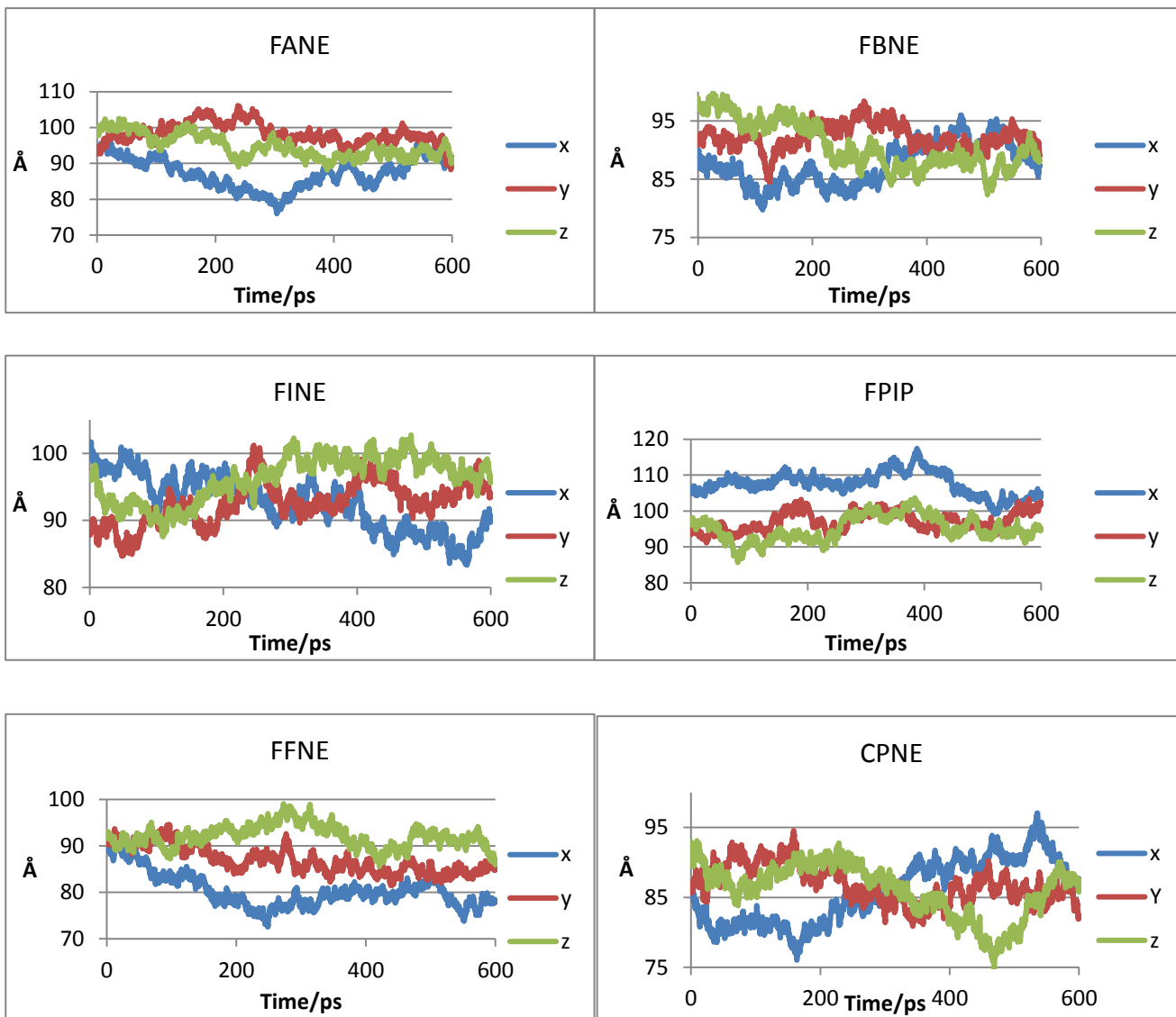


Figure 80. Variation in dimensions of the micelle for six of the neutral micelles during 600 ps dynamics simulation.

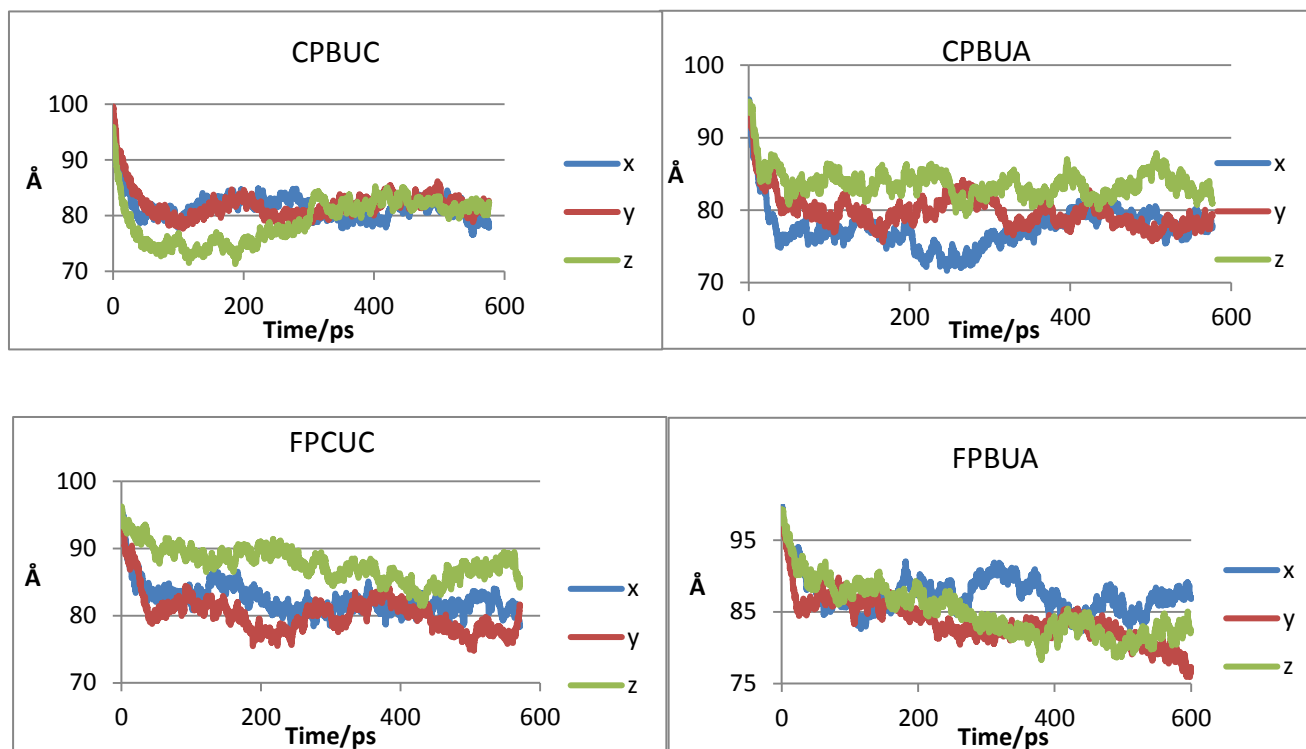


Figure 81. Dimensions of the micelle across three axes for the charged micelles during 600 ps of dynamics simulation.

The graphs in Figures 80 and 81 show the contraction and expansion of the micelle along the x, y and z axis. Both neutral and ionic micelles have an overall stable motion, with CPNE showing the most oscillation. In this particular micelle, the oscillation appeared to be present from the start of simulation, with a period of oscillation covering the 600 ps of simulation. A longer simulation would be required to confirm the presence of oscillations. It could also be argued that oscillations are dependent on what are essentially random starting conditions. Although the software can account for and cancel rotation and translations of the cell as a whole, a translation or flow of a subset of molecules within the micelle could feasibly set up oscillations that cause the micelle to oscillate during the course of simulation. The fact that micelle remained intact during oscillation points to the micelle being feasibly stable experimentally.

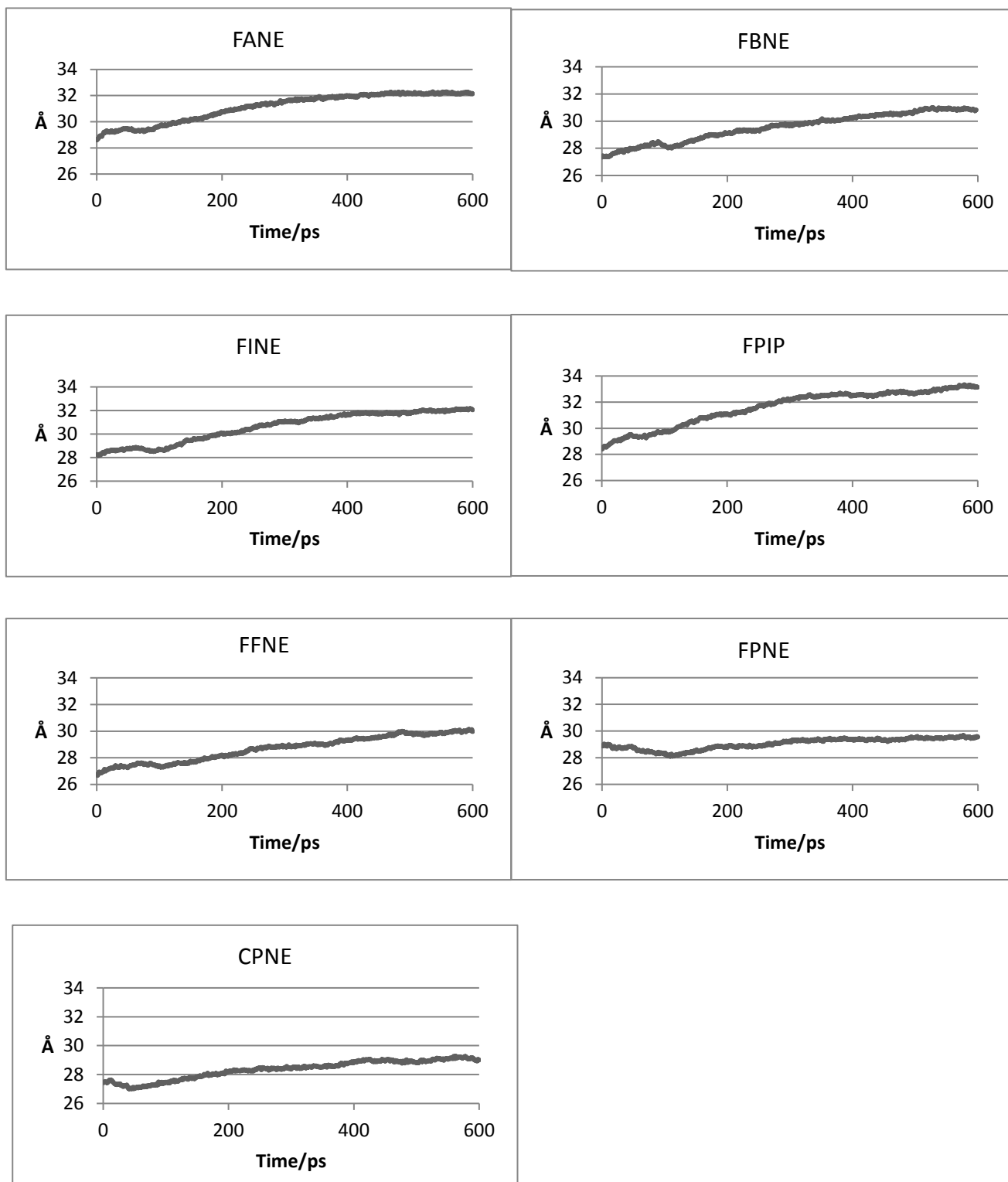


Figure 82. Radius of gyration for the neutral micelles during the course of simulation.

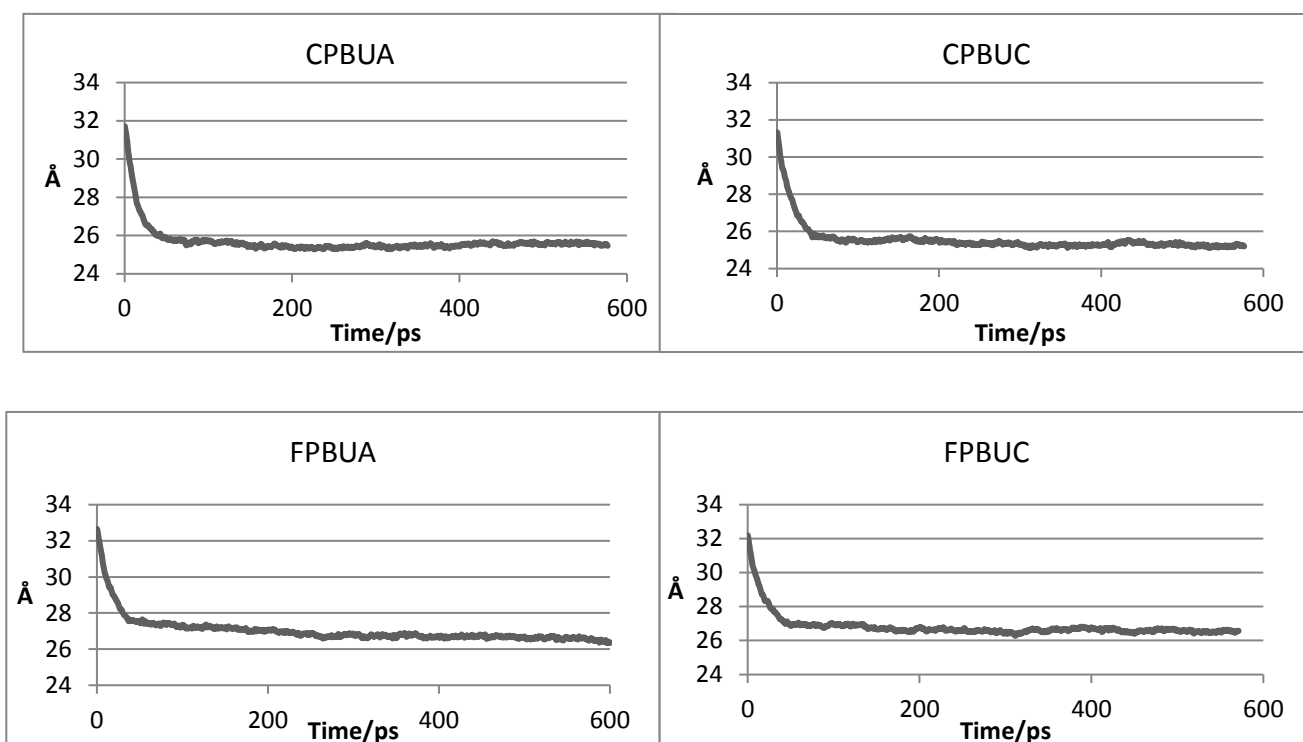


Figure 83. Radius of gyration for the charged micelles.

Another good indicator of micelle stability can be inferred by considering the radius of gyration. When looking at the micellar system one can determine the movements of the polymer chains in terms of mass moment of inertia, that is, specific points of mass moving about an axis of rotation. Graphs in Figure 83 show the evolution of the radius of gyration for the neutral micelles. The radius of gyration stabilizes in most cases towards the last 200 ps of the dynamics, attributed to stabilization of the micelle. The tails adopting a more disordered and peripheral stance within the micelle may have significant effect on this behaviour. These neutral micelles have a radius of gyration stabilizing between 28-32 Å. This difference may only be attributed to the amine derivatized head region.

In Figure 82, equilibration for the charged micelles shows a sharp decrease for approximately 40 ps and then stabilizes at 27 Å for nearly the entirety of the simulation. This adds support for the choice of method of construction of these micelles, with 90% of the micelle constructed from unionized surfactant and only 10% of the micelle remaining charged.

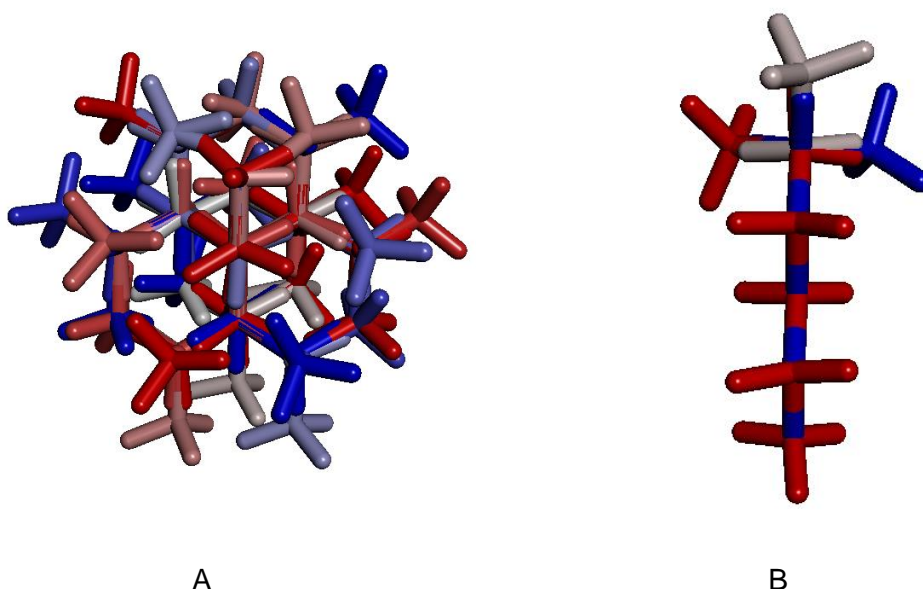


Figure 84. A: Chirality of several conformers; B: Chirality of three conformations illustrating an achiral conformation and conformers with equal and opposite chirality.

The carbon atoms of the hexane solvent were investigated for induced chirality by the micelle. Graphs were constructed to monitor the change in chirality of hexane in distance intervals moving further away from the chiral centre of the surfactant. The graphs in Figure 85 are for charged micelles (which contain the hexane on the inside core, and have a relatively small amount of hexane molecules). These graphs show the total chirality in regions away from the chiral head. The nearest distance (blue) thus shows a greater magnitude of chirality due to the larger numbers compared to the total chirality in the further region (red) exhibiting fewer hexane molecules (Figure 84). There appears to be an overall positive chiral influence on the hexane molecules filling the micelle core. These hexane molecules are likely to be found along the long hydrocarbon chains close to the sulfonamide head region. The graphs in Figure 86 track chirality of a neutral micelle. In these cases, hexane is the solvent surrounding the micelle; hence the greater number of hexane molecules in contact with chiral regions of the micelle surface leads to a greater total chirality. As one moves outwards, the number of hexane molecules to consider increases substantially and the trend for the nearest molecules is greatly over-shadowed by the trend for the more distant molecules. The chiral influence of only the furthest investigated hexane solvent is shown – this is clear evidence of the chiral influence far from the individual surfactants.

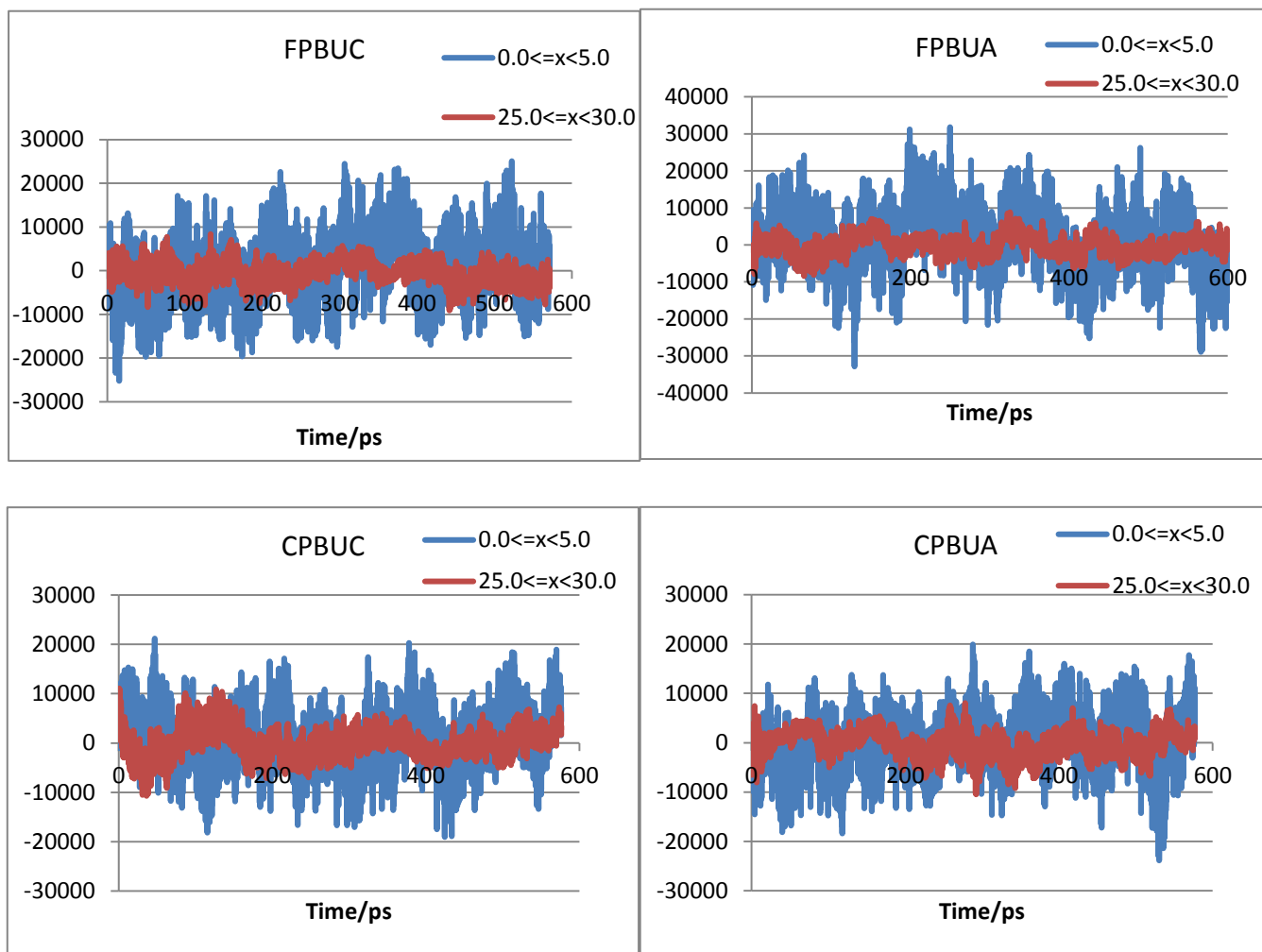


Figure 85. The sum of chirality indices for hexane molecules at a particular distance from the sulfonamide S of the micelle surfactants. For these micelles the hexane is the internal solvent.

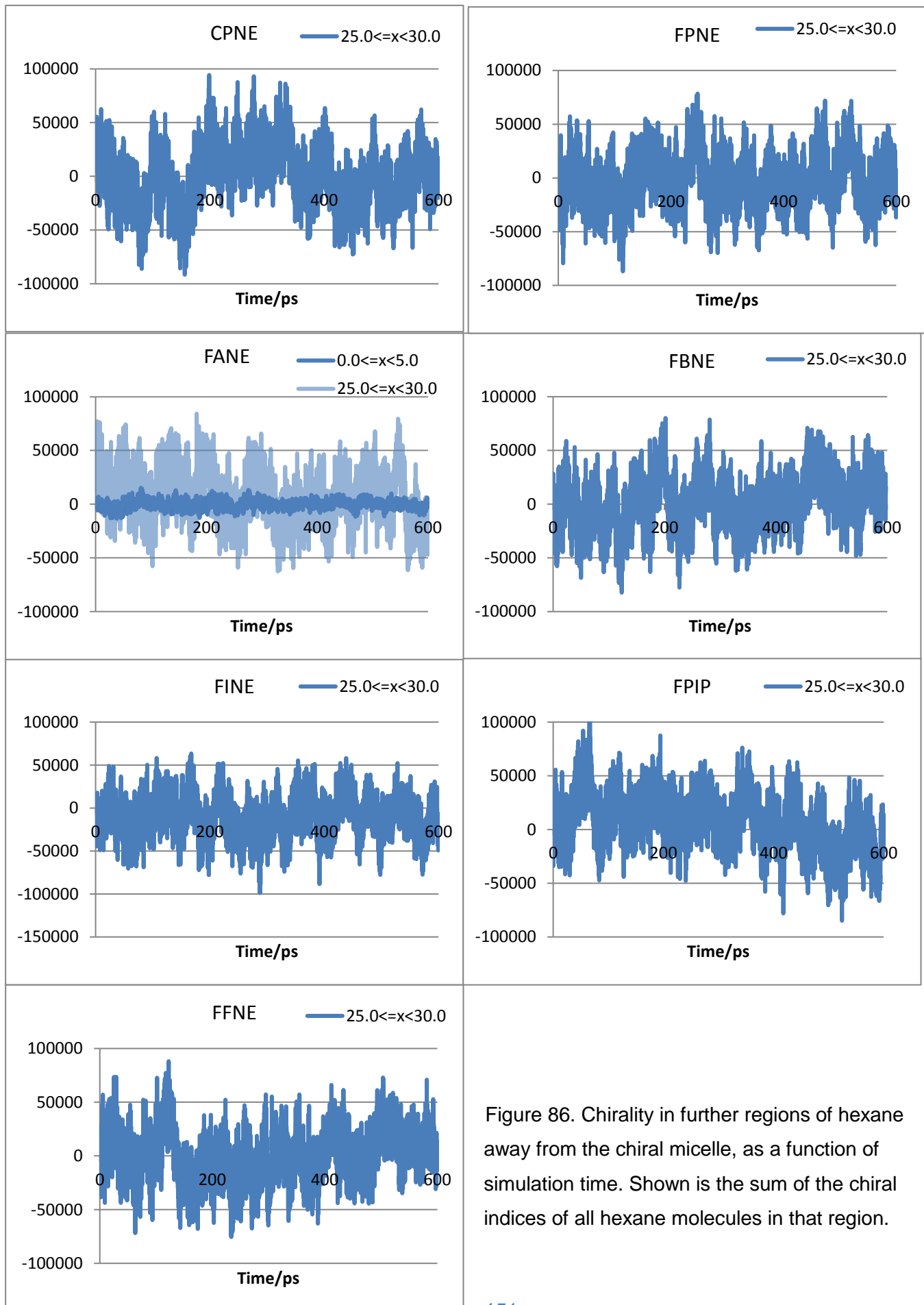


Figure 86. Chirality in further regions of hexane away from the chiral micelle, as a function of simulation time. Shown is the sum of the chiral indices of all hexane molecules in that region.

3.5.6 *Micelle studies conclusion*

Headway has been made in the synthesis of both normal and reverse micelles, while the focus of performing molecular dynamics simulations of a series of micelles has been accomplished. Full dynamics simulations were achieved for the tuneable picolylamine-derived surfactants for both camphor and fenchol moieties under neutral, acidic and basic conditions. A series of neutral fenchol-derived micelles were constructed *in silico* and successfully simulated. Overall, all micelles withstood the dynamics simulation and maintained their stability and general shape throughout the study. Further, there is evidence of chirality at regions far from the micelle interface. Reactions taking place at the interface will naturally experience a significant chiral environment. Therefore, these designed micelles are a viable and plausible vessel for experimental purposes, either for use in catalysis or as a chiral reaction environment.

Conclusions

The study and evaluation of substituted norbornyl systems, namely camphor and fenchol derivatives, have led to some unexpected observations which called for in-depth physical and mechanistic studies of these compounds. Detailed study of the racemization pathway following the decomposition of a camphor tosylate allowed for the exploration of rearrangement pathways *via* deuterium (^2H) labelling. Extensive ^1H and ^2H kinetic NMR studies were performed with the purpose of confirming the proposed mechanisms. The evidence supports the proposed highly concerted involvement of Wagner-Meerwein, 6,2-hydride shift and Wagner-Meerwein processes in the transformation of the kinetic product (**64**) to the thermodynamically favoured final product (**65**).

The synthesis of commercially unavailable fenchene has been successful; however, the first attempt at the fenchene synthesis led to a kinetic and conformational study stimulated by the observation of an unusual and surprising pair of dimer products. This pair of dimers was associated with the chirality of a single sulfur atom. The mechanism of formation of these dimers has been resolved.

Both camphor and fenchone derivatives were evaluated for applications in asymmetric synthesis, stemming from their optical purity. This took the form of a combined synthesis and molecular modelling study involving the design and construction of chiral normal and reverse micelles in a dual-solvent system.

The synthesis yielded a series of novel fenchol-derived sulfonamides for use in the head group region of the surfactant. An easy, green and highly efficient sulfonamide synthesis method was developed and applied for both camphor and fenchone derivatives producing excellent yields. Mass spectrometric studies revealed some unusual fragmentation pathways. Attention, however, was paid to the molecular modelling and simulation studies of the micellar system. A variety of in-house scripts and visualising programs such as DSV and CHARMM were used for the construction, assembly and simulation of the micellar systems. Data was obtained successfully for a series of seven neutral and four charged micelles. Results were very promising for all systems as all micelles withstood the equilibration and dynamics runs.

The concept of solvent induced chirality was explored primarily for the purpose of asymmetric synthesis and heterogeneous catalysis. There is definite evidence of induced chirality, more so for systems containing hexane in proximity to the micelle and interacting with the chiral micelle surface.

The objectives of this study were largely achieved. Further work in this area is expected to include:

- Further studies of rearrangements of similar systems using isotopic labelling. The carbocations involved can well be isolated at low temperatures and observed using NMR spectroscopy
- Synthesis of the designed series of surfactants and characterization of the micelles using techniques elaborated upon in the discussion
- The exploration of these chiral micelles for use in micro-heterogeneous catalysis

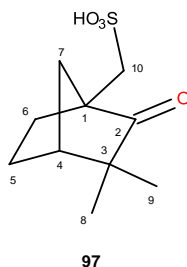
Experimental

4 Experimental Details

All syntheses were conducted in a fully equipped synthetic laboratory using chemicals supplied by Sigma Aldrich. Normal phase separations were performed using Silica-Gel 60 by means of flash chromatography, and thin layer chromatography was performed using a centrifugal chromatographic technique using a Chromatotron®. NMR techniques were performed either on a Bruker Avance 400 MHz spectrometer or a Bruker Avance II 600 MHz spectrometer with a broadband inverse detect (BBI) probe. High resolution mass spectrometry was performed by the University of Stellenbosch Central Analytical Facility. Spectra were acquired for both positive and negative ion source and performed on a Waters G2 TOF instrument with an ESI ion source. Infrared spectra were recorded on a Perkin-Elmer Spectrum 2000 spectrometer.

4.1 Fenchone derivatives

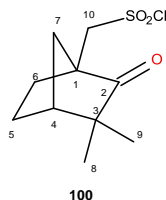
4.1.1 10-Fenchonesulfonic acid **97**



Fenchone (10.0 g, 66.0 mmol) was added dropwise to acetic anhydride (12 mL), followed by the addition of concentrated sulfuric acid (3.5 mL) to the stirred solution, and the temperature was kept below 20°C for 30 min. The mixture was allowed to warm and left to stir for 72 h at room temperature. The solution was poured directly onto ice and unreacted fenchone was extracted with dichloromethane (2 x 20 mL). NaCl was added to the aqueous layer to initiate product precipitation; the white powdery residue was collected *via* vacuum filtration to afford 10-fenchonesulfonic acid **97** (5.6 g, 56%); mp 199-201°C; δ_H (600 MHz, DMSO) 1.05 (6H, s, 8- and 9-Me), 2.01 and 2.13 (2H, 2 x d, $J = 11.6$, 7-CH₂), 1.65-1.79 (2H, series of multiplets, 6-CH₂), 1.18 and 2.33 (2H, series of multiplets, 5-CH₂), 2.19 (1H, s, 4-CH), 2.94 and 2.78 (2H,

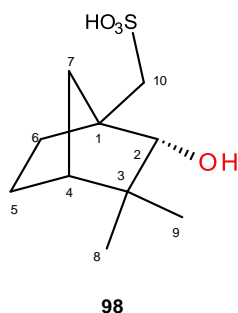
2 x d, $J = 15.2$, 10-CH₂); δ_C (150 MHz, DMSO) 22.0 (C-8), 23.3 (C-9), 24.3 (C-6), 29.0 (C-5), 38.7 (C-7), 44.8 (C-4), 47.3 (C-3), 50.6 (C-10), 55.4 (C-1), 218.7 (C-2).

4.1.2 10-Fenchonesulfonyl chloride **100**



Thionyl chloride (3.5 mL) was added dropwise to fenchonesulfonic acid **97** (1.00 g, 4.3 mmol), and the mixture was left to stir for 30-40 min at 50°C. It was then poured into ice and the resulting white precipitate was filtered off and recrystallized with hexane to yield white needle-like crystals of 10-fenchonesulfonyl chloride **100**. (0.23 g, 23%); mp 63-65°C; δ_H (600 MHz; CDCl₃) 1.12 (3H, s, 8-Me), 1.13 (3H, s, Me), 1.54-2.32 (6H, series of multiplets, 5- 6-, and 7-CH₂), 2.34 (1H, s, 4-CH), 4.03 and 4.33 (2H, 2 x d, $J = 15.1$, 10-CH₂); δ_C (150 MHz; CDCl₃) 21.4 (C-8), 23.0 (C-9), 24.1 (C-6), 29.9 (C-5), 38.2 (C-7), 45.2 (C-4), 47.3 (C-3), 54.6 (C-1), 66.1 (C-10).

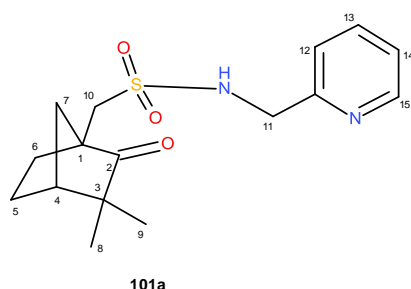
4.1.3 2-Hydroxy-10-fenchonesulfonic acid **98**



10-Fenchonesulfonic acid **97** (2.80 g, 12.0 mmol) was dissolved in methanol (15 mL), followed by the addition of NaBH₄ (0.92 g, 24.0 mmol) in small portions and the reaction mixture was stirred at room temperature for 1 h. The crude reaction mixture was washed with DCM (2 x 20 mL). Product was extracted *in vacuo* as a clear oil. (1.88 g, 60.7%) δ_H (600 MHz; 10% D₂O:90% H₂O) 0.76 (3H, s, 8-Me), 0.92 (3H, s, 9-Me), 1.32-1.72 (7H, series of multiplets, 5-, 6-, 7-CH₂ and 4-CH), 1.99 (1H, s, 2-CH), 3.04 and 3.09 (2H, 2 x d, $J = 15.0$, 10-CH₂), 3.57 (1H, s, OH); δ_C (150 MHz; 10% D₂O:90% H₂O) 19.7 (C-9), 22.9 (C-6), 24.9 (C-5), 29.7 (C-9), 38.3 (C-7), 38.5 (C-3), 47.3 (C-4), 49.6 (C-1) 55.1 (C-10), 82.9 (C-2).

4.2 Series of fenchone-10-sulfonamides

4.2.1 *N*-(Picolyl)fenchone-10-sulfonamide 101a



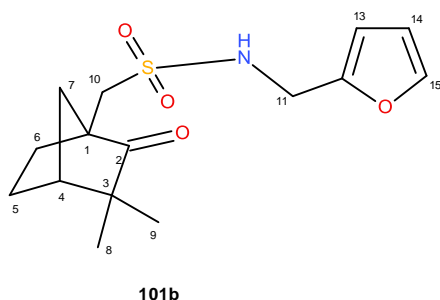
Method 1¹²⁸:

A solution of 10-fenchonesulfonyl chloride **100** (0.10 g, 0.45 mmol) in acetonitrile (5 mL) was added dropwise to a stirred solution of picolylamine (0.10 g, 0.92 mmol) and DMAP (0.06 g, 0.45 mmol) in acetonitrile (5 mL) under nitrogen at 0°C for 1 h. The crude reaction mixture was hydrolysed with water (1 mL), 10% HCl (1 mL) and extracted with EtOAc (3 x 15 mL). Organic layers were then combined, dried with MgSO₄, and concentrated *in vacuo* to give a green oil (0.045 g, 45%). δ_H (600 MHz; CDCl₃) 1.06 (6H, s, 8- and 9-Me), 1.40-2.03 (6H, series of multiplets, 5-, 6-, and 7-CH₂), 2.26 (1H, s, 4-CH), 3.24 and 3.62 (2H, 2 x d, $J = 14.8$, 10-CH₂), 4.46 (2H, multiplet, 11-CH₂), 5.79 (1H, s, NH), 7.22-8.57 (4H, series of multiplets, Ar-H); δ_C (150 MHz; CDCl₃) 21.5 (C-8), 23.2 (C-9), 23.9 (C-6), 30.5 (C-5), 38.4 (C-7), 45.2 (C-4), 47.3 (C-3), 47.4 (C-11), 52.0 (C-10), 54.5 (C-1), 121.9, 122.7, 136.9, 145.3, 155.1 (Ar-C), 218.2 (C-2).

Method 2:

10-Fenchonesulfonyl chloride **100** (0.50 g, 2.20 mmol) was stirred with picolylamine (0.47 g, 4.3 mmol) and silica gel (0.5 g) in EtOAc (10 mL) for 1 h. The resulting mixture was filtered and EtOAc removed *in vacuo*. Product isolated as a green oil (0.48 g, 97%); (Found $M^+ + H$ 323.1429; C₁₆H₂₂O₃N₂S requires 322.1351); ν_{max}/cm^{-1} (thin flim) 1735 (C=O) 3291 (NH); δ_H (600 MHz; CDCl₃) 1.06 (6H, s, 8- and 9-Me), 1.40-2.03 (6H, series of multiplets, 5-, 6-, and 7-CH₂), 2.26 (1H, s, 4-CH), 3.24 and 3.62 (2H, 2 x d, $J = 14.8$, 10-CH₂), 4.46 (2H, multiplet, 11-CH₂), 5.79 (1H, s, NH), 7.22-8.57 (4H, series of multiplets, Ar-H); δ_C (150 MHz; CDCl₃) 21.5 (C-8), 23.2 (C-9), 23.9 (C-6), 30.5 (C-5), 38.4 (C-7), 45.2 (C-4), 47.3 (C-3), 47.4 (C-11), 52.0 (C-10), 54.5 (C-1), 121.9, 122.7, 136.9, 145.3, 155.1 (Ar-C), 218.2 (C-2).

4.2.2 N-(2-Furfuryl)fenchone-10-sulfonamide 101b



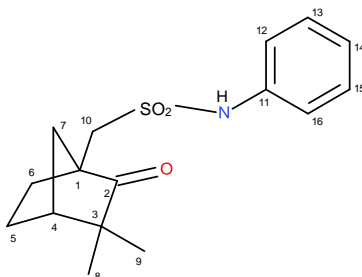
Method 1:

A solution of 10-Fenchonesulfonyl chloride **100** (0.10 g, 0.46 mmol) in acetonitrile (5 mL) was added dropwise to a stirred solution of furfurylamine (0.07 g, 0.69 mmol) and DMAP (0.06 g, 0.46 mmol) in acetonitrile (5 mL) under N₂ at 0°C for 1 h. The crude reaction mixture was hydrolysed with water (1 mL), 10% HCl (1 mL) and extracted with EtOAc (3 x 15 mL). Organic layers were combined, dried with MgSO₄, and concentrated *in vacuo* to give a light brown oil (0.05 g, 51%). δ_H (600 MHz; CDCl₃) 1.07 (3H, s, 8-Me), 1.08 (3H, s, 9-Me), 1.40-1.97 (6H, series of multiplets, 5-, 6-, and 7-CH₂), 2.24 (1H, s, 4-CH), 3.16 and 3.49 (2H, 2 x d, $J = 14.9$, 10-CH₂), 4.34 (2H, d, $J = 6.0$, 11-CH₂), 5.01 (1H, s, NH), 6.35 (2H, multiplet, ArH), 7.41 (1H, s, 15-CH); δ_C (150 MHz; CDCl₃) 21.4 (C-8), 23.3 (C-9), 24.0 (C-6), 30.4 (C-5), 38.6 (C-7), 40.0 (C-11), 45.2 (C-4), 47.5 (C-3), 52.9 (C-10), 54.5 (C-1), 220.2 (C-2), 108.6, 111.6, 142.8 and 150.1 (ArC).

Method 2:

10-Fenchonesulfonyl chloride **100** (0.50 g, 2.20 mmol) was stirred with furfurylamine (0.44 g, 4.70 mmol) and silica gel (0.50 g) in EtOAc (10 mL) for 1 h. The resulting mixture was filtered and EtOAc removed *in vacuo* to give a brown oil (0.46 g, 93%); ($M^+ + H$ 312.1270; C₁₅H₂₁O₄NS requires 311.1191); δ_H (600 MHz; CDCl₃) 1.07 (3H, s, 8-Me), 1.08 (3H, s, 9-Me), 1.40-1.97 (6H, series of multiplets, 5-, 6-, and 7-CH₂), 2.24 (1H, s, 4-CH), 3.16 and 3.49 (2H, 2 x d, $J = 14.9$, 10-CH₂), 4.34 (2H, d, $J = 6.0$, 11-CH₂), 5.01 (1H, s, NH), 6.35 (2H, multiplet, ArH), 7.41 (1H, s, 15-CH); δ_C (150 MHz; CDCl₃) 21.4 (C-8), 23.3 (C-9), 24.0 (C-6), 30.4 (C-5), 38.6 (C-7), 40.0 (C-11), 45.2 (C-4), 47.5 (C-3), 52.9 (C-10), 54.5 (C-1), 220.2 (C-2), 108.6, 111.6, 142.8 and 150.1 (ArC).

4.2.3 *N*-(Aniline)fenchone-10-sulfonamide **101c**



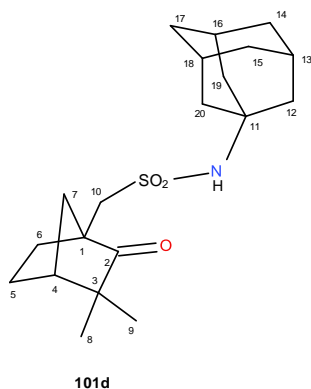
Method 1:

10-Fenchonesulfonyl chloride **100** (0.20 g, 0.74 mmol) in acetonitrile (5 mL) was added dropwise to a stirred solution of aniline (0.10 g, 1.10 mmol) and DMAP (0.10 g, 5.0 mmol) in acetonitrile (5 mL) under nitrogen at 0°C for 1 h. The crude reaction mixture was hydrolysed with water (1 mL), 10% HCl (1 mL) and extracted with EtOAc (3 x 15 mL). Organic layers were combined, dried with MgSO₄, and concentrated *in vacuo* to give a light brown oil (0.12 g, 61%). δ_H (600 MHz; CDCl₃) 1.09 (3H, s, 8-Me), 1.14 (3H, s, 9-Me), 1.49 and 2.40 (2H, series of multiplets, 5-CH₂), 1.46-1.95 (4H, series of multiplets, 6- and 7-CH₂), 2.28 (1H, s, 4-H), 3.26 and 3.64 (2H, 2 x d, $J = 14.8$, 10-CH₂), 7.00 (1H, s, NH), 7.18-7.38 (5H, overlapping signals, ArH); δ_C (150 MHz; CDCl₃) 21.4 (C-8), 23.3 (C-9), 23.9 (C-6), 30.6 (C-5), 39.2 (C-7), 45.3 (C-4), 47.8 (C-3), 51.4 (C-10), 55.1 (C-1), 121.2, 125.4, 129.5 & 137.0 (Ar-C), 217.9 (C=O).

Method 2:

10-Fenchonesulfonyl chloride **100** (0.50 g, 2.20 mmol) was stirred with aniline (0.26 g, 2.80 mmol) and silica gel (0.50 g) in EtOAc (10 mL) for 1 h. The resulting mixture was filtered and EtOAc removed *in vacuo* to give a light brown oil; (0.46 g, 93%); ($M^+ + H$ 308.1320; C₁₆H₂₁O₃NS requires 307.1242); δ_H (600 MHz; CDCl₃) 1.09 (3H, s, 8-Me), 1.14 (3H, s, 9-Me), 1.49 and 2.40 (2H, series of multiplets, 5-CH₂), 1.46-1.95 (4H, series of multiplets, 6- and 7-CH₂), 2.28 (1H, s, 4-H), 3.26 and 3.64 (2H, 2 x d, $J = 14.8$, 10-CH₂), 7.00 (1H, s, NH), 7.18-7.38 (5H, overlapping signals, ArH); δ_C (150 MHz; CDCl₃) 21.4 (C-8), 23.3 (C-9), 23.9 (C-6), 30.6 (C-5), 39.2 (C-7), 45.3 (C-4), 47.8 (C-3), 51.4 (C-10), 55.1 (C-1), 121.2, 125.4, 129.5 & 137.0 (Ar-C), 217.9 (C=O).

4.2.4 N-(Adamantyl)fenchone-10-sulfonamide 101d



Method 1:

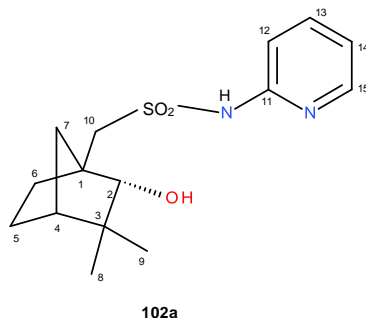
10-Fenchonesulfonyl chloride **100** (0.10 g, 0.46 mmol) in acetonitrile (5 mL) was added dropwise to a stirred solution of adamantylamine (0.07 g, 0.46 mmol) and DMAP (0.06 g, 0.46 mmol) in acetonitrile (5 mL) under N₂ at 0°C for 1 h. The crude reaction mixture was hydrolysed with water (1 mL), 10% HCl (1 mL) and extracted with EtOAc (3 x 15mL). Organic layers were combined, dried with MgSO₄, and concentrated *in vacuo* to give a light brown oil (0.05 g, 51%). δ_H (600 MHz; CDCl₃) 1.09 and 0.15 (6H, 2 x s, 8- and 9-Me), 1.43 (1H, m, 4-CH), 1.65-1.72 (6H, series of multiplets, 6-, 5-, and 7-CH₂), 1.92-2.22 (12H, series of multiplets, 12-, 14-, 15-, 17-, 19-, and 20-CH₂), 2.27 (3H, m, 13-, 16- and 18-CH), 3.32 and 3.65 (2H, 2 x d, $J = 14.1$, 10-CH₂), 4.23 (1H, br s, NH); δ_C (150 MHz; CDCl₃) 21.5 (C-8), 23.1 (C-9), 29.5 (C-13, 16, 18), 30.3 (C-5), 35.9 (C-19, 12, 14), 38.6 (C-6), 43.2 (C-15, 17, 20), 43.8 (C-4), 45.2 (C-3), 47.4 (C-1), 55.3 (C-11), 56.6 (C-10), 217.3 (C-2).

Method 2:

10-Fenchonesulfonyl chloride **100** (0.50 g, 2.20 mmol) was stirred with adamantylamine (0.44 g, 4.70 mmol) and silica gel (0.50 g) in EtOAc (10 mL) for 1 h. The resulting mixture was filtered and EtOAc removed *in vacuo* to give a light brown oil (0.36 g, 72%); (M⁺+H 366.2103; C₂₀H₃₁O₃NS requires 365.2025); ν_{max}/cm^{-1} (thin flim) 1738 (C=O) 3268 (NH); δ_H (600 MHz; CDCl₃) 1.09 and 0.15 (6H, 2 x s, 8- and 9-Me), 1.43 (1H, m, 4-CH), 1.65-1.72 (6H, series of multiplets, 6-, 5-, and 7-CH₂), 1.92-2.22 (12H, series of multiplets, 12-, 14-, 15-, 17-, 19-, and 20-CH₂), 2.27 (3H, m, 13-, 16- and 18-CH), 3.32 and 3.65 (2H, 2 x d, $J = 14.1$, 10-CH₂), 4.23

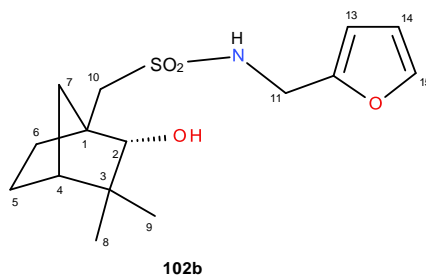
(1H, br s, NH); δ_C (150 MHz; CDCl₃) 21.5 (C-8), 23.1 (C-9), 29.5 (C-13, 16, 18), 30.3 (C-5), 35.9 (C-19, 12, 14), 38.6 (C-6), 43.2 (C-15, 17, 20), 43.8 (C-4), 45.2 (C-3), 47.4 (C-1), 55.3 (C-11), 56.6 (C-10), 217.3 (C-2).

4.2.5 2-Hydroxy-N-(picolyl)fenchane-10-sulfonamide 102a



N-(Picolyl)fenchone-10-sulfonamide **101a** (0.10 g, 0.45 mmol) was dissolved in methanol (5 mL) to which NaBH₄ (0.04 g, 1.10 mmol) was added in small portions and left to stir at room temperature for 1 h. The reaction mixture was then quenched with H₂O (1 mL), 10 % HCl (1 mL) and extracted with EtOAc (2 x 12 mL) to afford a light green oil. (0.049 g, 49%); δ_H (600 MHz; CDCl₃) 0.92 (3H, s, 8-Me), 1.02 (3H, s, 9-Me), 1.26-1.81 (6H, series of multiplets, 5-, 6- and 7-CH₂), 2.07 (1H, m, 4-CH), 3.28 and 3.33 (2H, 2 x d, $J = 14.7$, 10-CH₂), 3.71 (1H, s, 2-CH), 4.45 (2H, d, $J = 5.5$, 11-CH₂), 5.31 (1H, s, OH), 5.94 (1H, s, NH), 7.25-8.57 (4H, series of multiplets, Ar-H); δ_C (150 MHz; CDCl₃) 20.2 (C-8), 23.8 (C-9), 25.7 (C-6), 30.7 (C-5), 39.5 (C-7), 40.8 (C-4), 46.7 (C-3), 47.8 (C-11), 50.4 (C-10), 58.0 (C-1), 81.7 (C-2), 122.4, 123.1, 137.5, 149.1 (Ar-C).

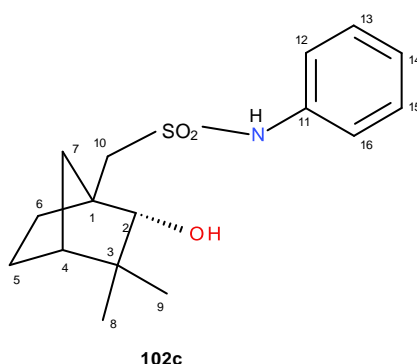
4.2.6 2-Hydroxy-N-(furfuryl)fenchane-10-sulfonamide 102b



N-(Furfuryl)fenchone-10-sulfonamide **101b** (0.10 g, 0.46 mmol) was dissolved in methanol (5 mL) to which NaBH₄ (0.03 g, 0.91 mmol) was added in small portions and left to stir at room temperature for 1 h. The reaction mixture was then quenched with H₂O (1 mL), 10% HCl (1 mL) and extracted with EtOAc (2 x 12 mL) to afford a light brown oil. (0.069 g, 69%) (M⁺+H)

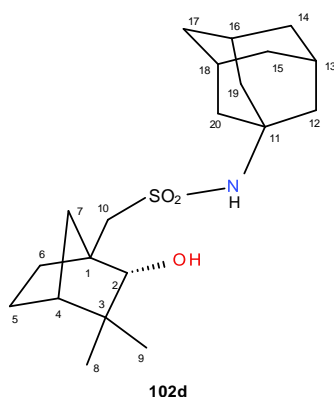
312.1270; expect M^+ 311.15); ν_{max}/cm^{-1} (thin film) 3409 (OH) 3123 (NH); δ_H (600 MHz; $CDCl_3$) 1.07 (3H, s, 8-Me), 1.09 (3H, s, 9-Me), 1.43-1.97 (6H, series of multiplets, 5-, 6-, and 7- CH_2), 2.24 (1H, s, 4-CH), 2.26 (1H, s, 2-CH), 3.17 and 3.49 (2H, 2 x d, $J = 14.6$, 10- CH_2), 3.47 (1H, s, OH), 4.35 (2H, d, $J = 5.6$, 11- CH_2), 4.97 (1H, s, NH), 6.36 (2H, m, 13-CH and 14CH), 7.42 (1H, s, 15-CH); δ_C (150 MHz; $CDCl_3$) 21.4 (C-8), 23.2 (C-9), 23.9 (C-6), 30.5 (C-5), 38.7 (C-7), 40.0 (C-11), 45.3 (C-4), 47.6 (C-3), 52.9 (C-10), 54.6 (C-1), 76.2 (C-2), 110.7, 143.1, 150.1 (Ar-C).

4.2.7 2-Hydroxy-N-(aniline)fenchane-10-sulfonamide 102c



N-(aniline)fenchone-10-sulfonamide (0.20 g, 0.65 mmol) was dissolved in methanol (5 mL) to which $NaBH_4$ (0.05 g, 1.30 mmol) was added in small portions and left to stir at room temperature for 1 h. The reaction mixture was then quenched with H_2O (1 mL), 10% HCl (1 mL) and extracted with EtOAc (2 x 12 mL) to afford a light brown oil. (0.11 g, 57%); δ_H (600 MHz; $CDCl_3$) 0.93 (3H, s, 8-Me), 1.04 (3H, s, 9-Me), 1.26-1.79 (6H, series of multiplets, 5-, 6-, and 7- CH_2), 2.07 (1H, s, 4-CH), 3.03 (1H, s, 2-CH), 3.34 & 3.38 (2H, 2 x d, $J = 14.8$, 10- CH_2), 3.65 (1H, s, OH), 5.32 (1H, s, NH), 7.15-7.39 (5H, overlapping signals, Ar-H); δ_C (150 MHz; $CDCl_3$) 21.5 (C-8), 23.2 (C-9), 23.9 (C-6), 29.8 (C-5), 39.1 (C-7), 45.3 (C-4), 50.4 (C-3), 52.4 (C-10), 62.8 (C-1), 76.1 (C-2), 121.3, 125.4, 129.6 (Ar-C).

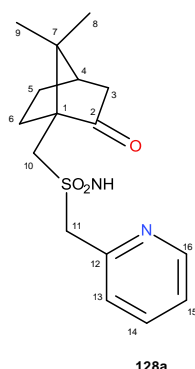
4.2.8 2-Hydroxy-N-(adamantyl) fenchane-10-sulfonamide **102d**



N-(Adamantyl) fenchone sulfonamide **101d** (0.27 g, 0.73 mmol) was dissolved in methanol (5 mL) to which NaBH₄ (0.027 g, 0.73 mmol) was added in portions and was left to stir at room temperature for 1 h. The reaction was then quenched with water (1 mL), 10% HCl (1 mL) and extracted with EtAOc (2 x 12 mL) to afford a light brown oil (0.82 g, 33%); ν_{max}/cm^{-1} (thin film) 3430 (OH) 3213 (NH); δ_H (600 MHz; CDCl₃) 0.93 and 1.06 (6H, 2 x s, 8- and 9-Me), 1.49 (1H, m, 4-CH), 1.63-1.74 (6H, series of multiplets, 5-, 6-, and 7-CH₂), 1.93-2.16 (12H, series of multiplets, 12-, 14-, 15-, 17-, 19-, and 20-CH₂), 2.13 (3H, m, 13-, 16-, and 18-CH), 2.19 (1H, s, 2-CH), 3.12 and 3.32 (2H, 2 x d, $J = 14.3$, 10-CH₂), 3.69 (1H, s, OH), 4.24 (1H, br s, NH); δ_C (150 MHz; CDCl₃) 21.5 (C-8), 21.6 (C-9), 29.4 (C-13, C-16, C-18), 30.0 (C-5), 35.9 (C-12, C-14, C-19), 38.4 (C-6), 45.2 (C-4), 43.2 (C-15, C-17, C-20), 45.3 (C-3), 47.3 (C-1), 54.7 (C-11), 56.6 (C-10), 75.4 (C-2).

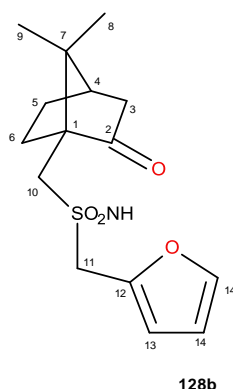
4.3 Synthesis of camphor-10-sulfonamides

4.3.1 *N*-(Picolyl)camphor-10-sulfonamide **128a**



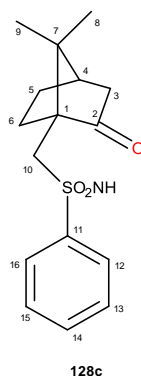
10-Camphorsulfonyl chloride **127** (0.50 g, 2.20 mmol) was stirred with picolylamine (0.47 g, 4.3 mmol) and silica gel (0.50 g) in EtOAc (10 mL) for 1 h. The resulting mixture was filtered and EtOAc removed *in vacuo*, giving a green oil. (0.46 g, 97%); ν_{max}/cm^{-1} (thin film) 1733 (C=O); δ_H (600 MHz; CDCl_3) 0.88 (3H, s, 9-Me), 1.07 (3H, s, 8-Me), 1.40-2.32 (6H, 5-, 6-, and 7- CH_2), 2.39 (1H, m, 4-CH), 2.96 and 3.52 (2H, 2 x d, $J = 14.9$, 10- CH_2), 4.54 (2H, m, 11- CH_2), 6.27 (1H, s, NH), 7.25 (1H, t, $J = 6.6$, ArH), 7.43 (1H, d, $J = 8.7$, ArH), 7.7 (1H, t, $J = 7.6$, ArH), 8.56 (1H, d, $J = 5.4$, ArH); δ_C (150 MHz; CDCl_3) 19.5 (C-8), 19.6 (C-9), 19.9 (C-5), 24.6 (C-6), 43.0 (C-3), 44.4 (C-4), 48.9 (C-1), 50.3 (C-10), 58.5 (C-7), 125.4, 126.9, 141.4, 145.7, 154.3 (ArC), 217.4 (C=O).

4.3.2 *N*-(Furfuryl)camphor-10-sulfonamide **128b**



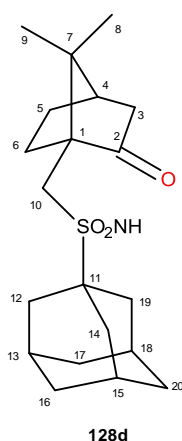
10-Camphorsulfonyl chloride **127** (0.50 g, 2.20 mmol) was stirred with furfurylamine (0.44 g, 4.70 mmol) and silica gel (0.50 g) in EtOAc (10 mL) for 1 h. The resulting mixture was filtered and EtOAc removed *in vacuo* to afford product as yellow-brown oil (0.47 g, 93%); δ_H (600 MHz; CDCl₃) 0.805 (3H, s, 8-Me), 0.97 (3H, s, 9-Me), 1.41-2.14 (6H, 5-, 6-, and 7-CH₂), 2.38 (1H, m, 4-CH), 2.89 and 3.15 (2 x d, $J = 14.9$, 10CH₂), 4.33 and 4.46 (2H, 2 x ddd, $J = 5.23$, 7.13, 7.61, 11-CH₂), 6.04 (1H, s, NH), 6.32 (2H, s, ArH), 7.38 (1H, s, ArH); δ_C (150 MHz; CDCl₃) 19.4 (C-9), 19.7 (C-8), 27.1 (C-5), 27.3 (C-3), 40.5 (CN), 42.7 (C-4), 42.9 (C-6), 48.8 (C-1), 51.3 (C-10), 59.4 (C-7), 108.6, 110.5, 142.6, 149.8 (ArC), 217.0 (C=O).

4.3.3 *N*-(Aniline)camphor-10-sulfonamide **128c**



10-Camphorsulfonyl chloride **127** (0.50 g, 2.20 mmol) was stirred with aniline (0.26 g, 2.80 mmol) and silica gel (0.50 g) in EtOAc (10 mL) for 1 h. The resulting mixture was filtered and EtOAc removed *in vacuo* to afford product as a dark brown oil (0.48 g, 93%); ν_{max}/cm^{-1} (thin flim) 1729 (C=O), 1148 (S=O), 3198, 1600 (N-H); δ_H (600 MHz; CDCl₃) 0.87 (3H, s, 9-Me), 0.97 (3H, s, 8-Me), 1.48-2.22 (6H, series of multiplets, 5-, 6- and 7-CH₂), 2.48 (1H, m, 4-CH), 2.88 and 3.38 (2H, 2 x d, $J = 15.3$, 10-CH₂), 7.19-7.38 (5H, overlapping signals, ArH); δ_C (150 MHz; CDCl₃) 19.4 (C-8), 20.7 (C-9), 27.2 (C-5), 27.7 (C-3), 42.8 (C-4), 43.1 (C-6), 48.9 (C-10), 49.1 (C-1), 59.7 (C-7), 122.2, 125.5, 129.4, 137.6 (ArC), 217.5 (C=O).

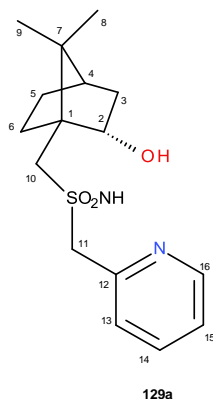
4.3.4 *N*-(1-Adamantyl)camphor-10-sulfonamide **128d**



10-Camphorsulfonyl chloride **127** (0.50 g, 2.20 mmol) was stirred with adamantylamine (0.47 g, 4.30 mmol) and silica gel (0.50 g) in EtOAc (10 mL) for 1 h. The resulting mixture was filtered and EtOAc removed *in vacuo* to afford the product as a clear oil (0.36 g, 72%) δ_H (600 MHz; CDCl_3) 0.85 (3H, s, 9-Me), 0.97 (3H, s, 8-Me), 1.47-2.32 (4H, series of multiplets, 5- and 6- CH_2), 1.68 (6H, m, 14-, 19- and 20- CH_2), 1.95 and 2.42 (2H, 2 x m, 3- CH_2), 2.03 (6H, m, 12-, 16-, and 17- CH_2), 2.06 (1H, s, 4-H), 2.12 3H, m, 13-, 15-, and 18-CH), 3.00 and 3.49 (2H, 2 x d, $J = 14.8$, 10- CH_2), 5.01 (1H, s, NH); δ_C (150 MHz; CDCl_3) 19.7 (C-8), 20.1 (C-9), 26.3 (C-5), 27.8 (C-6), 29.7 (C-13, C-15, and C-18), 36.5 (C-14, C-19, and C-20), 42.8 (C-4), 43.0 (C-3), 43.8 (C-12, C-16, & C-17), 48.2 (C-1), 54.5 (C-10), 55.8 (C-7), 59.8 (C-11), 218.9 (C=O).

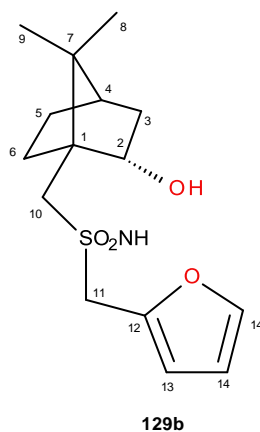
4.4 Camphor-sulfonamide reductions

4.4.1 2-Hydroxy-N-(picolyl)camphane-10-sulfonamide 129a



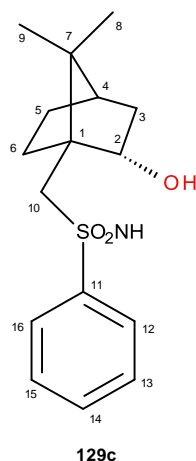
N-(Picolyl)camphor-10-sulfonamide **128a** (0.15 g, 0.67 mmol) was dissolved in methanol (5 mL) to which NaBH₄ (0.05 g, 1.30 mmol) was added in small portions and left to stir at room temperature for 1 h. The reaction mixture was then quenched with H₂O (1 mL), 10% HCl (1 mL) and extracted with EtOAc (2 x 12 mL) to afford a light green oil. (0.071 g, 49%); δ_H (600 MHz; CDCl₃) 0.85 (3H, s, 8-Me), 1.06 (3H, s, 9-Me), 1.41-2.20 (6H, 3-, 5-, and 6-CH₂), 2.37 (1H, m, 4-CH), 3.05 and 3.62 (2H, 2 x d, $J = 14.5$, 10-CH₂), 4.10 (1H, s, 2-CH), 4.86 (2H, m, 11-CH₂), 5.76 (1H, br s, OH), 7.53 (1H, s, NH), 7.83-8.89 (4H, overlapping signals, ArH); δ_C (150 MHz; CDCl₃) 19.8 (C-8), 20.0 (C-9), 20.6 (C-5), 27.3 (C-6), 43.8 (C-3), 44.4 (C-4), 49.0 (C-1), 52.7 (C-10), 58.5 (C-7), 75.9 (C-2), 125.6, 126.9, 141.7, 146.0, 154.3 (ArC).

4.4.2 2-Hydroxy-N-(furfuryl)camphane-10-sulfonamide 129b



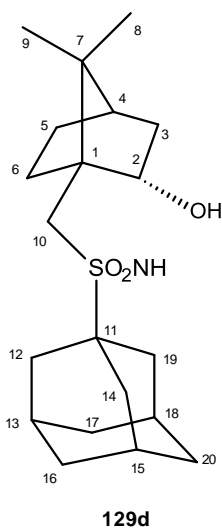
N-(Furfuryl)camphor-10-sulfonamide **128b** (0.18 g, 0.83 mmol) was dissolved in methanol (5 mL) to which NaBH₄ (0.06 g, 1.60 mmol) was added in small portions and left to stir at room temperature for 1 h. The reaction mixture was then quenched with H₂O (1 mL), 10% HCl (1 mL) and extracted with EtOAc (2 x 12 mL) to afford a light brown oil. (0.092 g, 69%); δ_H (600 MHz; CDCl₃) 0.75 (3H, s, 8-Me), 1.10 (3H, s, 9-Me), 1.40-2.16 (6H, series of multiplets, 3-, 5- and 6-CH₂), 2.39 (1H, m, 4-CH), 2.88 and 3.18 (2H, 2 x d, $J = 15.2$, 10-CH₂), 3.29 (1H, s, 2-CH), 4.07 (1H, s, OH), 4.37 (2H, m, 11-CH₂), 5.98 (1H, s, NH), 6.37 (1H, s, ArH), 7.37 (1H, s, ArH), 7.43 (1H, s, ArH); δ_C (150 MHz; CDCl₃) 19.7 (C-9), 20.5 (C-8), 27.0 (C-5), 30.3 (C-3), 40.5 (CN), 42.9 (C-4), 44.3 (C-6), 48.8 (C-1), 51.3 (C-10), 59.5 (C-7), 76.3 (C-2), 108.9, 110.8, 142.8, 143.0 (ArC).

4.4.3 2-Hydroxy-*N*-(aniline)camphane-10-sulfonamide **129c**



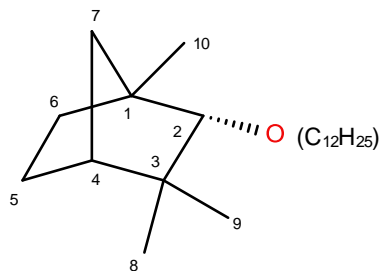
N-(Aniline)camphor-10-sulfonamide **128c** (0.10 g, 0.33 mmol) was dissolved in methanol (5 mL) to which NaBH₄ (0.025 g, 0.65 mmol) was added in small portions and left to stir at room temperature for 1 h. The reaction mixture was then quenched with H₂O (1 mL), 10% HCl (1 mL) and extracted with EtOAc (2 x 12 mL) to afford a light brown oil. (0.049 g, 57%); δ_H (600 MHz; CDCl₃) 0.70 (3H, s, 8-Me), 0.95 (3H, s, 9-Me), 1.44-1.79 (7H, series of multiplets, 3-, 5-, and 6-CH₂, and 4-CH), 1.98 (1H, s, 2-CH), 2.91 and 3.46 (2H, 2 x d, $J = 14.0$, 10CH₂), 4.07 (1H, m, OH), 6.58 (1H, s, NH), 7.07-7.32 (5H, overlapping signals, ArH); δ_C (150 MHz; CDCl₃) 19.8 (C-8), 20.5 (C-9), 24.0 (C-5), 27.4 (C-6), 39.1 (C-3), 44.3 (C-4), 49.0 (C-1), 50.3 (C-10), 54.5 (C-7), 76.4 (C-2), 120.3, 125.3, 129.4, 129.8, 136.7 (ArC).

4.4.4 2-Hydroxy-N-(adamantyl)camphane-10-sulfonamide **129d**



N-(Adamantyl)camphor-10-sulfonamide **128d** (0.10 g, 0.66 mmol) was dissolved in methanol (5 mL) to which NaBH₄ (0.050 g, 1.32 mmol) was added in small portions and left to stir at room temperature for 1 h. The reaction mixture was then quenched with H₂O (1 mL), 10% HCl (1 mL) and extracted with EtOAc (2 x 12 mL) to afford a light brown oil. (0.033 g, 33%); δ_H (600 MHz; CDCl₃) 0.91 (3H, s, 9-Me), 1.05 (3H, s, 8-Me), 1.47-2.35 (4H, series of multiplets, 5- and 6-CH₂), 1.72 (6H, m, 14-, 19-, 20-CH₂), 1.90 & 2.42 (2H, 2 x m, 3-CH₂), 2.07 (6H, m, 12-, 16-, and 17-CH₂), 2.09 (1H, s, 4-H) 2.15 (3H, m, 13-, 15-, and 18-CH), 3.07 and 5.51 (2H, 2 x d, $J = 15.0$, 10-CH₂), 3.78 (1H, s, OH) 5.10 (1H, s, NH) δ_C (150 MHz; CDCl₃) 19.9 (C-8), 20.5 (C-9), 26.0 (C-5), 26.8 (C-6), 31.0 (C-13, C-15, & C18), 36.8 (C-14, C-19, C-20), 43.1 (C-4), 43.4 (C-3), 44.2 (C-12, C-16, & C-17), 48.5 (C-1), 55.1 (C-10), 55.9 (C-7), 61.2 (C-11), 76.3 (C-2).

4.5 Attempted ether and ester synthesis



- Method 1:

A solution of bromododecane (0.50 g, 2.10 mmol), fenchol (0.30 g, 2.10 mmol), triethylamine (0.28 mL) and DMAP (0.25 g, 2.10 mmol) was stirred in THF (8 mL) under N_2 at $80^\circ C$ for 15 h. The solvent was removed *in vacuo* and residue dissolved in EtOAc (10 mL). The organic phase was then washed with water (2 x 5 mL) and brine (2 x 5 mL). The aqueous washings were extracted with EtOAc and, combined and dried with $MgSO_4$ anhydrous. Solvent removed *in vacuo* to provide the starting material unchanged.

Method 2:

Fenchol (0.15 g, 0.97 mmol) was dissolved in ethanol (EtOH) (6 mL). Sodium hydroxide (NaOH) (0.10 mL, 10 M) and bromododecane (0.25 g, 1.0 mmol) were added and reaction mixture was left to stir for 15 h at room temperature. The reaction mixture was extracted with DCM (2 x 10 mL). Organic layers were combined, dried over $MgSO_4$ anhydrous. Solvent removed *in vacuo* to provide the starting material unchanged.

- Method 3:

Fenchol (0.60 g, 3.9 mmol), sodium hydride (NaH) (0.10 g, 60% dispersion) and toluene (5 mL) were stirred for 2 h at $60^\circ C$. The bromododecane (1.00 g, 4.00 mmol) was then added and the reaction was refluxed for 18 h. The reaction mixture was quenched with sodium hydrogen carbonate ($NaHCO_3$) and organic layers were extracted with EtOAc (2 x 10 mL) and dried over $MgSO_4$ anhydrous. Solvent was removed *in vacuo* to provide the starting material unchanged.

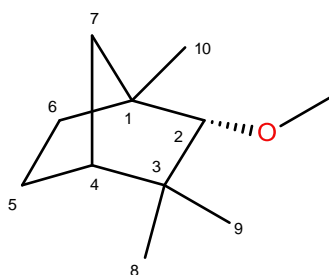
Method 4:

Dried fenchol (0.60 g, 4.00 mmol), NaH (0.1 g, 60% dispersion) and dried toluene (5 mL) were stirred for 2 h at 60°C. The bromododecane (1.00 g, 4.00 mmol) was then added and the reaction was refluxed for 18 h. The reaction mixture was quenched with NaHCO₃ and organic layers were extracted with EtOAc (2 x 10 mL) and dried over MgSO₄ anhydrous. Solvent was removed *in vacuo* to provide the starting material unchanged.

Method 5:

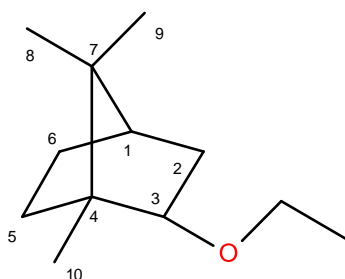
Dried fenchol (0.12 g, 0.65 mmol) and n-butyl lithium (BuLi) (0.40 mL) were stirred in THF (2 mL) for 30 min at 0°C. Bromododecane (0.16 g, 0.65 mmol) was added and the reaction mixture was allowed to warm up to room temperature and left to stir overnight under argon. The reaction mixture was quenched with NaHCO₃ and organic layers were extracted with EtOAc (3 x 5 mL) and dried over MgSO₄ anhydrous. Solvent was removed *in vacuo* to provide the starting material unchanged.

Method 6: - Methyl iodide



Fenchol (0.10 g, 0.65 mmol), NaH (0.10 g, 60% dispersion) and toluene (5 mL) were stirred for 2 h at 60°C. The methyl iodide (MeI) (0.04 mL) was added and the reaction mixture was refluxed for 18 h. The reaction mixture was quenched with NaHCO₃ and organic layers were extracted with EtOAc (3 x 5 mL) and dried over MgSO₄ anhydrous. Solvent was removed *in vacuo* to provide the starting material unchanged.

Method 7: - Borneol

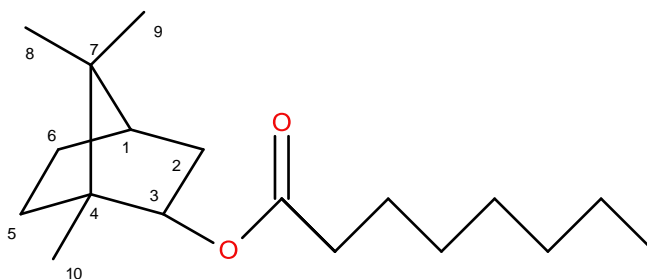


Borneol (0.52 g, 3.20 mmol) and NaH (0.078 g, 3.2 mmol) was left to stir for 1 h dry DMF (5 mL), ethyl bromide (0.24 mL) was then added and the reaction mixture was left to stir for 48 h under argon. Reaction was quenched with aqueous NaHCO₃ and extracted with EtOAc (3 x 10 mL). Solvent was removed *in vacuo* to provide the starting material unchanged.

- Method 8:

Borneol (0.10 g, 0.65 mmol) was added to a stirred solution of ethyl bromide (0.071 g, 0.65 mmol) and silver tetrafluoroborate (0.13 g, 0.65 mmol), The reaction mixture was refluxed in actone (5 mL) overnight. The reaction was quenched with aqueous NaHCO₃ and extracted with EtOAc (3 x 15 mL). Solvent was removed *in vacuo* to provide the starting material unchanged.

Method 9: ester



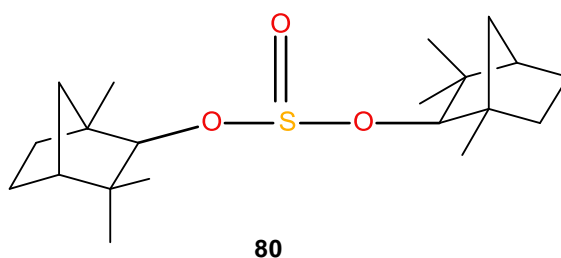
Carbonyldiimidazole (CDI) (0.11 g, 0.65 mmol) was added to a stirred solution of octanoic (0.12 g, 0.65 mmol) acid in dry DMF (5 mL). The mixture was stirred at room temperature for 30 min to allow for the evolution of CO₂. Borneol (0.12 g, 0.65 mmol) was then added to the mixture and was left to stir under argon overnight. DMF was removed *in vacuo* and the

remaining solution was run through a silica plug and washed with EtOAc. Solvent was removed *in vacuo* to provide the starting material unchanged.

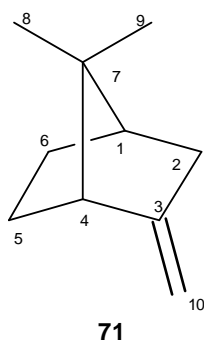
4.6 Fenchene Synthesis

Method 1¹¹³:

Fenchol **70** (2.0 g, 12.9 mmol) was stirred with thionyl chloride (1.1 mL) and pyridine (0.61 g, 7.8 mmol) at room temperature for 4 h. The resulting mixture was then added to cold NaHCO₃ and extracted with pentane (3 x 10 mL). The organic layers were then combined and washed with 10% HCl, water, and brine and dried over MgSO₄. The solvent was then removed *in vacuo* to afford white crystals of difenchyl sulfite, **80**. ν_{max}/cm^{-1} (thin film) 1459 (S=O); δ_H (600 MHz; CDCl₃) 0.92 and 0.89 (2xs, 6H, 3-*endo*-Me and 3'-*endo*-Me, major isomer), 0.97 and 0.85 (2xs, 6H, 2xs, 6H, 3-*endo*-Me and 3'-*endo*-Me, minor isomer), 1.03 (s, 6H, 3-*exo*-Me and 3'-*exo*-Me, major isomer), 1.12 and 1.07 (2xs, 6H, 1-Me and 1'-Me, major), 1.17-1.21(m, 2H, 7-*anti*- and 7'-*anti*-); δ_C (150 MHz; CDCl₃) 87.31 and 86.87 (C-2 and C-2', major), 87.27 and 86.91 (C-2 and C-2', minor), 19.17, 19.39, 21.54, 21.83, 29.37 and 29.39 (6 x CH₃, major), 20.14, 30.69, 29.43, 29.47, 21.58, 21.72 (6 x CH₃, minor), 47.99 and 48.03 (C-4 and C-4', major), 47.92 and 48.01 (C-4 and C-4', minor), 41.10 and 41.33 (C-7 and C-7' major), 40.97 and 41.35 (C-7 and C-7' minor), 25.88, 25.90, 25.98 and 26.19 (C-5, C-5', C-6 and C-6' major), 25.08, 25.84, 26.06 and 26.07 (C-5, C-5', C-6 and C-6', minor) 48.86, 49.00, 39.23 and 39.44 (C-1, C-1', C-5 and C-5' major), 48.89, 49.03, 39.26 and 39.33 (C-1, C-1', C-5 and C-5' minor).



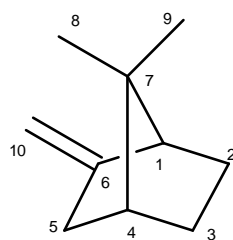
Method 2¹¹³:



Fenchol **70** (1.20 g, 7.80 mmol) and *p*-toluenesulfonyl chloride (1.90 g, 10.0 mmol) were refluxed in pyridine (12 mL) for 24 h.

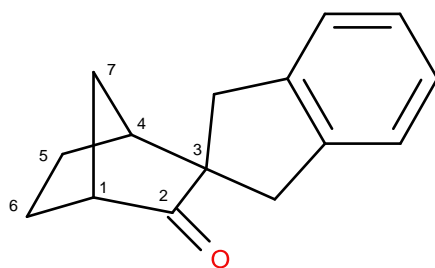
Work-up 1: The reaction mixture was quenched with NaOH (2 M) turning from red to yellow with a resulting white precipitate. The mixture was left stirring overnight in NaOH. The precipitate was filtered off and the product was then extracted with hexane (3 x 20 mL), washed with water (5 mL) and brine (5 mL). The organic layers were then combined, dried over MgSO₄ and solvent was removed *in vacuo*. Product was purified using flash chromatography on silica gel; elution with hexane:EtOAc (9:1) to afford fenchyl-*endo*-tosylate as an oil (0.89 g, 74 %) δ_H (600 MHz; CDCl₃) 0.82, 0.88 and 0.97 (9H, 3xs, 8-, 9-, and 10-Me), 1.00-1.69 (6H, series of multiplets, 5-, 6-, and 7-CH₂), 1.70 (1H, s, 4-CH), 2.45 (3H, s, Ar-Me), 4.05 (1H, s, 2-CHO), 7.33 (2H, d, $J = 7.5$, ArH), 7.81 (2H, d, $J = 7.9$, ArH).

Workup 2: The reaction mixture was quenched with aqueous NaHCO₃, and the product extracted with hexane (3 x 20 mL). The organic layers were combined and dried over MgSO₄. The hexane layer was then passed through a silica plug and solvent removed *in vacuo*. The product was purified using flash chromatography on silica gel; elution with hexane:EtOAc (9:1). The tosylate product was obtained.



Workup 3: The reaction mixture was quenched with aqueous NaHSO₃, and the product extracted with hexane (3 x 20 mL). The organic layers were combined and dried over MgSO₄. The hexane layer was then passed through a silica plug and solvent removed *in vacuo* to afford the product **71** as a brown oil (0.74 g, 62%) δ_H (600 MHz; CDCl₃) 0.99 and 1.00 (6H, 2xs, 8- and 9-Me), 1.33 (1H, m, 1-CH), 1.66-2.09 (6H, series of multiplets, 2-, 3-, & 5-CH₂), 2.43 (1H, m, 4-CH), 4.63 and 4.84 (2H, 2xs, 10-CH₂).

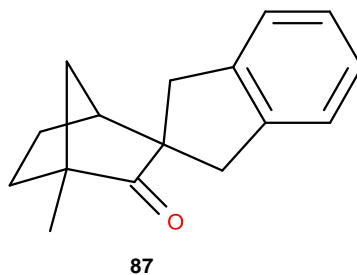
4.6.1 3,3'-Di-*o*-xylylnorcamphor **86**



86

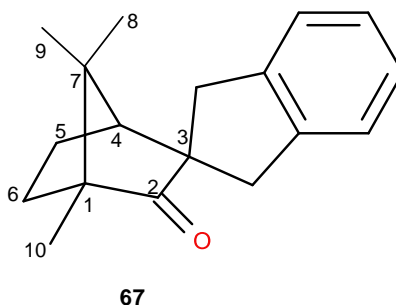
Norcamphor **85** (1.00 g, 9.00 mmol) and NaH (0.60 g, 60% dispersed in oil) in dry toluene (15 mL) was heated and stirred for 1 h. As the reaction mixture turned from clear to yellow, α,α' -dichloro-*o*-xylene (1.15 g, 6.60 mmol) was added and the resulting mixture was refluxed for 18 h. The reaction was quenched with saturated NaHCO₃, and extracted with EtOAc (3 x 30 mL). Organic layers were combined and dried over MgSO₄. The product was obtained as a yellow oil and purification done *via* flash chromatography on silica gel; eluant 100 % hexane. (0.74g, 74%) δ_H (600 MHz; CDCl₃) 1.54-2.02 (6H, series of multiplets, 5-, 6-, and 7-CH₂), 2.00 (1H, m, 1-CH), 2.47 (1H, s, 4-CH), 2.94 and 3.04 (2H, 2 x d, $J = 16.5$, xylyl-CH₂), 3.16 (2H, d, $J = 16.6$, xylyl-CH₂), 7.15 (4H, m, ArH). δ_C (150 MHz; CDCl₃) 23.4 (C-5), 25.2 (C-6), C1 (38.4), 35.6 and 42.6 (2 x xylyl-CH₂) 45.9 (C-4), 49.5 (C-3), 59.1 (C-7), 124.2, 126.5, 129.3 and 130.7 (Ar-C), 136.2 and 140.9 (4° Ar-C), 221.8 (C-2).

4.6.2 Attempted synthesis of 1-methyl-3,3'-di-o-xylynorcamphor 87



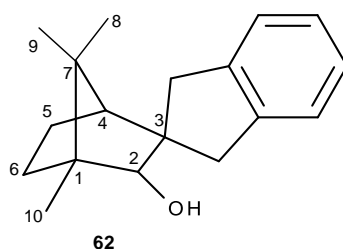
Tetramethylpiperidine (TMP) (0.085 g, 0.60 mmol) was stirred with butyllithium (0.056 mL) in THF (2 mL) at -78°C for 1 h. 3,3'-Di-o-xylynorcamphor **86** (0.13 g, 0.60 mmol) in THF (1 mL) was added to LiTMP and was stirred for 1 h at room temperature. Methyl iodide (0.037 mL) was then added and the resulting reaction mixture was left stirring overnight at room temperature. Solvent was removed *in vacuo* to provide the starting material unchanged.

4.6.3 3,3'-Di-o-xylylcamphor 67



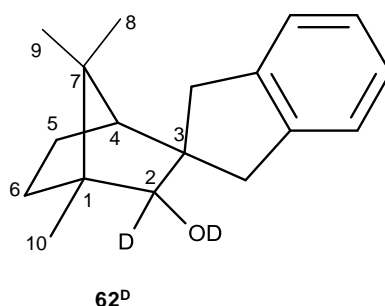
Camphor **1** (1.00 g, 6.50 mmol) and NaH (0.60 g) in dry toluene (15 mL) was heated and stirred for 1 h as the reaction mixture turned from white to yellow. α,α' -Dichloro-o-xylene (1.15 g, 6.60 mmol) was added and the resulting mixture was refluxed for 18 h. The reaction was quenched with saturated NaHCO₃ and extracted with EtOAc (3 x 30 mL). Organic layers were combined and dried over MgSO₄. Product was obtained as yellow crystals. Purification was *via* flash chromatography on silica gel; elution 100% hexane. (0.62 g, 62 %); mp 92-95 °C; δ_H (600 MHz; CDCl₃) 0.88, 1.04, and 1.08 (9H, 3 x s 8-, 9-, and 10-Me), 1.41-1.54 (2H series of multiplets, 6-CH₂), 1.80-1.93 (2H, series of multiplets, 5-CH₂), 2.14 (1H, s, 4-CH), 3.03 and 3.36 (2H, 2 x d, $J = 16.2$, xylyl-CH₂), 3.14 & 3.25 (2H, 2 x d, $J = 16.2$, xylyl-CH₂), 7.15-7.32 (4H, series of multiplets, Ar-H); δ_C (150 MHz; CDCl₃) 12.2, 21.9, 22.3 (C-8, C-9, and C-10), 24.4 (C-5), 34.3 (C-6), 40.9 & 47.4 (2 x xylyl CH₂), 45.0 (C-1), 51.0 (C-4), 56.2 (C-3), 57.3 (C-7), 123.7, 123.9, 126.0 and 126.3 (Ar-C), 141.9 and 144.8 (4°Ar-C), 227.9 (C-2).

4.6.4 2-Hydroxy-3,3'-di-o-xylylcamphor **62**



LAH (0.17 g, 4.50 mmol) was added to dry THF (5 mL) under argon and the solution was stirred at 50°C for 30 min. 3,3'-Di-o-xylylcamphor **67** (0.40 g, 1.50 mmol) in THF (2 mL) was added dropwise and the mixture was stirred at 50°C for 3 h. The reaction mixture was then stirred at room temperature overnight. NaOH (3 M, 1 mL) and water (1 mL) were added to the mixture, the precipitate was filtered off and washed with ethyl acetate (3 x 15 mL). The organic layers were combined and dried over MgSO₄ and solvent was removed *in vacuo*. The product was isolated as a yellow oil (0.32 g, 80%); δ_H (600 MHz; CDCl₃) 0.97, 0.98 and 1.33 (9H, 3 x s, 8-, 9-, & 10-Me), 1.37 (1H, m, 6-Ha), 1.56 (1H, br s, 2-OH), 1.61-1.82 (3H, series of multiplets, 5-CH₂ and 6-Hb), 1.83 (1H, s, 4-H), 2.83 and 3.26 (2H, 2 x d, $J = 15.1$, xylyl-CH₂), 2.89 & 3.73 (2H, 2 x d, $J = 15.8$, xylyl-CH₂), 3.41 (1H, s, 2-H), 7.12-7.27 (4H, series of multiplets, Ar-H); δ_C (150 MHz; CDCl₃) 12.0, 21.8, and 22.6 (C-8, C-9 & C-10), 24.4 (C-5), 34.4 (C-6), 40.9 and 47.4 (xylyl-CH₂), 49.1 (C-1), 51.0 (C-7), 56.2 (C-4), 57.3 (C-3), 89.3 (C-2), 123.7, 123.9, 126.0 and 126.3 (Ar-C), 141.8 and 144.8 (4° Ar-C).

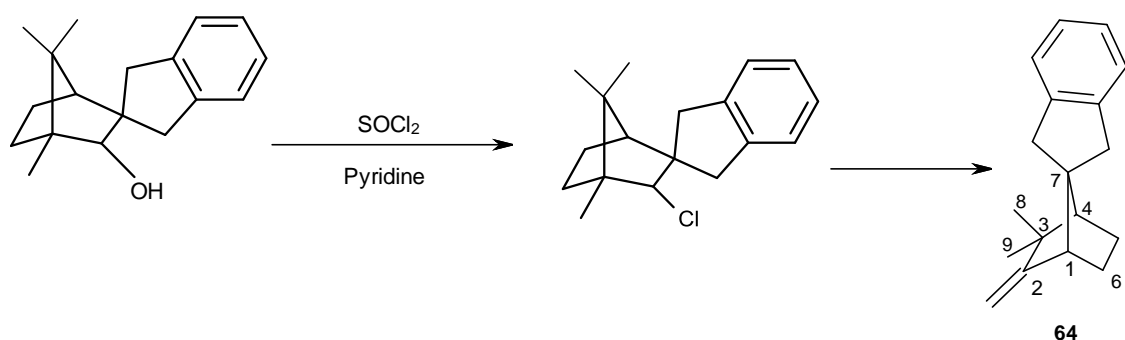
4.6.5 Deuterated 2-hydroxy-3,3'-di-o-xylylcamphor **62^D**



LAD (0.17 g, 4.50 mmol) was added to dry THF (5 mL) under argon and the solution was stirred at 50°C for 30 min. 3,3'-Di-o-xylylcamphor **67** (0.40 g, 1.50 mmol) in THF (2 mL) was

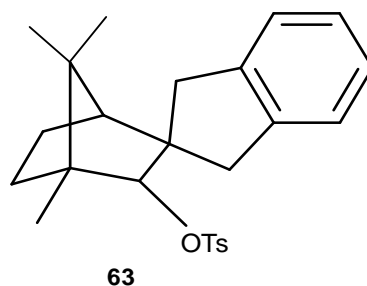
added dropwise and the mixture was stirred at 50°C for 3 h. The reaction mixture was then stirred at room temperature overnight. NaOH (3 M, 1 mL) and water (1 mL) were added to the mixture, the precipitate was filtered off and washed with ethyl acetate (2 x 15 mL). The organic layers were combined and dried over MgSO₄ and solvent was removed *in vacuo* (0.30 g, 75%).

4.6.6 Spiro[camphene-7,2'-indane] 64



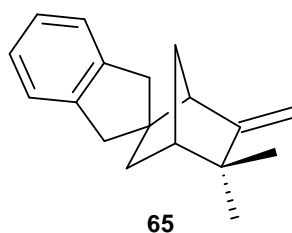
3,3'-Di-*o*-xylylcamphor (0.12 g, 0.49 mmol) was stirred with SOCl₂ (0.1 mL) and pyridine (2.0 mL) at room temperature for 4 h. The resulting mixture was added to cold saturated NaHCO₃ and the mixture was extracted with hexane (3 x 10 mL). The organic layers were combined and washed with 10% HCl, water, brine and dried over MgSO₄. Solvent was removed *in vacuo*. δ_{H} (600 MHz; CDCl₃) 1.19 and 1.29 (6H, 2 x s, 8-, 9-Me), 1.41 (1H, m, 5-*endo*-H), 1.68 (1H, m, 6-*exo*-H), 1.77 (1H, s, 1-H), 1.85 (1H, m, 6-*endo*-H), 1.97 (1H, m, 5-*exo*-H), 2.30 (1H, d, $J = 4.5$, 4-H), 2.95 (2H, s, xylyl-CH₂), 2.98 and 3.25 (2H, 2 x d, $J = 15.6$, xylyl-CH₂), 4.69 and 4.78 (2H, 2 x s, C=CH₂), 7.13 (4H, complex of multiplets, Ar-H) δ_{C} (150 MHz; CDCl₃) 24.3 (C-6), 26.7 (C-5) and 29.7 (2 x Me), 39.3 and 40.4 (xylyl-CH₂), 41.7 (C-2), 52.4 (C-4), 54.9 (C-1), 59.4 (C-7), 101.5 (C=CH₂), 124.1, 124.3, 125.91 and 125.96 (Ar-C), 142.1 and 143.8 (4°Ar-C) and 166.4 (C-3).

4.6.7 Spiro[bornane-3,2'-indan]-2-tosylate **63**¹¹³



Butyllithium (3.00 mL, 4.80 mmol) was added dropwise to a stirred solution of 2-hydroxy-3,3'-Di-o-xylylcamphor **62** (0.95 g, 4.00 mmol) in THF (25 mL) under argon at 0°C for 1 h. A solution of tosyl chloride (0.90 g, 9.60 mmol) in minimal volume THF was added and the resulting mixture was left to stir for 1 h. The reaction mixture was quenched with saturated NaHCO₃ and the extracted with EtOAc (2 x 50 mL). Organic layers were combined, dried over MgSO₄ and solvent was reduced to a minimum amount *in vacuo*. The resulting white crystals of the product **63** were kept refrigerated in minimal volume of EtOAc to prevent rearrangement of tosylate product.

4.6.8 Racemic-spiro[camphene-6,2'-indan] **65**



Camphor-tosylate crystals kept in EtOAc were vacuum dried in order to initialize rearrangement to the spiro[camphene-6,2'-indan].

4.7 Mechanistic study

4.7.1 LAD rearrangement

4.7.1.1 General procedure

Kinetics studies were carried out in CDCl_3 at 313 K, 318 K, 323 K and 328 K. The tosylate product was dried and weighed then made up to a standard solution of 5 mL with CDCl_3 to maintain a constant concentration at all temperatures (mol L^{-1}). The solution was then transferred equally into NMR tubes which were kept in dry ice until each respective kinetic run to minimize any rearrangement taking place prior to placement in NMR machine. The kinetics runs were carried out on the Bruker Biospin 600 MHz NMR spectrum.

Butyllithium (3.00 mL, 4.80 mmol) was added dropwise to a stirred solution of reduced deuterated camphor-xylene **62D** (0.95 g, 4.00 mmol) in THF (25 mL) under argon at 0°C for 1 h. A solution of tosyl chloride (0.90 g, 9.60 mmol) in minimal THF was added and the resulting mixture was left to stir for 1 h. The reaction mixture was quenched with saturated NaHCO_3 and then extracted with EtOAc (2 x 15 mL). The organic layers were combined, dried over MgSO_4 and the solvent reduced to a minimum amount *in vacuo*. The resulting white crystals were kept in the mother liquor at 0°C to prevent rearrangement of tosylate product. Yield (0.72 g, 76%), all isolated product was used for the kinetics study.

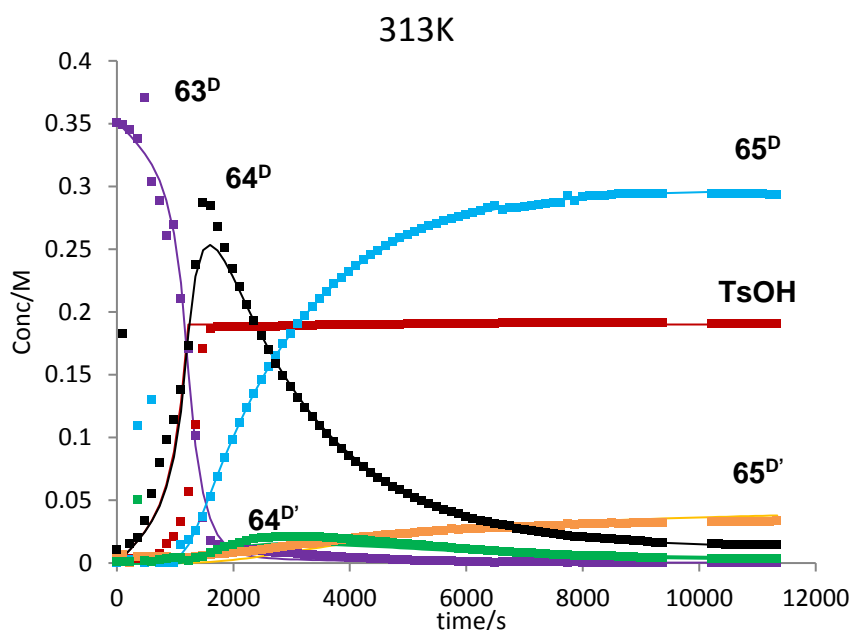


Figure 87: Molar concentration of all species in the decomposition of **63^D** at 313 K derived from ^1H data. The experimental data (points) are overlaid with the theoretical fit (lines).

Time/s	[TsOH]	[63 ^D]	[65 ^D]	[65 ^D]	[64 ^D]	[64 ^D]
0	0.003439	0.35122	0.000667853	0.005062	0.001319674	0.010921
100	0.003731	0.349576	0.001386265	0.006896	0.001180973	0.183046
225	0.003597	0.345333	0.002817876	0	0.0016592	0.015265
351	0.003527	0.338295	0.109478016	0.005256	0.050299067	0.020538
476	0.003366	0.37118	0	0.005353	0.00180859	0.033759
601	0.003678	0.303962	0.129802256	0.005545	0.001668142	0.055539
727	0.007701	0.288475	0	0.005502	0.002925518	0.08034
852	0.01539	0.260562	0	0.005447	0.003581798	0.098323
977	0.020934	0.269291	0	0.004555	0.004221276	0.114692
1103	0.032826	0.21063	0.01457124	0.00445	0.004084839	0.138666
1227	0.056651	0.170755	0.018647966	0.004767	0.002282877	0.173447
1352	0.110458	0.101947	0.025947701	0.004852	0.004339335	0.237417
1477	0.170621	0.036509	0.037204876	0.005733	0.005368837	0.287163
1603	0.187037	0.017779	0.053029828	0.006474	0.007884478	0.284656
1729	0.188632	0.014498	0.068672208	0.007122	0.010687238	0.268226
1854	0.188546	0.013306	0.084103529	0.007694	0.013026694	0.250954
1979	0.188566	0.012354	0.09887418	0.008262	0.015059308	0.234745
2104	0.188618	0.011717	0.111819945	0.008896	0.016615745	0.219754
2229	0.188727	0.011178	0.124136064	0.00963	0.018021238	0.205949
2354	0.188643	0.010634	0.135174189	0.010265	0.019084931	0.193054
2479	0.188527	0.009946	0.146503582	0.010949	0.01996959	0.181167
2604	0.188609	0.009392	0.156655122	0.011765	0.020593782	0.169905
2729	0.188813	0.008799	0.165670051	0.01241	0.020923458	0.159289
2855	0.189045	0.008318	0.17447663	0.013134	0.021182813	0.149472
2979	0.189217	0.007946	0.182655802	0.01394	0.021440048	0.140399
3104	0.189363	0.007428	0.190573231	0.01461	0.021409635	0.131935
3230	0.189545	0.00707	0.197372275	0.015321	0.02130951	0.123981
3355	0.18965	0.00652	0.204666094	0.015994	0.021141793	0.116602
3480	0.189739	0.006187	0.210755567	0.016786	0.020919214	0.109561
3606	0.189844	0.005822	0.216420037	0.017469	0.020563672	0.103035
3731	0.190002	0.005379	0.222427512	0.018111	0.020244404	0.097048
3857	0.190083	0.005009	0.227700098	0.018764	0.019816522	0.091421
3981	0.19011	0.004712	0.232362588	0.019397	0.019350855	0.086107
4107	0.190154	0.004404	0.237026672	0.019989	0.018959951	0.081255
4232	0.190063	0.004056	0.241532143	0.02067	0.018398502	0.076754
4358	0.190199	0.003763	0.245437609	0.02121	0.017936471	0.072387
4483	0.190184	0.003544	0.248799199	0.021707	0.01733774	0.068451
4609	0.190253	0.003303	0.252643829	0.022454	0.016869949	0.06477
4734	0.190286	0.003044	0.255917788	0.022921	0.016388924	0.061402
4860	0.190423	0.002757	0.259118805	0.023438	0.015809489	0.058131

4985	0.190511	0.002694	0.261417093	0.023906	0.015272997	0.055138
5111	0.190514	0.002461	0.264061838	0.024429	0.014830566	0.052302
5237	0.190631	0.002211	0.266867937	0.024837	0.014347823	0.049628
5362	0.190607	0.002067	0.26899057	0.025287	0.013754042	0.047151
5488	0.190658	0.002087	0.270738772	0.025848	0.013327373	0.04496
5613	0.190751	0.001895	0.272613876	0.026017	0.012771986	0.042777
5739	0.190762	0.001845	0.274297151	0.027434	0.012297528	0.040773
5865	0.190735	0.001481	0.276109365	0.026845	0.011822665	0.038996
5990	0.190618	0.00135	0.277785596	0.027274	0.011447928	0.03709
6116	0.190601	0.001083	0.279382432	0.027588	0.010988624	0.035323
6241	0.191018	0.000998	0.281073748	0.028005	0.010453242	0.034275
6366	0.190915	0.00082	0.283051383	0.028524	0.010265115	0.032963
6492	0.190858	0.000499	0.284621016	0.028703	0.009931903	0.031429
6617	0.191499	0.001697	0.281372827	0.028438	0.009237119	0.030352
6742	0.19138	0.001449	0.282858627	0.028644	0.008900572	0.029647
6867	0.191522	0.001487	0.283440819	0.029205	0.008605814	0.027975
6992	0.191575	0.001353	0.284163155	0.029322	0.008189026	0.026657
7117	0.1917	0.001276	0.285168011	0.02946	0.007939147	0.025837
7243	0.191717	0.001181	0.286029082	0.029703	0.007664606	0.024991
7368	0.191721	0.001155	0.286448017	0.029928	0.007348802	0.024375
7493	0.1917	0.001115	0.286965411	0.029958	0.007009932	0.023478
7618	0.191774	0.001133	0.287461395	0.030247	0.006786161	0.022933
7743	0.191269	0	0.292907751	0.031084	0.006817916	0.022366
7869	0.191767	0.000988	0.288477764	0.030524	0.006289071	0.021484
7993	0.191319	0	0.292365202	0.031167	0.006252456	0.021061
8119	0.191306	0	0.292837353	0.031485	0.006036929	0.020549
8243	0.191263	0	0.293075039	0.031269	0.006000607	0.020363
8368	0.191319	0	0.293181378	0.031699	0.005768985	0.019777
8494	0.191421	0	0.29370306	0.031873	0.00563672	0.019527
8619	0.191327	0	0.294073159	0.031736	0.005302538	0.018508
8745	0.191345	0	0.294051636	0.031798	0.005005911	0.018323
8870	0.191337	0	0.294134698	0.032191	0.004995767	0.017578
8995	0.191347	0	0.294710254	0.032234	0.004797618	0.01756
9120	0.19132	0	0.29426518	0.032192	0.004712759	0.016852
9245	0.191326	0	0.294403763	0.03235	0.004521824	0.016572
9370	0.191319	0	0.294343054	0.032492	0.004416526	0.01674
10210	0.191167	0	0.294262128	0.032935	0.003810055	0.015275
10335	0.191019	0	0.293952817	0.033039	0.003814299	0.015328
10460	0.190987	0	0.294294933	0.033071	0.003660049	0.015026
10585	0.19098	0	0.294355229	0.033198	0.003666717	0.014843

10710	0.190935	0	0.294064617	0.033205	0.003593245	0.014649
10835	0.190849	0	0.294461096	0.0333	0.003508548	0.014719
10961	0.190837	0	0.294230778	0.033336	0.00344335	0.014589
11087	0.190776	0	0.294173034	0.033285	0.003383649	0.014451
11212	0.190784	0	0.293919589	0.033278	0.003334758	0.014455
11337	0.190775	0	0.293815141	0.033464	0.003347519	0.01427

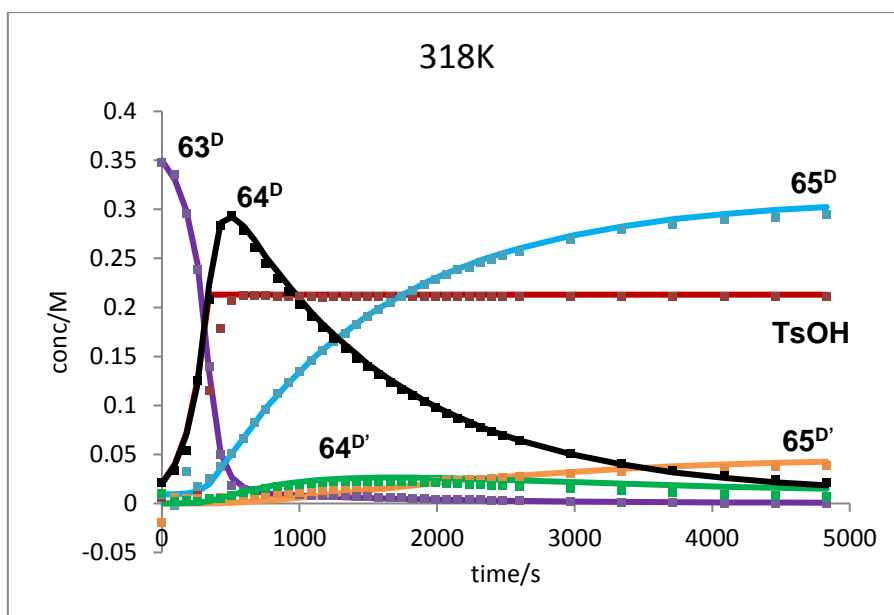


Figure 88: Molar concentration of all species in the decomposition of 63^D at 318 K derived from 1H data. The experimental data (points) are overlaid with the theoretical fit (lines)

Table 20: Molar concentration of all species in the decomposition of 63^D at 318 K derived from 1H data

Time/s	[TsOH]	[63^D]	[65^D]	[$65^{D'}$]	[$64^{D'}$]	[64^D]
0	0.005651	0.34762	0.009223	-0.01922	0.009968325	0.02078
94	0.004324	0.335637	-0.00182	0.005639	0.002348663	0.033702
177	0.002535	0.295151	0.032678	0.004789	0.002619884	0.053445
260	0.013897	0.239118	0.017136	0.004771	0.001658699	0.125811
343	0.115652	0.139223	0.025504	0.004823	0.004832673	0.207552
426	0.177923	0.050019	0.037983	0.005827	0.005008856	0.283151
508	0.207195	0.018529	0.050855	0.006722	0.007599055	0.294005
591	0.21148	0.013547	0.066554	0.007534	0.010645903	0.278342
673	0.211916	0.0121	0.082222	0.008349	0.013159476	0.260706

755	0.211638	0.011482	0.096094	0.008897	0.015315509	0.244657
838	0.210954	0.010172	0.111752	0.00989	0.017028595	0.229697
920	0.210876	0.009755	0.123431	0.010521	0.018454392	0.215921
1002	0.210746	0.009298	0.134989	0.011288	0.019655959	0.202808
1085	0.210498	0.008608	0.146019	0.012087	0.020492131	0.190608
1167	0.210423	0.008263	0.155652	0.012941	0.021277264	0.17888
1250	0.210491	0.007887	0.165632	0.014042	0.021871504	0.168062
1332	0.210585	0.007561	0.173735	0.01488	0.022164303	0.157637
1414	0.210529	0.006954	0.182982	0.015889	0.022434058	0.148299
1496	0.210507	0.006449	0.190708	0.016609	0.02245151	0.139524
1578	0.210483	0.006147	0.197934	0.017599	0.022424076	0.13141
1660	0.210543	0.005825	0.204568	0.018456	0.02227418	0.123819
1742	0.210528	0.00543	0.211146	0.019345	0.022093494	0.116428
1824	0.210624	0.005023	0.217198	0.020075	0.021817361	0.109742
1906	0.210649	0.004647	0.223368	0.021064	0.021585501	0.103484
1988	0.210656	0.004295	0.228655	0.021764	0.021098843	0.09757
2070	0.210687	0.004088	0.233325	0.022743	0.020638837	0.09192
2152	0.210775	0.003674	0.238299	0.023481	0.020189012	0.086842
2234	0.2109	0.003784	0.241117	0.024049	0.019715135	0.081947
2316	0.210988	0.003512	0.245195	0.024842	0.019171093	0.077505
2398	0.210898	0.003246	0.24912	0.025573	0.018670397	0.073429
2480	0.210842	0.003084	0.252435	0.026367	0.018249431	0.069561
2600	0.210851	0.002631	0.257466	0.0273	0.017460579	0.064289
2972	0.21087	0.001917	0.269023	0.029946	0.015093658	0.050894
3344	0.210715	0.000989	0.278946	0.032578	0.012931108	0.04113
3716	0.210709	0.00059	0.284689	0.034227	0.01088828	0.033879
4088	0.210658	0.000178	0.28946	0.035955	0.009291167	0.028507
4461	0.210906	0.000206	0.291389	0.037092	0.007781195	0.024635
4833	0.210804	-0.00031	0.294871	0.038159	0.006915632	0.021543

323K

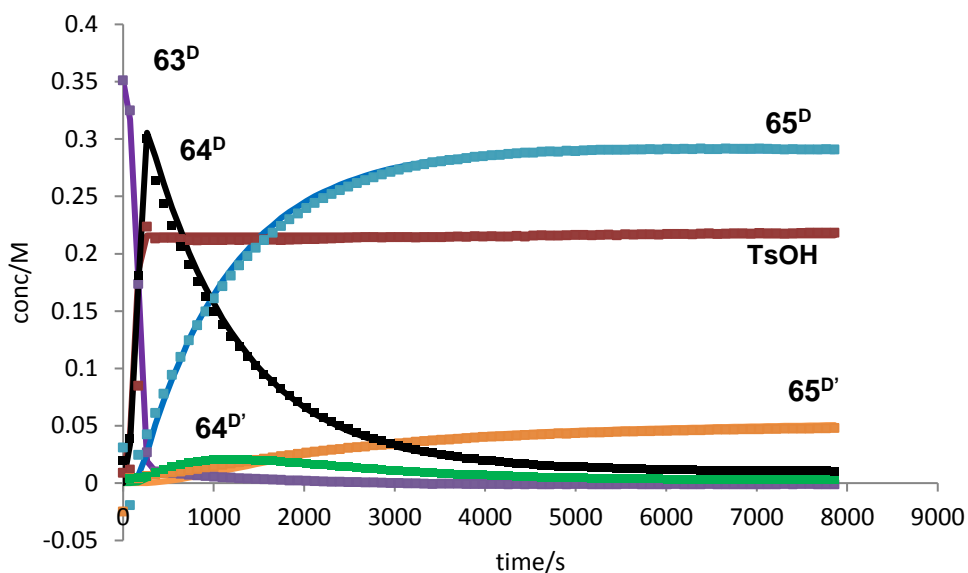


Figure 89: Molar concentration of all species in the decomposition of 63^D at 323 K derived from 1H data. The experimental data (points) are overlaid with the theoretical fit (lines)

Table 21: Molar concentration of all species in the decomposition of 63^D at 323 K derived from 1H data

Time/s	[TsOH]	[63^D]	[65^D]	[$65^D'$]	[$64^D'$]	[64^D]
0	0.009028	0.35122	0.031128	-0.02484	0.019775	0.019318
77	0.011827	0.324872	-0.01923	0.004226	0.003681	0.03861
170	0.085016	0.173557	0.024602	0.004255	0.004606	0.180865
263	0.223685	0.026731	0.042425	0.006201	0.005728	0.300146
355	0.213274	0.010052	0.061032	0.007229	0.008956	0.26393
448	0.213923	0.009333	0.07779	0.008267	0.012085	0.243724
541	0.213874	0.008733	0.09427	0.009124	0.014446	0.224627
634	0.212644	0.008023	0.10994	0.010192	0.016391	0.206655
726	0.211974	0.007284	0.124384	0.011302	0.017731	0.190499
819	0.211746	0.006651	0.137689	0.012424	0.018766	0.175671
911	0.211957	0.00619	0.149658	0.013589	0.019544	0.162219
1004	0.212016	0.005587	0.161166	0.014607	0.020038	0.149802
1097	0.212005	0.005106	0.171692	0.015859	0.020374	0.138168
1189	0.212223	0.0048	0.180994	0.016963	0.020478	0.127965
1282	0.211941	0.004332	0.189717	0.018055	0.02042	0.118676
1374	0.212171	0.003894	0.197935	0.019106	0.020213	0.110053
1467	0.212329	0.003646	0.205255	0.020175	0.019953	0.102171
1560	0.212311	0.003385	0.211966	0.021271	0.019584	0.094993

1653	0.212191	0.003026	0.218397	0.022362	0.01924	0.088174
1746	0.212008	0.002798	0.22424	0.023449	0.018705	0.082008
1839	0.212217	0.002382	0.229965	0.024396	0.018176	0.076282
1932	0.212453	0.002191	0.235007	0.025482	0.017598	0.070922
2025	0.21271	0.001876	0.239935	0.026525	0.016952	0.065913
2118	0.212848	0.001685	0.244258	0.027337	0.016406	0.061514
2211	0.212975	0.001408	0.248391	0.028137	0.015864	0.057399
2304	0.213337	0.001168	0.252188	0.02893	0.015199	0.053715
2397	0.213575	0.001028	0.255553	0.029735	0.014601	0.050283
2490	0.213745	0.00097	0.25847	0.030592	0.014088	0.047081
2583	0.214237	0.000738	0.261658	0.031179	0.013469	0.044155
2675	0.214467	0.000699	0.264148	0.031975	0.012902	0.041476
2769	0.214391	0.000447	0.266663	0.032858	0.012236	0.038996
2861	0.214187	0.000253	0.269104	0.033306	0.011801	0.036737
2955	0.214315	0.000134	0.271207	0.033924	0.011263	0.034671
3048	0.214463	-7.4E-05	0.273391	0.034573	0.010677	0.032633
3141	0.214297	-0.00031	0.275154	0.035294	0.010293	0.03077
3234	0.214062	-0.00038	0.276582	0.035904	0.009827	0.029264
3327	0.214362	-0.00052	0.278126	0.036599	0.009323	0.027668
3420	0.214344	-0.0007	0.279625	0.037149	0.008979	0.026151
3513	0.214336	-0.00067	0.280494	0.037767	0.008589	0.02502
3606	0.214734	-0.00066	0.281635	0.038111	0.008191	0.023927
3699	0.214945	-0.00057	0.282368	0.038669	0.007858	0.022872
3792	0.214774	-0.00079	0.283464	0.039144	0.007545	0.021836
3886	0.21512	-0.00083	0.284372	0.039565	0.007141	0.020955
3979	0.214989	-0.00078	0.284891	0.040217	0.006906	0.01997
4071	0.215376	-0.00088	0.285852	0.040397	0.00667	0.019164
4164	0.21508	-0.00085	0.286222	0.040814	0.006357	0.018657
4256	0.214874	-0.00104	0.287102	0.041173	0.006063	0.017905
4348	0.215482	-0.00095	0.287638	0.041464	0.005817	0.017233
4441	0.214923	-0.00116	0.288073	0.041926	0.005685	0.016678
4533	0.215709	-0.00091	0.288191	0.042246	0.005445	0.016234
4626	0.21595	-0.00098	0.288816	0.042448	0.005168	0.015749
4718	0.215782	-0.00099	0.289097	0.042715	0.004982	0.015399
4810	0.215871	-0.00082	0.28903	0.043158	0.004906	0.014927
4902	0.216058	-0.00099	0.289813	0.04312	0.004673	0.014587
4994	0.216223	-0.00086	0.289573	0.043592	0.004613	0.014284
5087	0.216464	-0.00087	0.289963	0.043754	0.004434	0.013921
5179	0.216143	-0.00108	0.290369	0.044136	0.004252	0.013519
5272	0.216387	-0.00105	0.290551	0.044251	0.004174	0.013274

5364	0.216524	-0.00098	0.290576	0.044527	0.00402	0.01306
5456	0.216203	-0.00101	0.290726	0.044601	0.00404	0.012844
5549	0.216825	-0.00092	0.290633	0.044897	0.003955	0.012631
5641	0.216618	-0.00092	0.290796	0.044975	0.003763	0.012588
5733	0.216787	-0.00099	0.290999	0.045232	0.003753	0.012204
5825	0.216931	-0.00096	0.29105	0.045331	0.003661	0.012117
5918	0.21665	-0.00096	0.290993	0.045607	0.003574	0.011983
6010	0.217333	-0.00097	0.291362	0.045592	0.003412	0.011806
6104	0.217068	-0.00091	0.291136	0.045856	0.003408	0.011715
6197	0.217118	-0.00104	0.291453	0.045875	0.003389	0.011519
6289	0.216785	-0.00105	0.291262	0.046148	0.003345	0.011493
6381	0.217378	-0.00117	0.291739	0.046143	0.003216	0.011268
6474	0.217616	-0.00086	0.291206	0.046415	0.003273	0.011165
6566	0.217217	-0.00104	0.291253	0.046539	0.003203	0.011241
6659	0.217573	-0.0011	0.291687	0.046672	0.003045	0.010901
6751	0.217719	-0.00107	0.291528	0.046642	0.00302	0.011075
6844	0.217871	-0.00099	0.291421	0.046796	0.003043	0.01093
6937	0.217399	-0.00106	0.291317	0.046954	0.002973	0.011011
7029	0.217996	-0.00108	0.291632	0.047032	0.002886	0.010726
7122	0.217637	-0.00109	0.291374	0.047113	0.00303	0.010771
7215	0.217754	-0.00097	0.29106	0.047206	0.002993	0.010908
7307	0.217559	-0.00089	0.290846	0.0474	0.003035	0.010806
7399	0.217813	-0.00108	0.291302	0.047403	0.002838	0.01074
7492	0.217912	-0.00094	0.291007	0.047509	0.002907	0.01072
7584	0.218175	-0.0009	0.290862	0.047557	0.002963	0.010718
7677	0.218211	-0.00097	0.290904	0.0477	0.002884	0.010679
7769	0.218172	-0.00119	0.291299	0.047648	0.002947	0.010496
7862	0.218428	-0.001	0.291006	0.047903	0.00285	0.010439

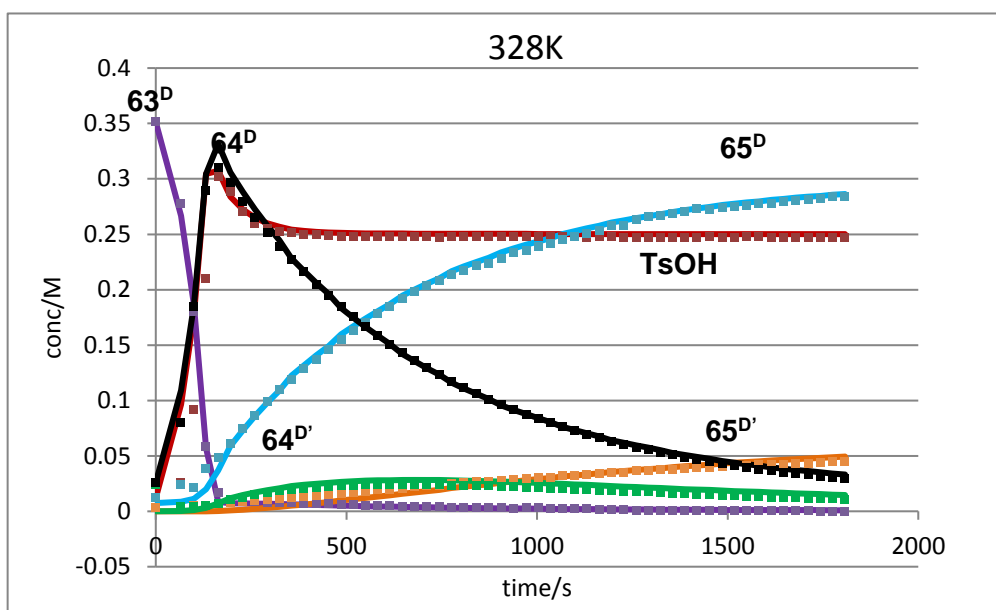


Figure 90: Molar concentration of all species in the decomposition of 63^D at 328 K derived from 1H data. The experimental data (points) are overlaid with the theoretical fit (lines)

Table 22: Molar concentration of all species in the decomposition of 63^D at 328 K derived from 1H data

Time/s	[TsOH]	[63^D]	[65^D]	[$65^{D'}$]	[$64^{D'}$]	[64^D]
0	0.011966	0.35122	0.012162	0.003299	0.023753	0.026078765
66	0.026068	0.277558	0.024012	0.004227	0.003793	0.079612538
100	0.091189	0.180151	0.021144	0.004439	0.004349	0.184239133
132	0.209924	0.058373	0.038137	0.0052	0.004725	0.28939512
164	0.301764	0.017025	0.048738	0.006611	0.007005	0.309814283
196	0.288699	0.010566	0.061003	0.007688	0.010067	0.296507032
228	0.269965	0.009164	0.07417	0.00866	0.012555	0.279762384
260	0.259544	0.008905	0.086082	0.00963	0.014784	0.264890598
292	0.255103	0.00814	0.098971	0.010677	0.016591	0.251396661
324	0.252584	0.007569	0.110118	0.011454	0.018148	0.238618043
356	0.251047	0.007381	0.118685	0.011937	0.019443	0.226925035
389	0.249635	0.007082	0.128524	0.013069	0.020444	0.215792039
421	0.249255	0.006811	0.137041	0.013961	0.021348	0.204815121
453	0.248407	0.006744	0.145719	0.015192	0.022135	0.194594835
486	0.247993	0.006058	0.154779	0.01587	0.022721	0.184892476

518	0.247955	0.005669	0.162754	0.016813	0.023103	0.175567296
550	0.247707	0.005545	0.169709	0.017885	0.023722	0.166831196
582	0.247584	0.004987	0.178247	0.019058	0.023805	0.158558729
614	0.247568	0.004513	0.184781	0.019881	0.024037	0.150759818
647	0.247767	0.004424	0.191377	0.020869	0.023978	0.143637971
679	0.247638	0.003899	0.198086	0.021876	0.02405	0.136370775
711	0.247488	0.003616	0.203526	0.022749	0.024126	0.129665879
744	0.247224	0.003603	0.207591	0.023427	0.023762	0.123172137
776	0.247542	0.003185	0.213581	0.024482	0.023472	0.117233831
808	0.247723	0.00352	0.217166	0.025604	0.023337	0.111713234
841	0.247629	0.003294	0.221712	0.026387	0.022902	0.10638237
873	0.24785	0.003408	0.223796	0.027129	0.022668	0.10087096
906	0.247636	0.003071	0.228077	0.027636	0.022134	0.096297499
938	0.247645	0.002456	0.233269	0.028582	0.021934	0.091522823
971	0.247619	0.002842	0.235264	0.029278	0.021458	0.087377023
1003	0.247753	0.002713	0.239039	0.030248	0.021046	0.083381937
1034	0.247501	0.002529	0.24165	0.030592	0.020449	0.079585764
1066	0.247582	0.002468	0.244866	0.031648	0.020154	0.076039381
1098	0.247455	0.002215	0.248076	0.032291	0.01969	0.07258679
1130	0.247404	0.002127	0.250532	0.032992	0.0192	0.069357289
1163	0.247587	0.001727	0.253643	0.033862	0.018799	0.066111259
1195	0.247476	0.001373	0.257441	0.034726	0.018299	0.063346909
1228	0.247158	0.001762	0.257438	0.035104	0.017973	0.06026598
1260	0.247069	0.00084	0.263424	0.036365	0.017365	0.057731983
1292	0.246841	0.0007	0.265683	0.036839	0.01716	0.055306703
1324	0.247174	0.00061	0.266948	0.037535	0.016703	0.052816388
1356	0.247154	0.00063	0.268784	0.037859	0.015864	0.050764451
1388	0.247049	0.000503	0.270366	0.038654	0.015899	0.048375508
1420	0.247286	0.000235	0.272557	0.039174	0.015093	0.046585218
1453	0.247632	0.000718	0.271805	0.039479	0.0148	0.044626615
1486	0.247303	0.000494	0.273625	0.039955	0.014059	0.042694482
1518	0.247018	0.000674	0.274433	0.040668	0.013781	0.0414854
1550	0.247434	0.000289	0.276159	0.041178	0.013369	0.039534756
1582	0.247554	0.000102	0.277667	0.041714	0.013072	0.037816302
1615	0.247185	0.000277	0.277985	0.042151	0.012547	0.036306782
1647	0.247371	0.000142	0.279104	0.042472	0.012127	0.035052714
1679	0.246581	0.000204	0.279976	0.043061	0.01186	0.033927327
1711	0.246757	0.000118	0.280932	0.043225	0.011367	0.032722298
1743	0.247329	-8.9E-05	0.282042	0.043894	0.01107	0.031542975
1775	0.247022	-0.00027	0.283944	0.044451	0.010972	0.030447577

4.8 Mechanistic study

4.8.1 Dimer study

4.8.1.1 General procedure

Kinetics studies were carried out in CDCl_3 at 298 K, 303 K, 313 K and 318 K. Fenchol (0.005 g, 0.032 mmol), thionyl chloride (0.0048 g, 0.040 mmol), pyridine (0.0015 g, 1.5 mmol) and a trimethoxybenzene standard (0.017 g) were each weighed out and kept in dry ice. A stock solution of the three reagents combined was made up to 5 mL with CDCl_3 and divided equally into NMR tubes used for the kinetics study. All NMR tubes were kept on dry ice until the time of experiment to ensure minimum reaction taking place. The kinetics runs were carried out on the Bruker Avance II 600 MHz NMR spectrometer.

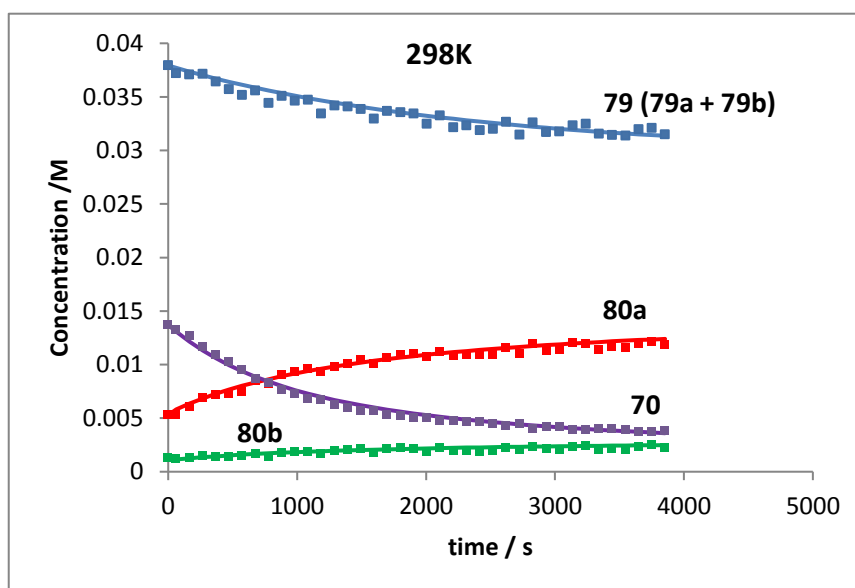
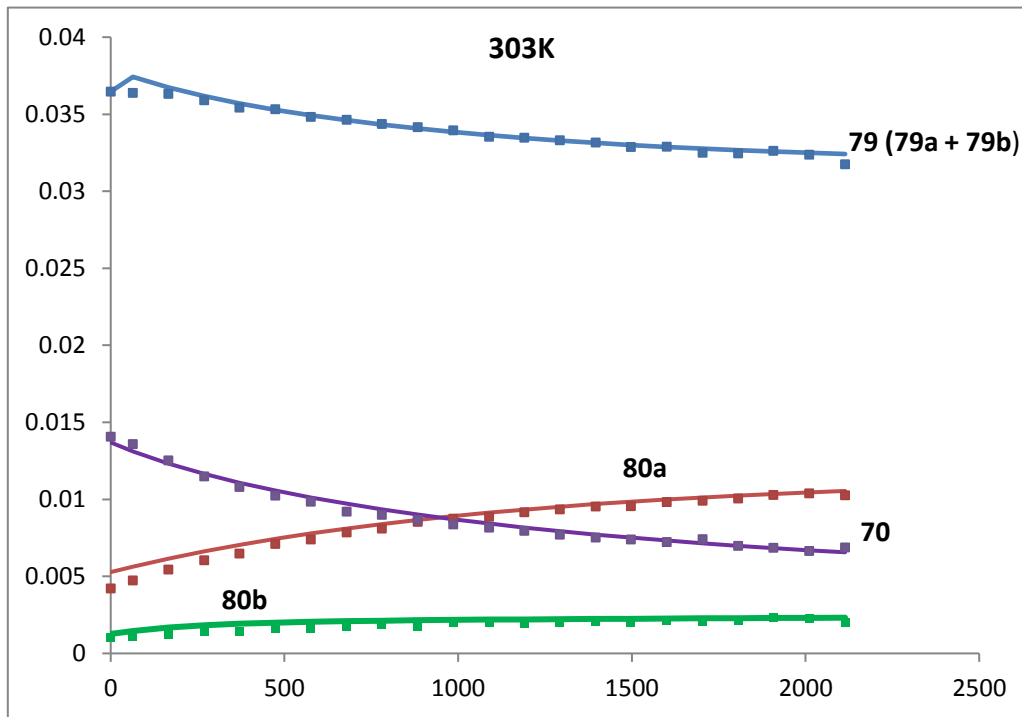


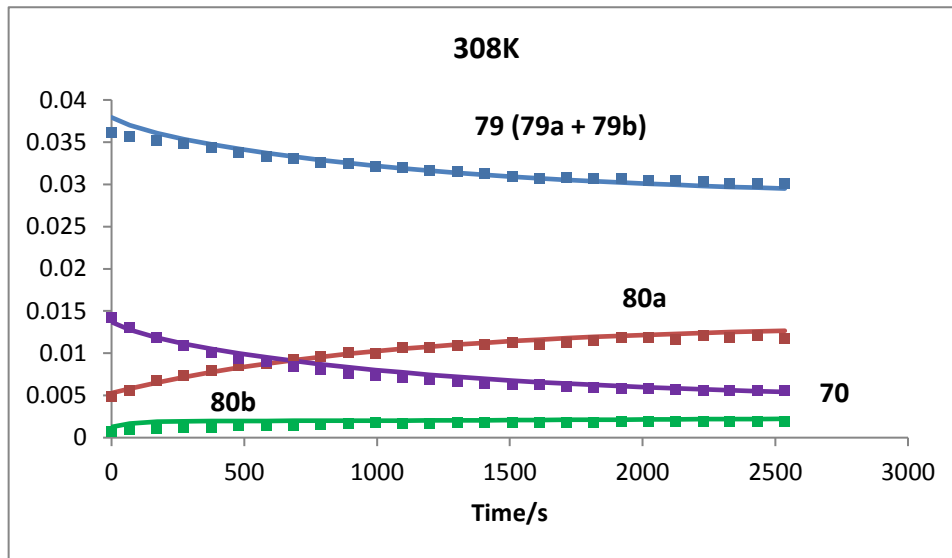
Figure 91: Molar concentration of all species in the decomposition of **70** at 298 K derived from ^1H data. The experimental data (points) are overlaid with the theoretical fit (lines)

Table 22: Molar concentration of all species in the decomposition of **70** at 298 K derived from ^1H data

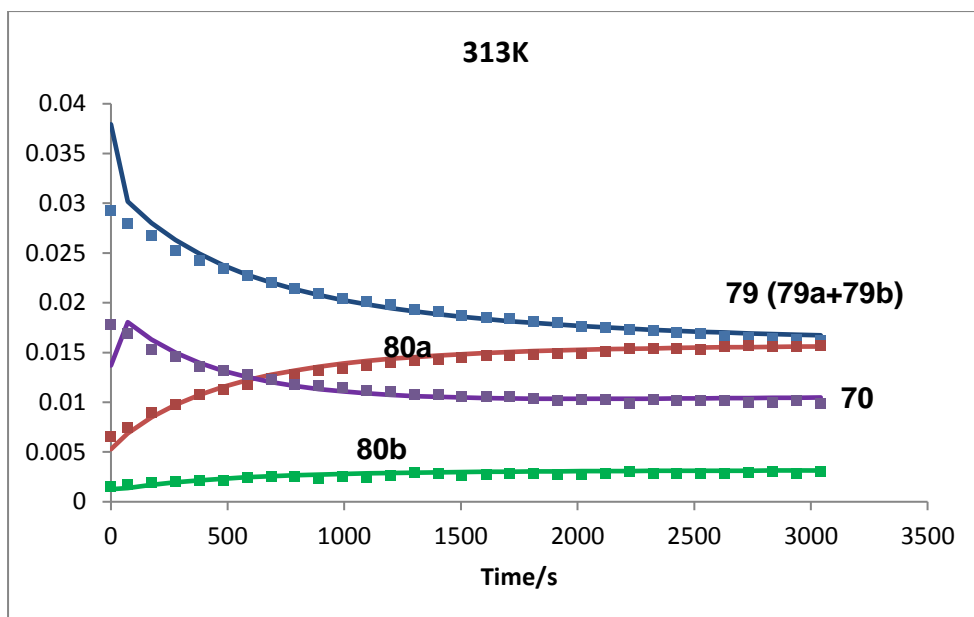
Time	[79]	[80a]	[80b]	[70]
0	0.037937	0.005279	0.001265	0.013696
62	0.037191	0.005368	0.001206	0.013265
164	0.037092	0.006131	0.001325	0.012727
267	0.037155	0.006938	0.001467	0.011703
369	0.036426	0.007163	0.00143	0.010939
472	0.035718	0.007324	0.001408	0.01023
574	0.035156	0.007483	0.001461	0.009497
676	0.035573	0.008528	0.00171	0.00873
779	0.034428	0.008226	0.001411	0.00831
881	0.035093	0.009003	0.001775	0.007667
983	0.034629	0.009388	0.001854	0.00724
1086	0.034715	0.009597	0.001889	0.006863
1188	0.033451	0.009373	0.001658	0.00672
1292	0.034174	0.009803	0.001932	0.006224
1394	0.034104	0.01006	0.002061	0.005963
1495	0.033847	0.010438	0.002099	0.005735
1597	0.032944	0.010117	0.001802	0.00571
1699	0.033674	0.01069	0.00215	0.005349
1802	0.033552	0.010971	0.002196	0.005179
1904	0.033422	0.011053	0.00215	0.005061
2006	0.032465	0.010745	0.001915	0.005039
2108	0.03325	0.011206	0.002268	0.004794
2212	0.032149	0.010836	0.001948	0.004806
2315	0.03234	0.010937	0.001976	0.004705
2418	0.031894	0.010923	0.001905	0.004668
2520	0.032011	0.010897	0.001952	0.004499
2623	0.032662	0.011563	0.002245	0.004255
2725	0.03146	0.011013	0.002021	0.004438
2829	0.032595	0.01192	0.002345	0.00406
2932	0.031694	0.011322	0.002115	0.004182
3035	0.031757	0.011373	0.002042	0.004208
3137	0.032342	0.012038	0.002366	0.003955
3240	0.032472	0.01195	0.00242	0.003922
3342	0.031565	0.01144	0.002057	0.00405
3444	0.031434	0.011668	0.002105	0.004025
3548	0.031363	0.011566	0.002064	0.00393
3650	0.031982	0.011953	0.002365	0.003753
3752	0.032103	0.012179	0.002489	0.003741
3854	0.031487	0.011874	0.002191	0.003837



Time	[79]	80a	80b	70
0	0.036469	0.004214	0.001019	0.014072
64	0.036384	0.004733	0.001113	0.013585
166	0.036321	0.005437	0.001254	0.012527
269	0.035914	0.006045	0.001446	0.011488
371	0.035427	0.006478	0.001437	0.010794
474	0.035325	0.007111	0.001598	0.010237
576	0.034821	0.007387	0.001632	0.009838
679	0.034631	0.007861	0.001759	0.009211
781	0.034373	0.008105	0.001857	0.008991
884	0.034153	0.008541	0.001759	0.008669
986	0.033949	0.008748	0.001994	0.008379
1089	0.033537	0.008875	0.001986	0.008162
1191	0.033475	0.00916	0.001971	0.007963
1293	0.033305	0.009358	0.002027	0.007713
1396	0.033161	0.009539	0.002105	0.007523
1498	0.03287	0.009567	0.002011	0.007393
1601	0.032893	0.00983	0.002119	0.007237
1704	0.032498	0.0099	0.002087	0.007427
1806	0.032451	0.010049	0.002111	0.006985
1908	0.03262	0.010278	0.002296	0.006862
2011	0.032381	0.010396	0.002234	0.006647
2114	0.03174	0.010264	0.001996	0.006867



time	[79]	[80a]	[80b]	70
0	0.036142	0.004881	0.000744	0.014234
69	0.035707	0.005582	0.000937	0.013088
172	0.035225	0.006708	0.001125	0.011874
274	0.034796	0.007365	0.001247	0.010868
378	0.034381	0.007977	0.001262	0.010048
481	0.033836	0.008482	0.001492	0.009322
584	0.033291	0.008845	0.00147	0.008998
686	0.033096	0.00922	0.001482	0.008439
789	0.032541	0.009616	0.001517	0.00807
892	0.032507	0.010107	0.001634	0.007627
995	0.032105	0.010012	0.001748	0.007364
1098	0.031983	0.010661	0.001696	0.007106
1200	0.031611	0.010693	0.001675	0.006932
1303	0.03153	0.010915	0.001757	0.006656
1406	0.031243	0.011022	0.001823	0.006457
1510	0.030966	0.011222	0.001814	0.006294
1612	0.030712	0.011049	0.001823	0.006249
1715	0.030848	0.011217	0.001826	0.006086
1818	0.030682	0.011575	0.001771	0.00597
1921	0.03074	0.011873	0.001888	0.005808
2023	0.030409	0.01184	0.001934	0.005793
2126	0.030393	0.011666	0.001982	0.00568
2229	0.030323	0.012055	0.001941	0.005621
2331	0.030085	0.011834	0.001923	0.005573
2434	0.030068	0.012041	0.001903	0.005578
2536	0.030122	0.01176	0.001913	0.005537



time	[79]	[80a]	[80b]	[70]
0	0.029289	0.006521	0.00147	0.017748
72	0.027962	0.007506	0.00169	0.016866
174	0.026737	0.008895	0.001965	0.015312
276	0.025294	0.009706	0.001975	0.014597
379	0.024187	0.010745	0.002137	0.013596
481	0.02343	0.01121	0.00213	0.01316
584	0.022705	0.011745	0.00238	0.012814
686	0.022077	0.012348	0.002504	0.01228
788	0.021421	0.012804	0.002507	0.011757
891	0.020927	0.01316	0.002359	0.011705
994	0.020451	0.013414	0.002518	0.011513
1096	0.020089	0.013689	0.00244	0.011154
1199	0.019772	0.014015	0.002617	0.011028
1301	0.019337	0.014145	0.002918	0.010755
1403	0.019079	0.014299	0.002804	0.010727
1505	0.018742	0.014449	0.002665	0.010505
1608	0.018474	0.014672	0.002763	0.010527
1710	0.018361	0.014727	0.002781	0.010563
1813	0.018136	0.014796	0.002833	0.010374
1915	0.017993	0.014918	0.002773	0.010154
2017	0.017613	0.014894	0.002758	0.010246
2120	0.01753	0.015061	0.00285	0.010231
2222	0.01732	0.015391	0.002977	0.009861
2325	0.017207	0.015371	0.002823	0.010233
2427	0.017031	0.015351	0.002854	0.010171
2529	0.016848	0.015319	0.002867	0.01015
2632	0.016628	0.015558	0.002818	0.010117

2734	0.016509	0.015696	0.002955	0.009978
2837	0.016386	0.015636	0.002974	0.010017
2939	0.016283	0.015557	0.002871	0.010164
3042	0.016194	0.015743	0.003018	0.009919

Bibliography

1. Dimitrov, V., Simova, S. and Kostova, K. Highly Effective and Practical Stereoselective Synthesis of New Homoallylic Alcohols with (+) -Camphor and (-) -Fenchone Skeleton. *Tetrahedron* **52**, 1699-1706 (1996).
2. Chen, W., Vermaak, I. and Viljoen, A. Camphor--a fumigant during the Black Death and a coveted fragrant wood in ancient Egypt and Babylon--a review. *Molecules* **18**, 5434–54 (2013).
3. Brown, B. Y. H. C., Rothberg, I., Schleyer, P. von. R., Donaldson, M. M. and Harper, J. J. The slow rates of solvolysis of endo-5,6-trimethylene-endo-(2 and 8)-norbornyl tosylates: steric hinderance to ionization and the Foote-Schleyer correlation. *Proc. Nat. Acad. Sci.* **56**, 1653–1660 (1966).
4. Olah, G.A., Prakash, G. K. (Ed) Carbocation Chemistry (John Wiley, 2004)
5. Meerwein, H., van Emster, K. Über die Gleichgewichts - Isomerie zwischen Bornylchlorid, Isobornylchlorid und Camphen - chlorhydrat. *Ber. Dtsch. Chem. Ges* **55**, 2500–2528 (1922).
6. Olah, G. A. The α -Bridged 2-Norbornyl Cation and Its Significance to Chemistry. *Acc. Chem. Res* **9**, 41–52 (1976).
7. Kropp, P. J., Poindexter, G. S., Pienta, N. J. and Hamilton, D. C. Photochemistry of alkyl halides. 1-norbornyl, 1-norbornylmethyl, 1- and 2-adamantyl, and 1-octyl bromides and iodides. *J. Am. Chem. Soc* **98**, 8135–8144 (1976).
8. Fomenko, V. V, Korchagina, D. V, Salakhutdinov, N. F. and Barhash, V. A. Some aliphatic-aromatic alcohols in organized medium. *Butlerov Commun.* **2**, 35–38 (2002).
9. Mosley, J. D., Young, J., W. Agarwal, J., Schaefer, H.F., Schleyer, P. von. R., and Duncan, M. A. Structural isomerization of the gas-phase 2-norbornyl cation revealed with infrared spectroscopy and computational chemistry. *Angew. Chem. Int. Ed. Engl.* **53**, 5888–91 (2014).
10. Lobb, K. A. Isomerization of the 2-Norbornyl Carbocation. *Eur. J. Org. Chem.* **2015**, 5370–5380 (2015).
11. Jalife, S. Martinez-Guajardo, G. Zavala-Oseguera, C. Fernandez-Herrera, M. A. Schleyer, P. von. R. and Merino, G. Mechanistic Elucidation of the 2-Norbornyl to 1,3-Dimethylcyclopentenyl Cation Isomerization. *Eur J. Org. Chem.* **2014**, 7955–7959 (2014).
12. Meerwein, H. Über unsymmetrische cyclische und acyclische Pinakone und deren Umlagerungsprodukte; ein Beitrag zur Kenntnis der Pinakolinumlagerung. *Justus Liebigs Ann. Chem.* **396**, 200 (1913).
13. Birladeanu, L. The Story of the Wagner – Meerwein Rearrangement *J. Chem. Edu.* **77**, 858–863 (2000).
14. Lee, C. C., Hahn, S. and Lam, L. K. M. 3,2-hydride shifts in the norbornyl system under acetolysis conditions. *Tetrahedron Lett.* 3049–3052 (1969).
15. Schleyer, P. von. R., Watts, W. E., Jr, R. C. F., Comisarow, M. B. and Olah, G. A. Stable Carbonium Ions. X.1 Direct Nuclear Magnetic Resonance Observation of the 2-Norbornyl Cation. **2700**, 5679–5680 (1964).

16. Roberts, J. D., and Lee, C. C. The nature of the Intermediate in the Solvolysis of Norbornyl Derivatives. *J. Am. Chem. Soc.* **73**, 5009–5010 (1951).
17. Olah, G. A. My search for carbocations and their role in chemistry. *Nobel Lect.* (1994).
18. Sorensen, T. S. Terpene Rearrangements from a Superacid Perspective. *Acc. Chem. Res.* **9**, 257–265 (1976).
19. Vaughan, W. R., Goetschel, C. T., Goodrow, M. H., and Warren, C. L. The Nature of Camphene Racemization. *J. Am. Chem. Soc.* **85**, 2282–2289 (1963).
20. Smith, W. B. A DFT Study of the Camphene Hydrochloride Rearrangement. *J. Org. Chem.* **64**, 60–64 (1999).
21. Bartlett, P. D., Pockel, I. The Wagner-Meerwein Rearrangement. A Kinetic Reinvestigation of the Isomerization of Camphene Hydrochloride'. **60**, (1938).
22. Brunelle, P., Sorensen, T.S., and Taeschler, C. The Historic Camphenyl Cation : A Detailed Structure Evaluation Including Solvation Energy Calculations. *J. Org. Chem.* **66**, 4 (2001).
23. Kong, J., Schleyer, P. von. R., and Rzepa, H. S. Successful computational modeling of isobornyl chloride ion-pair mechanisms. *Can. J. Chem.* **53**, 1056–1066 (2010).
24. Weininger, S. J. “ What's in a name?” from designation to denunciation - The nonclassical cation controversy . *Bull. Hist. Chem* **25**, (2000).
25. Lecture, C. Nonclassical Ions and Homoaromaticity. (1967).
26. Saunders, M. & Hugo, A. Recent Studies of Carbocations. *Chem. Rev.* **91**, 375-397 (1991).
27. Moss, R. A. The 2-norbornyl cation: A retrospective. *J. Phys. Org. Chem.* **27**, 374–379 (2014).
28. Wintein, S., Trifan, D. The structure of the bicyclo[2,2,1]-heptyl (norbornyl) carbonium ion. *J. Am. Chem. Soc* **71**, 2953 (1949).
29. Winstein, S., Trifan, D. Neighboring Carbon and Hydrogen. X. Solvolysis of endo-Norbornyl Arylsulfonates. *J. Am. Chem. Soc.* **74**, 1147–1154 (1952).
30. Bentley, TW., Bowen, CT., Morten, DH., Schleyer, PVR. The SN2-SN1 spectrum 3. Solvolyses of secondary and tertiary alkyl sulfonates in fluorinated alcohols. Further evidence for the SN2 intermediate mechanism. *J. Am. Chem. Soc.* **103**, 5466–5475 (1981).
31. Brown, C. The Energy of the Transition States and the Intermediate Cation in the Ionization of 2-Norbornyl Derivatives. Where is the Nonclassical Stabilization Energy?'. *Acc. Chem. Res.* **16**, 432–440 (1983).
32. Solomon, J.J., and Field, F. H. Reversible Reactions of Gaseous Ions. X. The Intrinsic Stability. *Reversible React. Gaseous Ions* 1567–1569 (1975).
33. Nevell, T.P., deSalas, E., and Wilson, C. L. Use of Isotopes in Chemical Reactions. Part I. The Mechanism of the Wagner-Meerwein Rearrangement. Exchange of Radioactive Chlorine and of Deuterium between Camphene Hydrochloride and Hydrogen Chloride. *J. Chem. Soc.* 1188–1199 (1939).
34. Carey, F. and Sunderberg. R. J. *Advanced Organic Chemistry.* (Springer, 2002).

35. Prakash, G K S, Olah, G. A., Saunders, M. Conclusion of the Classical-Nonclassical Ion Controversy. *Am. Chem. Soc.* **16**, 440–448 (1983).
36. Christl, M., Leininger, H., and Bruckner, D. On the Nature of the Bicyclo[3.2.1]octa-3,6-dien-2-yl Anion. A ¹³C NMR Spectroscopic Study. *J. Am. Chem. Soc.* **105**, 4843–4844 (1983).
37. Goetz, D.W., Schlegel, H., and Allen, L. C. Ab Initio Electronic Structure Calculations for Classical and Nonclassical Structures of the 2-Norbornyl Cation. *J. Am. Chem. Soc.* **18**, 8118–8120 (1977).
38. Scholz, F., Himmel, D., Heinemann, F.W., Schleyer, P. von. R., Meyer, K., and Kossing, I.. Crystal structure determination of the nonclassical 2-norbornyl cation. *Science* **341**, 62–4 (2013).
39. Wang, S. Chirality Transfer from Chiral Solutes and Surfaces to Achiral Solvents : Insights. (2009).
40. Yang, K. and Chen, K. Diastereoselective Baylis – Hillman Reactions : The Design and Synthesis of a Novel Camphor-Based Chiral Auxiliary. *Org. Lett.* **2**, 1999–2001 (2000).
41. Zhao, G., Yang, C., Sun, H., Lin, R. and Xia, W. (+)-Camphor Derivative Induced Asymmetric [2 +2]Photoaddition Reaction. *Org. Lett.* **14**, 776–779 (2012).
42. Le Paih, J., Derien, S., Demerseman, B., Bruneau, C., Dixneuf, P. H., Toupet, L., Dazinger, G., and Kirchner, K. Ruthenium-catalyzed synthesis of alkylidenecyclobutenes via head-to-head dimerization of propargylic alcohols and cyclobutadiene-ruthenium intermediates. *Chemistry* **11**, 1312–24 (2005).
43. Lee, D-S., Chang, S-M., Ho, C-Y., Lu, T-J. Enantioselective Addition of Diethylzinc to Aldehydes Catalyzed by Chiral O , N , O-tridentate Phenol Ligands Derived From Camphor. *Chirality* (2015).
44. Trillo, R. B., Leven, M., Neudorfl, J. M. and Goldfuss, B. Electronegativity Governs Enantioselectivity : Alkyl-Aryl Halide Cross-Coupling with Fenchol-Based Palladium-Phosphorus Halide Catalysts. *Adv. Synth. Catal.* **354**, 1451–1465 (2012).
45. Wang, Y., Xu, J., Wang, Y. and Chen, H. Emerging chirality in nanoscience. *Chem. Soc. Rev.* **42**, 2930–62 (2013).
46. Horváth, B., Kubincová, J. and Devínsky, F. Synthesis, surface and antimicrobial properties of some quaternary ammonium homochiral camphor sulfonamides. *Eur. J. Pharm. Sci.* **65**, 29–37 (2014).
47. Edwards, D. A., Luthy, R. G. and Liu, Z. Solubilization of Polycyclic Aromatic Hydrocarbons in Micellar Nonionic Surfactant Solutions. *Environ. Sci. Tech.* **25**, 127–133 (1991).
48. Salanger, J.-L. Surfactants:Types and Uses. (FIRP booklet # E300-A, 2000)
49. Schmiedel, P., and Rybinski, V. Chemistry and Technology of Surfactants. (Blackwell publishing, 2006).
50. Everett, D. H. *Basic principles of colloid science*. (RSC Paperbacks, 1988).
51. Ross, S. & Morrison, I. D. *Colloidal systems and interfaces*. (John Wiley, 1988).

52. Nagarajan, R. Solubilization in aqueous solutions of amphiphiles. *Curr. Opin. Colloid Interface Sci.* **1**, 391–401 (1996).
53. Milton, J. Surfactants and interfacial phenomena. (John Wiley, 1989).
54. Myers, D. Surfactant science and technology. (John Wiley, 2005).
55. Dwars, T., Paetzold, E. and Oehme, G. Reactions in micellar systems. *Angew. Chem. Int. Ed. Engl.* **44**, 7174–99 (2005).
56. Hill, J., Shrestha, L., Ishihara, S., Ji, Q. and Ariga, K. Self-Assembly: From Amphiphiles to Chromophores and Beyond. *Molecules* **19**, 8589–8609 (2014).
57. Letchford, K. & Burt, H. A review of the formation and classification of amphiphilic block copolymer nanoparticulate structures: micelles, nanospheres, nanocapsules and polymersomes. *Eur. J. Pharm. Biopharm.* **65**, 259–69 (2007).
58. Noguchi, H. Structure formation in binary mixtures of lipids and detergents: Self-assembly and vesicle division. (2012).
59. Chu, Z. and Feng, Y. Empirical Correlations between Krafft Temperature and Tail Length for Amidosulfobetaine Surfactants in the Presence of Inorganic Salt. *J. Am. Chem. Soc.* **28**, 1175–1181 (2012).
60. Bales, B. L., Benrraou, M. and Zana, R. Krafft Temperature and Micelle Ionization of Aqueous Solutions of Cesium Dodecyl Sulfate. *J. Phys. Chem. B* **106**, 9033–9035 (2002).
61. IUPAC Compendium of Chemical Terminology 2nd Edition (1997).
62. Rösler, A., Vandermeulen, G. W. M. and Klok, H.-A. Advanced drug delivery devices via self-assembly of amphiphilic block copolymers. *Adv. Drug Deliv. Rev.* **64**, 270–279 (2012).
63. Kalhapure, R. S., Suleman, N., Mocktar, C., Seedat, N. and Govender, T. Nanoengineered drug delivery systems for enhancing antibiotic therapy. *J. Pharm. Sci.* **104**, 872–905 (2015).
64. Zhao, L., Wang, X., Ma, Y. L. R., A. Y., and Shi, L., Chiral Micelles of Achiral TPPS and Diblock Copolymer Induced by Amino Acids. *Macromolecules* **42**, 6253–6260 (2009).
65. Mero, A., Pasut, G., Dalla, L., Fijten, M. W. M. & Schubert, U. S. Synthesis and characterization of poly (2-ethyl 2-oxazoline)-conjugates with proteins and drugs : Suitable alternatives to PEG-conjugates ? *J. Cont. Res.* **125**, 87–95 (2008).
66. Radovic-moreno, A. F. *et al.* Surface Charge-Switching Polymeric Nanoparticles for Bacterial Cell Wall- Targeted Delivery of Antibiotics. *Am. Chem. Soc.* **6**, 4279–4287 (2012).
67. Matini, T. Francini, N., Battocchio, A., Spain, S.G., Mantovani, G., Vicent, M. J., Sanhis, J., Gallon, E., Mastrotto, F., Salmaso, S. and Alexander, C. Synthesis and characterization of variable conformation pH responsive block co-polymers for nucleic acid delivery and targeted cell entry. *Polym. Chem* **5**, 1626–1636 (2014).
68. Cserhati, T., Forgacs, E. and Oros, G. Biological activity and environmental impact of anionic surfactants. *Environ. Int.* **28**, 337–348 (2002).
69. Zhang, Y., Han, Y., Chu, Z., He, S., Zhang, J and Feng, Y. Thermally induced structural transitions from fluids to hydrogels with pH-switchable anionic wormlike micelles. *J. Colloid Interface Sci.* **394**, 319–328 (2013).

70. Tsai, C.-H., Vivero-Escoto, J. L., Slowing, I. I., Fang, I.-J., Trewyn, B. G., and Lin, V. S. Y. Surfactant-assisted controlled release of hydrophobic drugs using anionic surfactant templated mesoporous silica nanoparticles. *Biomaterials* **32**, 6234–44 (2011).
71. McNally, C. S., Turner, D. P., Kulak, A. N., Meldrum, F. C. and Hyett, G. The use of cationic surfactants to control the structure of zinc oxide films prepared by chemical vapour deposition. *Chem. Commun.* **48**, 1490–2 (2012).
72. Bhardwaj, V. Ankla, D.D., Gupta, S. C., Schneider, M., Lehr, C.M., Ravi, M. N. V. PLGA nanoparticles stabilized with cationic surfactant: safety studies and application in oral delivery of paclitaxel to treat chemical-induced breast cancer in rat. *Pharm. Res.* **26**, 2495–503 (2009).
73. Kadajji, V. G. and Betageri, G. V. Water Soluble Polymers for Pharmaceutical Applications. *Polymers.* **3**, 1972–2009 (2011).
74. Jeirani, Z., Jan, M. J., Ali, B. S., Noor, I. M., See, C. H., and Saphanuchart, W. Formulation, optimization and application of triglyceride microemulsion in enhanced oil recovery. *Ind. Crops Prod.* **43**, 6–14 (2013).
75. Fernandes, S. C., de Souza F. D., de Souza, S. B., Nome, F. and Vieira, I. C. Gold nanoparticles dispersed in zwitterionic surfactant for peroxidase immobilization in biosensor construction. *Sens. Actuators B.* **173**, 483–490 (2012).
76. Geagea, R., Aubert, P., Banet, P. and Sanson, N. Signal enhancement of electrochemical biosensors via direct electrochemical oxidation of silver nanoparticle labels coated with zwitterionic polymers. *Chem. Commun.* **51**, 402–405 (2014).
77. Pileni, M.-P. The role of soft colloidal templates in controlling the size and shape of inorganic nanocrystals. *Nat. Mater.* **2**, 145–50 (2003).
78. Carreto, M. L., Rubio, S. and Perez-bendito, D. Organic Microheterogeneous Systems in Kinetic Analysis . Self-assembled Systems A Review. **121**, 33–44 (1996).
79. Manohar, C. and Narayanan, J. Average packing factor approach for designing micelles, vesicles and gel phases in mixed surfactant systems. *Colloids Surf.* **403**, 129–132 (2012).
80. Minkler, S. R. K., Lipshutz, B. H. and Krause, N. Gold Catalysis in Micellar Systems. *Angew. Chem* **123**, 7966–7969 (2011).
81. Falcone, R. D., Baruah, B., Gaidamaukas, E., Ritner, C. D., Correa, N. M., Silber, J. J., Crans, D. C., and Lvinger, N. E. Layered structure of room-temperature ionic liquids in microemulsions by multinuclear NMR spectroscopic studie.. *Euro. J. Chem***17**, 6837–46 (2011).
82. Illanes, A. *Enzyme Biocatalysis*. (Springer, 2008).
83. Iyer, P.V., and Ananthanarayan, L. Enzyme stability and stabilization — Aqueous and non - aqueous environment. *Process Biochem.* **43**, 1019-1178 (2008).
84. Sintra, T. E., Ventura, S. P. M. and Coutinho, J. A. P. Superactivity induced by micellar systems as the key for boosting the yield of enzymatic reactions. *J. Mol. Catal. B: Enzym.* **107**, 140–151 (2014).
85. Kamranfar, P. and Jamialahmadi, M. Effect of surfactant micelle shape transition on the microemulsion viscosity and its application in enhanced oil recovery processes. *J. Mol. Liq.* **198**, 286–291 (2014).

86. Lu, J., Liyanage, P. J., Solairaj, S., Adkins, S., Arachchilage, G. P., Kim, D. H., Britton, C., Weerasooriya, U. and Pope, G. A. New surfactant developments for chemical enhanced oil recovery. *J. Pet. Sci. Eng.* **120**, 94–101 (2014).
87. Bernal, E., Marchena, M. and Sánchez, F. Microheterogeneous catalysis. *Molecules* **15**, 4815–74 (2010).
88. Caumul, P. The role of surfactants and their intermediates in environmental chemistry. *J. Env Res and Dev.* **5**, 495–508 (2011).
89. Morris, K. F. Billiot, E. J., Billiot, F. H., Lipkowitz, K. B., Southerland, W. M., and Fang, Y. Investigation of Chiral Molecular Micelles by NMR Spectroscopy and Molecular Dynamics Simulation. *J. Phys. Chem.* **2012**, 240–251 (2012).
90. Goldberg, S. I., Baba, N., Green, R. I., Pandian, R., and Stowers, J. Micelle-Enzyme Analogy: Stereochemical and Substrate Selectivity. *J. Am. Chem. Soc* **100**, 97–98 (1978).
91. Zhang, L., Qin, L., Wang, X., Cao, H. and Liu, M. Supramolecular chirality in self-assembled soft materials: regulation of chiral nanostructures and chiral functions. *Adv. Matter.* **26**, 6959–64 (2014).
92. Diego-Castro, M. J., Hailes, H. C. and Lawrence, M. J. Synthesis and Characterization of Optically Active Surfactants Derived from Phenylalanine and Leucine. *J. Colloid Interface Sci.* **234**, 122–126 (2001).
93. Davidson, T. A., Mondal, K. and Yang, X. Use of a chiral surfactant for enantioselective reduction of a ketone. *J. Colloid Interface Sci.* **276**, 498–502 (2004).
94. Rispens, T. and Engberts, J. B. F. N. Micellar Catalysis of Diels - Alder Reactions : Substrate Positioning in the Micelle. *J. Med. Chem.* **67**, 7369–7377 (2002).
95. Otto, S. and Engberts, J. A. N. B. F. N. Diels-Alder Reactions in Micellar Media. *Reactions and Synthesis in Micellar Media.* 247–263 (2001) Marcel Dekker, New York.
96. Otto, S., Bertoncin, F. and Engberts, J. B. F. N. Lewis Acid Catalysis of a Diels - Alder Reaction in Water. *J. Am. Chem. Soc.* **118**, 7702–7707 (1996).
97. Diego-Castro, M. J. and Hailes, H. C. Novel application of chiral micellar media to the Diels – Alder reaction. *Chem. Commun.*, 1549–1550 (1998).
98. Fujiki, M. Supramolecular Chirality: Solvent Chirality Transfer in Molecular Chemistry and Polymer Chemistry. *Symmetry.* **6**, 677–703 (2014).
99. Fowler, P. W. Quantification of chirality : attempting the impossible. *Symmetry: culture and Science.* **16**, 321–334 (2007).
100. Aswal, V. K. and Goyal, P. S. Small-angle neutron scattering from micellar solutions. *Pramana* **63**, 65–72 (2004).
101. Goyal, P. S. and Aswal, V. K. Micellar structure and inter-micelle interactions in micellar solutions : Results of small angle neutron scattering studies. *Curr. Sci.* **80**, (2001).
102. Jensen, G. V., Lund, R., Gummel, J., Narayanan, T. and Pedersen, J. S. Monitoring the transition from spherical to polymer-like surfactant micelles using small-angle X-ray scattering. *Angew. Chem. Int. Ed. Engl.* **53**, 11524–8 (2014).

103. Tadras, T. F. *Applied Surfactants: Principles and applications*. (Wiley, Hoboken, 2006).
104. Gila, T. and Borbe, S. SANS Study of the Structure of Sodium Alkyl Sulfate Micellar Solutions in Terms of the One-Component Macrofluid Model. *J. Phys. Chem* **104**, 2073–2081 (2000).
105. Jusufi, A., Hynninen, A., Haataja, M. and Panagiotopoulos, A. Z. Electrostatic Screening and Charge Correlation Effects in Micellization of Ionic Surfactants. *J. Phys. Chem.* **113**, 6314–6320 (2009).
106. Furó, I. NMR spectroscopy of micelles and related systems. *J. Mol. Liq.* **117**, 117–137 (2005).
107. Villeneuve, M., Ootsu, R., Ishiwata, M. and Nakahara, H. Research on the Vesicle - Micelle Transition by ¹H NMR Relaxation Measurement. *J. Phys. Chem.* **110**, 17830–17839 (2006).
108. Lu, X-Y., Jiang, Y., Cui, X-H., Mao, S-Z., Lui, M-L. and Du, Y-R. NMR Study of Surfactant Micelle Shape Transformation with Concentration. *Acta Phys. Chim. Sin* **25**, 1357–1361 (2009).
109. Karaborni, S. and Smit, B. Computer simulations of surfactant structures. *Curr. Opin. Colloid Interface Sci.* **1**, 411–415 (1996).
110. Wilfred, B., Gunsteren, V. and Berendsen, C. Computer Simulation of Molecular Dynamics: Methodology, Applications, and Perspectives in Chemistry. **29**,
111. Bruce, C. D., Berkowitz, M. L., Perera, L. and Forbes, M. D. E. Molecular Dynamics Simulation of Sodium Dodecyl Sulfate Micelle in Water: Micellar Structural Characteristics and Counterion Distribution. *J. Phys. Chem.* **106**, 3788–3793 (2002).
112. Maillet, J.-B., Lachet, V. and Coveney, P. V. Large scale molecular dynamics simulation of self-assembly processes in short and long chain cationic surfactants. *Phys. Chem. Chem. Phys.* **1**, 5277–5290 (1999).
113. Lobb, K. A. and Kaye, P. T. ¹H NMR-based kinetic and mechanistic study of unusual skeletal rearrangements of a spirobornyl tosylate derivative. *J. Phys. Org. Chem.* **24**, 38–44 (2011).
114. Biali, S.E., and Rappoport, Z. Stable Simple Enols. Synthesis and Keto - Enol Equilibrium; of the Elusive 2,2-Dimesitylethanal and 1,2,2-Trimesitylethanone. Conformations of 1,2,2-Trimesitylethanone and 1,2,2-Trimesitylethanol. *J. Am. Chem. Soc.* **107**, 1007–1015 (1985).
115. Kraus, G. A. and Kiriara, M. Annulations in Bridged Systems. An Approach to the Synthesis of Shikodonin. *Tetrahedron Lett.* **33**, 7727–7728 (1993).
116. Martinez, A. G., Vilar, E. T., Fraile, A. G., Cerero, S. de la M., Herrero, M. E. R., Luiz, P. M., Subramanian, L. R. and Gancedo, A. G. Synthesis of Substituted 1-Norbornylamines with Antiviral Activity. *J. Med. Chem.* **38**, 4474–4477 (1995).
117. Schumann, R., and Pendleton, P. Dehydration products of 2-methylisoborneol. *Water Res* **31**, 1243–1246 (1997).
118. Soucy, P., Deslonc, P. and Villiger, B.-. Thermal decomposition of ozonides. A complementary method to the Baeyer-Villiger oxidation of hindered ketones. *Can. J. Chem.* **10**, (1979).
119. Lana, E. J. L., da Silva Rocha, K. A., Kozhevnikov, I. V. and Gusevskaya, E. V. One-pot synthesis of diisobornyl ether from camphene using heteropoly acid catalysts. *J. Mol. Catal. A Chem.* **243**, 258–263 (2006).

120. Brooks, P. R. and Bishop, R., Counter, J.A., and Tiekink, R. T. Chemistry and Structure of anti-(Z)- and syn-(E)-Bis(fenchyldiene). *J. Org. Chem.* **59**, 1365–1368 (1994).
121. Duggan, A. R., Mciteka, L. P., Lobb, K. A. and Kaye, P. T. H NMR-Based Kinetic-Mechanistic Study of the Intramolecular Trans-esterification of 2-exo-3-exo-Dihydroxybornane Monoacrylate Esters. *S. Afr. J. Chem.* **58**, 140–144 (2013).
122. Lobb, K. A. kl_kinint (unpublished in-house script).
123. Bandgar, B.P., Kinkar, S.N., Kanble, V.T., and Bettigeri, S. V. Highly rapid and direct synthesis of diaryl sulfoxides. *Synlett* **13**, 2029 (2003).
124. Cervantes, H., Khac, D. D., Fetizon, M. and Guir, F. Model studies in the taxane diterpene series - Part I. *Tetrahedron.* **42**, 3491–3502 (1986).
125. Werstuijk, N.H., Timmins, G., Sayer, B. High-field ²Hmr spectrometry of deuteriated 1,3,3-trimethylbicyclo[2.2.1]heptan-2-ones. Determination of geminal deuterium isotope effects on deuterium chemical shift. *Can. J. Chem* **64**, 1465–1466 (1986).
126. Chandrasekhar, J., Maitra, U. Use of Isotopes for Studying Reaction Mechanisms. *Resonance* (1997).
127. Bartlett, P.D. and Knox, L. H. D,L-10-Camphorsulfonic Acid (Reychler's Acid). *Org. Synth.* **45**, 12 (1965).
128. Mciteka, L. P. Novel applications of Morita-Baylis-Hillman methodology in organic synthesis. Rhodes Thesis (2012).
129. Jafarpour, M., Rezaeifard, A. and Aliabadi, M. Catalytic activity of silica gel in the synthesis of sulfonamides under mild and solvent-free conditions. *Appl. Catal, A.* **358**, 49–53 (2009).
130. Banerjee, A. K., Laya, M. S. and Vera, W. J. Silica gel in organic synthesis. *Russ. Chem. Rev.* **70**, 971–990 (2001).
131. Mendes, S. R. Thurow, S., Fortes, M. P., Penteado, F., Lenardo, E. J., Alves, D., Perin, G. and Jacob, R. Synthesis of bis(indolyl)methanes using silica gel as an efficient and recyclable surface. *Tetrahedron Lett.* **53**, 5402–5406 (2012).
132. Evans, P., McCabe, T., Morgan, B. S. and Reau, S. Double Reduction of Cyclic Aromatic Sulfonamides : A Novel Method for the Synthesis of 2- and 3-Aryl-Substituted Cyclic Amines. *Org. Lett.* **7**, 43–46 (2005).
133. Nukina, Shogo and Searles, S. Cleavage and rearrangement of sulfonamides. *Chem.Rev.* **59**, 1077–1103 (1959).
134. Osby, J.O., Heinzman, S. W. and Ganem, B. Studies on the Mechanism of Transition-Metal-Assisted Sodium Borohydride and Lithium Aluminum Hydride Reductions. *J. Am. Chem. Soc.* **108**, 67–72 (1986).
135. Chaikin, S.W., and Brown, G. W. Reduction of Aldehydes, Ketones and Acid Chlorides by Sodium Borohydride. *J. Am. Chem. Soc.* **71**, 122–125 (1949).
136. Freedman, H.H., and Dubois, R. A. An improved Williamson ether synthesis using phase transfer catalyst. *Tetrahedron Lett.* **38**, 3251–3254 (1975).

137. Schlatterer, J. C. and Jäschke, A. Universal initiator nucleotides for the enzymatic synthesis of 5'-amino- and 5'-thiol-modified RNA. *Biochem. Biophys. Res. Commun.* **344**, 887–92 (2006).
138. Shintou, T. and Mukaiyama, T. Efficient Methods for the Preparation of Alkyl - Aryl and Symmetrical or Unsymmetrical Dialkyl Ethers between Alcohols and Phenols or Two Alcohols by Oxidation - Reduction Condensation. *J. Am. Chem. Soc.* **126**, 7359–7367 (2004).
139. Oberg, K. M. Martin, T. J., Oinen, M. E., Dalton, D. M., Friedman, R. K., Neely, J. M., and Rovis, T. Enantioselective Rhodium-Catalyzed [2+2+2] Cycloaddition of Pentenyl Isocyanate and 4-Ethynylanisole: Preparation and Use of Taddol-pyrrolidine Phosphoramidite. *Org. Synth.* **91**, 150–161 (2014).
140. Poulsen, P.H., Overgaard, M., Jensen, K.L., and Anker, K. Enantioselective Organocatalytic α -Arylation of Aldehydes. *Org. Synth.* **91**, 175–184 (2014).
141. Kuroda, H. K. and Sasaki, K. H. Facile Conversions of Carboxylic Acids into Amides, Esters, and Thioesters Using 1,1'-Oxalyldiimidazole and 1.1'-oxalyldi(1,2,4-triazole). *Chem. Pharm. Bull.* **35**, 4294–4301 (1987).
142. Lanzillotto, M., Konnert, L., Lamaty, F., Martinez, J. and Colacino, E. Mechanochemical 1,1'-Carbonyldiimidazole-Mediated Synthesis of Carbamates. *ACS Sustainable. Chem. Eng.* **3**, 2882–2889 (2015).
143. Kallenbach, M., Baldwin, I. T. and Bonaventure, G. A rapid and sensitive method for the simultaneous analysis of aliphatic and polar molecules containing free carboxyl groups in plant extracts by LC-MS/MS. *Plant Methods* **5**, 11 (2009).
144. Martínez, L., Andrade, R., Birgin, E. G. and Martínez, J. M. Packmol: A Package for Building Initial Configurations for Molecular Dynamics simulations. *J. Comput. Chem.* **30**, 2157–2164 (2009).
145. Humphrey, W., Dalke, A., and Schulten, K. VMD: Visual Molecular Dynamics. *J. Mol. Graph.* **14**, 33–38 (1996).
146. Phillips, J. C. Braun, R., Wang, W., Gumbart, J., Tajkhorshid, E., Villa, E., Chipot, C., Skeel, R., Kale, L., and Schulten, K. Scalable molecular dynamics with NAMD. *J. Comput. Chem.* **26**, 1781–802 (2005).
147. Pedretti, A., Villa, L., Vistoli, G. VEGA-an open platform to develop chemo-bio-informatics applications, using plug-in architecture and script programming. *J.C.A.M.D* **18**, 167–173 (2004).
148. Pedretti, A., Villa, L., Vistoli, G. VEGA: A versatile program to convert, handle and visualize molecular structure on windows-based pcs. *J. Mol. Graph* **21**, 47–49 (2002).
149. Vanommeslaeghe, K., Hatcher, E., Acharya, C., Kundu, S., Zhong, S., Shim, J., Darian, E., Guvench, O., Lopes, P., Vorobyov, I., and MacKerell Jr., A. D. CHARMM General Force Field: A Force field for Drug-Like Molecules Compatible with the CHARMM All-Atom Additive Biological Force Field. *J. Comput. Chem* **31**, 671–690 (2010).
150. Yu, W., He, X., Vanommeslaeghe, K, and MacKerell Jr., A. D. Extension of the CHARMM General Force Field to Sulfonyl-Containing Compounds and Its Utility in Biomolecular Simulations. *J. Comput. Chem.* **33**, 2451–2468 (2012).
151. Desmond, J. L., Rodger, P. M. and Walsh, T. R. Testing the inter-operability of the CHARMM and SPC/Fw force fields for conformational sampling. *Mol. Simul.* **40**, 912–921 (2013).

152. Patel, S. and Brooks, C. L. Fluctuating charge force fields: recent developments and applications from small molecules to macromolecular biological systems. *Mol. Simul.* **32**, 231–249 (2006).
153. 00setupcrdstr.pl, a perl script written within the research group for the assembly of surfactants into a micelle.
154. Carlson, C. How I Made Wine Glasses from Sunflowers. *Wolfram Blog* (2011).
155. Buda, A. B. and Mislow, K. A Hausdorff Chirality Measure. *J. Am. Chem. Soc.*, **114**, 6006–6012. (1992).
156. Sijbren, O. and Engberts, J. B. F. N, Diels-Alder Reactions in Micellar Media. *Pure Appl. Chem.*, **72**, 1365-1372 (2000).
157. Goering, B. K. *Ph.D. Dissertation*, Cornell University (1995).
158. Engberts, J. B. F. N., Fernández, E., García-Río, L and Leis, J. R. Water in oil microemulsions as reaction media for a Diels-Alder reaction between *N*-ethylmaleimide and cyclopentadiene. *J. Org. Chem.*, **71**, 4111-4117. (2006).
159. Otsuka, K. and Terabe, S. Enantiomer separation of drugs by micellar electrokinetic chromatography using chiral surfactants. *J. Chromatogr. A.* **875**, 163-178. (2000).
160. Balasubramanian, S., and Abell, C. Synthesis of [6-2H]enolpyruvylshikimate-3-phosphate. *Tetrahedron. Lett.*, **34**, 963-966. (1991).
161. Zhang, Y. and Wu, W. Enantioselective synthesis of oxiranes by the reactions of dimethylsulfonium nethylide and aromatic aldehydes and ketones in the presence of chiral micelles. *Tetrahedron: Asymmetry*, **8**, 2723-2725. (1997).
162. Li, J., Tang, Y., Wang, Q., Li, X., Cun, L., Zhang, X., Zhu, J., Li, L. and Deng, J. Chiral surfactant-type catalysis for asymmetric reduction of aliphatic ketones in water. *J. Am. Chem. Soc.*, **134**, 18522-18525. (2012).